frontiers | Research Topics

Pharmaceutical materials for tumor imaging and therapy

Edited by
Wenliang Li, Jianxun Ding, Leijiao Li, Na Kong and Junqing Wang

Published in
Frontiers in Bioengineering and Biotechnology
Frontiers in Materials

FRONTIERS EBOOK COPYRIGHT STATEMENT

The copyright in the text of individual articles in this ebook is the property of their respective authors or their respective institutions or funders. The copyright in graphics and images within each article may be subject to copyright of other parties. In both cases this is subject to a license granted to Frontiers.

The compilation of articles constituting this ebook is the property of Frontiers.

Each article within this ebook, and the ebook itself, are published under the most recent version of the Creative Commons CC-BY licence. The version current at the date of publication of this ebook is CC-BY 4.0. If the CC-BY licence is updated, the licence granted by Frontiers is automatically updated to the new version.

When exercising any right under the CC-BY licence, Frontiers must be attributed as the original publisher of the article or ebook, as applicable.

Authors have the responsibility of ensuring that any graphics or other materials which are the property of others may be included in the CC-BY licence, but this should be checked before relying on the CC-BY licence to reproduce those materials. Any copyright notices relating to those materials must be complied with.

Copyright and source acknowledgement notices may not be removed and must be displayed in any copy, derivative work or partial copy which includes the elements in question.

All copyright, and all rights therein, are protected by national and international copyright laws. The above represents a summary only. For further information please read Frontiers' Conditions for Website Use and Copyright Statement, and the applicable CC-BY licence.

ISSN 1664-8714
ISBN 978-2-83251-113-8
DOI 10.3389/978-2-83251-113-8

About Frontiers

Frontiers is more than just an open access publisher of scholarly articles: it is a pioneering approach to the world of academia, radically improving the way scholarly research is managed. The grand vision of Frontiers is a world where all people have an equal opportunity to seek, share and generate knowledge. Frontiers provides immediate and permanent online open access to all its publications, but this alone is not enough to realize our grand goals.

Frontiers journal series

The Frontiers journal series is a multi-tier and interdisciplinary set of open-access, online journals, promising a paradigm shift from the current review, selection and dissemination processes in academic publishing. All Frontiers journals are driven by researchers for researchers; therefore, they constitute a service to the scholarly community. At the same time, the *Frontiers journal series* operates on a revolutionary invention, the tiered publishing system, initially addressing specific communities of scholars, and gradually climbing up to broader public understanding, thus serving the interests of the lay society, too.

Dedication to quality

Each Frontiers article is a landmark of the highest quality, thanks to genuinely collaborative interactions between authors and review editors, who include some of the world's best academicians. Research must be certified by peers before entering a stream of knowledge that may eventually reach the public - and shape society; therefore, Frontiers only applies the most rigorous and unbiased reviews. Frontiers revolutionizes research publishing by freely delivering the most outstanding research, evaluated with no bias from both the academic and social point of view. By applying the most advanced information technologies, Frontiers is catapulting scholarly publishing into a new generation.

What are Frontiers Research Topics?

Frontiers Research Topics are very popular trademarks of the *Frontiers journals series*: they are collections of at least ten articles, all centered on a particular subject. With their unique mix of varied contributions from Original Research to Review Articles, Frontiers Research Topics unify the most influential researchers, the latest key findings and historical advances in a hot research area.

Find out more on how to host your own Frontiers Research Topic or contribute to one as an author by contacting the Frontiers editorial office: frontiersin.org/about/contact

Pharmaceutical materials for tumor imaging and therapy

Topic editors

Wenliang Li — Jilin Medical University, China

Jianxun Ding — Changchun Institute of Applied Chemistry, Chinese Academy of Sciences (CAS), China

Leijiao Li — Changchun University of Science and Technology, China

Na Kong — Harvard Medical School, United States

Junqing Wang — Sun Yat-sen University, China

Citation

Li, W., Ding, J., Li, L., Kong, N., Wang, J., eds. (2023). *Pharmaceutical materials for tumor imaging and therapy*. Lausanne: Frontiers Media SA.

doi: 10.3389/978-2-83251-113-8

Table of contents

frontiers | Frontiers in Bioengineering and Biotechnology

TYPE Editorial
PUBLISHED 08 December 2022
DOI 10.3389/fbioe.2022.1099762

Check for updates

OPEN ACCESS

EDITED AND REVIEWED BY
Hasan Uludag,
University of Alberta, Canada

*CORRESPONDENCE
Bo Zhou,
hottank3210@163.com

SPECIALTY SECTION
This article was submitted to Biomaterials, a section of the journal Frontiers in Bioengineering and Biotechnology

RECEIVED 16 November 2022
ACCEPTED 17 November 2022
PUBLISHED 08 December 2022

CITATION
Li W, Wang J, Ding J, Kong N, Li L, Sun Y and Zhou B (2022), Editorial: Pharmaceutical materials for tumor imaging and therapy.
Front. Bioeng. Biotechnol. 10:1099762.
doi: 10.3389/fbioe.2022.1099762

COPYRIGHT
© 2022 Li, Wang, Ding, Kong, Li, Sun and Zhou. This is an open-access article distributed under the terms of the Creative Commons Attribution License (CC BY). The use, distribution or reproduction in other forums is permitted, provided the original author(s) and the copyright owner(s) are credited and that the original publication in this journal is cited, in accordance with accepted academic practice. No use, distribution or reproduction is permitted which does not comply with these terms.

Editorial: Pharmaceutical materials for tumor imaging and therapy

Wenliang Li[1,2], Junqing Wang[3], Jianxun Ding[4], Na Kong[5], Leijiao Li[6], Yu Sun[1] and Bo Zhou[1]*

[1]Key Laboratory of Jinlin Province for Zoonosis Prevention and Control, Military Veterinary Institute, AMMS, Changchun, China, [2]Jilin Collaborative Innovation Center for Antibody Engineering, Jilin Medical University, Jilin, China, [3]School of Pharmaceuticals Sciences (Shenzhen), Sun Yat-sen University, Guangzhou, China, [4]Key Laboratory of Polymer Ecomaterials, Changchun Institute of Applied Chemistry, Chinese Academy of Sciences, Changchun, China, [5]Center for Nanomedicine and Department of Anesthesiology, Brigham and Women's Hospital, Harvard Medical School, Boston, MA, United States, [6]School of Chemistry and Environmental Engineering, Changchun University of Science and Technology, Changchun, China

KEYWORDS

pharmaceutical material, imaging-guided therapy, photo-sensitive agent-mediated therapy, gene therapy, pharmacokinetics

Editorial on the Research Topic
Pharmaceutical materials for tumor imaging and therapy

1 Introduction

Biomedicine is undergoing a complete transformation, brought about by the development of nanotechnology. Cancer is a major public health problem worldwide. Therefore, a wide variety of pharmaceutical nanomaterials exhibiting antitumor activities have been designed and prepared for the improvement of human health. In this Research Topic "Pharmaceutical Materials for Tumor Imaging and Therapy", we focused on diagnostic imaging, available therapies, pharmaco-mechanisms, and pharmacokinetics specific to antitumor pharmaceutical materials. Nine articles are presented and are divided into five themes: 1) imaging-guided therapy, 2) photo-sensitive agent-mediated therapy, 3) gene therapy, 4) pharmacokinetics, and 5) research progress in pharmaceutical materials.

2 Imaging-guided therapy

One article has been published related to imaging-guided therapy. Xin et al. designed and prepared an iodine (I)-rich amphiphilic copolymer, poly(ethylene glycol)-poly(2-hydroxyethyl methacrylate)-I (PEG-PHEMA-I, INA), for computed tomography (CT) imaging–guided photo-dynamic immunotherapy of breast cancer. INA, as a CT contrast

agent, successfully illuminated the tumors in CT imaging. Under the guidance of CT imaging, photo-dynamic therapy (PDT) triggered by INA induced immunogenic cell death (ICD) to trigger the release of immune-associated cytokines. Good anticancer efficacy both *in vitro* and *in vivo* were obtained.

3 Photo-sensitive agent-mediated therapy

With the rapid development of nanotechnology, various photo-sensitive nano-agents have been added to pharmaceutical nanomaterials. Photo-sensitive nano-agents cover a wide range of materials, such as photo-responsive nanoparticles and photo-sensitizers for photo-thermal or photo-dynamic therapy (PTT/PDT). For example, a series of thermo- and light-responsive copolymers consisting of poly(*N*-isopropylacrylamide) (PNIPAM) and 6-[4-(4-methoxy phenyl azo)-phenoxyl-hexyl methacrylate) (AzoMA); PNIPAM-*b*-PAzoMA, were synthesized by Cui et al. *via* reversible addition-fragmentation chain transfer (RAFT) radical polymerization. PNIPAM-*b*-PAzoMA was used as a carrier for the delivery of ferroferric oxide (Fe_3O_4) nanoparticle. The photo-sensitive agent showed no significant cytotoxicity and good stability in physiological environments, demonstrating its potential for cancer therapy.

Wang et al. reported a charge-reversal nanoplatform (chlorin e6-poly(lactic-co-glycolic acid)@polydopamine-poly(allylamine hydrochloride)-dimethyl maleic acid nanoparticle (Ce6-PLGA@PDA-PAH-DMMA NP)), including PDA and Ce6 for enhancing synergistic PTT/PDT. The PAH-DMMA charge-reversal layer enabled Ce6-PLGA@PDA-PAH-DMMA NP to circulate for a long time in the blood at normal physiological condition and to successfully realize charge reversal in a weakly acidic tumor microenvironment, thereby improving cell uptake. This strategy provided a promising approach for the synergistic PTT/PDT for breast cancer.

4 Gene therapy

Delving further into the study of cancer pathogenicity mechanisms, researchers have realized that tumors are a type of gene disease. In the past two decades, approximately 1,000 clinical cancer trials based on gene drugs have been conducted. Yang et al. investigated the effects of sulfured polysaccharide from Undaria pinnatifida (SPUP) on the biological behaviors of ovarian cancer cells. The authors found that SPUP inhibited the proliferation, migration, and invasion of ovarian cancer cells, and induced their apoptosis by inhibiting the activation of Hedgehog signaling pathway at the protein level. In light of this discovery, natural products, particularly SPUP may be utilized as gene therapeutic agents for cancer therapy.

5 Pharmacokinetics

Doxorubicin (DOX), a potent anthracycline cytotoxic drug, has been routinely used as a frontline chemotherapeutic agent for the treatment of various cancers. The article by Xu et al. reported the molecular dynamic behaviors of free DOX and DOX-conjugated lipid prodrug molecule using molecular dynamics simulations. The authors concluded that free DOX loaded in a nanodisc system experienced rapid dissociation due to the unfavorable orientation of DOX attached to the lipid surface. The authors also investigated the conformational variation of nanodisc components, as well as intermolecular interactions, solvent accessible surface areas, and the flexibility of the individual membrane scaffold protein 1 residue.

A lipiodol nanoformulation, to overcome the drawbacks of interventional embolization chemotherapy, was introduced by Peng et al. The study demonstrated that superstable, homogeneous, and intermixed formulation technology allowed the clever combination of lipiodol and hydrophilic chemotherapeutic drugs to prepare an effective and superstable homogeneous lipiodol and DOX, exhibiting improved clinical transformation and application value.

6 Research progress in pharmaceutical materials

This sub-theme covers three reviews related to recent research progress in pharmaceutical materials. For example, Xiao et al. surveyed recent advances in research on polymeric nanoparticles used for controlled cancer drug delivery. This research reviewed the current state of cancer drug loading systems by presenting a series of published articles that highlighted the novelty and functions of a variety of different architectures, including micelles, liposomes, dendrimers, polymersomes, hydrogels, and metal-organic frameworks. This article may contribute to the development of useful polymeric nanoparticles to achieve different therapeutic purposes. Moreover, another article summarized the recent research on lipid nanoparticle (LNP) vehicles, utilized as powerful mRNA delivery tools for mRNA cancer therapy. The formulation components of mRNA-LNPs were discussed, and future challenges and directions were also highlighted. Furthermore, Wang et al. performed a systematic review of inorganic nanomaterials for the prevention and treatment of bacterial infection. Several classical, metal-based, metal-like, and carbon-based nanomaterials, used as PTT agents, were reviewed, and their advantages were discussed and summarized. These discussions may provide valuable suggestions for future research on near-infrared (NIR) photo-thermal conversion inorganic nanomaterials.

7 Conclusion

In summary, this Research Topic on "*Pharmaceutical Materials for Tumor Imaging and Therapy*" presents articles on different types of pharmaceutical materials for diagnosis and treatment of cancers. These articles describe advances in tumor imaging and therapy, highlighting exciting and transformative accomplishments.

Author contributions

WL, JW, JD, NK, LL, and YS wrote the article. BZ edited the article. All authors read and approved the final version.

Conflict of interest

The authors declare that the research was conducted in the absence of any commercial or financial relationships that could be construed as a potential conflict of interest.

Publisher's note

All claims expressed in this article are solely those of the authors and do not necessarily represent those of their affiliated organizations, or those of the publisher, the editors and the reviewers. Any product that may be evaluated in this article, or claim that may be made by its manufacturer, is not guaranteed or endorsed by the publisher.

frontiers in Materials

ORIGINAL RESEARCH
published: 13 December 2021
doi: 10.3389/fmats.2021.795061

Sulfated Polysaccharide From Undaria Pinnatifida Induces Apoptosis and Inhibits Proliferation, Migration, and Invasion in Ovarian Cancer *via* Suppressing the Hedgehog Signaling Pathway

*Yi Yang, Qin Zhang, Yongping Xu, Gang Chen and Yukuan Qiu**

Department of Oncology, China Coast Guard Hospital of the People's Armed Police Force, Jiaxing, China

OPEN ACCESS

Edited by:
Jianxun Ding,
Changchun Institute of Applied Chemistry (CAS), China

Reviewed by:
Nenad Filipovic,
University of Kragujevac, Serbia
Qinghua Xu,
Purdue University, United States

***Correspondence:**
Yukuan Qiu
qiuyukuan@163.com

Specialty section:
This article was submitted to Biomaterials, a section of the journal Frontiers in Materials

Received: *14 October 2021*
Accepted: *16 November 2021*
Published: *13 December 2021*

Citation:
Yang Y, Zhang Q, Xu Y, Chen G and Qiu Y (2021) Sulfated Polysaccharide From Undaria Pinnatifida Induces Apoptosis and Inhibits Proliferation, Migration, and Invasion in Ovarian Cancer via Suppressing the Hedgehog Signaling Pathway. Front. Mater. 8:795061. doi: 10.3389/fmats.2021.795061

Objective: To investigate the effects of sulfured polysaccharide from Undaria pinnatifida (SPUP) on the biological behaviors of ovarian cancer (OC) cells and its potential mechanism.

Methods: Sulfated polysaccharide from Undaria pinnatifida (SPUP) was extracted and characterized through a combination of chemical analysis, IR spectra, UV-Vis, gas chromatography, and high-performance gel permeation chromatography. OC and human ovarian surface epithelial cells were used as working model *in vitro* for evaluation of SPUP's therapeutic effects. A combination of CCK-8, Transwell, and flow cytometry assay was used to measure the proliferation, migration, invasion, and apoptosis of OC cells, respectively. In addition, the protein expression levels of cells were also measured by Western blot.

Results: SPUP suppressed OC development from three different perspectives: 1) SPUP treatment significantly inhibited the proliferation of OC in a dosage-dependent manner ($p < 0.05$); 2) SPUP inhibited the migration and invasion of OC cells confirmed by scratch and Transwell experiments ($p < 0.05$); 3) SPUP induced apoptosis in OC cells and thus further inhibited the growth of OC cells evaluated using flow cytometry ($p < 0.05$). The underlying mechanism of the suppressing effects of SPUP might be related to the inhibition of the hedgehog (Hh) signaling pathway in OC cells after SPUP treatment. With additional suppression of the Hh signaling pathway, the anticancer effects of SPUP were enhanced ($p < 0.05$).

Conclusion: Taken together, SPUP could inhibit the proliferation, migration, and invasion and induce apoptosis of OC cells by inhibiting the activation of the Hh signaling pathway, which proposes SPUP as a novel drug to treat OC clinically.

Keywords: sulfated polysaccharide from undaria pinnatifida, epithelial ovarian cancer, hedgehog signaling pathway, apoptosis, proliferation, migration, invasion

INTRODUCTION

There are approximately 239,000 new cases of ovarian cancer (OC), the deadliest gynecological tumor in women, developed and 152,000 deaths worldwide every year (Ferlay et al., 2015). Due to the difficulty of early diagnosis and the drug resistance of chemotherapy, OC has become the leading cause of death in patients with gynecological malignant tumors (Torre et al., 2018), among which epithelial OC is the most critical pathological subtype of OC, accounting for 90% of primary ovarian malignant tumors (Mutch and Prat, 2014; Fu et al., 2016). Till now, cytoreductive surgery combined with platinum and paclitaxel-based chemotherapy is the standard treatment strategy for epithelial OC. However, about 70% of patients relapse after the initial treatment and often develop resistance to platinum chemotherapy after recurrence (Chien et al., 2013). OC can metastasize rapidly in a short time and has a high degree of malignancy. Due to the fact that there is no satisfactory treatment for advanced patients, the 5-year survival rate of patients with advanced epithelial OC is only 29% (Reid et al., 2017). Therefore, it is urgent to develop a new, safe, and effective drug with minor side effects to control the progression of OC and reduce patient mortality.

In recent years, natural antitumor polysaccharides have gradually attracted the attention of cancer experts and scholars because of their significant anticancer effects with less toxic and side effects (Zong et al., 2015). It has been reported that polysaccharides could inhibit the proliferation of tumor cells and directly induce apoptosis or trigger immune enhancement activity combined with chemotherapy (Zong et al., 2012; Chowdhury et al., 2015). Undaria pinnatifida (UP), as seafood, is distributed worldwide (Zhou et al., 2015). The main compounds of UP are protein, polysaccharides, and minerals. Further, studies reported that UP had various biological functions, including immune regulation and anticancer (Wu et al., 2019; Yu et al., 2019). Sulfated polysaccharide from Undaria pinnatifida (SPUP), a critical component of US, is a hot research topic especially in the field of cancer treatment. It has been proved that SPUP plays a critical role in anti-breast cancer treatment by inhibiting the proliferation and migration of as well as inducing apoptosis in breast cancer cells (Wu et al., 2019). In addition, other studies have shown that SPUP could be encapsulated into nanoparticles and delivered through injection to inhibit the migration and invasion of pancreatic cancer cells; thus, SPUP was identified as a target drug for pancreatic cancer treatment (Song et al., 2019). However, the effects and activity of SPUP in OC remain unclear and require further studies.

The hedgehog (Hh) signaling pathway plays an important role in determining cell fate including regulating proliferation, migration, and invasion (Liu et al., 2018). It was reported that the aberrant activation of the Hh signaling pathway was associated with tumorigenesis and progression of human cancer (Skoda et al., 2018). In OC, Liu et al. found that DHA could induce apoptosis and inhibit proliferation, migration, and invasion in ovarian cancer cell *via* suppressing the Hh signaling pathway (Liu et al., 2018). However, there is no study about the effects of SPUP on OC progression.

Taken together, this study aimed to study the effects of SPUP on cell proliferation, migration, invasion, and apoptosis in OC epithelial cells and further investigate its potential mechanism, providing novel insights for further potential identification of SPUP as a therapeutic drug in OC treatment.

MATERIALS AND METHODS

Extraction and Identification of SPUP

SPUP was prepared as previously published (Zhao et al., 2018). The UP was purchased from the local seafood market and rinsed with precooled ultrapure water to remove impurities. The cleaned UP was cut into 3–5-cm-long pieces and crushed with a high-speed grinder. The obtained homogenate was continuously stirred in absolute ethanol to remove lipids and other impurities. The suspension was centrifuged at room temperature at 5,000 rpm for 30 min and air-dried to obtain powder. A volume of 20 g UP powder was resuspended in distilled water with a ratio of 1:20 (powder mass and water volume, g/mL), extracted for 5 h in the reflux device, and centrifuged at room temperature at 5,000 rpm for 20 min. The supernatant was collected and concentrated to about 50 ml with a vacuum rotary evaporator. It was then deproteinized by the Sevag method (Sevag et al., 1938). After that, the solution was mixed with four times the volume of absolute ethanol and stirred violently and overnight at 4°C. The next day, the mixture was centrifuged at 4°C at 5,000 rpm for 20 min. The sediment was collected following by vacuuming and stored in the refrigerator at −80°C. To identify the properties of SPUP, chemical analysis, gas chromatography (GC), high-performance gel permeation chromatography (HPGPC), infrared spectroscopy, and ultraviolet, visible spectroscopy (UV-1800 spectrophotometer, Shimadzu, Kyoto, Japan) were used for evaluation.

Cell Culture

OC cell lines (SKOV3, A2780) and human ovarian surface epithelial cells (HOSEPICs) were purchased from Shanghai Fuheng Biotechnology Co., Ltd. The cells were incubated in a humidified incubator at 37°C and 5% CO_2 using RPMI 1640 medium with 10% fetal bovine serum and 1% penicillin and streptomycin.

Cell Proliferation was Measured by Cell Counting Kit-8

OC cells in the logarithmic growth stage were inoculated into 96-well plates (10^4 cells/well) and cultured in an incubator at 37°C and 5% CO_2 for 24 h. The cells were divided into the control and different-concentration SPUP treatment groups (the concentrations were 25, 50, 100, 150, and 200 μg/ml), incubated for 24 h after corresponding treatment. After addition of 10 μl CCK-8 solution, the cells were cultured for another 2 h in the incubator. The 96-well plates were placed in a

spectrophotometer to measure the absorbance value at 450-nm wavelength.

Cell Migration Activity was Detected by the Transwell Method

The cells were divided into the control and SPUP treatment groups (100 μg/ml) and inoculated into the Transwell upper chamber (Corning, NY, USA) at the density of 10^5 cells/well. The corresponding culture medium without fetal bovine serum was added into the upper chamber for 24 h 600 μl RPMI 1640 medium containing 20% fetal bovine serum which was added in the lower chamber simultaneously. After 24 h, the non-migrating cells on the top of Transwell ependyma were removed with a cotton swab. The cells were fixed with 1% paraformaldehyde at room temperature for 30 min and stained with 2% crystal violet for 30 min. The transmembrane cells on the ventricular membrane were imaged with an inverted microscope.

Transwell Method was Used to Detect the Invasive Activity of Cells

The cells were inoculated into the Transwell upper chamber (Corning, USA) with Matrigel glue at 2×10^5/well density. The cells in the upper chamber were cultured with a corresponding culture medium without fetal bovine serum for 24 h with 600 μl RPMI 1640 medium containing 20% fetal bovine serum in the lower chamber simultaneously. After 24 h, the non-migrating cells on the top of Transwell ependyma were removed with a cotton swab. After 1% paraformaldehyde was fixed at room temperature for 30 min and stained with 2% crystal violet for 30 min, the transmembrane cells on the ventricular membrane in 3 randomly selected fields of each group were imaged with an inverted microscope to count the cell number.

Flow Cytometry was Utilized to Measure Apoptosis

Apoptosis was determined by Annexin V-FITC/PI double staining. The cells were divided into control and SPUP treatment groups, inoculated in 6-well plates at the density of 10^5/well, and treated the next day. After 24 h of culture, the cells were trypsinized and transferred to the centrifuge tube and washed with precooled PBS 3 times with centrifuging 5 min each. After cell pellets were obtained, 500 μl combined buffer was added and incubated in the dark, in which 5 μl Annexin V-FITC was added with 10 μl PI staining solution. The cells were cultured in the dark at room temperature for 15 min. Then, flow cytometry was performed and analyzed using FlowJo software to evaluate cell apoptosis.

Western Blot was Used to Detect the Protein Expression of Cells

RIPA (Beyotime Technology, China) containing PMSF and phosphotransferase inhibitor was used for cell protein extraction. The BCA protein concentration analysis kit (Beyotime Technology, Shanghai, China) was used to determine the protein concentration. An equal amount of proteins was separated using SDS-PAGE gel (12%) and transferred to the PVDF membrane (Millipore, Bedford, MA, USA). Subsequently, the membrane was blocked with 5% skimmed milk at room temperature for 1 h and incubated with the corresponding primary antibody at 4°C overnight. The horseradish peroxidase bound secondary antibody was used to incubate at room temperature for 1 h. Protein fluorescence imaging was performed in the developing system using an ECL luminescent solution (Millipore, USA). Primary reactance includes β-actin (1:3,000, ab8226, Abcam, United Sates), Shh (1,000, ab53281, Abcam), Gli1 (1:1,000, ab134906, Abcam), Ptch1 (1:500, ab53715, Abcam), and Smo (1:1,000, ab72130, Abcam).

Statistical Analysis

All experiments were repeated three times independently. All measurement data in this study were expressed as mean ± standard deviation. SPSS 20.2 (SPSS, Chicago, IL, USA) was used. Under the same conditions, one-way ANOVA was used for intragroup comparison. Different groups were compared using Student's t-test. When $p < 0.05$, the difference was significant.

RESULTS

Identification of Physical and Chemical Properties of SPUP

Through chemical analysis, the main contents of SPUP were identified as total sugar (80.21%), uronic acid (3.56%), and protein (7.32%). Notably, the percentage of sulfate in SPUP was 29.47%, suggesting that SPUP was an acid-free polysaccharide. As shown in **Figure 1A**, consistent with chemical composition analysis, the UV-Vis spectrum of SPUP reported an obvious absorption at almost 280 nm, indicating the existence of protein or nucleic acid in SPUP (Feng et al., 2010; Zhao et al., 2018).

Following, the monosaccharide composition of SPUP was analyzed and cross referenced with the chromatogram of monosaccharide standard. As shown in **Figure 1B**, monosaccharide standards of rhamnose, arabinose, fucose, xylose, mannose, glucose, and galactose were separated well under GC conditions. In contrast, SPUP was mainly composed of fucose, glucose, and galactose, with a molar ratio of 27.22:19.32:53.46 (**Figure 1C**).

In addition, the bond structure of SPUP was determined by infrared spectroscopy. Similar to common carbohydrate features, SPUP exhibited a stretching vibration of the O–H bond at 3,437.1 cm-1 (**Figure 1D**). A stretching vibration of the C–H key could then be seen at 2,981.3 cm-1. The moderate-intensity absorption peaks appeared at 1,661.2 and 1,638.7 cm-1, manifested explicitly in the deformation vibration of the O–H bond. There was a strong absorption peak at about 1,000–1,200 cm^{-1}, suggesting the stretching of the coupled

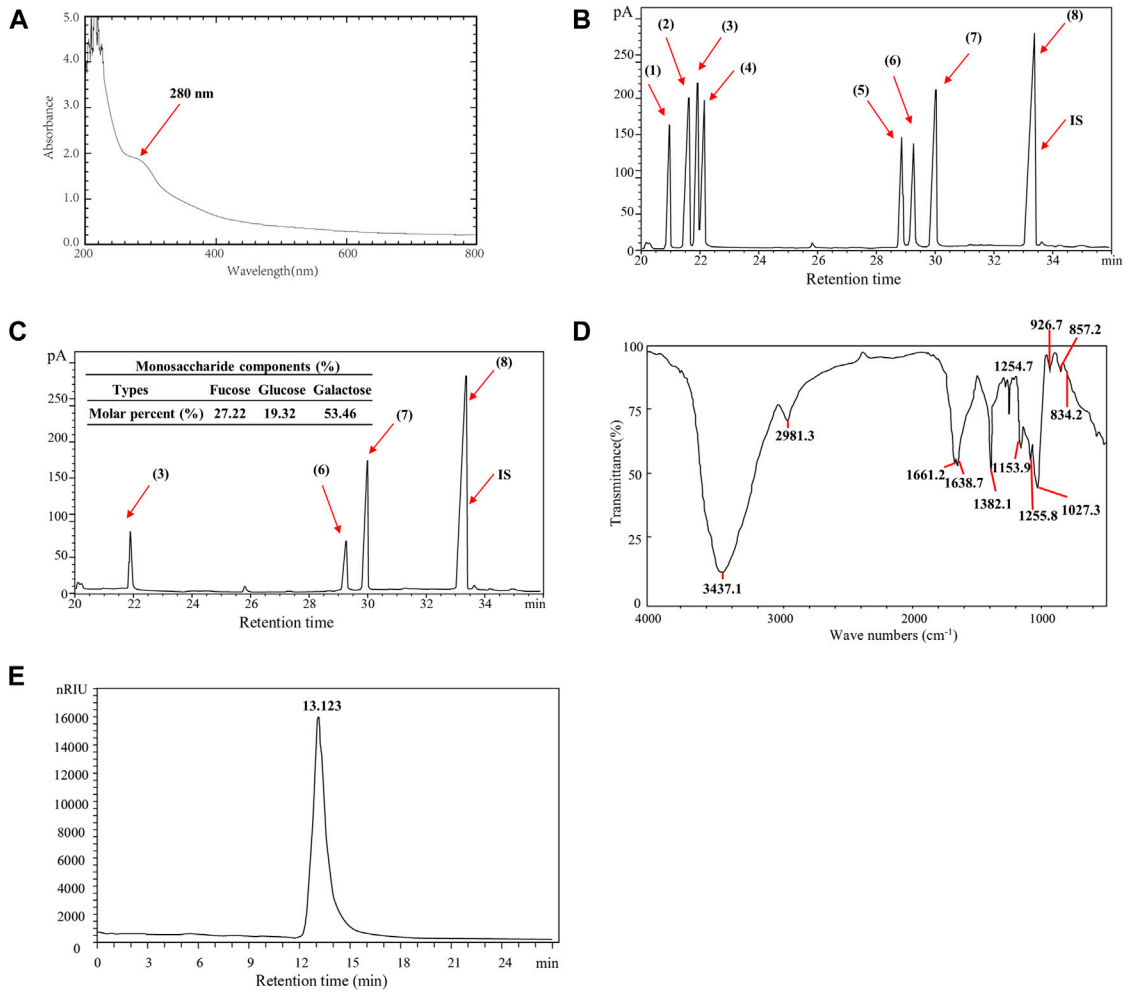

FIGURE 1 | Identification of physical and chemical properties of SPUP; **(A)** UV-vis spectra of SPUP; **(B,C)** GC diagram of standard monosaccharide and SPUP; **(D)** infrared spectrum of SPUP; **(E)** HPGPC chromatogram of SPUP. Note: 1): rhamnose; 2): arabinose; 3): fucose; 4): xylose; 5): mannose; 6): glucose; 7): galactose; 8): inositol; IS: internal standard. SPUP inhibited the proliferation of OC cells.

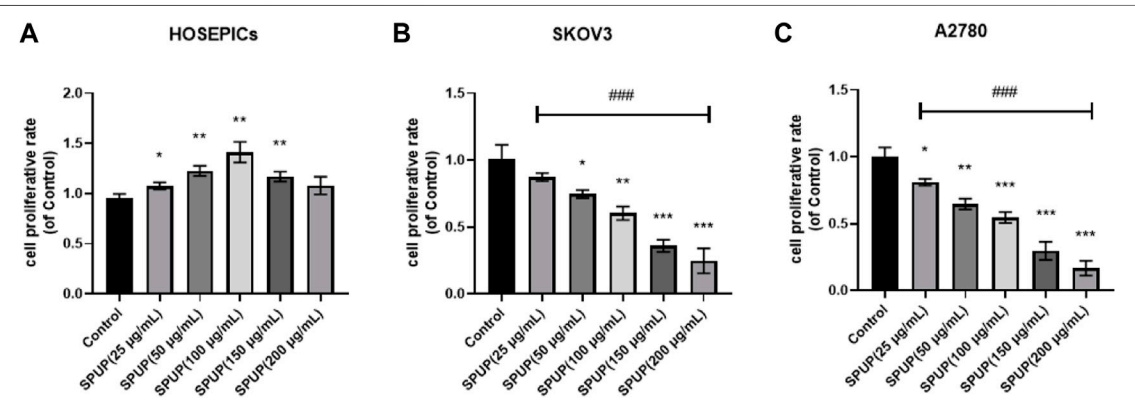

FIGURE 2 | Effect of SPUP on the proliferation activity of two kinds of OC cells and human normal ovarian epithelial cells. Compared with the control group, $^{*}p < 0.05$, $^{**}p < 0.01$, $^{***}p < 0.001$; comparison between groups with different concentrations of SPUP, $^{\#\#\#}p < 0.001$. **(A)** HOSEPICs, **(B)** SKOV3, and **(C)** A2780.

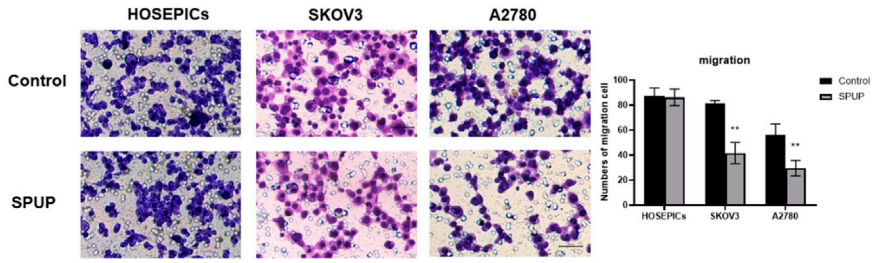

FIGURE 3 | Effect of SPUP on the migration ability of two kinds of OC cells and human normal ovarian epithelial cells. Compared with the control group, $^{**}p < 0.01$.

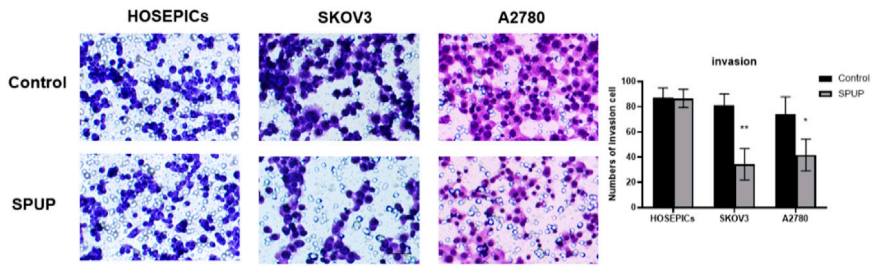

FIGURE 4 | SPUP on the invasion ability of two kinds of OC cells and human normal ovarian epithelial cells. Compared with the control group, $^{*}p < 0.05$, $^{**}p < 0.01$.

C–O bond and C–C bond, as well as the bending vibration of O–H. The absorption peak signal at 926.7 cm^{-1} might be due to the presence of β-d-galactopyranose. In addition, according to previous studies, it could be determined that the absorption peak at 834.2 or 857.2 and 1,255.8 cm^{-1} was sulfate (Mao et al., 2008). In addition, the characteristic absorption, peaking at 834.2 or 857.2, suggested the existence of an α-type glycosidic bond in SPUP.

As shown in **Figure 1E**, the retention time of SPUP in HPGPC chromatography was 13.123 min. According to the calibration curve-fitting equation established by the dextran standard with different molecular weights, the calculation method of retention time was substituted into the calibration curve equation. The average molecular weight of SPUP was 97.9 kDa.

SPUP Inhibited the Proliferation of OC Cells

Through the proliferation assay analysis, with the increase in SPUP concentration, the proliferative activity of two OC cells decreased in a concentration-dependent manner ($p < 0.05$) (**Figure 2**). The cell proliferation rate was decreased under 0.5 when the concentration of SPUP reached 150 μg/ml. In contrast, in human normal ovarian epithelial cells, the capacity of cell proliferation increased with SPUP treatment within the range of 25–100 μg/ml ($p < 0.05$). However, the increase in cell proliferation rate caused by SPUP reached its maximum at 100 μg/ml and no additional effects were observed with further increasing of SPUP. Taken from the results, SPUP could inhibit the proliferation of OC cells in a dosage-dependent manner. As determined, the concentrations of 150 and 200 μg/ml of SPUP inhibited cell proliferation most violently; the concentration of 100 μg/ml SPUP was used for further study otherwise indicated.

SPUP Reduced OC Cell Migration

To study the effect of SPUP on the migration ability of HOSEPICs, SKOV3, and A2780 cells, Transwell cell migration experiments were used to determine the migration ability of cells. As shown in **Figure 3**, SPUP treatment could significantly inhibit the migration ability of OC cells (all $p < 0.05$) than the control group. In contrast, there are no significant changes observed in the migration ability of normal cells ($p > 0.05$).

SPUP Treatment Inhibited OC Cell Invasion

The invasion ability of OC cells was measured by the Transwell chamber. Compared with the control group, SPUP treatment could significantly inhibit the invasion ability of OC cells (all $p < 0.05$) (**Figure 4**). In comparison, the migration ability of normal cells did not change significantly ($p > 0.05$).

SPUP Promoted OC Cell Apoptosis

As shown in **Figure 5**, SPUP treatment could significantly induce the apoptosis of OC cells (all $p < 0.05$) but not in normal cells ($p > 0.05$).

SPUP Inhibited the Activation of Hedgehog Signaling Pathway in OC Cells

As shown in **Figure 6A**, OC cells had different degrees of Hh signal pathway activation compared with HOSEPICs cells (all $p < 0.05$). To clarify whether SPUP plays an anti-OC role by

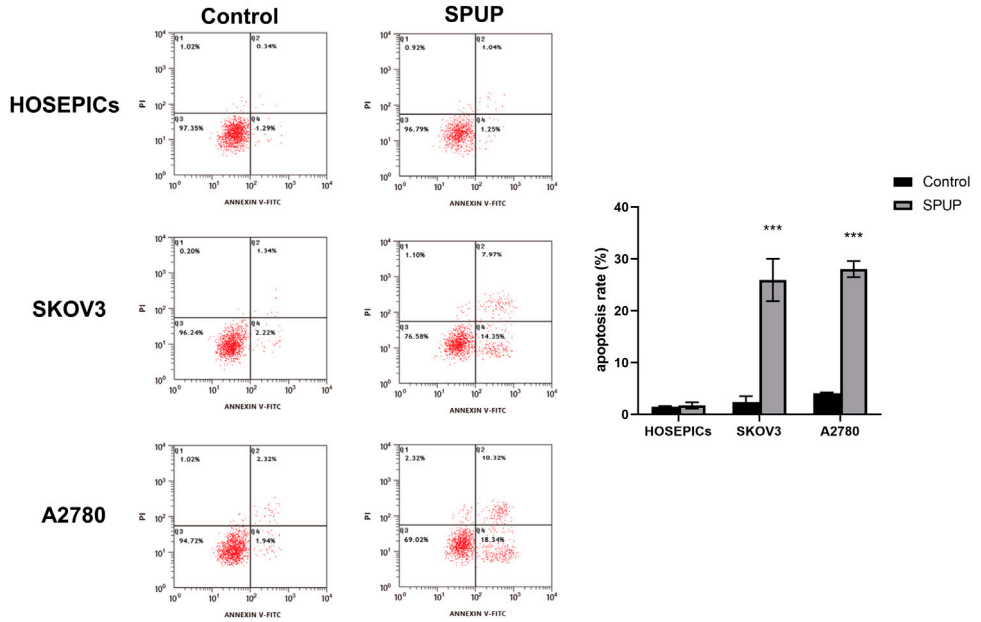

FIGURE 5 | Effects of SPUP on apoptosis of two kinds of OC cells and human normal ovarian epithelial cells. ***$p < 0.001$ compared with the control group. SPUP inhibited the activation of the hedgehog signaling pathway in OC cells.

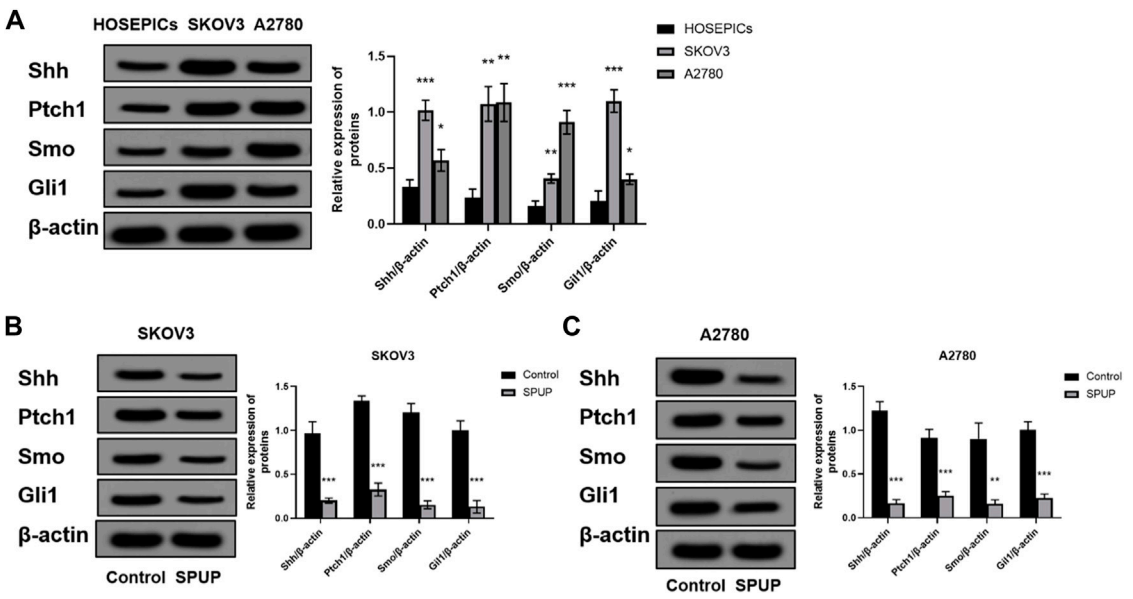

FIGURE 6 | Effect of SPUP on Hh signal pathway activity of OC cells; **(A)** protein expression of OC cells and HOSEPICs cells; **(B,C)** protein expression of SKOV3 and A2780 cells. *$p < 0.05$, **$p < 0.01$, ***$p < 0.001$ compared with HOSEPICs or control group. SPUP could inhibit the proliferation, invasion, and migration and promoted apoptosis by regulating the activation of the Hh signaling pathway.

inhibiting the Hh pathway, we evaluated the expressions of Shh, Ptch1, Smo, and Gli1 upon SPUP treatment. As shown in **Figures 6B,C**, compared with the control group, the expression of Shh, Ptch1, Smo, and Gli1 proteins in OC cells in the SPUP treatment group decreased to varying degrees (all $p < 0.05$). The results suggested that SPUP might take effects in anticancer through inhibiting the activation of the Hh signal pathway in OC cells.

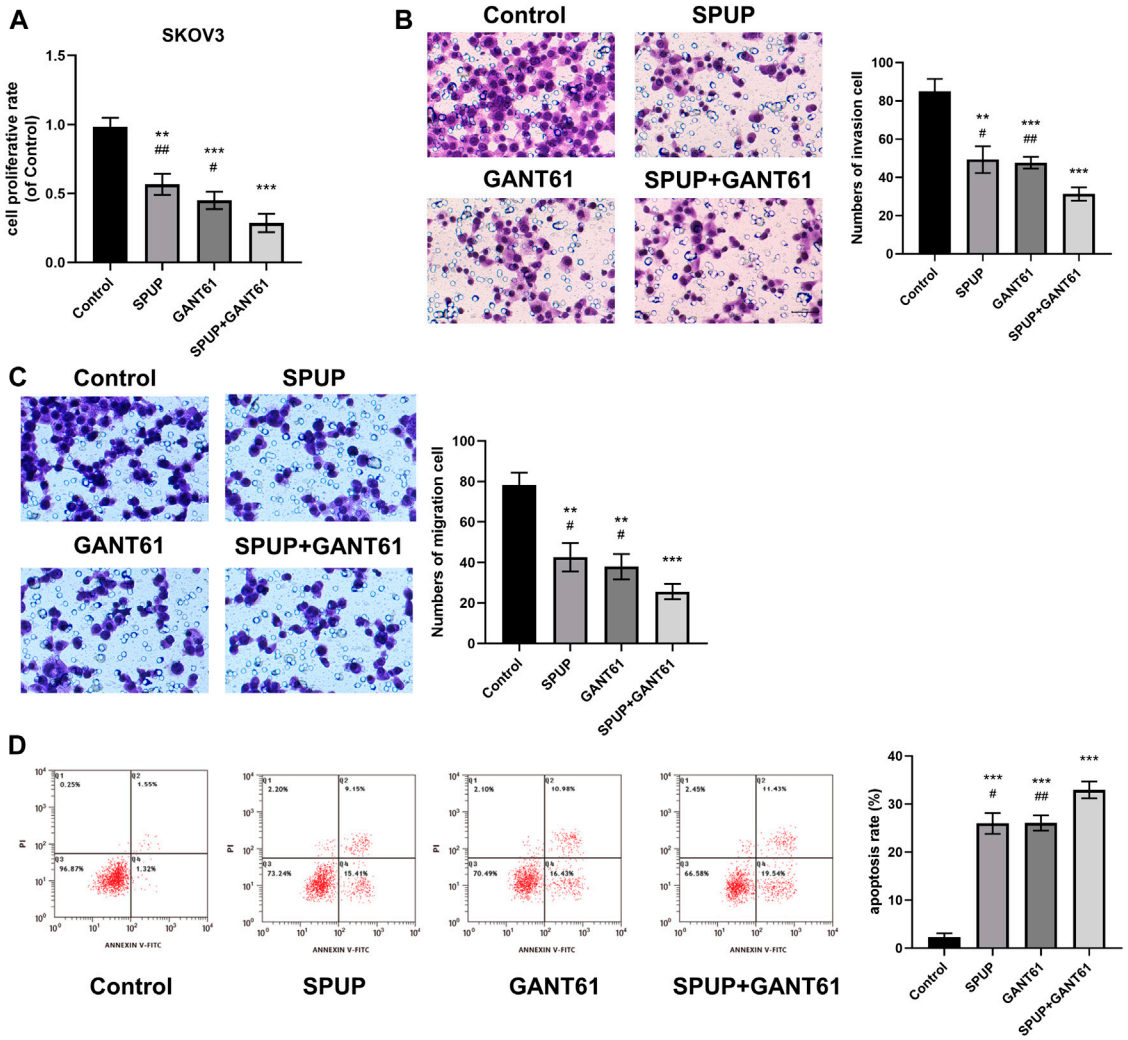

FIGURE 7 | SPUP plays a role in regulating cell function by inhibiting the activation of the Hh signaling pathway. **(A)** The CCK-8 method was used to determine the proliferation ability of cells after the Hh pathway inhibitor was applied; **(B,C)** the Transwell method was used to determine the invasion and migration ability of cells after Hh pathway inhibitor was applied; **(D)** the apoptosis of cells after the Hh pathway inhibitor was measured by flow cytometry. $^{**}p < 0.01$, $^{***}p < 0.001$ compared with the control group, $^{\#}p < 0.01$, $^{\#\#}p < 0.01$ compared with the SPUP + GANT61 group.

SPUP Could Inhibit Proliferation, Invasion, and Migration and Promote Apoptosis by Regulating the Activation of the Hh Signaling Pathway

As shown in **Figure 7**, SPUP or GANT61 alone or in combination with SPUP and GANT61 could inhibit the proliferation, migration, and invasion of OC cells (all $p < 0.05$) and promote apoptosis (all $p < 0.05$) in SKOV3 cells. The inhibitory effects of the SPUP + GANT61 group were more obvious than those of the SPUP or GANT61 group (all $p < 0.05$), respectively. Thus, SPUP played an anticancer role by regulating the activation of the Hh signaling pathway.

DISCUSSION

As known, SPUP is an effective apoptosis inducer for a variety of cancer cells (Yang et al., 2013). In addition to anticancer, antiproliferative, and anticoagulant activities, some studies have also found that SPUP can activate exogenous or endogenous apoptosis pathways in various cancer cell lines through regulating the expression of apoptosis-related or signal proteins, cell-cycle regulatory proteins, and transcription factors (Hyun et al., 2009; Yamasaki-Miyamoto et al., 2009). This study found that SPUP could inhibit the proliferation, migration, and invasion of OC cells and induce apoptosis. In addition, SPUP significantly reduced the activation of the Hh signaling pathway at the protein level.

As previous study has shown that SPUP could inhibit the proliferation and migration and induce the apoptosis of breast cancer cells (Wu et al., 2019), we thought to investigate the role of SPUP in OC cells. A systematic evaluation of cell proliferation, migration, invasion, and apoptosis was conducted using a combination of CCK-8 assay, Transwell assay, and flow cytometry. We, for the first time, confirmed that SPUP could inhibit the cell proliferation of OC cells (SKOV3 and A2780) in a dose-dependent manner. The concentrations of SPUP (25, 50, 100, 150, and 200 μg/ml) we used in this study are consistent with Wu et al. (Wu et al., 2019), who once found that SPUP treatment could inhibit the proliferation and migration and induce the apoptosis of breast cancer cells. Considering that there are few studies that focus on the effects of SPUP in cancers, more experimental studies are still needed.

Moreover, this study also provided novel insights in the effects of SPUP on normal human ovarian epithelial cells. It was found that SPUP could promote the proliferation of human ovarian epithelial cells, suggesting that the side effects of SPUP treatment could be reduced to the minimum by administering a proper amount of SPUP. Migration and invasion are known to play an essential role in the progression of tumors. Our study also found for the first time that SPUP could significantly inhibit the migration and invasion of OC cells and induce the apoptosis of SPUP-treated OC cells.

The Hh pathway is very important for embryonic development (Wang et al., 2017). Many previous studies have shown that activation of the Hh pathway could promote the occurrence and development of tumors, including OC (Chen et al., 2013; Wu et al., 2019). The Hh pathway is known to have a high expression level in OC (Schmid et al., 2011). Taken together, inhibition of Hh signals could induce apoptosis and inhibit cell viability and migration. Nevertheless, inhibition of the Hh pathway may be an effective target for OC treatment. Corresponding to previous studies, this study also investigated the relationship between SPUP and the Hh signaling pathway. In our study, we compared the expression of the Hh signaling pathway-related proteins in human normal ovarian epithelial cells and OC cells and found that the levels of Shh, Ptch1, Smo, and Gli1 protein in OC cells were significantly increased, indicating that the Hh signaling pathway was activated in OC. Moreover, we were the first time to find that the activation of the Hh signaling pathway was diminished upon SPUP treatment in SKOV3 and A2780 cells. Therefore, we speculated that SPUP might play an anticancer role in OC by inhibiting Hh signal activation. Till now, there are few studies that reported the regulatory effects of polysaccharide on the Hh signaling pathway in cancers. Yamasaki et al. once found that protein-bound polysaccharide-K could inhibit the induction of a malignant phenotype in pancreatic cancer by suppressing the Hh signaling pathway (Yamasaki et al., 2016), suggesting that polysaccharide might suppress the progression of cancers by modulating the activation of Hh signaling. In our study, we also found similar results; however, the underlying mechanism effects of SPUP in OC still needs further research.

In this study, SKOV3 cells were used as a disease model and treated with SPUP, GANT61 (Hh pathway inhibitor), and SPUP and GANT61 to investigate the underlying mechanism of SPUP on the Hh signal pathway. We found that SPUP could induce apoptosis of OC cells and inhibit cell proliferation, migration, and invasion. The effect of the GANT61 treatment was similar to that of SPUP. In addition, the anticancer effect of SPUP combined with GANT61 was more efficient than that of GANT61 alone, suggesting that SPUP could enhance the anticancer effects of GANT61. The above results indicated that SPUP might induce OC cell apoptosis and inhibit cell proliferation, migration, and invasion by reducing the protein expression of Hh signal pathway proteins Shh, Ptch1, Smo, and Gli1, similar to other Hh signal pathway inhibitors.

In conclusion, this study identified SPUP, for the first time, as an effective drug which induced apoptosis and inhibited cell proliferation, migration, and invasion by inhibiting Hh pathway conduction in OC cells. However, the exact mechanism of how SPUP regulating Hh pathway in OC was still in need for further studies.

DATA AVAILABILITY STATEMENT

The original contributions presented in the study are included in the article/Supplementary Material; further inquiries can be directed to the corresponding author.

AUTHOR CONTRIBUTIONS

YY and YQ proposed and designed the experiments. YY and QZ carried out the experiments with the help of YX and GC. YY and QZ drafted the article and interpreted the data. GC, YX, and YQ revised the article. All the authors approved the final version of this article.

FUNDING

The project was supported by the Jiaxing Science and Technology Plan Project (No. 2018AD32182).

REFERENCES

Chen, Q., Gao, G., and Luo, S. (2013). Hedgehog Signaling Pathway and Ovarian Cancer. *Chin. J. Cancer Res.* 25 (3), 346–353. doi:10.3978/j.issn.1000-9604.2013.06.04

Chien, J., Kuang, R., Landen, C., and Shridhar, V. (2013). Platinum-sensitive Recurrence in Ovarian Cancer: the Role of Tumor Microenvironment. *Front. Oncol.* 3, 251. doi:10.3389/fonc.2013.00251

Chowdhury, S. R., Sengupta, S., Biswas, S., Sen, R., Sinha, T. K., Basak, R. K., et al. (2015). Low Fucose Containing Bacterial Polysaccharide Facilitate Mitochondria-dependent ROS-Induced Apoptosis of Human Lung Epithelial Carcinoma via Controlled Regulation of MAPKs-Mediated Nrf2/Keap1 Homeostasis Signaling. *Mol. Carcinog.* 54 (12), 1636–1655. doi:10.1002/mc.22236

Feng, L., Jia, X.-B., Shi, F., and Chen, Y. (2010). Identification of Two Polysaccharides from Prunella Vulgaris L. And Evaluation on Their Anti-lung Adenocarcinoma Activity. *Molecules* 15 (8), 5093–5103. doi:10.3390/molecules15085093

Ferlay, J., Soerjomataram, I., Dikshit, R., Eser, S., Mathers, C., Rebelo, M., et al. (2015). Cancer Incidence and Mortality Worldwide: Sources, Methods and Major Patterns in GLOBOCAN 2012. *Int. J. Cancer* 136 (5), E359–E386. doi:10.1002/ijc.29210

Fu, X., Li, Y., Alvero, A., Li, J., Wu, Q., Xiao, Q., et al. (2016). MicroRNA-222-3p/GNAI2/AKT axis Inhibits Epithelial Ovarian Cancer Cell Growth and Associates with Good Overall Survival. *Oncotarget* 7 (49), 80633–80654. doi:10.18632/oncotarget.13017

Hyun, J.-H., Kim, S.-C., Kang, J.-I., Kim, M.-K., Boo, H.-J., Kwon, J.-M., et al. (2009). Apoptosis Inducing Activity of Fucoidan in HCT-15 colon Carcinoma Cells. *Biol. Pharm. Bull.* 32 (10), 1760–1764. doi:10.1248/bpb.32.1760

Liu, Y., Gao, S., Zhu, J., Zheng, Y., Zhang, H., and Sun, H. (2018). Dihydroartemisinin Induces Apoptosis and Inhibits Proliferation, Migration, and Invasion in Epithelial Ovarian Cancer via Inhibition of the Hedgehog Signaling Pathway. *Cancer Med.* 7 (11), 5704–5715. doi:10.1002/cam4.1827

Mao, W.-J., Fang, F., Li, H.-Y., Qi, X.-H., Sun, H.-H., Chen, Y., et al. (2008). Heparinoid-active Two Sulfated Polysaccharides Isolated from marine green Algae Monostroma Nitidum. *Carbohydr. Polym.* 74 (4), 834–839. doi:10.1016/j.carbpol.2008.04.041

Mutch, D. G., and Prat, J. (2014). 2014 FIGO Staging for Ovarian, Fallopian Tube and Peritoneal Cancer. *Gynecol. Oncol.* 133 (3), 401–404. doi:10.1016/j.ygyno.2014.04.013

Reid, B. M., Permuth, J. B., and Sellers, T. A. (2017). Epidemiology of Ovarian Cancer: a Review. *Cancer Biol. Med.* 14 (1), 9–32. doi:10.20892/j.issn.2095-3941.2016.0084

Schmid, S., Bieber, M., Zhang, F., Zhang, M., He, B., Jablons, D., et al. (2011). Wnt and Hedgehog Gene Pathway Expression in Serous Ovarian Cancer. *Int. J. Gynecol. Cancer* 21 (6), 975–980. doi:10.1097/igc.0b013e31821caa6f

Sevag, M. G., Lackman, D. B., and Smolens, J. (1938). The Isolation of the Components of Streptococcal Nucleoproteins in Serologically Active Form. *J. Biol. Chem.* 124 (1), 42–49. doi:10.1016/s0021-9258(18)74048-9

Skoda, A. M., Simovic, D., Karin, V., Kardum, V., Vranic, S., and Serman, L. (2018). The Role of the Hedgehog Signaling Pathway in Cancer: A Comprehensive Review. *Bosn J. Basic Med. Sci.* 18 (1), 8–20. doi:10.17305/bjbms.2018.2756

Song, Z., Li, H., Liang, J., Xu, Y., Zhu, L., Ye, X., et al. (2019). Sulfated Polysaccharide from Undaria Pinnatifida Stabilizes the Atherosclerotic Plaque via Enhancing the Dominance of the Stabilizing Components. *Int. J. Biol. Macromolecules* 140, 621–630. doi:10.1016/j.ijbiomac.2019.08.173

Torre, L. A., Trabert, B., DeSantis, C. E., Miller, K. D., Samimi, G., Runowicz, C. D., et al. (2018). Ovarian Cancer Statistics, 2018. *CA: A Cancer J. Clinicians* 68 (4), 284–296. doi:10.3322/caac.21456

Wang, X., Wei, S., Zhao, Y., Shi, C., Liu, P., Zhang, C., et al. (2017). Anti-proliferation of Breast Cancer Cells with Itraconazole: Hedgehog Pathway Inhibition Induces Apoptosis and Autophagic Cell Death. *Cancer Lett.* 385, 128–136. doi:10.1016/j.canlet.2016.10.034

Wu, J., Li, H., Wang, X., Zhang, X., Liu, W., Wang, Y., et al. (2019). Effect of Polysaccharide from Undaria Pinnatifida on Proliferation, Migration and Apoptosis of Breast Cancer Cell MCF7. *Int. J. Biol. Macromolecules* 121, 734–742. doi:10.1016/j.ijbiomac.2018.10.086

Yamasaki, A., Onishi, H., Imaizumi, A., Kawamoto, M., Fujimura, A., Oyama, Y., et al. (2016). Protein-bound Polysaccharide-K Inhibits Hedgehog Signaling through Down-Regulation of MAML3 and RBPJ Transcription under Hypoxia, Suppressing the Malignant Phenotype in Pancreatic Cancer. *Anticancer Res.* 36 (8), 3945–3952.

Yamasaki-Miyamoto, Y., Yamasaki, M., Tachibana, H., and Yamada, K. (2009). Fucoidan Induces Apoptosis through Activation of Caspase-8 on Human Breast Cancer MCF-7 Cells. *J. Agric. Food Chem.* 57 (18), 8677–8682. doi:10.1021/jf9010406

Yang, L., Wang, P., Wang, H., Li, Q., Teng, H., Liu, Z., et al. (2013). Fucoidan Derived from Undaria Pinnatifida Induces Apoptosis in Human Hepatocellular Carcinoma SMMC-7721 Cells via the ROS-Mediated Mitochondrial Pathway. *Mar. Drugs* 11 (6), 1961–1976. doi:10.3390/md11061961

Yu, Y., Zhang, Y., Hu, C., Zou, X., Lin, Y., Xia, Y., et al. (2019). Chemistry and Immunostimulatory Activity of a Polysaccharide from Undaria Pinnatifida. *Food Chem. Toxicol.* 128, 119–128. doi:10.1016/j.fct.2019.03.042

Zhao, Y., Zheng, Y., Wang, J., Ma, S., Yu, Y., White, W., et al. (2018). Fucoidan Extracted from Undaria Pinnatifida: Source for Nutraceuticals/Functional Foods. *Mar. Drugs* 16 (9), 321. doi:10.3390/md16090321

Zhou, A. Y., Robertson, J., Hamid, N., Ma, Q., and Lu, J. (2015). Changes in Total Nitrogen and Amino Acid Composition of New Zealand Undaria Pinnatifida with Growth, Location and Plant Parts. *Food Chem.* 186, 319–325. doi:10.1016/j.foodchem.2014.06.016

Zong, A., Cao, H., and Wang, F. (2012). Anticancer Polysaccharides from Natural Resources: a Review of Recent Research. *Carbohydr. Polym.* 90 (4), 1395–1410. doi:10.1016/j.carbpol.2012.07.026

Zong, A., Liu, Y., Zhang, Y., Song, X., Shi, Y., Cao, H., et al. (2015). Anti-tumor Activity and the Mechanism of SIP-S: A Sulfated Polysaccharide with Anti-metastatic Effect. *Carbohydr. Polym.* 129, 50–54. doi:10.1016/j.carbpol.2015.04.017

Conflict of Interest: The authors declare that the research was conducted in the absence of any commercial or financial relationships that could be construed as a potential conflict of interest.

Publisher's Note: All claims expressed in this article are solely those of the authors and do not necessarily represent those of their affiliated organizations, or those of the publisher, the editors, and the reviewers. Any product that may be evaluated in this article, or claim that may be made by its manufacturer, is not guaranteed or endorsed by the publisher.

Copyright © 2021 Yang, Zhang, Xu, Chen and Qiu. This is an open-access article distributed under the terms of the Creative Commons Attribution License (CC BY). The use, distribution or reproduction in other forums is permitted, provided the original author(s) and the copyright owner(s) are credited and that the original publication in this journal is cited, in accordance with accepted academic practice. No use, distribution or reproduction is permitted which does not comply with these terms.

frontiers in Bioengineering and Biotechnology

ORIGINAL RESEARCH
published: 18 February 2022
doi: 10.3389/fbioe.2022.836468

pH-Sensitive and Charge-Reversal Polymeric Nanoplatform Enhanced Photothermal/Photodynamic Synergistic Therapy for Breast Cancer

Wenyan Wang[1†], Zimu Li[1†], Xiaozhong Nie[2†], Wenfeng Zeng[1], Yi Zhang[1], Yimin Deng[1], Hongzhong Chen[1], Xiaowei Zeng[1], Hualin Ma[3], Yi Zheng[4]* and Nansha Gao[1]**

[1]Institute of Pharmaceutics, School of Pharmaceutical Sciences (Shenzhen), Sun Yat-sen University, Shenzhen, China, [2]School of Food and Drug, Shenzhen Polytechnic, Shenzhen, China, [3]Shenzhen Key Laboratory of Kindey Diseases, Department of Nephrology, Shenzhen People's Hospital (The Second Clinical Medical College, Jinan University, The First Affiliated Hospital, Southern University of Science and Technology), Shenzhen, China, [4]Central Laboratory, University of Chinese Academy of Sciences-Shenzhen Hospital, Shenzhen, China

OPEN ACCESS

Edited by:
Wenliang Li,
Jilin Medical University, China

Reviewed by:
Yuce Li,
Sungkyunkwan University, South Korea
Dongfang Zhou,
Southern Medical University, China

***Correspondence:**
Hualin Ma
mahualin0796@sina.com
Yi Zheng
zhengyi1205@126.com
Nansha Gao
gaonsh@mail.sysu.edu.cn

[†]These authors have contributed equally to this work

Specialty section:
This article was submitted to Biomaterials, a section of the journal Frontiers in Bioengineering and Biotechnology

Received: 15 December 2021
Accepted: 18 January 2022
Published: 18 February 2022

Citation:
Wang W, Li Z, Nie X, Zeng W, Zhang Y, Deng Y, Chen H, Zeng X, Ma H, Zheng Y and Gao N (2022) pH-Sensitive and Charge-Reversal Polymeric Nanoplatform Enhanced Photothermal/Photodynamic Synergistic Therapy for Breast Cancer. Front. Bioeng. Biotechnol. 10:836468. doi: 10.3389/fbioe.2022.836468

As reported, breast cancer is one of the most common malignancies in women and has overtaken lung cancer as the most commonly diagnosed cancer worldwide by 2020. Currently, phototherapy is a promising anti-tumor therapy due to its fewer side effects, less invasiveness, and lower cost. However, its application in cancer therapeutics is limited by the incomplete therapeutic effect caused by low drug penetration and monotherapy. Herein, we built a charge-reversal nanoplatform (Ce6-PLGA@PDA-PAH-DMMA NPs), including polydopamine (PDA) and chlorin e6 (Ce6) for enhancing photothermal/photodynamic synergistic therapy. The PAH-DMMA charge-reversal layer enabled Ce6-PLGA@PDA-PAH-DMMA NPs to have long blood circulation at the normal physiological environment and to successfully realize charge reversal under the weakly acidic tumor microenvironment, improving cellular uptake. Besides, *in vitro* tests demonstrated that Ce6-PLGA@PDA-PAH-DMMA NPs had high photothermal conversion and greater anti-tumor activity than no charge-reversal nanoparticles, which overcame the limited tumor therapeutic efficacy of PTT or photodynamic therapy alone. Overall, the design of pH-responsive and charge-reversal nanoparticles (Ce6-PLGA@PDA-PAH-DMMA NPs) provided a promising approach for synergistic PTT/PDT therapy against breast cancer.

Keywords: cancer nanotechnology, charge-reversal, photodynamic therapy, photothermal therapy, pH-sensitive

INTRODUCTION

According to World Health Organization (WHO) statistics, almost 19.3 million cancer patients have been diagnosed, and close to 10.0 million deaths have occurred in 2020 worldwide (Ferlay et al., 2021; Sung et al., 2021). Every fifth people in the world have cancer in their lifetime, reflecting that cancer is one of the most critical public health issues. Based on the population growth and aging, the global burden of cancer incidence and mortality increases rapidly (Gersten and Wilmoth, 2002; Omran, 2005). Amazingly, breast cancer in women has become the most frequently diagnosed cancer, exceeding lung cancer (Printz, 2021).

Nowadays, conventional clinical cancer therapies for breast cancer, such as surgery, chemotherapy, and radiotherapy, have high toxicity and aggressiveness, low selectivity, and low efficacy (Dolmans et al., 2003; Bonavida and Chouaib, 2017; Cai et al., 2019). In recent years, some new approaches, including gene therapy, immunotherapy, and phototherapy, have been developed to improve breast cancer treatment (Wang et al., 2021). Phototherapy consisting of photodynamic therapy (PDT) and photothermal therapy (PTT) is a promising option for anti-breast cancer therapy because of its apparent advantages, such as fewer side effects, less invasiveness, high curative rate, and lower cost (Zeng et al., 2020; Zou et al., 2021). In PDT, the photosensitizer could transfer energy to oxygen to generate reactive oxygen species (ROS) after irradiating specific light wavelengths, killing neighboring cancer cells (Dolmans et al., 2003; Lucky et al., 2015). PTT can efficiently damage the tumor tissues by transforming near-infrared NIR light energy into heat (Zhang et al., 2020). However, monotherapy of PTT or PDT is limited by incomplete anti-tumor treatment caused by insufficient light penetration, heat resistance, or hypoxia (Jaque et al., 2014; Wang W. et al., 2020). Moreover, low drug penetration of the tumor tissue and low drug uptake of cancer cells weaken the therapeutic efficacy of monotherapy (Yang et al., 2020; Cao et al., 2021). Studies have found that the combination of PDT and PTT had a synergistic effect (Sun et al., 2021; Zhang et al., 2021). Under heat generated by the low-energy laser, the photothermal agent could not only improve the permeability of the cell membrane and increase the cellular uptake of the photosensitizer (Shi et al., 2013), but also increase the blood flow of the tumor tissue and relieve the hypoxia (Song et al., 2015).

It has been reported that nanoplatform-based phototherapy received considerable attention for breast cancer treatment (Dang and Guan, 2020; Shi et al., 2020; Huang et al., 2021; Yang et al., 2021). Nanoparticles (NPs) loading the photosensitizer and the photothermal agent could efficiently deliver to the tumor tissue *via* enhanced permeability and retention (EPR) effect (Zeng et al., 2020). Besides, NPs with positive surface charges were easier to be taken up by cancer cells with negative charge due to the charge interaction, while negatively charged NPs could effectively reduce the immune clearance, increasing circulation time (Liu et al., 2019). Thus, NPs with the charge-reversal layer could promote cellular uptake and reduce the side effects (Gao et al., 2019). In this study, we engineered the pH-responsive and charge-reversed NPs (Ce6-PLGA@PDA-PAH-DMMA NPs) to achieve synergistic PTT/PDT therapy against breast cancer.

As we all know, poly-lactic-co-glycolic acid (PLGA) has been widely applied in biomedical applications based on its excellent biocompatibility and biodegradability (Thamake et al., 2012; Peng et al., 2018). Meanwhile, PLGA has a good loading content and can satisfy the requirement of drug delivery (Park et al., 2012; Zeng et al., 2013). In this design, chlorin e6 (Ce6) was loaded into PLGA. Polydopamine (PDA), an excellent photothermal agent with good biocompatibility (Zeng et al., 2018; Li et al., 2021a; Li et al., 2021b; Hou et al., 2021), was applied to decorate Ce6-PLGA NPs. Then, positively charged poly-(allyamine) (PAH) produced by amino groups was connected to Ce6-PLGA@PDA NPs. Finally, the negatively charged polymer dimethyl-maleic acid (DMMA) was attached to shield the positive charge of PAH, assembling the PAH-DMMA charge-reversal layer (Feng et al., 2016; Xu et al., 2017). The amide bond of DMMA would break and expose positively charged amino groups under the weakly acidic tumor microenvironment (Li et al., 2021c), resulting in the surface charge reversal of Ce6-PLGA@PDA-PAH-DMMA NPs from negative to positive, facilitating cellular endocytosis and accumulating at the tumor tissue. Subsequently, after irradiating with the 808-nm and 660-nm lasers, the NPs produced a large amount of heat and toxic ROS, damaging the tumor tissue (Cui et al., 2019; Wang Y. et al., 2020) (**Figure 1**) In conclusion, the NPs (Ce6-PLGA@PDA-PAH-DMMA NPs) we developed offer a promising approach for efficient cancer synergistic PTT/PDT and have extensive clinical application prospects.

METHODS

Synthesis of Ce6-PLGA@PDA NPs

First, Ce6 (5 mg) and PLGA copolymers (200 mg) were dissolved in acetone (16 ml) and added into TPGS aqueous solution (200 ml, 0.03%). The solution was stirred overnight in the dark. The final reactant was centrifuged (20,000 rpm, 20 min) to obtain Ce6-PLGA NPs. Afterward, dopamine (15 mg) was dispersed in 150 ml of Tris-HCl buffer and stirred in darkness (12 h). Ce6-PLGA@PDA NPs were gained by centrifugation. Synthesis of Ce6-PLGA@PDA-PAH-DMMA NPs.

Briefly, Ce6-PLGA@PDA NPs and PAH were added in Tris-HCl buffer and stirred overnight. The PLGA@PDA-PAH NPs were obtained by centrifuging (20,000 rpm, 20 min) and washing twice. Subsequently, Ce6-PLGA@PDA-PAH NPs were dispersed in DMSO (5 ml) and then DMMA (30 mg) and triethylamine (130 μl) were added to stir for 24 h. Finally, Ce6-PLGA@PDA-PAH-DMMA NPs were obtained by centrifugation. The Ce6-PLGA@PDA-PEG NPs were prepared by replacing PAH with PEG-NH_2.

Characterization of NPs

The morphology was determined by a transmission electron microscope (TEM, JEOL Ltd., Japan). Fourier transform infrared (FTIR) absorption spectrometry was used to observe the chemical bond connection after modification. X-ray photoelectron spectroscopy (XPS; ESCALAB 250Xi, Japan) was applied to analyze the surface chemistry. A UV-vis spectroscopy (LAMBDA365) was employed to evaluate the loading of Ce6. The 808-nm laser (BOHR-the 808-FCIR8) was used for photothermal therapy. An IR thermal imaging camera was used to record the temperature changes. The production of ROS by the cells and the NPs cellular uptake efficiency were detected by confocal laser scanning microscopy (CLSM). The cell viability was analyzed by a Spectra M2 plate reader (SpectraMax®i3x). An IR thermal camera (Fluke Ti480) was used to examine *in vitro* photothermal performance.

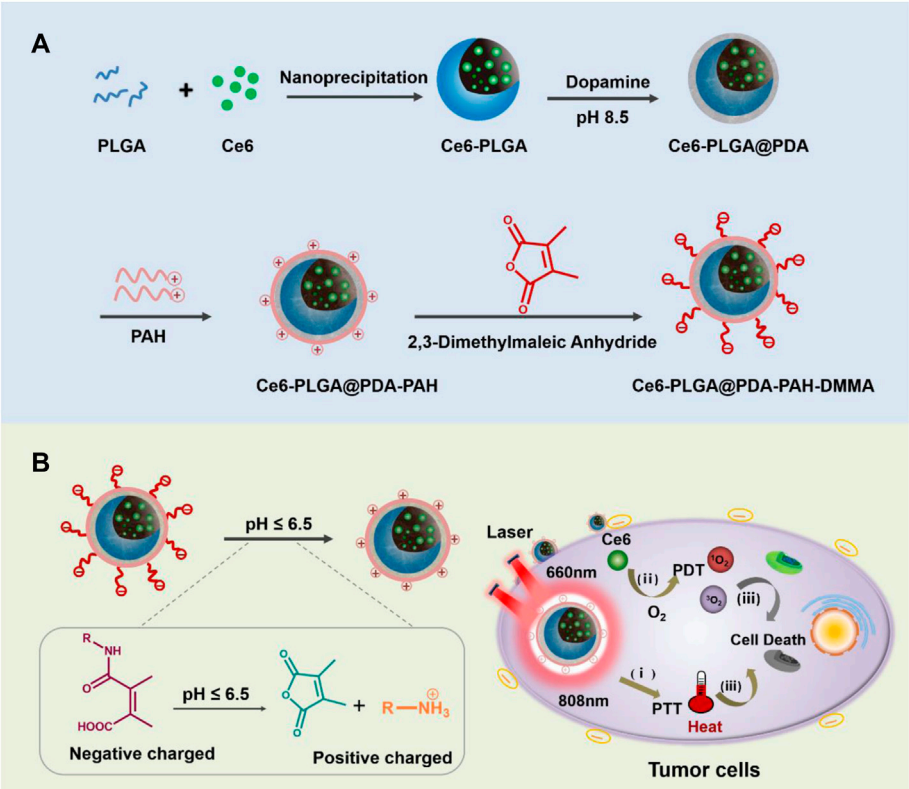

FIGURE 1 | (A) Schematic diagram of the preparation progress of Ce6-PLGA@PDA-PAH-DMMA NPs. **(B)** Ce6-PLGA@PDA-PAH-DMMA NPs applied to PTT/PDT synergistic breast cancer therapy.

In Vitro Photothermal Property

For analyzing the photothermal property of different NPs, various solutions (PBS, Ce6-PLGA NPs, Ce6-PLGA@PDA NPs, Ce6-PLGA@PDA-PAH NPs, and Ce6-PLGA@PDA-PAH-DMMA NPs) were irradiated for 10 min *via* the 808-nm laser. To test the concentration effect of the NPs, different concentrations of Ce6-PLGA@PDA-PAH-DMMA NPs (0.25, 2.5, 12.5, 25, and 50 μg/ml) were irradiated for 10 min (808 nm, 1.5 W/cm^2). The Ce6-PLGA@PDA-PAH-DMMA NPs solution (25 μg/ml) was irradiated for 10 min under various power densities. Finally, to observe the photothermal stability of the Ce6-PLGA@PDA-PAH-DMMA NPs solution (25 μg/ml), the solution was irradiated for 10 min in five times laser on/off cycles (1.5 W/cm^2).

Cellular Uptake Experiments

MCF-7 cells were cultured in confocal dishes for 12 h in an incubator (37°C, 5% CO_2). Then, medium, including various Ce6 preparations labeled with Cy5 (Ce6 = 2 μg/ml), was added. After co-incubation for 2 h, the cells were fixed with 4% paraformaldehyde and dyed with DAPI. The results were analyzed by CLSM (DAPI and Cy5 fluorescent channels). Moreover, MCF-7 cells were seeded in plates in an incubator (37°C, 5% CO_2) for 24 h. Then, the medium including Ce6-PLGA@PDA-PAH-DMMA-Cy5 NPs and Ce6@PDA-PEG-Cy5 NPs was added, followed by incubating for 2 h. Finally, the MCF-7 cells were collected for flow cytometer analysis.

In Vitro Cytotoxicity Assay

Dark Toxicity

First, 4T1 or MCF-7 cells (5×10^3 per well) were cultured for 12 h in an incubator (37°C, 5% CO_2) until complete adhesion. Then, the medium containing different concentrations of Ce6-PLGA@PDA-PAH-DMMA NPs (7.8, 15.6, 31.3, 63.5, 125, and 250 μg/ml) at pH 7.4 was added.

The Photo-Cytotoxicity

The cells (5 × 10^3 per well) were cultured for 12 h in an incubator (37°C, 5% CO_2) until complete adhesion. Then, some medium, containing free Ce6, Ce6-PLGA@PDA-PEG NPs, Ce6-PLGA@PDA-PEG NPs, and Ce6-PLGA@PDA-PAH-DMMA NPs, was added separately, each group with concentrations of Ce6 (1, 2, and 4 μg/ml). After incubation for 6 h, the cells were treated with the 660-nm laser (200 mV/cm^2, 5 min) and cultured for another 24 h.

Combination Therapy

For the combined therapy experiment, cells (5 × 10^3 per well) were cultured for 12 h. Then, some medium containing PBS, Ce6-PLGA@PDA-PEG NPs, and Ce6-PLGA@PDA-PAH-DMMA NPs (Ce6 = 2 μg/ml) was added, with or without

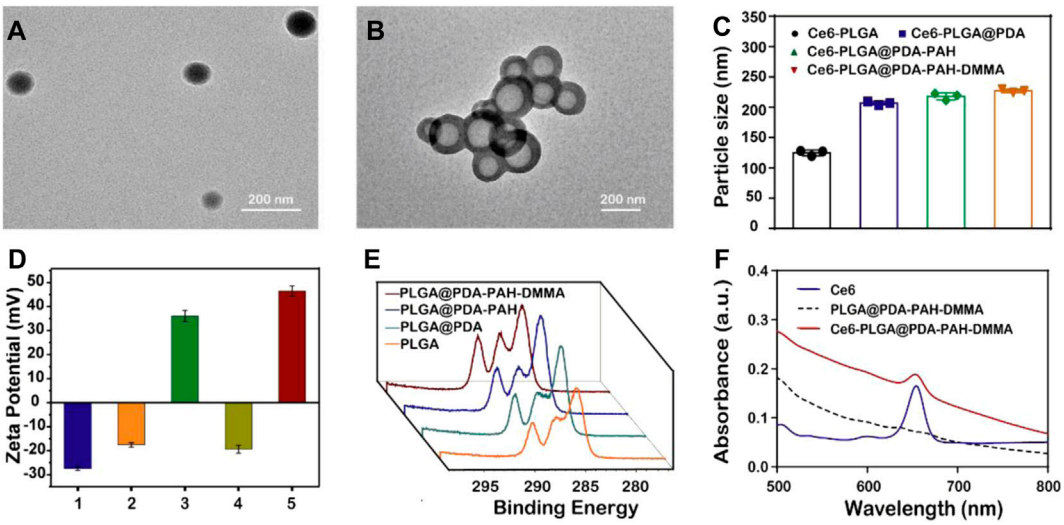

FIGURE 2 | Characterization of the synthesized NPs. TEM images of **(A)** Ce6-PLGA NPs; **(B)** Ce6-PLGA@PDA-PAH-DMMA NPs. **(C)** Particle size of synthesized NPs. **(D)** Surface zeta potentials of different NPs (1, 2, 3, 4, and 5 present Ce6-PLGA NPs, Ce6-PLGA@PDA NPs, Ce6-PLGA@PDA-PAH NPs, Ce6-PLGA@PDA-PAH-DMMA NPs-pH 7.4, and Ce6-PLGA@PDA-PAH-DMMA NPs-pH 5.5). **(E)** XPS spectra of PLGA NPs, PLGA@PDA NPs, PLGA@PDA-PAH NPs, and PLGA@PDA-PAH-DMMA NPs. **(F)** UV-vis spectra of Ce6, PLGA@PDA-PAH-DMMA NPs, and Ce6-PLGA@PDA-PAH-DMMA NPs.

irradiation by laser. After being co-cultured for 6 h, the drug-containing medium was removed. Then, the related groups were treated with the 660-nm laser (200 mV/cm^2, 5 min) or the 808-nm laser (1.5 W/cm^2, 10 min), or both, and cultured for another 24 h.

In Vitro $^1O_2$ Generation

MCF-7 cells were seeded in confocal dishes for 12 h until complete adhesion (37°C, 5% CO_2). Then, cells were treated with medium including Ce6-PLGA@PDA-PAH-DMMA NPs and Ce6@PDA-PEG NPs (Ce6 = 2 μg/ml), followed by incubating for 6 h. Next, the cells were co-cultured with DCFH-DA for 30 min and irradiated with the 660-nm laser (200 mV/cm^2, 5 min). After that, MCF-7 cells after treatment were observed with CLSM.

RESULTS AND DISCUSSION

Preparation of Ce6-PLGA@PDA-PAH-DMMA NPs

The preparation of Ce6-PLGA@PDA-PAH-DMMA NPs was illustrated in **Figure 1A**, which included three steps. Briefly, Ce6, a photosensitizer with poor solubility, was loaded into PLGA by nanoprecipitation (Ce6-PLGA NPs). Secondly, Ce6-PLGA NPs were coated with PDA through an oxidative polymerization reaction in an alkaline environment (Ce6-PLGA@PDA NPs), which endowed Ce6-PLGA@PDA NPs with photothermal performance and groups (amino and carboxyl groups) for further modification. Finally, Ce6-PLGA@PDA NPs were modified with PAH-DMMA charge-reversal layer through the Michael addition reaction and electrostatic interaction.

Characterization of NPs

The morphology of Ce6-PLGA NPs and Ce6-PLGA@PDA-PAH-DMMA NPs was observed by transmission electron microscopy (TEM). **Figures 2A,B** show that Ce6-PLGA NPs were spherical at approximately 125 nm, but after modification, the surface of Ce6-PLGA NPs had significant coatings resulting in increased particle size of Ce6-PLGA@PDA-PAH-DMMA NPs (about 225 nm). Similarly, the increased size was also verified in the results of dynamic light scattering (**Figure 2C**, **Supplementary Table S1**). As we can see from the surface zeta potential results (**Figure 2D**), both Ce6-PLGA NPs and Ce6-PLGA@PDA NPs appeared as negative charges, but Ce6-PLGA@PDA-PAH NPs showed a positive potential (36.0 ± 2.3 mv) because of the cationic layer PAH. After being modified by 2,3-dimethylmaleic anhydride, the zeta potential of Ce6-PLGA@PDA-PAH-DMMA NPs became negative, increasing the circulation of the NPs. As reported, the negatively charged polymer PAH-DMMA could be hydrolyzed and become a positively charged polymer under a weakly acidic environment. To prove it, we analyzed the zeta potential of Ce6-PLGA@PDA-PAH-DMMA NPs at different pH. We found that Ce6-PLGA@PDA-PAH-DMMA NPs had a negative charge under normal physiological conditions (pH 7.4), while it had apparent charge-reversal capability from negative potential to positive potential under a mildly acidic environment. This phenomenon indicated that this nanoparticle could potentially flip into a positive charge under the weakly acidic tumor microenvironment, which may help the penetration of Ce6-PLGA@PDA-PAH-DMMA NPs in the tumor tissue.

In addition, we verified the successful loading of PDA and the charged layer on the surface of PLGA NPs by FT-IR and XPS analysis. After modifying PDA, a prominent absorption peak between 1,600 cm^{-1} and 1,530 cm^{-1} was observed, which was assigned to the overlap of the C=C resonance vibrations and the

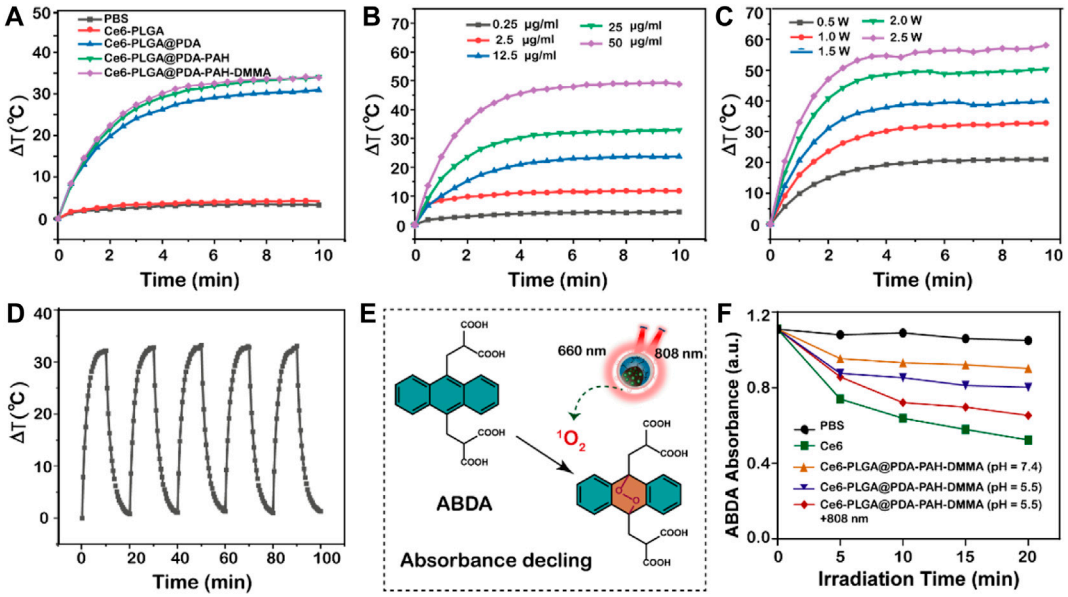

FIGURE 3 | Photothermal properties. **(A)** Heating curves of different NPs after irradiating by the 808-nm laser. **(B)** Photothermal heating curves of different concentrations of Ce6-PLGA@PDA-PAH-DMMA NPs irradiated by the 808-nm laser (1.5 W/cm^2, 10 min). **(C)** Temperature changes of Ce6-PLGA@PDA-PAH-DMMA NPs exposed to the 808-nm laser in different power densities. **(D)** Heating/cooling curves for 10 min-on–10 min-off laser irradiations (808 nm, 1.5 W/cm^2, 5 times). **(E)** Detection mechanism of ABDA for $^1O_2$. **(F)** Absorption spectra of ABDA for $^1O_2$ generation in different formulations treated in different ways.

N–H bending vibrations, suggesting that the PDA layer successfully adhered to the surface of PLGA NPs (**Supplementary Figure S2A**). Furthermore, the results of the XPS analysis also verified it. Bands of the C–C group (~284 eV) and C–O group (~286 eV) intensities of PLGA@PDA NPs, PLGA@PDA-PAH NPs, and PLGA@PDA-PAH-DMMA NPs showed an increasing trend, which is attributed to the PDA layers and the successful connection of PAH and DMMA (**Figure 2E**). As for the N1s spectrum (**Supplementary Figure S2B**), the NPs appeared to significantly increase the band intensity at 400 eV. These results confirmed the successful synthesis of PLGA@PDA-PAH-DMMA NPs. The photosensitizer Ce6 had a characteristic ultraviolet absorption peak at 654 nm. Based on it, we measured the UV characteristic peak of NPs to confirm the success of Ce6-loaded. Compared to pure PLGA@PDA-PAH-DMMA NPs, Ce6-PLGA@PDA-PAH-DMMA NPs had an apparent absorption band at approximately 654 nm, indicating that Ce6 was successfully encapsulated into PLGA@PDA-PAH-DMMA NPs (**Figure 2F**). To test the encapsulation efficiency and loading content, we measured the free Ce6 in the supernatant after loading the drug by UV-vis absorption spectra. Results showed that the encapsulation efficiency (EE) and loading content of Ce6 were approximately 78% and 4.2%, respectively (**Supplementary Figure S3**).

Photothermal Performance

As reported, PDA had an excellent photothermal effect and could be used for photothermal therapy. To investigate the photothermal performance of NPs, we recorded the temperature of NPs under the 808-nm laser irradiation *in vitro*. We observed that the temperatures of the NPs with the PDA layer all increased rapidly by approximately 30°C in 10 min under NIR irradiation (1.5 W/cm^2), performing excellent light and heat heating effect, while others did not (**Figure 3A**). Moreover, the temperature rise of Ce6-PLGA@PDA-PAH-DMMA NPs depended on nanoparticle concentration and irradiation intensity (**Figures 3B,C**), suggesting that we could adjust the concentration of the NPs and the irradiation intensity to meet actual application needs. Furthermore, the photothermal stability of the photothermal agent was crucial for the application of photothermal therapy. Thus, we irradiated Ce6-PLGA@PDA-PAH-DMMA NPs solution in five on/off cycles through NIR laser (2 W/cm^2), finding no significant difference in temperature changes (**Figure 3D**). In summary, Ce6-PLGA@PDA-PAH-DMMA NPs had superior light-to-heat conversion performance and great light-to-heat stability.

In Vitro ROS Generation

Limited by the content of Ce6 and instrument sensitivity, we indirectly reflected the release of Ce6 by measuring the ability of drug release solutions of each group to generate ROS under the 660-nm laser irradiation. To explore the ability of NPs to generate ROS (such as $^1O_2$) *in vitro*, we used ABDA as a singlet oxygen ($^1O_2$) indicator for determining. ABDA could react with single oxygen to generate corresponding endoperoxides, causing a drop in UV absorption at 400 nm (**Figure 3E**). Results showed that the ABDA fluorescence intensity of Ce6-PLGA@PDA-PAH-DMMA NPs (pH 5.5 + 808 nm) declined to 65.38%, which was slightly lower than 52.3% of Ce6 and higher than other groups after irradiating with the 660-nm laser (**Figure 3F**). Therefore, we anticipated that Ce6-PLGA@PDA-PAH-DMMA NPs increased

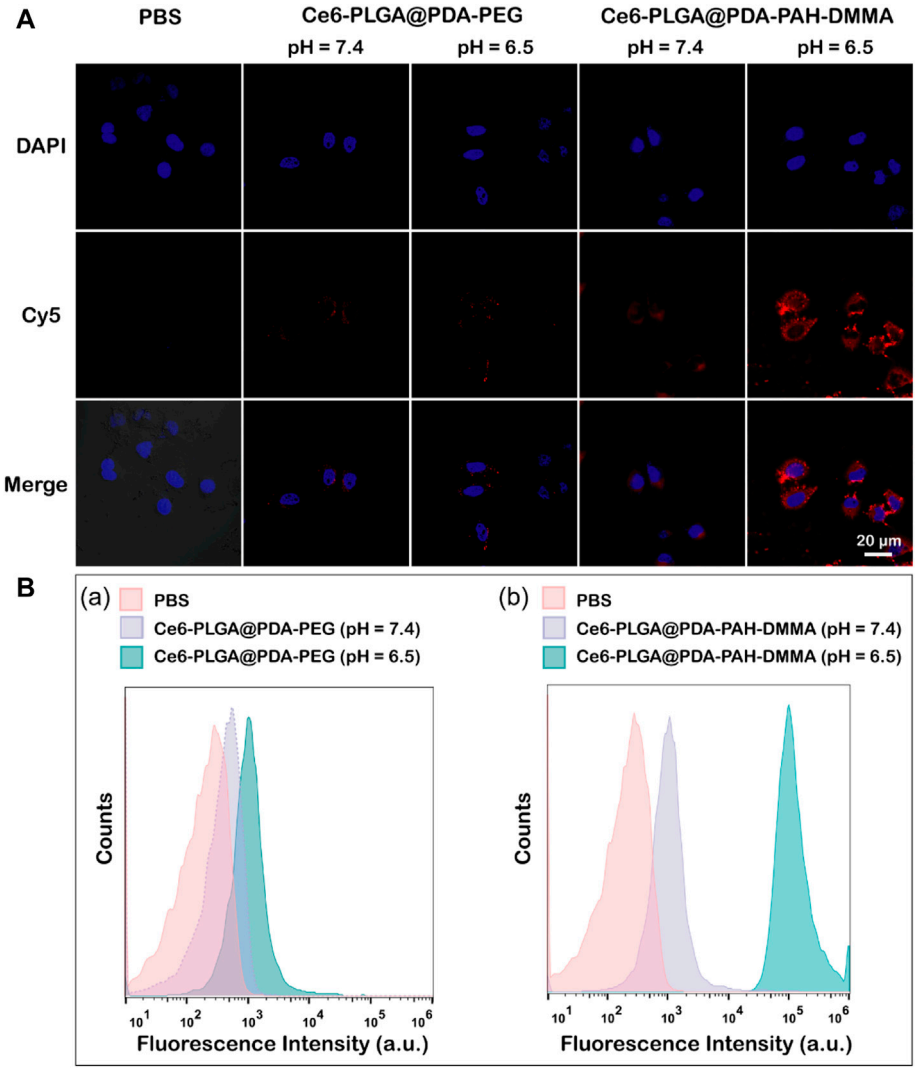

FIGURE 4 | (A) Confocal images of MCF-7 cells cultured separately with the NPs at pH 7.4 and 6.5 for 2 h at 37°C (Blue: DAPI; Red: Cy5 fluorescence). **(B)** Flow cytometric analysis of MCF-7 cells after treating with Ce6-PLGA@PDA-PEG NPs **(A)** and Ce6-PLGA@PDA-PAH-DMMA NPs **(B)** at pH 7.4 and 6.5.

the release of Ce6 at pH 5.5 and irradiated with the 808-nm laser, and could effectively produce toxic.

In Vitro Cellular Uptake

Owing to a weakly acidic environment, the surface charge of Ce6-PLGA@PDA-PAH-DMMA NPs would flip into the positive charge, which could interact with the negatively charged cell membrane of cancer cells, promoting cellular uptake. Thus, we evaluated its internalization by MCF-7 cells at pH 6.5 and pH 7.4 for 2 h. The Cy5 was used to label the Ce6-PLGA@PDA-PEG NPs and Ce6-PLGA@PDA-PAH-DMMA NPs. As revealed by confocal images, after 2 h co-incubation with MCF-7 cells, the group of Ce6-PLGA@PDA-PAH-DMMA NPs (pH = 6.5) had a strong red fluorescence signal distributed in the cytoplasm, which was much higher than it was at pH 7.4 and the groups of Ce6-PLGA@PDA-PEG NPs. This phenomenon demonstrated that Ce6-PLGA@PDA-PAH-DMMA NPs could promote the uptake of cancer cells under a weakly acidic environment (**Figure 4A**). At the same time, cell flow cytometry was also used to certify the internalization of Ce6-PLGA@PDA-PAH-DMMA NPs by MCF-7 cells and similar results were found. As shown in **Figure 4B**, we discovered that, after culturing with Ce6-PLGA@PDA-PAH-DMMA NPs for 2 h, the mean fluorescence intensity of MCF-7 cells at pH 6.5 is four times more than that at pH 7.4. In contrast, it was very weak when co-incubation with Ce6-PLGA@PDA-PEG NPs at pH 6.5 or pH 7.4.

In Vitro Cellular Cytotoxicity

To evaluate the ability of Ce6-PLGA@PDA-PAH-DMMA NPs to inhibit MCF-7 cells and 4T1 cells, a cell counting kit (cck8) was used. As we can see from **Figure 5A**, the survival rate of MCF-7 and 4T1 cells were all over 85% after co-cultivation with different concentrations of Ce6-PLGA@PDA-PAH-DMMA NPs for 24 h, indicating it had excellent biocompatibility in no near-infrared

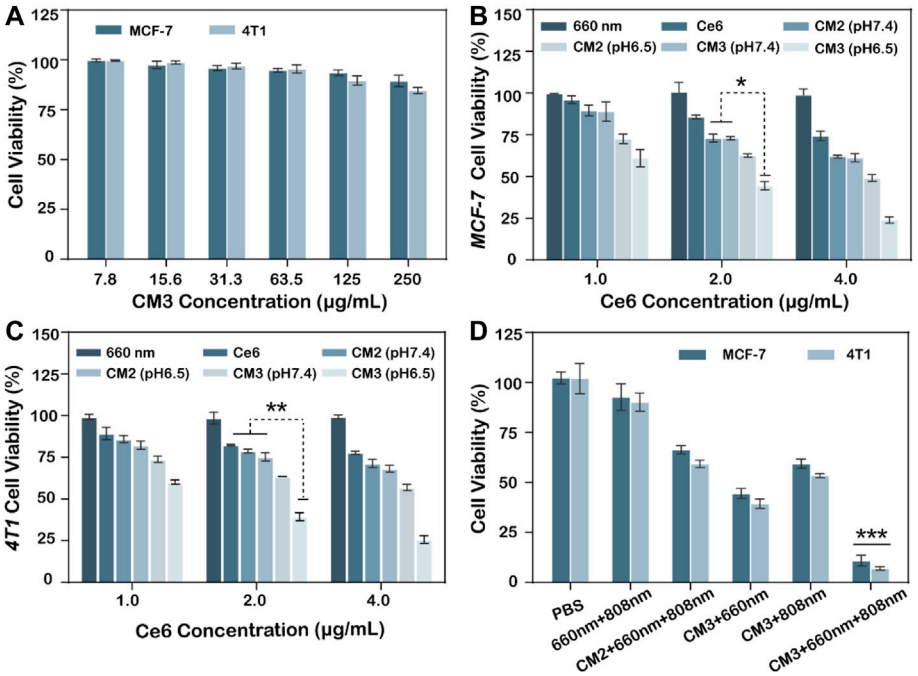

FIGURE 5 | (A) Viability of MCF-7, 4T1 cells after treating with different concentrations of Ce6-PLGA@PDA-PAH-DMMA (CM3) without lasers. Viability of MCF-7 cells **(B)** and 4T1 cells **(C)** after incubation with Ce6-PLGA@PDA-PEG NPs (CM2) and Ce6-PLGA@PDA-PAH-DMMA NPs (CM3) at concentrations of Ce6 (1.0 μg/ml, 2.0 μg/ml, and 4.0 μg/ml) under the 660-nm laser irradiation (200 mW/cm^2, 5 min) at pH 6.5. **(D)** Viability of cancer cells after PTT or PDT alone and PTT/PDT treatments (*t*-test, $^*p < 0.05$, $^{**}p < 0.01$, $^{***}p < 0.001$ and $n = 3$); Q value method: Q = V (a + b)/(Va + Vb—Va* Vb). V (a + b) is the inhibition rate of combined A and B drug, Va and Vb are the A and B drugs alone (Q < 0.85 is antagonism, 0.85 ≤ Q < 1.15 is additive, and Q ≥ 1.15 is synergy).

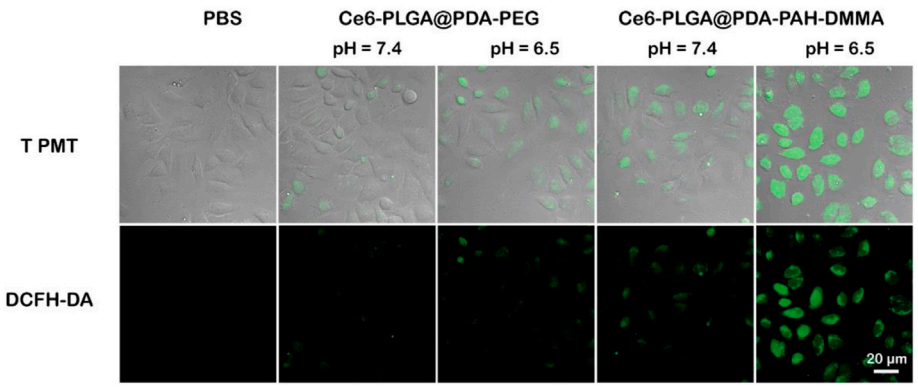

FIGURE 6 | Confocal images of ROS generation by cells treated with PBS (control), Ce6-PLGA@PDA-PEG NPs, and Ce6-PLGA@PDA-PAH-DMMA NPs.

radiation. On the contrary, Ce6-PLGA@PDA-PAH-DMMA NPs containing different concentrations of Ce6 inhibited the growth of the cells under the 660-nm laser irradiation (**Figures 5B,C**). Furthermore, after irradiation with the 660-nm laser (200 mW/cm^2, 5 min), Ce6-PLGA@PDA-PAH-DMMA NPs had a better-killing effect on cancer cells at pH 6.5 than that at pH 7.4. Reasons for this result may be more cell uptake promoted by charge flipping and faster drug release caused by the decomposition of PDA in a weakly acidic environment. Subsequently, to explore the effect of the combined PTT/PDT therapy, we selected Ce6-PLGA@PDA-PEG NPs or Ce6-PLGA@PDA-PAH-DMMA NPs with a Ce6 content of 2 ug/ml as therapeutic agents. As shown in **Figure 5D**, a significantly reduced cell survival rate (MCF-7: 59.43%; 4T1: 53.46%) was observed when the cancer cells were treated with Ce6-PLGA@PDA-PAH-DMMA NPs at pH 6.5 under the 808-nm laser irradiation, which was attributed to the photothermal ability of PDA. As expected, we found that the combination therapy (Ce6-PLGA@PDA-PAH-DMMA NPs + 660 nm + 808 nm) showed the lowest viability of MCF-7 (10.9%) and 4T1 cells (7.05%), compared with other groups.

The above results indicated that, under weakly acidic conditions, the ability to inhibit cancer cell growth of synergistic PTT/PDT therapy was stronger than PTT or PDT alone. Furthermore, according to the Q value method: Q = V (a + b)/(Va + Vb—Va* Vb), we obtain the following results: Q_{MCF-7} = 1.212; Q_{4T1} = 1.178. Both of them are greater than 1.15, proving that PDT and PTT are working synergistically.

In Vitro $^1O_2$ Generation

To further verify the ability of Ce6-PLGA@PDA-PAH-DMMA NPs to generate ROS during intracellular PDT, the DCFH-DA kit, a molecule that could enter cells and react with $^1O_2$ to emit fluorescence, was used to detect the intracellular $^1O_2$ level. The results were observed by confocal images of MCF cells incubated with different NPs at different pH values (pH 6.5 and pH 7.4) and treated with DCFH-DA for 30 min before irradiating with the 660-nm laser. As shown in **Figure 6**, compared with other groups, the strongest intracellular fluorescence was discovered when treated with Ce6-PLGA@PDA-PAH-DMMA NPs at pH 6.5, illustrating that most $^1O_2$ were generated. The cells incubated with Ce6-PLGA@PDA-PEG NPs at pH 6.5 and pH 7.4 or Ce6-PLGA@PDA-PAH-DMMA NPs at pH 7.4 showed weak fluorescence. In conclusion, Ce6-PLGA@PDA-PAH-DMMA NPs could efficiently generate massive toxic $^1O_2$ at pH 6.5, which may be attributed to the mass internalization of Ce6-PLGA@PDA-PAH-DMMA NPs by cells at pH 6.5.

CONCLUSION

In conclusion, we built a pH-responsive and charge-reversal nanoplatform (Ce6-PLGA@PDA-PAH-DMMA NPs) that can enhance breast cancer therapeutic efficiency. Ce6-PLGA@PDA-PAH-DMMA NPs with a charge-reversal layer, which could maintain a negative potential at pH 7.4 and become a positive potential at the tumor extracellular microenvironment (pH 6.5), promoted their enrichment in the tumor and uptake by cancer cells. Subsequently, after irradiation with the 808-nm laser and the 660-nm laser, the photothermal effect of PDA and the ROS produced by Ce6 can synergistically damage breast cancer. *In vitro* experiments manifested that Ce6-PLGA@PDA-PAH-DMMA NPs showed increased uptake by cancer cells and overcame the limited tumor therapeutic efficacy of PTT or PDT alone. Taken together, Ce6-PLGA@PDA-PAH-DMMA NPs offer a promising approach with enhanced therapeutic efficiency for breast cancer treatment.

DATA AVAILABILITY STATEMENT

The original contributions presented in the study are included in the article/**Supplementary Material**, Further inquiries can be directed to the corresponding authors.

AUTHOR CONTRIBUTIONS

NG, HM, and YZ designed the research project; WW, ZL, and XN had full control of the experiments, data analysis, and preparation of article; WZ, YZ, YD, HC, and XZ were involved in planning the analysis and drafting the article. The final draft was approved by all the authors.

ACKNOWLEDGMENTS

We are grateful for the financial support from the Shenzhen Fund for Guangdong Provincial High-level Clinical Key Specialties (No. SZGSP001), the Shenzhen Key Laboratory of Kidney Diseases (No. ZDSYS201504301616234), the Science, Technology and Innovation Commission of Shenzhen Municipality (2021A18 and JCYJ20180301170030277), the Key Project of Guangzhou Municipal Science and Technology Bureau (201903010039), the Natural Science Foundation of Guangdong Province (2020A1515011353), the Science and Technology Innovation Strategic Foundation of Guangdong Province (pdjh 2020b1180), the Shenzhen Educational Science Planning Project (zdfz20019), and the Guangming District Economic Development Special Fund (2020R01072 and 2021R01120).

SUPPLEMENTARY MATERIAL

The Supplementary Material for this article can be found online at: https://www.frontiersin.org/articles/10.3389/fbioe.2022.836468/full#supplementary-material

REFERENCES

Bonavida, B., and Chouaib, S. (2017). Resistance to Anticancer Immunity in Cancer Patients: Potential Strategies to Reverse Resistance. *Ann. Oncol.* 28, 457–467. doi:10.1093/annonc/mdw615

Cai, X., Xie, Z., Ding, B., Shao, S., Liang, S., Pang, M., et al. (2019). Monodispersed Copper(I)-Based Nano Metal-Organic Framework as a Biodegradable Drug Carrier with Enhanced Photodynamic Therapy Efficacy. *Adv. Sci.* 6, 1900848. doi:10.1002/advs.201900848

Cao, S., Shao, J., Wu, H., Song, S., De Martino, M. T., Pijpers, I. A. B., et al. (2021). Photoactivated Nanomotors via Aggregation Induced Emission for Enhanced Phototherapy. *Nat. Commun.* 12. doi:10.1038/s41467-021-22279-w

Cui, T., Yan, Z., Qin, H., Sun, Y., Ren, J., and Qu, X. (2019). A Sequential Target-Responsive Nanocarrier with Enhanced Tumor Penetration and Neighboring Effect *In Vivo*. *Small* 15, 1903323. doi:10.1002/smll.201903323

Dang, Y., and Guan, J. (2020). Nanoparticle-based Drug Delivery Systems for Cancer Therapy. *Smart Mater. Med.* 1, 10–19. doi:10.1016/j.smaim.2020.04.001

Dolmans, D. E. J. G. J., Fukumura, D., and Jain, R. K. (2003). Photodynamic Therapy for Cancer. *Nat. Rev. Cancer* 3, 380–387. doi:10.1038/nrc1071

Feng, T., Ai, X., An, G., Yang, P., and Zhao, Y. (2016). Charge-Convertible Carbon Dots for Imaging-Guided Drug Delivery with Enhanced *In Vivo* Cancer Therapeutic Efficiency. *ACS Nano* 10, 4410–4420. doi:10.1021/acsnano.6b00043

Ferlay, J., Colombet, M., Soerjomataram, I., Parkin, D. M., Piñeros, M., Znaor, A., et al. (2021). Cancer Statistics for the Year 2020: An Overview. *Int. J. Cancer* 149, 778–789. doi:10.1002/ijc.33588

Gao, N., Xing, C., Wang, H., Feng, L., Zeng, X., Mei, L., et al. (2019). pH-Responsive Dual Drug-Loaded Nanocarriers Based on Poly (2-Ethyl-2-Oxazoline) Modified Black Phosphorus Nanosheets for Cancer Chemo/Photothermal Therapy. *Front. Pharmacol.* 10, 270. doi:10.3389/fphar.2019.00270

Gersten, O., and Wilmoth, J. R. (2002). The Cancer Transition in Japan since 1951. *DemRes* 7, 271–306. doi:10.4054/DemRes.2002.7.5

Hou, M., Zhong, Y., Zhang, L., Xu, Z., Kang, Y., and Xue, P. (2021). Polydopamine (PDA)-activated Cobalt Sulfide Nanospheres Responsive to Tumor Microenvironment (TME) for Chemotherapeutic-Enhanced Photothermal Therapy. *Chin. Chem. Lett.* 32, 1055–1060. doi:10.1016/j.cclet.2020.08.009

Huang, P., Lian, D., Ma, H., Gao, N., Zhao, L., Luan, P., et al. (2021). New Advances in Gated Materials of Mesoporous Silica for Drug Controlled Release. *Chin. Chem. Lett.* 6 (3), e1902242. doi:10.1016/j.cclet.2021.06.034

Jaque, D., Martínez Maestro, L., del Rosal, B., Haro-Gonzalez, P., Benayas, A., Plaza, J. L., et al. (2014). Nanoparticles for Photothermal Therapies. *Nanoscale* 6, 9494–9530. doi:10.1039/C4NR00708E

Li, Z., Liu, Q., Zhang, Y., Yang, Y., Zhou, X., Peng, W., et al. (2021a). Charge-reversal Nanomedicine Based on Black Phosphorus for the Development of A Novel Photothermal Therapy of Oral Cancer. *Drug Deliv.* 28, 700–708. doi:10.1080/10717544.2021.1909176

Li, Z., Shan, X., Chen, Z., Gao, N., Zeng, W., Zeng, X., et al. (2021b). Applications of Surface Modification Technologies in Nanomedicine for Deep Tumor Penetration. *Adv. Sci.* 8, 2002589. doi:10.1002/advs.202002589

Li, Z., Yang, Y., Wei, H., Shan, X., Wang, X., Ou, M., et al. (2021c). Charge-reversal Biodegradable MSNs for Tumor Synergetic Chemo/photothermal and Visualized Therapy. *J. controlled release* 338, 719–730. doi:10.1016/j.jconrel.2021.09.005

Liu, Q., Zhao, K., Wang, C., Zhang, Z., Zheng, C., Zhao, Y., et al. (2019). Multistage Delivery Nanoparticle Facilitates Efficient CRISPR/dCas9 Activation and Tumor Growth Suppression *In Vivo*. *Adv. Sci.* 6, 1801423. doi:10.1002/advs.201801423

Lucky, S. S., Soo, K. C., and Zhang, Y. (2015). Nanoparticles in Photodynamic Therapy. *Chem. Rev.* 115, 1990–2042. doi:10.1021/cr5004198

Omran, A. R. (2005). The Epidemiologic Transition: A Theory of the Epidemiology of Population Change. *Milbank Memorial Fund Q.* 49, 509–538. doi:10.1111/j.1468-0009.2005.00398.x

Park, W., Kim, D., KangKang, H. C., Bae, Y. H., and Na, K. (2012). Multi-arm Histidine Copolymer for Controlled Release of Insulin from Poly(lactide-Co-Glycolide) Microsphere. *Biomaterials* 33, 8848–8857. doi:10.1016/j.biomaterials.2012.08.042

Peng, Y., Nie, J., Cheng, W., Liu, G., Zhu, D., Zhang, L., et al. (2018). A Multifunctional Nanoplatform for Cancer Chemo-Photothermal Synergistic Therapy and Overcoming Multidrug Resistance. *Biomater. Sci.* 6, 1084–1098. doi:10.1039/c7bm01206c

Printz, C. (2021). Female Breast Cancer Most Commonly Diagnosed Cancer Globally. *Cancer* 127, 1952–1953. doi:10.1002/cncr.33637

Shi, S., Zhu, X., Zhao, Z., Fang, W., Chen, M., Huang, Y., et al. (2013). Photothermally Enhanced Photodynamic Therapy Based on Mesoporous Pd@Ag@mSiO2 Nanocarriers. *J. Mater. Chem. B* 1, 1133–1141. doi:10.1039/c2tb00376g

Shi, Z., Zhou, Y., Fan, T., Lin, Y., Zhang, H., and Mei, L. (2020). Inorganic Nano-Carriers Based Smart Drug Delivery Systems for Tumor Therapy. *Smart Mater. Med.* 1, 32–47. doi:10.1016/j.smaim.2020.05.002

Song, G., Liang, C., Gong, H., Li, M., Zheng, X., Cheng, L., et al. (2015). Core-Shell MnSe@Bi2Se3Fabricated via a Cation Exchange Method as Novel Nanotheranostics for Multimodal Imaging and Synergistic Thermoradiotherapy. *Adv. Mater.* 27, 6110–6117. doi:10.1002/adma.201503006

Sun, W., Yu, H., Wang, D., Li, Y., Tian, B., Zhu, S., et al. (2021). MnO2 Nanoflowers as a Multifunctional Nano-Platform for Enhanced Photothermal/photodynamic Therapy and MR Imaging. *Biomater. Sci.* 9, 3662–3674. doi:10.1039/d1bm00033k

Sung, H., Ferlay, J., Siegel, R. L., Laversanne, M., Soerjomataram, I., Jemal, A., et al. (2021). Global Cancer Statistics 2020: GLOBOCAN Estimates of Incidence and Mortality Worldwide for 36 Cancers in 185 Countries. *CA A. Cancer J. Clin.* 71, 209–249. doi:10.3322/caac.21660

Thamake, S. I., Raut, S. L., Gryczynski, Z., Ranjan, A. P., and Vishwanatha, J. K. (2012). Alendronate Coated Poly-Lactic-Co-Glycolic Acid (PLGA) Nanoparticles for Active Targeting of Metastatic Breast Cancer. *Biomaterials* 33, 7164–7173. doi:10.1016/j.biomaterials.2012.06.026

Wang, S., Zhang, L., Zhao, J., He, M., Huang, Y., and Zhao, S. (2021). A Tumor Microenvironment-Induced Absorption Red-Shifted Polymer Nanoparticle for Simultaneously Activated Photoacoustic Imaging and Photothermal Therapy. *Sci. Adv.* 7. doi:10.1126/sciadv.abe3588

Wang, W., Tang, Z., Zhang, Y., Wang, Q., Liang, Z., and Zeng, X. (2020a). Mussel-Inspired Polydopamine: The Bridge for Targeting Drug Delivery System and Synergistic Cancer Treatment. *Macromol. Biosci.* 20, 2000222. doi:10.1002/mabi.202000222

Wang, Y., Luo, S., Wu, Y., Tang, P., Liu, J., Liu, Z., et al. (2020b). Highly Penetrable and On-Demand Oxygen Release with Tumor Activity Composite Nanosystem for Photothermal/Photodynamic Synergetic Therapy. *ACS Nano* 14, 17046–17062. doi:10.1021/acsnano.0c06415

Xu, J., Kuang, Y., Lv, R., Yang, P., Li, C., Bi, H., et al. (2017). Charge Convertibility and Near Infrared Photon Co-enhanced Cisplatin Chemotherapy Based on Upconversion Nanoplatform. *Biomaterials* 130, 42–55. doi:10.1016/j.biomaterials.2017.03.041

Yang, R., Zhang, Z., Fu, S., Hou, T., Mu, W., Liang, S., et al. (2020). Charge and Size Dual Switchable Nanocage for Novel Triple-Interlocked Combination Therapy Pattern. *Adv. Sci.* 7, 2000906. doi:10.1002/advs.202000906

Yang, Y., Zeng, W., Huang, P., Zeng, X., and Mei, L. (2021). Smart Materials for Drug Delivery and Cancer Therapy. *View* 2, 20200042. doi:10.1002/VIW.20200042

Zeng, W., Zhang, H., Deng, Y., Jiang, A., Bao, X., Guo, M., et al. (2020). Dual-response Oxygen-Generating MnO2 Nanoparticles with Polydopamine Modification for Combined Photothermal-Photodynamic Therapy. *Chem. Eng. J.* 389, 124494. doi:10.1016/j.cej.2020.124494

Zeng, X., Luo, M., Liu, G., Wang, X., Tao, W., Lin, Y., et al. (2018). Polydopamine-Modified Black Phosphorous Nanocapsule with Enhanced Stability and Photothermal Performance for Tumor Multimodal Treatments. *Adv. Sci.* 5, 1800510. doi:10.1002/advs.201800510

Zeng, X., Tao, W., Mei, L., Huang, L., Tan, C., and Feng, S.-S. (2013). Cholic Acid-Functionalized Nanoparticles of star-shaped PLGA-Vitamin E TPGS Copolymer for Docetaxel Delivery to Cervical Cancer. *Biomaterials* 34, 6058–6067. doi:10.1016/j.biomaterials.2013.04.052

Zhang, F., Lu, G., Wen, X., Li, F., Ji, X., Li, Q., et al. (2020). Magnetic Nanoparticles Coated with Polyphenols for Spatio-Temporally Controlled Cancer Photothermal/immunotherapy. *J. Controlled Release* 326, 131–139. doi:10.1016/j.jconrel.2020.06.015

Zhang, W., Yu, L., Jiang, Y., and Guo, C. (2021). Phycocyanin-functionalized Black Phosphorus Quantum Dots Enhance PDT/PTT Therapy by Inducing ROS and Irreparable DNA Damage. *Biomater. Sci.* 9, 5302–5318. doi:10.1039/d1bm00106j

Zou, Y., Long, S., Xiong, T., Zhao, X., Sun, W., Du, J., et al. (2021). Single-Molecule Förster Resonance Energy Transfer-Based Photosensitizer for Synergistic Photodynamic/Photothermal Therapy. *ACS Cent. Sci.* 7, 327–334. doi:10.1021/acscentsci.0c01551

Conflict of Interest: The authors declare that the research was conducted in the absence of any commercial or financial relationships that could be construed as a potential conflict of interest.

Publisher's Note: All claims expressed in this article are solely those of the authors and do not necessarily represent those of their affiliated organizations, or those of the publisher, the editors, and the reviewers. Any product that may be evaluated in this article, or claim that may be made by its manufacturer, is not guaranteed or endorsed by the publisher.

Copyright © 2022 Wang, Li, Nie, Zeng, Zhang, Deng, Chen, Zeng, Ma, Zheng and Gao. This is an open-access article distributed under the terms of the Creative Commons Attribution License (CC BY). The use, distribution or reproduction in other forums is permitted, provided the original author(s) and the copyright owner(s) are credited and that the original publication in this journal is cited, in accordance with accepted academic practice. No use, distribution or reproduction is permitted which does not comply with these terms.

frontiers in Bioengineering and Biotechnology

ORIGINAL RESEARCH
published: 25 February 2022
doi: 10.3389/fbioe.2022.859255

An in Silico Approach to Reveal the Nanodisc Formulation of Doxorubicin

Daiyun Xu[1†], Xu Chen[1†], Zhidong Chen[1†], Yonghui Lv[1], Yongxiao Li[1], Shengbin Li[1], Wanting Xu[1], Yuan Mo[1], Xinpei Wang[1], Zirui Chen[1], Tingyi Chen[1], Tianqi Wang[1], Zhe Wang[2], Meiying Wu[1]* and Junqing Wang[1]**

[1]School of Pharmaceutical Sciences (Shenzhen), Sun Yat-sen University, Shenzhen, China, [2]Department of Pathology, The Eighth Affiliated Hospital, Sun Yat-sen University, Shenzhen, China

OPEN ACCESS

Edited by:
Mingqiang Li,
Third Affiliated Hospital of Sun Yat-sen University, China

Reviewed by:
Chengchao Chu,
Xiamen University, China
Jingxiao Chen,
Jiangnan University, China
Yuan Xiong,
Huazhong University of Science and Technology, China

***Correspondence:**
Zhe Wang
wangzh379@mail.sysu.edu.cn
Meiying Wu
wumy53@mail.sysu.edu.cn
Junqing Wang
wangjunqing@mail.sysu.edu.cn

†These authors have contributed equally to this work

Specialty section:
This article was submitted to Biomaterials, a section of the journal Frontiers in Bioengineering and Biotechnology

Received: 21 January 2022
Accepted: 08 February 2022
Published: 25 February 2022

Citation:
Xu D, Chen X, Chen Z, Lv Y, Li Y, Li S, Xu W, Mo Y, Wang X, Chen Z, Chen T, Wang T, Wang Z, Wu M and Wang J (2022) An in Silico Approach to Reveal the Nanodisc Formulation of Doxorubicin. Front. Bioeng. Biotechnol. 10:859255. doi: 10.3389/fbioe.2022.859255

Molecular dynamic behaviors of nanodisc (ND) formulations of free doxorubicin (DOX) and DOX conjugated lipid prodrug molecules were investigated by molecular dynamics (MD) simulations. We have unveiled how formulation design affects the drug release profile and conformational stability of ND assemblies. Our simulation results indicate that free DOX molecules loaded in the ND system experienced rapid dissociation due to the unfavorable orientation of DOX attached to the lipid surface. It is found that DOX tends to form aggregates with higher drug quantities. In contrast, lipidated DOX-prodrugs incorporated in ND formulations exhibited sufficient ND conformational stability. The drug loading capacity is dependent on the type of lipid molecules grafted on the DOX-prodrug, and the drug loading quantities in a fixed area of NDs follow the order: DOX-BMPH-MP > DOX-BMPH-TC > DOX-BMPH-PTE. To gain further insight into the dynamic characteristics of ND formulations governed by different kinds of lipidation, we investigated the conformational variation of ND components, intermolecular interactions, the solvent accessible surface area, and individual MSP1 residue flexibility. We found that the global conformational stability of DOX-prodrug-loaded ND assemblies is influenced by the molecular flexibility and lipidated forms of DOX-prodrug. We also found that the spontaneous self-aggregation of DOX-prodrugs with increasing quantities on ND could reduce the membrane fluidity and enhance the conformational stability of ND formulations.

Keywords: molecular dynamics, Doxorubicin, nanodiscs, prodrugs, Drug delivery, lipidation

INTRODUCTION

Doxorubicin (DOX), a potent anthracycline cytotoxic drug, has been routinely used as a frontline chemotherapeutic agent in the treatment of various cancers. The anticancer mechanisms of DOX are known to involve multiple mechanisms, including intercalation of DOX into DNA double helix (Coldwell et al., 2008), inhibitions of several molecular targets (topoisomerase enzymes I and II, DNA and RNA polymerase) (Momparler et al., 1976; Foglesong et al., 1992; Marinello et al., 2018), generation of reactive oxygen species (ROS) (Davies and Doroshow, 1986), upregulation of C6 ceramide level (Ji et al., 2010), induction of autophagic cell death (Velez et al., 2011), and immunostimulatory effects (Mattarollo et al., 2011).

However, its clinical utility is restricted by dose-dependent toxicity on noncancerous cells of major organs, including the heart, liver, kidney, and brain (Chatterjee et al., 2010; Octavia et al., 2012; Tacar et al., 2013). Due to these unspecific side effects of conventional DOX therapy, various drug delivery systems (DDSs) such as liposomes, micelles, dendrimers, and inorganic nanoparticles have

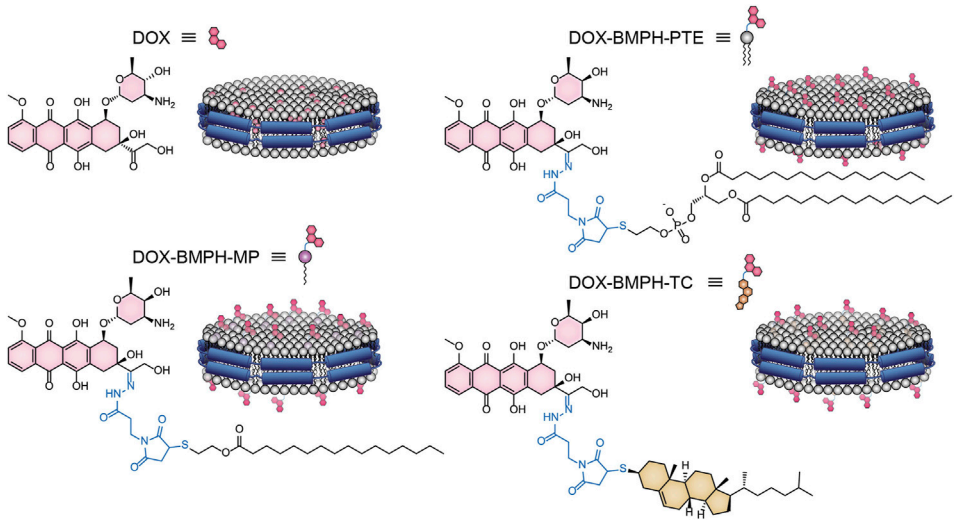

FIGURE 1 | A flow chart summarizes the individual steps for the MD simulation of ND systems.

been developed to enhance therapeutic efficacy minimize the adverse effects of DOX. However, the optimized biocompatibility and pharmacokinetics of these DDSs are critically dependent on PEGylation technology. This approach potentially results in several negative aspects, including restriction of cellular uptake, anti-PEG immune response, non-degradability, and heterogeneity in production. These unfavorable impacts have plagued the clinical translation of most DDS, and hence this has motivated the discovery of alternative PEG-free DDSs.

Endogenous and synthetic lipoproteins, such as high-density lipoprotein (HDL)-like nanodiscs, have rapidly evolved as a promising DDS for small molecules, peptides, and nucleic acids because of their intrinsic long *in vivo* half-lives and passive targeting properties (Kuai et al., 2017; Kuai et al., 2018; Kadiyala et al., 2019). Therefore, nanodisc drug formulation has attracted significant attention in the field of nanomedicine (Lacko et al., 2015; Wang et al., 2018; Tang et al., 2021). Several studies regarding nanodisc-based DOX delivery that employed different encapsulation strategies have shown increased efficacy and reduced side effects in anticancer therapy (Murakami et al., 2010; Yuan et al., 2013; Wang et al., 2014; Kuai et al., 2018). However, nanodisc (ND) formulation of DOX approached by different encapsulation designs can lead to variable drug-loading capacity (DLC), distinct drug release profiles, altered structures, and surface charges, as well as stability of the ND system. These characteristics are critical for DOX-DDS development. Although conventional trial and error approaches may provide sufficient guidance on formulation development, this process is usually sophisticated, time-consuming, and costly (Boruah et al., 2019). Besides, the rational design of DDS formulation depends on a detailed understanding of molecular principles; the mechanistic insights at the molecular level are hard to obtain through experimental research (Ramezanpour et al., 2016). Theoretical studies based on computational modeling methods enable the initial screening of formulation variables to predict potential conditions to accelerate the experimental process (Mehta et al., 2019). In this regard, molecular dynamics (MD) simulations offer a powerful tool to inspect structural, molecular interactions, and dynamic features of drugs and carriers (Bunker and Rog, 2020). Taking into account these considerations, it appears desirable to initially predict the optimum ND formulation of DOX through computational methods.

Here we present an in silico approach that adopted the ND modeling and MD simulation techniques to investigate the effect of different formulation designs on DOX loaded ND DDS (**Figure 1**). Free DOX and lipidated-DOX prodrugs are designed to access the formulation variables on the structural and dynamical behavior of ND assemblies. The present study focuses on the influence of different lipidated forms of DOX and the drug-to-lipid ratio (D/L ratio) on drug release profile, the structural and dynamic properties of ND-DOX formulations. Moreover, the mechanism of the interaction between DOX and the ND lipid bilayer is poorly understood. This drove us to investigate the behavior of free DOX and lipidated-DOX prodrug molecules in the DPPC bilayer ND through MD simulations.

MATERIALS AND METHODS

Preparation of the Nanodisc System

Membrane scaffold protein 1 (MSP1) and 1,2-dipalmitoyl-sn-glycero-3-phosphocholine (DPPC) were assembled into NDs using CHARMM-GUI (Qi et al., 2019). The diameter of all nanodiscs was 9.8 nm. For preparing four different ND formulation systems: 1. Free DOX, 2. DOX-BMPH-PTE (DOX-N-β-maleimidopropionic acid hydrazide-1,2-Dipalmitoyl-sn-Glycero-3-Phosphothioethanol), 3. DOX-BMPH-MP (DOX-N-β-maleimidopropionic acid hydrazide-2-Mercaptoethyl

TABLE 1 | The composition of each ND formulation system.

Proportion (number)	DOX (%)		Lipidated-DOX					
	DPPC	DOX	DPPC	DOX*	DPPC	DOX#	DPPC	DOX†
10	180	20	172	18	180	20	180	20
25	156	52	142	48	168	56	156	52
50	116	116	94	96	128	128	116	116

DOX denotes DOX-BMPH-PTE; DOX# denotes DOX-BMPH-MP; DOX† denotes DOX-BMPH-TC.*

palmitate), and 4. DOX-BMPH-TC (DOX-N-β-maleimidopropionic acid hydrazide- Thiocholesterol), four corresponding structural analogs (1. Sitosteryl Glucoside, 2. DPPC, 3. Hexadecanoate, and 4. Campesteryl Glucoside) were selected from CHARMM-GUI for subsequent positional labeling. The selected structural analogs were randomly inserted into the ND system with a predefined set of proportions (10, 25, and 50%). Then DOX and Lipidated-DOX were superimposed to the labeled analog using flexible docking, and the labeled analog was subsequently removed. To eliminate the impact of the wrong docking poses on simulation accuracy, only the pose where the DOX sugar moiety is at the hydrophilic interface, and the molecule as a whole is wrapped in the pocket of the membrane layer is preserved. Each step in the process is presented in a flowchart (**Figure 2**). The control system (empty ND) consists of two MSP1 and 190 DPPCs, and the concrete composition of other ND formulation systems is described in **Table 1**. Each MSP1 contained 200 residues and a total of 400 residues in each ND system. The system was protonated at 298 K, the salt concentration was set to 0.145 M, and the pH was set to 7.35. All systems were solvated in cubic boxes using TIP3P water and neutralized by adding 0.145 M NaCl. Energy minimization for up to 10,000 steps was performed using the gradient descent algorithm to optimize the system.

Parameter Settings of Molecular Dynamics Simulations

0.25 ns of NVT equilibration and 1.625 ns of NPT equilibration were performed. System temperature and pressure were maintained at 298 K, and at 1 bar using the Berendsen algorithm, respectively. The Nose-Hoover and Parrinello-Rahman algorithms were used to maintain temperature and pressure in the production simulation (Martyna et al., 1992). The constraints of heavy atoms in the system were gradually released until free in the equilibration stage. The simulation with the time step of 2 fs lasting 100 ns was performed for each system. The CHARMM36 force field was applied to all simulations (Huang and MacKerell Jr, 2013). The LINCS algorithm was used to constrain hydrogen bonds, and Coulomb interactions were calculated using particle-mesh Ewald (Hess et al., 1997). The root-mean-square deviation (RMSD), root-mean-square fluctuation (RMSF), solve accessible surface areas (SASA), and hydrogen bonds of the system were calculated in the trajectory analysis. All structures in the trajectory were clustered based on the RMSD of MSP1, and the structure in the largest cluster with the lowest RMSD relative to all other structures was defined as the central structure. All simulations were performed using GROMACS 2020.5 accelerated by CUDA modules, and all programs ran on AMD Ryzen™ Threadripper™ PRO 3995WX and The GeForce RTX™ 3080 Ti graphics card (Van Der Spoel et al., 2005).

RESULTS AND DISCUSSION

Dynamic Behaviour of DOX Molecules in DPPC ND Formulation

We initially investigated the MSP1/DPPC ND formulations of free DOX molecules through 100 ns all-atom MD simulations. Three different proportions of DOX ranging from 10 to 25% and 50% of total lipids were randomly placed into the ND bilayer. Considering the structural stability of ND and molecular motion of DOXs in the DPPC membrane, the root-mean-square deviation (RMSD) of DOX, DPPC, MSP (MSP1), and ND complex is determined in **Figures 3A–E** as a function of time. In the case of an empty ND system (**Figure 3A**), DPPC and MSP1 reach equilibrium in the first 12 ns of the 100 ns trajectories. Both DPPC and MSP show similar trends with an average RMSD (after 50 ns of simulation) of 1.00 and 1.20 nm, respectively. The global motions of the ND complex are plotted by the RMSD values comprising of DPPC and MSP in the trajectory, with RMSD quickly reaching a plateau of ~1 nm after about 12 ns of simulation. In contrast to the empty ND system (control), the 10% DOX-incorporated ND assembly was unstable during the 100 ns of simulation (**Figure 3B**), with RMSD values undergoing a progressive increase of approximately 2.5-fold higher than control at the end of the simulation. However, The average RMSD value (after 50 ns of simulation) of DPPC and MSP1 is 1.18 and 1.22 nm, respectively. This indicates the significant RMSD increment of the ND complex is attributed to the random motion of DOXs.

To further study the role of DOX content in ND stability, ND with elevated DOX content of 25 and 50% were simulated under the same conditions. The structure of the ND complex (25% DOX) was increasingly unstable throughout the simulations, with the highest RMSD above 3.5 nm (**Figure 3C**). In contrast, the ND complex with higher DOX content (50%) generally shows lower RMSD with a maximum value of ~2.6 nm (**Figure 3D**). However, the RMSD values of DPPC display the same increasing trend in 25 and 50% DOX of ND complex by maintaining an average of 1.31 and 1.35 nm during the second half of 50 ns, respectively. This implies the loss of constraints or reduced density between

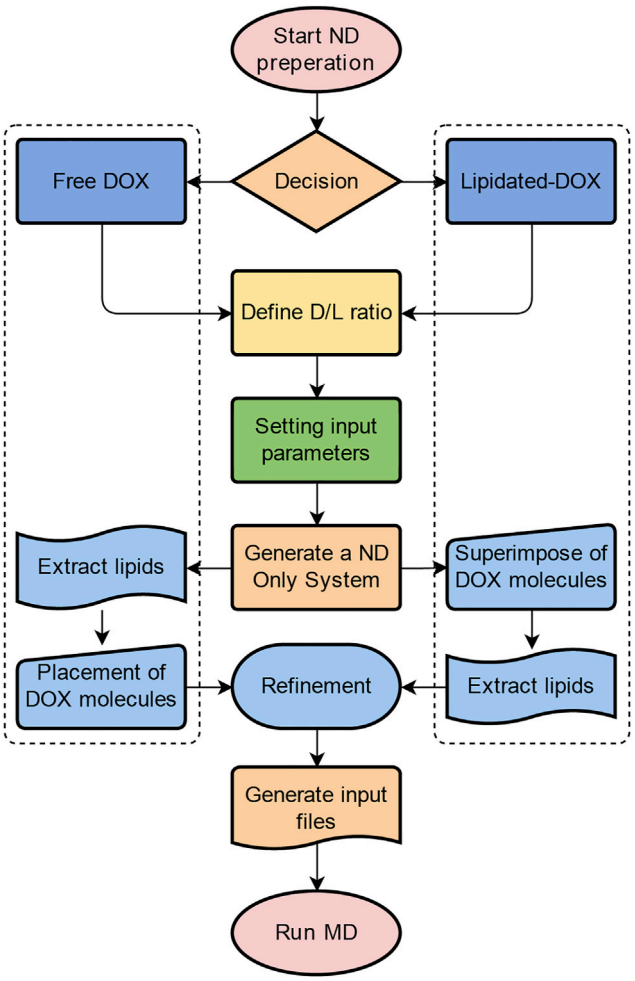

FIGURE 2 | MD simulation results of free-DOX incorporated DPPC ND formulation. The RMSD trajectory of DPPC, MSP1, and ND complex as a function of simulation time in nanoseconds (ns) for **(A)** the empty ND, **(B)** 10% DOX-ND, **(C)** 25% DOX-ND, and **(D)** 50% DOX-ND. **(E)** The RMSD trajectory of DOX molecules with increasing proportions (10, 25, and 50%) as a function of simulation time in ns. The initial and final snapshot of the simulation for each DOX-ND formulation: **(F)** 10% DOX-ND, **(H)** 25% DOX-ND, and **(J)** 50% DOX-ND. The interactions of the DOX molecules with the ND differed depending on the proportions of DOX: **(G)** 10% DOX, **(I)** 25% DOX, and **(K)** 50% DOX.

DPPC molecules. Moreover, all simulations show that an increase in the ratio of DOX results in little effect on the RMSD of MSP1. In this regard, the global instability mainly comes from the dissociation of DOX from the ND complexes. Interestingly, the RMSD profiles of 10 and 25% of DOX molecules in ND formulations show a similar trend with increasing RMSD values along the trajectories, while a higher proportion of DOX (50%) in the ND formulation leads to improved global stability, as reflected in lower RMSD pattern of the DOX molecules (**Figure 3E**). The simulation results suggest the self-aggregation propensity of DOX molecules.

In order to gain further insight into the dynamic behavior of DOX molecules, the first and last snapshots of MD trajectories are illustrated, and DOX-DPPC/MSP1 interactions are analyzed (**Figures 3F–K**). The drug leakage evaluation shows that 55% of DOX quantities were dissociated from the ND (10% DOX) throughout 100 ns MD simulations, suggesting variable interactions between DOX and DPPC ND bilayer (**Figure 3F**). However, the degree of DOX dissociation behavior is dropped to 25 and 15%, with increases in DOX-loading content from 25 to 50%, respectively (**Figures 3H,J**), indicating multiple network interactions were created via homomolecular and heteromolecular interactions. In the case of the low content of DOX (10%), DOX can interact with the DPPC molecules because of its amphiphilic structure. The positively charged amino sugar moiety can readily interact with the negatively charged phosphate group of DPPC through electrostatic interactions. The anthraquinone (AQ) ring of DOX can insert into the DPPC bilayer *via* hydrophobic interaction. In the case of the mid content of DOX (25%) (**Figure 3I**), additional interactions were formed between the DOX and polar or charged residues in MSP1. Specifically, Arg, Lys, and Glu residues frequently interact with the amino sugar and AQ moieties of DOX molecules. This results in the relocation of DOX molecules toward the ND rim, which is also reflected in the decrease of average RMSD values of MSP1 (**Figures 3A–D**). In addition to DOX-MSP1 interactions, the high content of DOX (50%) can form a giant network of DOX

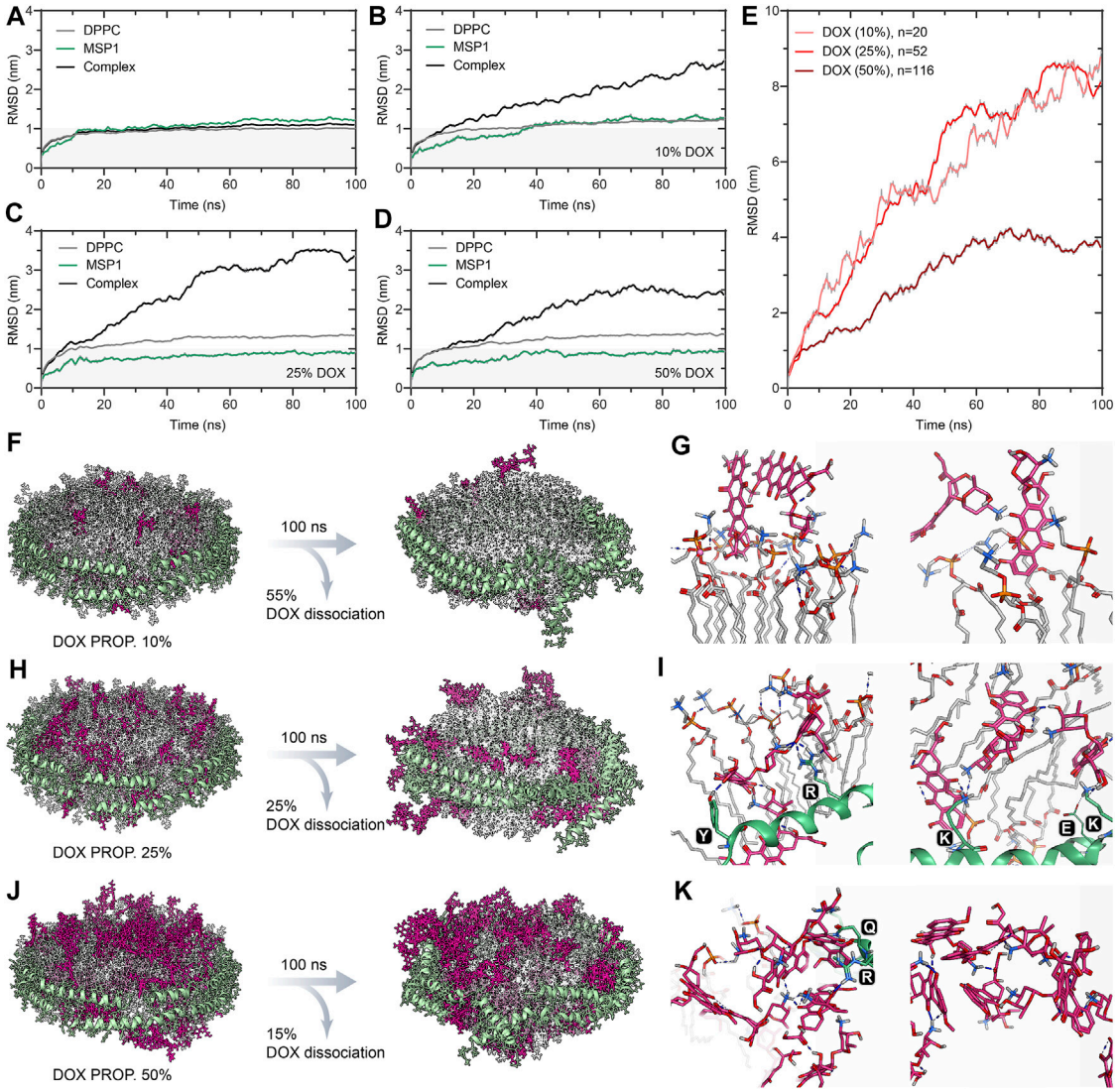

FIGURE 3 | RMSD trajectories and snapshots of center clusters for various types of lipidated-DOX prodrug ND formulations with increasing drug proportions (10, 25, and 50%). **(A)** ND formulation of DOX-BMPH-PTE. **(B)** ND formulation of DOX-BMPH-MP. **(C)** ND formulation of DOX-BMPH-TC.

molecules on the interface of ND *via* both hydrogen bonding and hydrophobic π-π interactions (**Figure 3K**). This self-aggregation led to an arrested molecular motion and improved association of DOX with the ND. Therefore, we consider that the design of ND formulation involved free DOX molecules should be primarily concerned with the increased self-aggregation tendency at higher DOX concentrations (Fonseca et al., 1997; Fülöp et al., 2013). Such spontaneous homomolecular interactions may distort the orientational-dependent interactions between DOX and ND assembly.

The Impact of Drug Conjugation on ND Formulation

Three existing types of DOX lipidation are evaluated by a similar MD simulation approach. MD simulation results of ND formulation containing increasing quantities (10, 25, 50%) of BMPH-PTE, BMPH-MP, and BMPH-TC conjugated pH-sensitive DOX prodrugs and their corresponding central structure with the lowest RMSD score in the cluster are illustrated in **Figure 4**. In the group of ND formulations of DOX-BMPH-PTE (**Figure 4A**), no DOX leakage was observed during the MD simulations. Visual inspection on the ND complexes showed that DOX-BMPH-PTE molecules were tightly assembled with DPPC NDs. The RMSD profile of each component trajectory remains generally stable after 50 ns of simulations. Lower average RMSD values of DOX-BMPH-PTE and MSP1 are observed with an increase in DOX-BMPH-PTE proportion (**Figure 4A**). This implies the loss in the degree of ND conformational freedom and plausibly relative to the concentration-dependent DOX self-aggregation and DOX-MSP1 interactions.

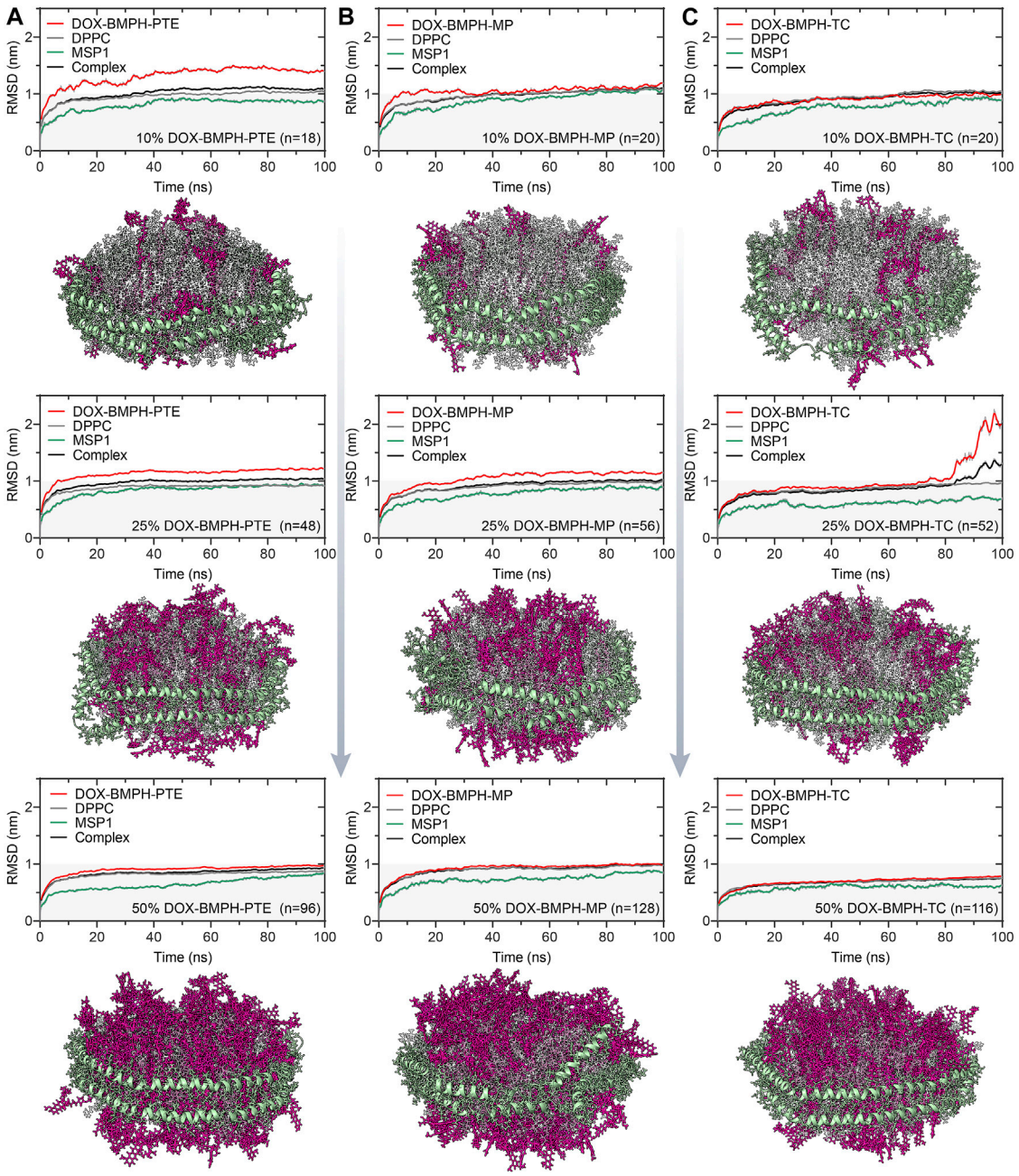

FIGURE 4 | MD simulation analysis of hydrogen bonds formed between DOX prodrug molecules and MSP1 protein in ND complexes. Dynamic measurements of hydrogen bond numbers in ND formulations of **(A)** DOX-BMPH-PTE (10%), DOX-BMPH-MP (10%), and DOX-BMPH-TC (10%). **(B)** DOX-BMPH-PTE (25%), DOX-BMPH-MP (25%), and DOX-BMPH-TC (25%). **(C)** DOX-BMPH-PTE (50%), DOX-BMPH-MP (50%), and DOX-BMPH-TC (50%). Dynamic measurements of hydrogen bonds per drug molecule in ND formulations of **(D)** DOX-BMPH-PTE. **(E)** DOX-BMPH-MP. **(F)** DOX-BMPH-TC. Electrostatic interactions between DOX prodrug molecules and MSP1 protein in ND formulations of **(G)** DOX-BMPH-PTE. **(H)** DOX-BMPH-MP. **(I)** DOX-BMPH-TC.

Similar dynamic behavior was observed in ND formulations of DOX-BMPH-MP and DOX-BMPH-TC. It is worth noting that each ND assembly possessed the same initial surface area, and the packing capacity is dependent on the surface area per lipid molecule. In this regard, the DOX-BMPH-PTE molecule occupies the largest area (63.0 $Å^2$) on the ND among the simulated prodrugs, followed by DOX-BMPH-TC (40 $Å^2$) and DOX-BMPH-MP (30 $Å^2$). Therefore, ND formulated DOX-BMPH-MP appears to have the highest packing capacity. However, a parallel comparison between DOX-BMPH-PTE and DOX-BMPH-MP ND formulations shows that more DOX-BMPH-MP loading quantities do not seem to govern the stability of the MPS1 and ND complex significantly (**Figures 4A,B**). But the single acyl-chain characteristics of MP may subsequently influence membrane curvature. As the large head groups (DOX) of

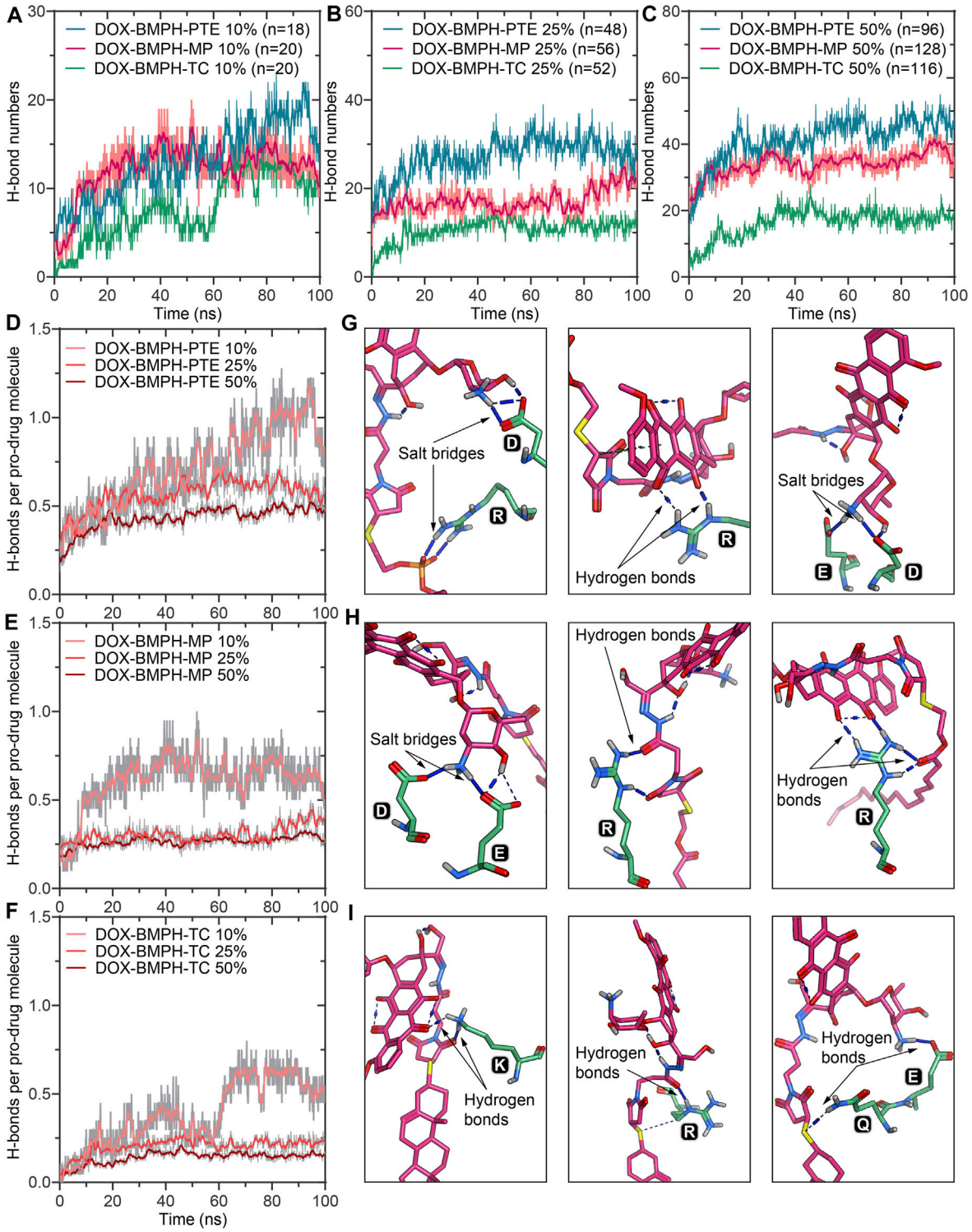

FIGURE 5 | A schematic illustration of the ND formulation designs for free DOX and lipidated DOX-prodrugs.

lipid clusters group together, DOX-BMPH-MPs impose a positive curvature on both sites of the ND membrane. Notably, the MD trajectory of DOX-BMPH-TC ND formulation exhibits the lowest RMSD values and fluctuations (except the case with a drug loading of 25%) than the formerly discussed ND formulations, which can be typically observed in the case with a 50% drug loading ratio (**Figure 4C**). We speculated that this significant RMSD improvement is primarily attributed to the cholesterol domain of

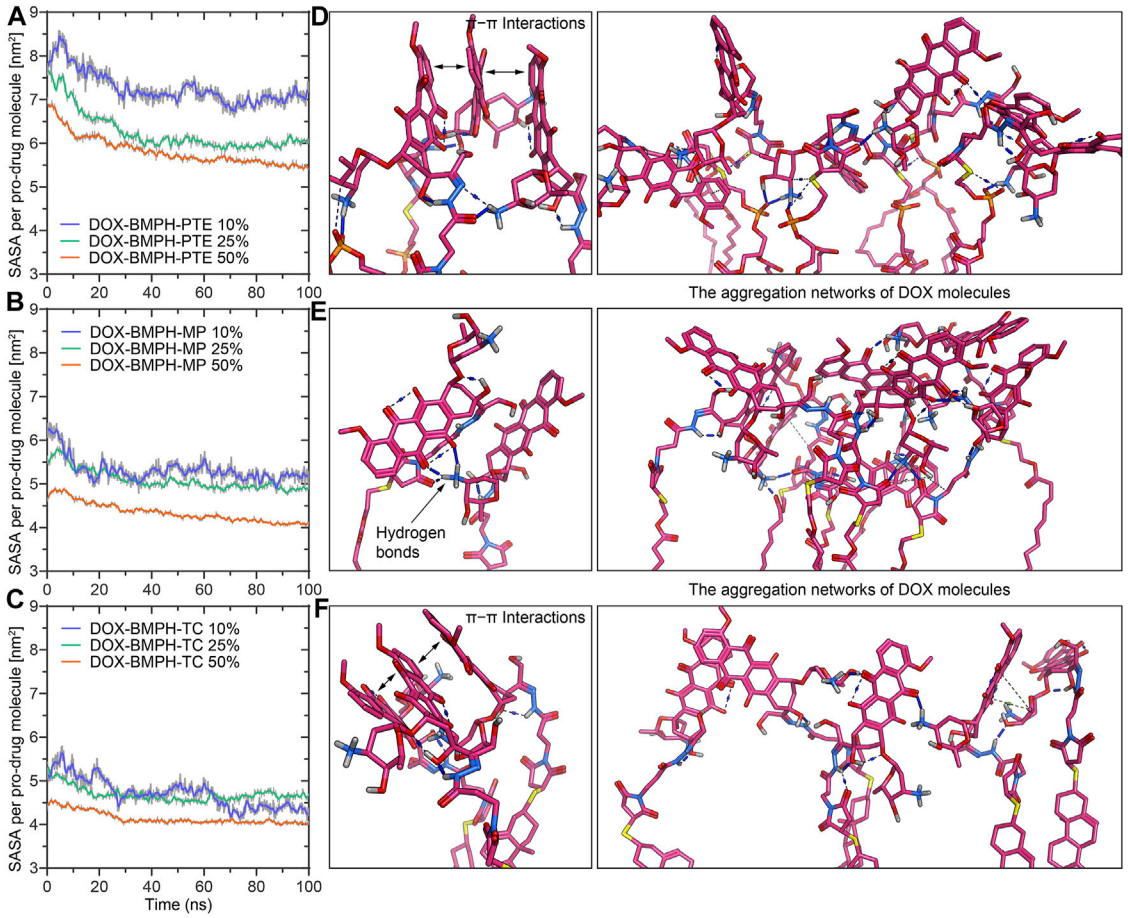

FIGURE 6 | MD simulation analysis of the solvent accessible surface area (SASA) and self-aggregation behavior of DOX-prodrug ND formulations. Time evolution of the SASA per prodrug molecule during 100 ns of MD simulation for ND formulations of **(A)** DOX-BMPH-PTE. **(B)** DOX-BMPH-MP. **(C)** DOX-BMPH-TC. The aggregation networks of DOX molecules in ND formulations of **(D)** DOX-BMPH-PTE. **(E)** DOX-BMPH-MP. **(F)** DOX-BMPH-TC. Overall Stability and Flexibility of MSP1 Protein Assembled with Different DOX-ND Formulations.

DOX-BMPH-TC, which can stabilize the ND by increasing the order of the lipid packing, enhancing the rigidity, and reducing the fluidity of the membrane. Moreover, DOX-BMPH-TC with fewer rotatable bonds than DOX-BMPH-PTE and DOX-BMPH-MP can also result in reduced structural flexibility and lower RMSD.

The Electrostatic Interactions between DOX-Prodrug molecules and MSP1 Proteins

In MD simulations of DOX-prodrug ND formulations, we observed that the number of hydrogen bonds between DOX-prodrug molecules and MSP1 proteins is proportional to the loading quantities in all types of ND formulations (**Figures 5A–C**). The DOX-BMPH-PTE ND formulation consistently has the highest average counts of hydrogen bonds (after 50ns of simulation) across different loading quantities (10%, H_n = 16.1; 25%, H_n = 29.5; 50%, H_n = 45.5), followed by a consistent pattern for DOX-BMPH-MP ND formulation (10%, H_n = 13.1; 25%, H_n = 18.2; 50%, H_n = 35.8), and received the lowest average counts for DOX-BMPH-TC ND formulation (10%, H_n = 10.3; 25%, H_n = 11.5; 50%, H_n = 17.8). This regularity difference between the different types of ND formulations could be explained by the fact that the number of rotatable bonds and the structural flexibility of DOX-prodrug molecules are in descending order: DOX-BMPH-PTE > DOX-BMPH-MP > DOX-BMPH-TC (**Figure 1**). The loss of conformational freedom in DOX-prodrug molecules results in limited DOX-MSP1 interactions, and hence the less number of hydrogen bonds. This implies that increasing in conformational restriction of drug molecules may have a reduced influence on MSP1 dynamics.

The fluctuations of hydrogen bonds per-DOX interaction with MSP1 over the simulation time show that hydrogen bonds per-DOX are significantly reduced with increasing DOX quantities (**Figures 5D–F**), and the minimum limits are achieved when the proportions of DOX rise to above 25%. In accordance with the center clusters of DOX-BMPH-PTE ND, we found abundant electrostatic interactions between DOX prodrugs and MSP1 proteins, including salt bridges and hydrogen bonds (**Figures 5G–I**). Similar interactions are observed in DOX-BMPH-MP ND

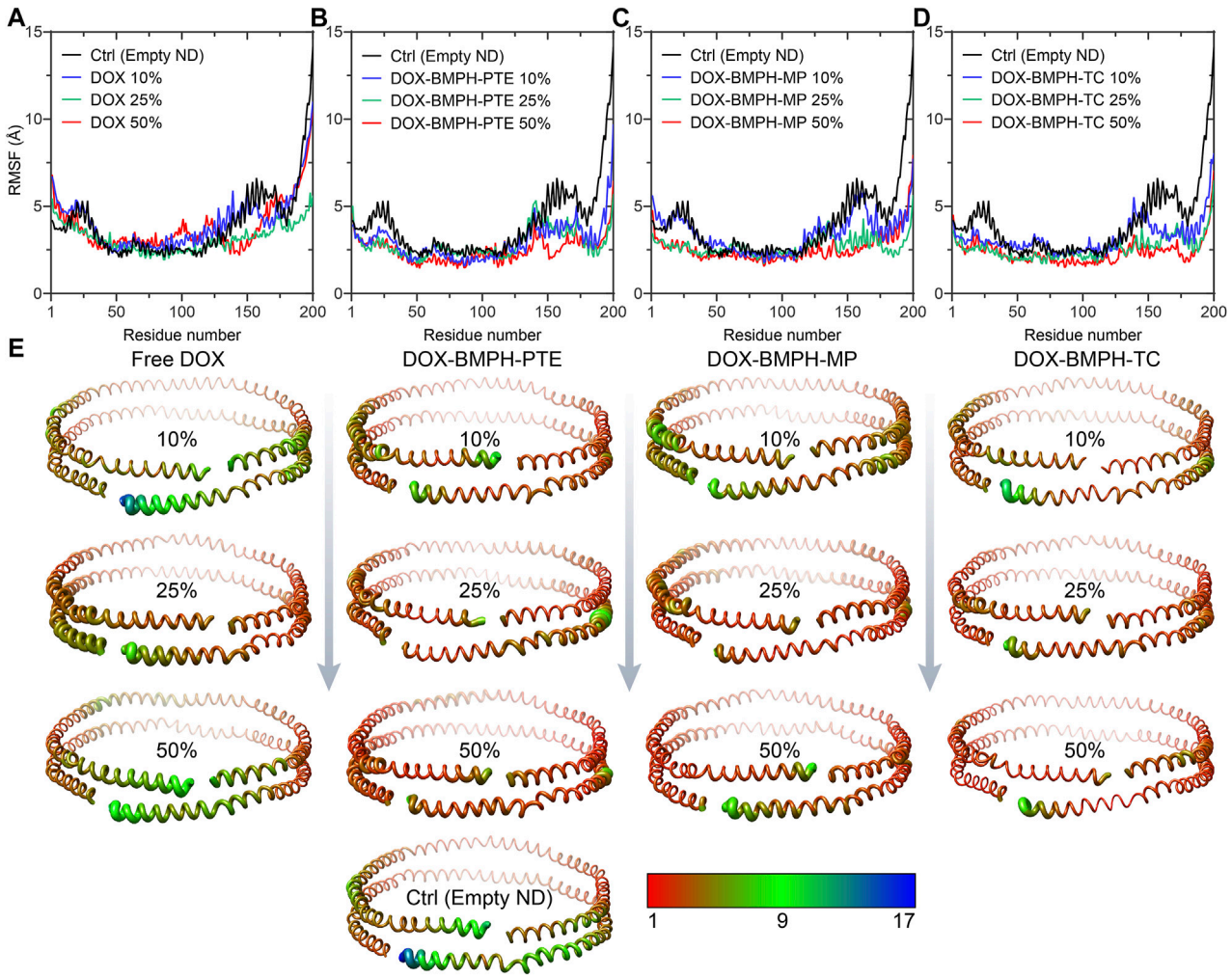

FIGURE 7 | Root Mean Square Fluctuation (RMSF) analyses MSP1 protein assembled with different DOX-ND formulations. Each MSP1 contained 200 residues, and the abscissa in the line charts represents the average value of RMSF in the same residue of two MSP1 proteins. RMSF of four systems compared with MSP1 residues in the empty ND: **(A)** MSP1 residues in the free DOX-ND formulations. **(B)** MSP1 residues in DOX-BMPH-PTE ND formulations. **(C)** MSP1 residues in DOX-BMPH-MP ND formulations. **(D)** MSP1 residues in DOX-BMPH-TC ND formulations. **(E)** Comparison of the fluctuations of each residue between four ND formulations and the empty ND with variants colored and sized according to its RMSF contribution. The coloring-thickness scale varies from deep red and thin (low fluctuations) to dark blue and thick (high fluctuations).

central structures, whereas in DOX-BMPH-TC ND central structures, only a few hydrogen bonds were formed with MSP1 proteins. Collectively, Arg, Lys, Asp, and Glu residues of MSP1 proteins have commonly participated in hydrogen bonding and salt-bridge interactions with DOX-prodrug molecules.

SOLVENT ACCESSIBLE SURFACE AREA AND STABILITY OF DOX-PRODRUG LOADED ND ASSEMBLIES

Solvent accessible surface area (SASA) of DOX-prodrug loaded ND assemblies could be an important factor in stability studies. The SASA per prodrug molecule of different ND formulations is shown in **Figures 6A–C**. We noticed that a smaller head moiety of lipidated DOX-prodrugs can lower SASA per prodrug molecule. Besides, comparable trajectories are observed for 10 and 25% of both DOX-BMPH-MP ND and DOX-BMPH-TC ND (**Figures 6B,C**), which suggests rigidity of the DOX-BMPH-MP and DOX-BMPH-TC head moieties. It is notable that the SASA per prodrug molecule appears to be dropped at high proportions of DOX-prodrug quantity (50%), indicating that the tendency of decreasing in SASA could be governed by the quantity-dependent self-aggregation of DOX (Fülöp et al., 2013). Various interactions such as hydrogen bonding, π-π, π-alkyl stacking, and hydrophobic interaction are frequently involved in the aggregation networks of DOX. The visual inspection of central structures found that the presence of six-membered daunosamine sugar of DOX molecules plays a dominant role in forming

hydrogen-bonding networks (**Figures 6D–F**). Other substructures, including aglycone moiety, phosphate groups, glycerol groups, and maleimide groups, also facilitated the intermolecular and intramolecular electrostatic interactions.

To observe and compare the motion of MSP1 residues, we performed the root mean square fluctuation (RMSF) analyses for both the empty ND (reference structure) and different DOX-ND Formulations (**Figure 7**). In all cases, the most flexible regions are the C-terminal residues of the MSP1 (**Figures 7A–D**). As the DOX loading increased, each type of formulation followed a similar tendency with varying degrees of reduction in global RMSF values (**Figure 7E**). It is observed that residues of the ND formulation of DOX-BMPH-TC are more rigid than other ND formulations. This is in agreement with RMSD results and indicates that there were relatively strong interactions between the lipids/Drugs and MSP1 proteins, as well as lower fluidity of the membrane, which stabilized the DOX-BMPH-TC ND in a more compact conformation than others. Nevertheless, the rigidity of residues could be improved by loading a higher proportion of lipidated-prodrugs except for free DOX ND formulation.

CONCLUSION

The molecular dynamic behavior of both free DOX and DOX conjugated lipid prodrug molecules loaded in ND formulations was investigated in depth by a series of all-atom MD simulations. We found that the interactions between free DOX molecules and the ND system are labile due to the strong electrostatic interaction between the amino sugar moiety of DOX and the phosphate head group of DPPC. These hydrogen bonds and intrinsic steric hindrance altered the ideal binding mode of DOX and resulted in an unfavorable orientation of DOX attached on the lipid surface rather than the vertical insertion of the AQ ring. Such amphiphilic characteristics of DOX may enable rapid membrane penetration and diffusion (Toroz and Gould, 2019). The stability of DOX binding modes to the ND membrane could be dependent on lipid composition (Siani et al., 2022). Through the comparison between three types of ND formulations of lipidated-DOX prodrugs, we observed that lipidation approaches could provide sufficient conformational stability for prodrug loading and different lipid used for lipidation led to variable loading capacity. ND formulation of DOX-BMPH-MP may be selected for more drug loading quantities as compared to other formulations. Our results also demonstrated that the global conformational stability of DOX-prodrug-loaded ND Assemblies is influenced by the molecular flexibility and lipid composition of DOX-prodrug molecules. Thus, ND formulation of DOX-BMPH-TC may be considered for better dynamic stability. We have also demonstrated that the increase in proportions of DOX-prodrug within a specific range (e.g., 10–50%) could induce DOX self-aggregation and hydrogen bonding with MSP1 residues, incidentally lowering the membrane fluidity and hence improving the conformational stability of ND formulations.

The main limitation of our study lies in the assumption that ND formulations of DOX satisfy the discoidal double-belt model and can be properly prepared under experimental conditions. Although this study mainly focused on comparing ND formulations with one another, simulated time could be another limitation that affects the accuracy. Besides, the effect of drug loading quantity on ND solubility was not within the scope of the study. Nevertheless, our findings offered a molecular insight into how lipidation of DOX influences the dynamic performance of ND formulations. The obtained information may guide the practical design and optimization of the ND formulation of DOX. The in silico approach adopted here exhibits future potential as a virtual screening or evaluation method to develop ND formulations.

DATA AVAILABILITY STATEMENT

The raw data supporting the conclusions of this article will be made available by the authors, without undue reservation.

AUTHOR CONTRIBUTIONS

JW conceived the idea, designed the study, directed the project. JW, XC, and ZHC developed the ND formulation dynamic simulation method and wrote the manuscript. XC, ZHC, and DX performed all the experiments and analyzed the data. MW, ZHW, XC and ZHC evaluated the computational modeling for formulation design and supervised the experimental procedure. DX, YLV, YLI, SL, WX, YM, ZIC, and TC provided technical support and revised the manuscript. All authors contributed text to the article and approved the submitted version.

FUNDING

This work was supported by the National Natural Science Foundation of China (82001887 to JW and 81900105 to ZW), in part by a horizontal project of Sun Yat-sen University (K21-75110-007), Science and Technology Innovation Committee of Shenzhen Municipality (JCYJ20210324115003009), and the Guangdong Basic and Applied Basic Research Foundation (2019A1515110326).

REFERENCES

Boruah, N., Sarma, H., and Sharma, H. (2019). *Computational Formulation Development and Drug Delivery*. Tamil Nadu: i-manager Publications, 191–195.

Bunker, A., and Róg, T. (2020). Mechanistic Understanding from Molecular Dynamics Simulation in Pharmaceutical Research 1: Drug Delivery. *Front. Mol. Biosci.* 7, 604770. doi:10.3389/fmolb.2020.604770

Chatterjee, K., Zhang, J., Honbo, N., and Karliner, J. S. (2010). Doxorubicin Cardiomyopathy. *Cardiology* 115 (2), 155–162. doi:10.1159/000265166

Coldwell, K. E., Cutts, S. M., Ognibene, T. J., Henderson, P. T., and Phillips, D. R. (2008). Detection of Adriamycin-DNA Adducts by Accelerator Mass Spectrometry at Clinically Relevant Adriamycin Concentrations. *Nucleic Acids Res.* 36 (16), e100. doi:10.1093/nar/gkn439

David Foglesong, P., Reckord, C., and Swink, S. (1992). Doxorubicin Inhibits Human DNA Topoisomerase I. *Cancer Chemother. Pharmacol.* 30 (2), 123–125. doi:10.1007/BF00686403

Davies, K. J., and Doroshow, J. H. (1986). Redox Cycling of Anthracyclines by Cardiac Mitochondria. I. Anthracycline Radical Formation by NADH Dehydrogenase. *J. Biol. Chem.* 261 (7), 3060–3067. doi:10.1016/s0021-9258(17)35746-0

Fonseca, M. J., van Winden, E. C. A., and Crommelin, D. J. A. (1997). Doxorubicin Induces Aggregation of Small Negatively Charged Liposomes. *Eur. J. Pharmaceutics Biopharmaceutics* 43 (1), 9–17. doi:10.1016/S0939-6411(96)00018-5

Fülöp, Z., Gref, R., and Loftsson, T. (2013). A Permeation Method for Detection of Self-Aggregation of Doxorubicin in Aqueous Environment. *Int. J. Pharmaceutics* 454 (1), 559–561. doi:10.1016/j.ijpharm.2013.06.058

Hess, B., Bekker, H., Berendsen, H. J. C., and Fraaije, J. G. E. M. (1997). LINCS: A Linear Constraint Solver for Molecular Simulations. *J. Comput. Chem.* 18 (12), 1463–1472. doi:10.1002/(sici)1096-987x(199709)18:12<1463::aid-jcc4>3.0.co;2-h

Huang, J., and MacKerell, A. D., Jr (2013). CHARMM36 All-Atom Additive Protein Force Field: Validation Based on Comparison to NMR Data. *J. Comput. Chem.* 34 (25), 2135–2145. doi:10.1002/jcc.23354

Ji, C., Yang, B., Yang, Y.-L., He, S.-H., Miao, D.-S., He, L., et al. (2010). Exogenous Cell-Permeable C6 Ceramide Sensitizes Multiple Cancer Cell Lines to Doxorubicin-Induced Apoptosis by Promoting AMPK Activation and mTORC1 Inhibition. *Oncogene* 29 (50), 6557–6568. doi:10.1038/onc.2010.379

Kadiyala, P., Li, D., Nuñez, F. M., Altshuler, D., Doherty, R., Kuai, R., et al. (2019). High-Density Lipoprotein-Mimicking Nanodiscs for Chemo-Immunotherapy against Glioblastoma Multiforme. *ACS Nano* 13 (2), 1365–1384. doi:10.1021/acsnano.8b06842

Kuai, R., Ochyl, L. J., Bahjat, K. S., Schwendeman, A., and Moon, J. J. (2017). Designer Vaccine Nanodiscs for Personalized Cancer Immunotherapy. *Nat. Mater* 16 (4), 489–496. doi:10.1038/nmat4822

Kuai, R., Yuan, W., Son, S., Nam, J., Xu, Y., Fan, Y., et al. (2018). Elimination of Established Tumors with Nanodisc-Based Combination Chemoimmunotherapy. *Sci. Adv.* 4 (4), eaao1736. doi:10.1126/sciadv.aao1736

Lacko, A. G., Sabnis, N. A., Nagarajan, B., and McConathy, W. J. (2015). HDL as a Drug and Nucleic Acid Delivery Vehicle. *Front. Pharmacol.* 6. doi:10.3389/fphar.2015.00247

Marinello, J., Delcuratolo, M., and Capranico, G. (2018). Anthracyclines as Topoisomerase II Poisons: From Early Studies to New Perspectives. *Ijms* 19 (11), 3480. doi:10.3390/ijms19113480

Martyna, G. J., Klein, M. L., and Tuckerman, M. (1992). Nosé-Hoover Chains: The Canonical Ensemble via Continuous Dynamics. *J. Chem. Phys.* 97 (4), 2635–2643. doi:10.1063/1.463940

Mattarollo, S. R., Loi, S., Duret, H., Ma, Y., Zitvogel, L., and Smyth, M. J. (2011). Pivotal Role of Innate and Adaptive Immunity in Anthracycline Chemotherapy of Established Tumors. *Cancer Res.* 71 (14), 4809–4820. doi:10.1158/0008-5472.CAN-11-0753

Mehta, C. H., Narayan, R., and Nayak, U. Y. (2019). Computational Modeling for Formulation Design. *Drug Discov. Today* 24 (3), 781–788. doi:10.1016/j.drudis.2018.11.018

Momparler, R. L., Karon, M., Siegel, S. E., and Avila, F. (1976). Effect of Adriamycin on DNA, RNA, and Protein Synthesis in Cell-free Systems and Intact Cells. *Cancer Res.* 36 (8), 2891–2895.

Murakami, T., Wijagkanalan, W., Hashida, M., and Tsuchida, K. (2010). Intracellular Drug Delivery by Genetically Engineered High-Density Lipoprotein Nanoparticles. *Nanomedicine* 5 (6), 867–879. doi:10.2217/nnm.10.66

Octavia, Y., Tocchetti, C. G., Gabrielson, K. L., Janssens, S., Crijns, H. J., and Moens, A. L. (2012). Doxorubicin-induced Cardiomyopathy: From Molecular Mechanisms to Therapeutic Strategies. *J. Mol. Cell Cardiol.* 52 (6), 1213–1225. doi:10.1016/j.yjmcc.2012.03.006

Qi, Y., Lee, J., Klauda, J. B., and Im, W. (2019). CHARMM-GUI Nanodisc Builder for Modeling and Simulation of Various Nanodisc Systems. *J. Comput. Chem.* 40 (7), 893–899. doi:10.1002/jcc.25773

Ramezanpour, M., Leung, S. S. W., Delgado-Magnero, K. H., Bashe, B. Y. M., Thewalt, J., and Tieleman, D. P. (2016). Computational and Experimental Approaches for Investigating Nanoparticle-Based Drug Delivery Systems. *Biochim. Biophys. Acta (Bba) - Biomembranes* 1858 (7, Part B), 1688–1709. doi:10.1016/j.bbamem.2016.02.028

Siani, P., Donadoni, E., Ferraro, L., Re, F., and Di Valentin, C. (2022). Molecular Dynamics Simulations of Doxorubicin in Sphingomyelin-Based Lipid Membranes. *Biochim. Biophys. Acta (Bba) - Biomembranes* 1864 (1), 183763. doi:10.1016/j.bbamem.2021.183763

Tacar, O., Sriamornsak, P., and Dass, C. R. (2012). Doxorubicin: an Update on Anticancer Molecular Action, Toxicity and Novel Drug Delivery Systems. *J. Pharm. Pharmacol.* 65 (2), 157–170. doi:10.1111/j.2042-7158.2012.01567.x

Tang, Z., Xiao, Y., Kong, N., Liu, C., Chen, W., Huang, X., et al. (2021). Nano-bio Interfaces Effect of Two-Dimensional Nanomaterials and Their Applications in Cancer Immunotherapy. *Acta Pharmaceutica Sinica B* 11 (11), 3447–3464. doi:10.1016/j.apsb.2021.05.004

Toroz, D., and Gould, I. R. (2019). A Computational Study of Anthracyclines Interacting with Lipid Bilayers: Correlation of Membrane Insertion Rates, Orientation Effects and Localisation with Cytotoxicity. *Sci. Rep.* 9 (1), 2155. doi:10.1038/s41598-019-39411-y

Van Der Spoel, D., Lindahl, E., Hess, B., Groenhof, G., Mark, A. E., and Berendsen, H. J. C. (2005). GROMACS: Fast, Flexible, and Free. *J. Comput. Chem.* 26 (16), 1701–1718. doi:10.1002/jcc.20291

Velez, J. M., Miriyala, S., Nithipongvanitch, R., Noel, T., Plabplueng, C. D., Oberley, T., et al. (2011). p53 Regulates Oxidative Stress-Mediated Retrograde Signaling: a Novel Mechanism for Chemotherapy-Induced Cardiac Injury. *PLoS One* 6 (3), e18005. doi:10.1371/journal.pone.0018005

Wang, B., Yuan, Y., Han, L., Ye, L., Shi, X., and Feng, M. (2014). Recombinant Lipoproteins Reinforce Cytotoxicity of Doxorubicin to Hepatocellular Carcinoma. *J. Drug Target.* 22 (1), 76–85. doi:10.3109/1061186X.2013.839687

Wang, J., Wang, A. Z., Lv, P., Tao, W., and Liu, G. (2018). Advancing the Pharmaceutical Potential of Bioinorganic Hybrid Lipid-Based Assemblies. *Adv. Sci.* 5 (9), 1800564. doi:10.1002/advs.201800564

Yuan, Y., Wang, W., Wang, B., Zhu, H., Zhang, B., and Feng, M. (2013). Delivery of Hydrophilic Drug Doxorubicin Hydrochloride-Targeted Liver Using apoAI as Carrier. *J. Drug Target.* 21 (4), 367–374. doi:10.3109/1061186X.2012.757769

Conflict of Interest: The authors declare that the research was conducted in the absence of any commercial or financial relationships that could be construed as a potential conflict of interest.

The handling editor ML declared a shared affiliation, though no other collaboration, with all authors at the time of the review.

Publisher's Note: All claims expressed in this article are solely those of the authors and do not necessarily represent those of their affiliated organizations, or those of the publisher, the editors and the reviewers. Any product that may be evaluated in this article, or claim that may be made by its manufacturer, is not guaranteed or endorsed by the publisher.

Copyright © 2022 Xu, Chen, Chen, Lv, Li, Li, Xu, Mo, Wang, Chen, Chen, Wang, Wang, Wu and Wang. This is an open-access article distributed under the terms of the Creative Commons Attribution License (CC BY). The use, distribution or reproduction in other forums is permitted, provided the original author(s) and the copyright owner(s) are credited and that the original publication in this journal is cited, in accordance with accepted academic practice. No use, distribution or reproduction is permitted which does not comply with these terms.

frontiers | Frontiers in Bioengineering and Biotechnology

OPINION
published: 21 June 2022
doi: 10.3389/fbioe.2022.952194

A Superstable Homogeneous Lipiodol-Nanoformulation to Overcome the Dilemma of Interventional Embolization Chemotherapy

Yisheng Peng, Pan He, Xing Gao, Gang Liu and Hongwei Cheng**

State Key Laboratory of Molecular Vaccinology and Molecular Diagnostics, Center for Molecular Imaging and Translational Medicine, School of Public Health, Xiamen University, Xiamen, China

Keywords: hepatocellular carcinoma, transcatheter arterial chemoembolization, drug delivery, drug dispersion, lipiodol

OPEN ACCESS

Edited by:
Junqing Wang,
Sun Yat-sen University, China

Reviewed by:
Xiaowei Zeng,
Sun Yat-sen University, China
Chengchao Chu,
Xiamen University, China

****Correspondence:***
Gang Liu
gangliu.cmitm@xmu.edu.cn
Hongwei Cheng
hongwei1026@hotmail.com

Specialty section:
This article was submitted to Biomaterials, a section of the journal Frontiers in Bioengineering and Biotechnology

Received: *24 May 2022*
Accepted: *03 June 2022*
Published: *21 June 2022*

Citation:
Peng Y, He P, Gao X, Liu G and Cheng H (2022) A Superstable Homogeneous Lipiodol-Nanoformulation to Overcome the Dilemma of Interventional Embolization Chemotherapy. Front. Bioeng. Biotechnol. 10:952194. doi: 10.3389/fbioe.2022.952194

INTRODUCTION

Hepatocellular carcinoma (HCC) is one of the leading cancer-related death, with morbidity and mortality rates increasing annually. As the most common treatment for HCC, transcatheter arterial embolization (TACE) plays an important role in HCC therapy (Singal et al., 2020). However, clinical practice has shown that the choice of embolic agents is limited by postoperative recanalization, non-targeted embolization, etc. (Chen et al., 2020b; Jiang et al., 2022). Furthermore, TACE also suffers from rapid drug release and insufficient therapeutic doses, which might contribute to drug resistance and poor therapeutic effects (Cao et al., 2021). Therefore, manufacture of the homogeneous drug dispersion in embolic agents is a revolutionary progress. Recently, He *et al.* reported a superstable homogeneous lipiodol-hydrophilic chemodrug formulation for TACE of HCC (He et al., 2022), which significantly enhanced the dispersion of chemotherapeutic drugs in lipiodol, thereby increasing the drug bioavailability of TACE in HCC patients and overcoming the shortcoming of rapid drug-releasee in clinic. Compared with the conventional surfactant emulsion strategy to increase drug dispersibility (Zhu et al., 2022), this superstable homogeneous intermixed formulation technology (SHIFT) is a green manufacture with any additions (Chen et al., 2020a; Cheng et al., 2020). And the chemotherapeutic drugs are assembled into nanostructures under the condition of cardon dioxide supercritical fluid. The specific nano-size effect offers the better dispersibility of chemotherapeutic drugs in lipiodol, suggesting this technology is universal in TACE. The chemotherapeutic drugs with nanostructures exhibit the better cellular uptake and sustained drug release properties. In general, this opinion prospects the interpretation of recent progress in the interventional embolization therapy of HCC, and focuses on the advantages of SHIFT technology in improving the stability of embolic reagents, improving the bioavailability of chemodrugs, and improving the prognosis of HCC.

THE DILEMMA OF TACE IN CLINICAL HCC

Recent studies reported over 900,000 new HCC global cases by 2020, and by 2025, over one million people are expected to suffer with HCC every year (Siegel et al., 2022). For many years, surgical resection and liver transplantation have proved as primary methods for curative HCC treatment. However, liver decompensation after hepatectomy is a great concern for surgeons. Small-

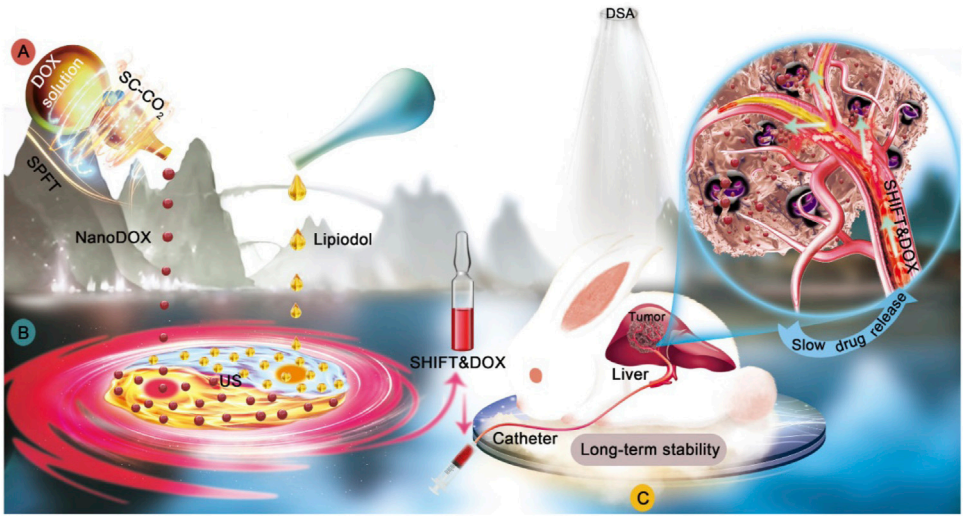

FIGURE 1 | Illustration of superstable homogeneous lipiodol-chemodrug formulation in TACE. **(A)** SPFT was applied to produce nanoDOX with a nanoscale size and excellent uniformity. **(B)** nanoDOX was homogeneously dispersed into lipiodol *via* ultrasonication to achieve the superstable homogeneous lipiodol-DOX formulation (SHIFT&DOX). **(C)** The SHIFT&DOX embolic formulation showed the sustained drug release and enhanced therapeutic effects. Reproduced with permission (He et al., 2022). Copyright 2022, Ivyspring International Publisher.

disseminated nidus or multi-center occurrences may exist before surgery, therefore the 5-year recurrence rate for HCC patients after surgery is close to 70%, and the 5-year survival rate is only 10% (Llovet et al., 2021). The long-term prognosis of HCC patients undergoing liver transplantation is superior to those patients with surgical resection. However, donor shortages often deprive HCC patients with optimal transplantation opportunities due to tumor progression. Therefore, main treatments for unresectable HCC patients are local ablation, chemotherapy, radiotherapy or interventional embolization, all of which are called palliative treatments. Among them, TACE is the most widely used in clinical practice.

In a normal liver, hepatic arterial blood supply accounts for approximately 25% and portal venous blood supply for approximately 75%, while in HCC tissue, hepatic artery blood supply accounts for approximately 90%, and portal vein blood supply is lower to 10% (Shiraishi et al., 2008). These blood flow parameters constitute the theoretical foundation of vascular interventional therapy. TACE exploits this by dissolving chemotherapeutic drugs, such as doxorubicin or carboplatin, in embolic agents and injecting them into tumor feeding arteries, causing serious tumor cytotoxicity, ischemia and hypoxia, while inhibiting and killing tumor cells (Wei and Zhang, 2021; Reig et al., 2022). Compared to systemic chemotherapy, TACE significantly increases drug concentrations in liver cancer tissue and reduces systemic adverse events. However, for unresectable HCC tumors with a diameter over 10 cm, these therapeutic effects remain largely unsatisfactory and may cause serious adverse reactions, including iodine oil ectopic embolism, oncolytic reactions, fever, liver abscess, bone marrow suppression after chemotherapy, and other risks (Kishore et al., 2020). One possible reason for this is that the current hand-emulsifier lipiodol with hydrophilic chemotherapy drugs such as doxorubicin, epirubicin, and fluorouracil, displaying the rapid drug release into systemic blood circulation after TACE (<30 min), which unfortunately elevate postoperative patient side effects and reduce therapeutic efficacy. Therefore, a novel technology is urgently required to stably disperse hydrophilic chemotherapeutic drugs in lipiodol to improve the therapeutic effects and safety of TACE treatments.

SUPERSTABLE HOMOGENEOUS INTERMIXED FORMULATION TECHNOLOGY FOR ENHANCED TACE

SHIFT was developed to stably disperse chemotherapeutic drugs in lipiodol, overcoming the above mentioned issues during TACE (**Figure 1**). This technology skillfully combined lipiodol and hydrophilic chemotherapeutic drugs to prepare an effective and superstable homogeneous lipiodol and doxorubicin hydrochloride mixture (SHIFT and DOX), which was verified in several animal models, including decellularized liver, N1S1 rat orthotopic liver tumor and VX2 rabbit orthotopic liver tumor, showing improved clinical transformation and application value.

Doxorubicin (DOX), a hydrophilic chemotherapeutic drug, was transformed into pure nano-doxorubicin by supercritical technology and then dispersed in a stable and uniform manner in the lipiodol with a simple low-power ultrasound. In addition to improving the stability of doxorubicin in lipiodol, the SHIFT and DOX formulation did not contain any additional additives. These benefits have ensured its safety and effectiveness, with great prospects in translational medicine. When compared with traditional lipiodol chemotherapy, this strategy significantly reduced chemotherapy levels reaching the systemic circulation, while ultra-high sustained-release properties were maintained for up to 21 days, thereby increasing local drug concentrations and anti-tumor efficacy.

Animal studies reported that SHIFT and DOX showed good drug-specific deposition and sustained drug-release effects, therapeutic effects, and safety in tumor areas. Therefore, SHIFT and DOX could address issues with drug burst release, poor stability, poor efficacy, poor repeatability, serious side effects in current conventional TACE. Additionally, for those patients who cannot undergo surgery, SHIFT and DOX could ameliorate the transformation efficiency of patients with large and advanced liver cancer, favoring HCC patients enduring curative tumor resection. Furthermore, for HCC patients with a high risk of tumor recurrence after surgery, retrospective studies have demonstrated that postoperative TACE treatment can reduce recurrence and prolong survival (Chen W. et al., 2020). Considering the better performance of SHIFT and DOX in nanoscale size, it is believed SHIFT and DOX could penetrate into tiny lesions and kill tumors, thereby reducing tumor recurrence and improving the prognosis of patients with large and advanced liver cancer.

DISCUSSION

With the application of nanotechnology in clinical cancer treatments, it has shown remarkable prospects in improving drug solubility, increasing drug bioavailability, enhancing therapeutic efficacy and reducing side effects. Nab paclitaxel is a good example of nanotechnology in cancer treatment, which combined paclitaxel with albumin protein to assemble into nanostructure, improving the water solubility of paclitaxel and avoiding the severe immune response caused by the addition of castor oil (Ma et al., 2021). Similar examples are irinotecan and mitoxantrone liposome complexes for the enhancement of tumor chemotherapy (Li et al., 2021). However, while utilizing nanotechnology to enhance the efficacy of drugs, the potential side effects of vector introduction are also worthy of vigilance. Therefore, pure drug nanomedicine has received more and more attention in recent years. On the one hand, it makes effective use of nanotechnology in drug delivery and efficacy enhancement, and on the other hand, it avoids potentials risks caused by the introduction of additional carriers. For the application, SHIFT technology is to exploit this mechanism of pure drug nano-assembly to prepare homogeneous lipiodol formulation.

In addition, SHIFT technology could also be used in other medical field fields. While not just used for mixing lipiodol and chemotherapeutics, it can be used for the superstable and uniform mixture of lipiodol and indocyanine green (ICG) to improve ICG fluorescence properties and guide the complete resection of liver cancer (Chen et al., 2020a; Zhang et al., 2021). Based on the SHIFT approach, it is believed that the superstable homogeneous lipiodol-hydrophilic drug can be applied to the interventional treatment of colorectal tumors and pancreatic tumor liver metastases, and even internal irradiation based on nuclides (Chen et al., 2022). In summary, the formulation of hydrophilic lipiodol chemotherapy drugs based on SHIFT technology has significant clinical perspectives and translational value for interventional embolization therapy. In future translational clinical applications, this technology would fill existing technology gaps and modify palliative treatment strategies for patients with advanced liver cancer.

AUTHOR CONTRIBUTIONS

YP and HC wrote the original manuscript, PH and XG conducted the literature analysis. HC and LG reviewed and edited the manuscript. All authors agreed to submit the final version of the article.

FUNDING

This work was supported by the Major State Basic Research Development Program of China (No. 2017YFA0205201), and the National Natural Science Foundation of China (NSFC, Nos 81925019 and U1705281).

REFERENCES

Cao, L., Zhu, Y., Wang, W., Wang, G., Zhang, S., and Cheng, H. (2021). Emerging Nano-Based Strategies against Drug Resistance in Tumor Chemotherapy. *Front. Bioeng. Biotechnol.* 9, 798882. doi:10.3389/fbioe.2021.798882

Chen, H., Cheng, H., Dai, Q., Cheng, Y., Zhang, Y., Li, D., et al. (2020a). A Superstable Homogeneous Lipiodol-ICG Formulation for Locoregional Hepatocellular Carcinoma Treatment. *J. Control. Release* 323, 635–643. doi:10.1016/j.jconrel.2020.04.021

Chen, H., Cheng, H., Wu, W., Li, D., Mao, J., Chu, C., et al. (2020b). The Blooming Intersection of Transcatheter Hepatic Artery Chemoembolization and Nanomedicine. *Chin. Chem. Lett.* 31, 1375–1381. doi:10.1016/j.cclet.2020.03.024

Chen, H., Teng, M., Zhang, H., Liang, X., Cheng, H., and Liu, G. (2022). Advanced Radionuclides in Diagnosis and Therapy for Hepatocellular Carcinoma. *Chin. Chem. Lett.* 33, 3371–3383. doi:10.1016/j.cclet.2022.03.079

Chen, W., Ma, T., Zhang, J., Zhang, X., Chen, W., Shen, Y., et al. (2020c). A Systematic Review and Meta-Analysis of Adjuvant Transarterial Chemoembolization after Curative Resection for Patients with Hepatocellular Carcinoma. *HPB* 22, 795–808. doi:10.1016/j.hpb.2019.12.013

Cheng, H., Yang, X., and Liu, G. (2020). Superstable Homogeneous Iodinated Formulation Technology: Revolutionizing Transcatheter Arterial Chemoembolization. *Sci. Bull.* 65, 1685–1687. doi:10.1016/j.scib.2020.06.029

He, P., Ren, E., Chen, B., Chen, H., Cheng, H., Gao, X., et al. (2022). A Super-Stable Homogeneous Lipiodol-Hydrophilic Chemodrug Formulation for Treatment of Hepatocellular Carcinoma. *Theranostics* 12, 1769–1782. doi:10.7150/thno.68456

Jiang, Y., Zhang, Y., Lu, Z., Wang, X., Bai, S., Chen, Y., et al. (2022). Liquid Embolic Agents for Interventional Embolization. *ChemPhysMater* 1, 39–50. doi:10.1016/j.chphma.2021.09.008

Kishore, S. A., Bajwa, R., and Madoff, D. C. (2020). Embolotherapeutic Strategies for Hepatocellular Carcinoma: 2020 Update. *Cancers (Basel)* 12 (4), 791. doi:10.3390/cancers12040791

Li, J., Zhou, S., Yu, J., Cai, W., Yang, Y., Kuang, X., et al. (2021). Low Dose Shikonin and Anthracyclines Coloaded Liposomes Induce Robust Immunogenetic Cell Death for Synergistic Chemo-Immunotherapy. *J. Control. Release* 335, 306–319. doi:10.1016/j.jconrel.2021.05.040

Llovet, J. M., Kelley, R. K., Villanueva, A., Singal, A. G., Pikarsky, E., Roayaie, S., et al. (2021). Hepatocellular Carcinoma. *Nat. Rev. Dis. Prim.* 7, 6. doi:10.1038/s41572-020-00240-3

Ma, Y., Yu, S., Ni, S., Zhang, B., Kung, A. C. F., Gao, J., et al. (2021). Targeting Strategies for Enhancing Paclitaxel Specificity in Chemotherapy. *Front. Cell Dev. Biol.* 9, 626910. doi:10.3389/fcell.2021.626910

Reig, M., Forner, A., Rimola, J., Ferrer-Fàbrega, J., Burrel, M., Garcia-Criado, Á., et al. (2022). BCLC Strategy for Prognosis Prediction and Treatment Recommendation: The 2022 Update. *J. Hepatol.* 76, 681–693. doi:10.1016/j.jhep.2021.11.018

Shiraishi, J., Sugimoto, K., Moriyasu, F., Kamiyama, N., and Doi, K. (2008). Computer-aided Diagnosis for the Classification of Focal Liver Lesions by Use of Contrast-Enhanced Ultrasonography. *Med. Phys.* 35, 1734–1746. doi:10.1118/1.2900109

Siegel, R. L., Miller, K. D., Fuchs, H. E., and Jemal, A. (2022). Cancer Statistics, 2022. *CA A Cancer J. Clin.* 72, 7–33. doi:10.3322/caac.21708

Singal, A. G., Lampertico, P., and Nahon, P. (2020). Epidemiology and Surveillance for Hepatocellular Carcinoma: New Trends. *J. Hepatology* 72, 250–261. doi:10.1016/j.jhep.2019.08.025

Wei, Z.-Q., and Zhang, Y.-W. (2021). Transcatheter Arterial Chemoembolization Followed by Surgical Resection for Hepatocellular Carcinoma: A Focus on its Controversies and Screening of Patients Most Likely to Benefit. *Chin. Med. J. Engl.* 134, 2275–2286. doi:10.1097/cm9.0000000000001767

Zhang, Y., Cheng, H., Chen, H., Xu, P., Ren, E., Jiang, Y., et al. (2021). A Pure nanoICG-Based Homogeneous Lipiodol Formulation: toward Precise Surgical Navigation of Primary Liver Cancer after Long-Term Transcatheter Arterial Embolization. *Eur. J. Nucl. Med. Mol. Imaging* (in press). doi:10.1007/s00259-021-05654-z

Zhu, J., Chu, C., Li, D., Zhang, Y., Cheng, Y., Lin, H., et al. (2022). Superior Fluorescent Nanoemulsion Illuminates Hepatocellular Carcinoma for Surgical Navigation. *Front. Bioeng. Biotechnol.* 10, 890668. doi:10.3389/fbioe.2022.890668

Conflict of Interest: The authors declare that the research was conducted in the absence of any commercial or financial relationships that could be construed as a potential conflict of interest.

The reviewer CC declared a shared parent affiliation with the authors to the handling editor at the time of review.

Publisher's Note: All claims expressed in this article are solely those of the authors and do not necessarily represent those of their affiliated organizations, or those of the publisher, the editors and the reviewers. Any product that may be evaluated in this article, or claim that may be made by its manufacturer, is not guaranteed or endorsed by the publisher.

Copyright © 2022 Peng, He, Gao, Liu and Cheng. This is an open-access article distributed under the terms of the Creative Commons Attribution License (CC BY). The use, distribution or reproduction in other forums is permitted, provided the original author(s) and the copyright owner(s) are credited and that the original publication in this journal is cited, in accordance with accepted academic practice. No use, distribution or reproduction is permitted which does not comply with these terms.

frontiers | Frontiers in Bioengineering and Biotechnology

ORIGINAL RESEARCH
published: 12 July 2022
doi: 10.3389/fbioe.2022.931830

Thermo- and Light-Responsive Polymer-Coated Magnetic Nanoparticles as Potential Drug Carriers

Guihua Cui[1,2], Hao Wang[1†], Shengsen Long[1], Tianshuo Zhang[1], Xiaoyu Guo[3], Shuiying Chen[2], Toyoji Kakuchi[4], Qian Duan[2] and Donghai Zhao[1]**

[1]Science and Technology Division, Jilin Medical University, Jilin, China, [2]Department of Materials Science and Engineering, Changchun University of Science and Technology, Jilin, China, [3]Jilin Vocational College of Industry and Technology, Jilin, China, [4]Division of Biotechnology and Macromolecular Chemistry, Graduate School of Engineering, Hokkaido University, Sapporo, Japan

OPEN ACCESS

Edited by:
Junqing Wang,
Sun Yat-sen University, China

Reviewed by:
Shuangxi Xing,
Northeast Normal University, China
Sanjun Shi,
Chengdu University of Traditional Chinese Medicine, China

***Correspondence:**
Qian Duan
duanqian88@hotmail.com
Donghai Zhao
cuiyuhan1981_0@sohu.com

†These authors have contributed equally to this work

Specialty section:
This article was submitted to Biomaterials, a section of the journal Frontiers in Bioengineering and Biotechnology

Received: 29 April 2022
Accepted: 13 June 2022
Published: 12 July 2022

Citation:
Cui G, Wang H, Long S, Zhang T, Guo X, Chen S, Kakuchi T, Duan Q and Zhao D (2022) Thermo- and Light-Responsive Polymer-Coated Magnetic Nanoparticles as Potential Drug Carriers. Front. Bioeng. Biotechnol. 10:931830. doi: 10.3389/fbioe.2022.931830

A series of thermo- and light-responsive copolymers of poly (*N*-isopropylacrylamide) (PNIPAM) and 6-[4-(4-methoxy phenyl azo)-phenoxyl-hexyl methacrylate) (AzoMA) (PNIPAM-b-PAzoMA) were synthesized *via* reversible addition–fragmentation chain transfer (RAFT) radical polymerization. The resulting copolymers had a narrow molecular weight distribution range of 1.06–1.24, in which M_n changed regularly with the monomer concentration. Subsequently, the diblock copolymers were successfully modified on the surface of iron oxide nanoparticles through the interaction between the chemical bonds to prepare Fe_3O_4@(PNIPAM-b-PAzoMA) nanoparticles. The size of fabricated nanoparticles with excellent thermo-sensitivity and photo-sensitivity was controlled at about 40–50 nm. Cell viability assays suggested that the nanoparticles showed no significant cytotoxicity and potential drug delivery in the tumor microenvironment.

Keywords: Poly(N-isopropylacrylamide) (PNIPAM), magnetic nanoparticles, thermo-sensitive, light-sensitive, Poly(6-[4-(4-methoxy phenyl azo)-phenoxyl- hexyl methacrylate]) (PAzoMA)

1 INTRODUCTION

The cancer burden had risen to 19.3 million new cases and 10.0 million cancer deaths in 2020 (IARC, 2020). Cancer is characterized by highly metastatic and recurrent, traditional treatments such as surgery, chemotherapy, and radiation and is difficult to cure completely (Couzin-Frankel, 2013; Gotwals et al., 2017). Therefore, continuous endeavors by the researchers are being made to develop new low-cost and effective solutions for cancer treatments with few side effects, high specificity, and anti-metastasis (Lu et al., 2020; Baggiolini et al., 2021; Eberhardt et al., 2021). Polymeric nanomedicine has become crucial in clinical application with its precise and efficient targeting therapy of tumors (Farokhzad and Langer, 2006; Hawkins et al., 2008; Girase et al., 2019; Chen et al., 2021). A few drug-carrying polymeric nanoparticles (NPs) have been used in preclinical oncology treatment (Tong et al., 2012; Li et al., 2018; He et al., 2019). Stimulus-responsive NP drug delivery systems have attracted extensive attention because of their specificity, selectivity, and efficacy in tumor tissues and biocompatibility for normal cells (Karimi et al., 2016; Jia et al., 2018). The endogenous and exogenous (or external) stimuli could induce drug release from polymer vesicles. External stimulus-responsive factors included pH, magnetism, temperature, ultrasound, and light

(Satarkar and Hilt, 2008; Brazel, 2009; Schroeder et al., 2009; Ge et al., 2012; Huo et al., 2014; Liu et al., 2014; Shanmugam et al., 2014; Olejniczak et al., 2015; Rwei et al., 2015; Alimoradi et al., 2016). Slight changes in the external environment could trigger the release of the polymer vesicles to the drug. The integration of multiple functions and various chemical nature of compounds to improve their functionalities was an innovative approach to obtaining nanoscale drug carriers.

Light-responsive nanocarriers have attracted extensive attention in the field of drug delivery (Olejniczak et al., 2015; Rwei et al., 2015). Using light as a trigger has many beneficial advantages. Light is easy to manipulate and make tiny adjustments. The photo-responsive nano-carrier acts as a biofriendly material, which could achieve accurate control of the location, time, and dose of released species (Sortino, 2012). The first example is azobenzene units, which could be handily transformed between *trans*- and *cis*-configuration to release encapsulated antineoplastic drugs. There are so many distinctions of azobenzene derivatives in physical, chemical, optical, and biological properties which are caused by *E*-to-*Z* isomerization. It is the reason that azobenzene compounds could be utilized to tune the characteristics of host materials. A growing number of studies were using azobenzene derivatives covalently linked to polymers as photoactivated drug delivery systems in NPs formed *via* self-assembly of polymers (Shibaev et al., 2003; Wang et al., 2015; Zhang et al., 2019; Shi et al., 2021a; Yao et al., 2021). It was reasonable to expect that as soon as the hydrophobic forces and π-π interactions are removed under UV irradiation, the vesicles with drugs dominated by electrostatic forces would expand rapidly to open the "gate" to achieve drug release (Yao et al., 2021).

Fe_3O_4 NPs are excellent nanoparticles for cancer therapy, which have been approved by the U.S. Food and Drug Administration (FDA) for the clinical treatment due to magnetic targeting and T_2-weighted magnetic resonance imaging (MRI) (Ge et al., 2018). However, individual Fe_3O_4 NPs have no antitumor effect. Thus, composite materials based on ions have emerged, especially anti-tumor composites. In recent years, many substances have been used to combine with Fe_3O_4 to prepare antitumor nanoparticles, such as oxide-graphene (Lin et al., 2014), poly (ethylene glycol)-block-poly (lactic-co-glycolic acid) copolymer-encapsulated (Liu et al., 2022), and polymers (Swain et al., 2015; Du et al., 2017; Shi et al., 2021b; Ndebele et al., 2021). These composite Fe_3O_4 NPs showed great potential for cancer therapy. In the past few decades, the temperature sensitivity of poly (*N*-isopropylacrylamide) (PNIPAM) has been utilized to successfully synthesize so many drug nanocarriers with temperature responsiveness and high loading capacity. PNIPAM could respond to changes in the microenvironment temperature, which caused changes in the carrier structure and interactions with cells to achieve temperature-sensitive drug delivery and release (Liu et al., 2015; Bathfield et al., 2016; Nguyen et al., 2016). In our previous study, a series of biomaterials containing PNIPAM were also synthesized, and their lower critical solution temperature (LCST) was close to human body temperature (Cui G. et al., 2020; Cui G. H. et al., 2020). In this work, we took advantage of the thermo- and light-responsive properties of the polymer to synthesize polymer-coated magnetic nanoparticles, which may be used for drug delivery in the tumor microenvironment.

2 MATERIALS AND METHODS

2.1 Materials and Instrumentation

N- isopropylacrylamide (Aldrich, 98%) was recrystallized twice from a hexane/benzene mixture (3/2, v/v). 2,2′-Azobis (2-methylpropionitrile) (AIBN) (J&K chemical, 98%), 1,3,5-trioxane (Sigma-Aldrich, 99%), 1-dodecanethiol (Sigma-Aldrich, ≥98%), tetrabutylammonium bromide (Sigma-Aldrich, 99%), carbon disulfide (Sigma-Aldrich, 99.9%), p-anisidine (Aladdin, 99%), 1,6-dibromohexane (Aladdin, 99%), phenol (Aladdin, 99%), methacrylic acid (J&K chemical, 98%), and MTT (3-[4,5-dimethylthiazol-2-yl]-2,5-diphenyltetrazolium were purchased from Acros. Human breast cancer cell (MCF-7) culture and NCTC clone 929 (L-929) were purchased from the Type Culture Collection of the Chinese Academy of Sciences, Shanghai.

The ^{1}H nuclear magnetic resonance (NMR) spectra of polymers in $CDCl_3$ were obtained on a Varian Unity 400 NMR spectrometer. The molecular weights (M_n) and polydispersity (M_w/M_n) were measured by gel permeation chromatography (GPC) using a Waters 510 pump and a Model 410 differential refractometer at 25°C. The LCSTs of the polymer solutions were determined by turbidimetry, using a Shimadzu-2600 UV-Vis spectrophotometer with a heating rate of 0.1°C·min^{-1}. FTIR spectra were recorded on a Shimadzu IR-8400S spectrometer. The average particle size and size distribution of the nanoparticles were characterized by dynamic light scattering (DLS) with a Malvern470 instrument at a fixed scattering angle of 90°, after being filtered by 0.45-μm Millipore filters. The scanning electron microscopy (SEM) images were obtained with JEOL JSM-6701SF. The morphologies of the nanoparticles were determined by transmission electron microscopy (TEM) with JEOL JEM-2100. Powder X-Ray Diffraction (XRD) was performed by using an X′-Pert PRO Philips X-ray。diffractometer using Cu radiation (wavelength λ is 1.514056 *A*) in the 2θ range of 10 ~100° with a scan rate of 20°/min. X-ray photoelectron spectra (XPS) were examined on a PHI-5702 instrument using Mg Ka radiation with a pass energy of 29.35 eV. The optical density (OD) was measured at 570 nm with a microplate reader, model 550 (Bio-Rad, United States). Cell viability was determined as a percentage of the negative control (untreated cells).

2.2 General Procedure for the Thermo- and Light-Responsive Block Polymer Synthesis

2.2.1 Synthesis of Dual-responsive Block Polymers

The procedure of AzoMA synthesis is shown in **Supplementary Scheme S1**. $NaNO_2$ (3.0094 g, 43.6 mmol) was dissolved in deionized water (20 ml). Then, it was added to the hydrochloric acid solution of p-anisidine (5.0984 g and 41.4 mmol) solution and stirred at 0°C for 2 h. Miscible liquids were shifted to sodium hydroxide solution (4 g and 0.1 mol) of phenol (4.0902 g and 43.4 mmol) and stirred at 0°C for 2 h, and the pH was adjusted to neutral to obtain 4-hydroxy-4′-

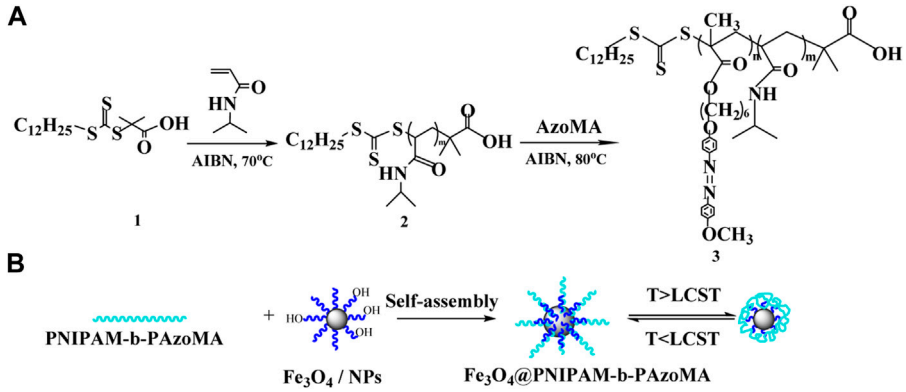

SCHEME 1 | Fabrication strategy for thermo- and light-responsive polymer-coated magnetic nanoparticles.

methoxy-azobenzene. The aforementioned product (2.43 g and 10 mmol) and 1, 6-dibromohexane (14.67 g and 53.6 mmol) and anhydrous K_2CO_3 (7.3922 g and 53.6 mmol) were added to acetone (100 ml) and stirred at 75°C for 24 h. The mixture was precipitated in petroleum ether (30~60°C) and recrystallized by thermal filtration in ethyl acetate twice to obtain 1-bromo-6 -(4-methoxyazobenzene-4′-oxygen) hexane.

Methacrylic acid (0.2004 g, 2 mmol) and $KHCO_3$(0.1002 g and 1 mmol) were dissolved in *N*,*N*-dimethylformamide(10 ml); then, 1-bromo-6-(4-methoxyazobenzene-4′-oxygen) hexane(0.3912 g, 1.09 mmol) was added dropwise under whisk and stirred at 65°C for 4 h. The pure AzoMA was acquired by column chromatography (the results are shown in **Supplementary Figures S1, S2**).

2.2.2 Synthesis of PNIPAM-b-PAzoMA

PNIPAM-b-PAzoMA was synthesized using NIPAM and AzoMA as monomers by RAFT, as shown in **Scheme 1**. There were three steps for the synthesis of block copolymers. First, *S*-1-dodecyl-*S*′-(*α*,*α*′-dimethyl-*α*′′-acetic acid) trithio-carbonate (DMP) (1) was synthesized as a chain transfer agent (CTA). DMP was synthesized by a method derived from Lai et al. (2002), and we have reported in previous research (Cui G. et al., 2020). Subsequently, the synthesis of macromolecular chain transfer agents 2) *via* reversible addition–fragmentation chain transfer (RAFT) was mentioned in our study (Cui G. et al., 2020).

Finally, for the synthesis of PNIPAM-b-PAzoMA, a mixture of AzoMA (0.132 g and 0.5 mmol), macro CTA (152.7 mg and 0.015 mmol), 1,3,5-trioxane (50.44 mg and 0.56 mmol), and AIBN (1.70 mg and 0.01 mmol) was added to anhydrous DMF: H_2O (7.5 ml and 95:5, v/v) and was sealed on the middle side of an H-shaped ampoule glass and stirred. Nitrogen was bubbled through both mixtures for 20 min to remove any oxygen. Three freeze-pump-thaw cycles were performed to degas the solutions. The ampoule was placed at 80°C for 24 h. Polymerization was quenched by exposing the solution to air. The solution was concentrated under a vacuum, and the polymer was precipitated into petroleum ether (30~60°C) thrice; then, the product was dried under a vacuum.

2.3 Synthesis of Polymer-Coated Magnetic Nanoparticles

Fe_3O_4 nanoparticles were synthesized by chemical coprecipitation (Wu et al., 2012). The details are mentioned in our report (Cui G. H. et al., 2020). The Fe_3O_4 nanoparticles were dissolved in *N*, *N*-dimethylformamide (20 ml) and dispersed by ultrasonic concussion. Then PNIPAM-b-PAzoMA (0.3 mmol), EDC·HCl (10 mg and 0.052 mmol), and DMAP (7.1 mg and 0.058 mmol) were added successively under stirring and stirred at 80°C in an oil bath for 24 h. The compound was washed continuously with excess methanol in order to remove the unreacted polymer after magnetic separation and dried under vacuum to obtain polymer-coated magnetic nanoparticles.

2.4 Biocompatibility Study

The cell viabilities of macro-CTA, PNIPAM-b-PAzoMA, and Fe_3O_4@PNIPAM-b-PAzoMA nanoparticles were preliminarily investigated by using NCTC clone 929 (L-929) and human breast cancer cell (MCF-7) culture. Specific details were referred to in our previous studies (Cui G. H. et al., 2020). Six replicate wells were used for the control and test concentrations for each sample. The optical density was measured using a microplate reader at 492 nm. The cell viability (%) was calculated according to the following **Eq. 1**:

$$\text{Cell viability}\,(\%) = \left(A_{\text{sample}}/A_{\text{control}}\right) \times 100\%, \qquad (1)$$

where A_{sample} was the absorbance of the cells incubated in DMEM and mixture, and A_{control} was the absorbance of the cells incubated in DMEM.

3 RESULTS AND DISCUSSION

3.1 Architecture Analysis

The morphologies of Fe_3O_4@PNIPAM-b-PAzoMA nanoparticles were investigated by SEM (**Figure 1A**) and TEM (**Figure 1B**). The diameter of the Fe_3O_4@PNIPAM-b-PAzoMA

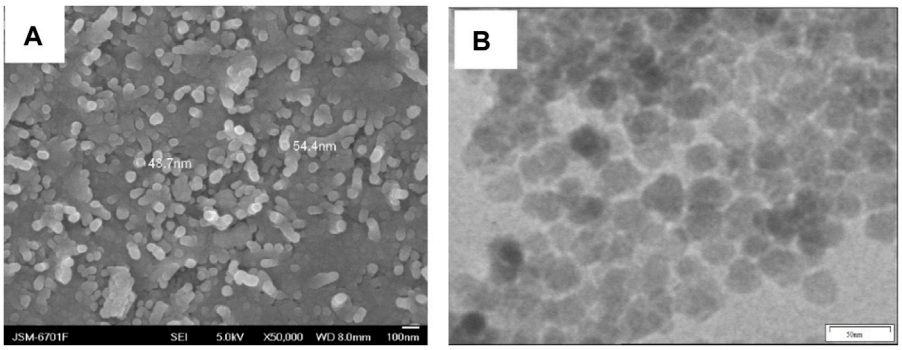

FIGURE 1 | SEM and TEM images of Fe_3O_4@ PNIPAM-b-PAzoMA nanoparticles.

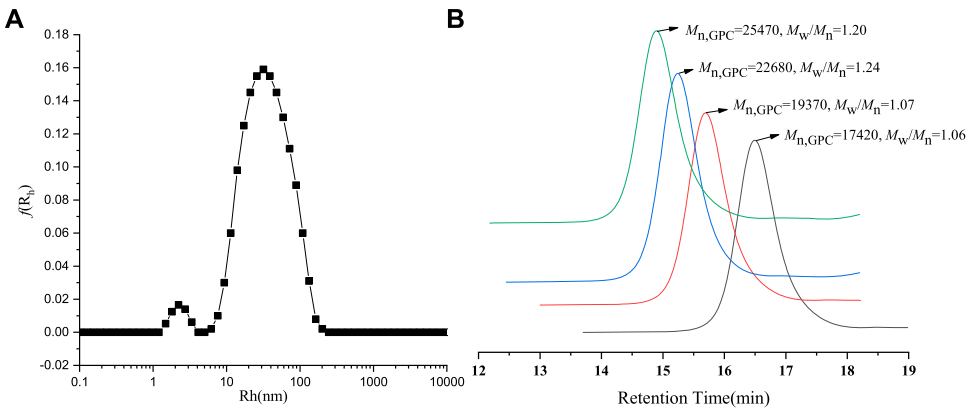

FIGURE 2 | (A) DLS spectrogram for Fe_3O_4@ PNIPAM-b-PAzoMA nanoparticles. **(B)** GPC traces of PNIPAM-b-PAzoMA.

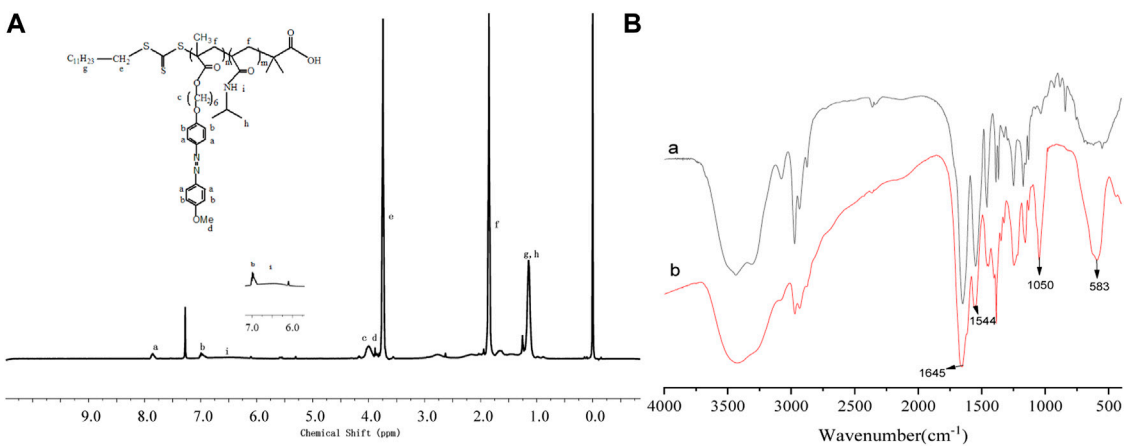

FIGURE 3 | [1]HNMR spectra of PNIPAM-b-PAzoMA **(A)**, FT-IR spectra of PNIPAM-b-PAzoMA, and Fe_3O_4@PNIPAM-b-PAzoMA nanoparticles **(B)**.

nanoparticles ranged from 40 to 50 nm. The size was basically identical to the intensity-average hydrodynamic radius distribution f (R_h) which was measured by DLS in **Figure 2A**. The nanoparticles had an almost spherical shape since the polymer shells of Fe_3O_4@PNIPAM-b-PAzoMA nanoparticles were mostly formed by esterification.

The PNIPAM-b-PAzoMA was synthesized by the different feed ratios of AzoMA/macro-CTA/AIBN, which could obtain

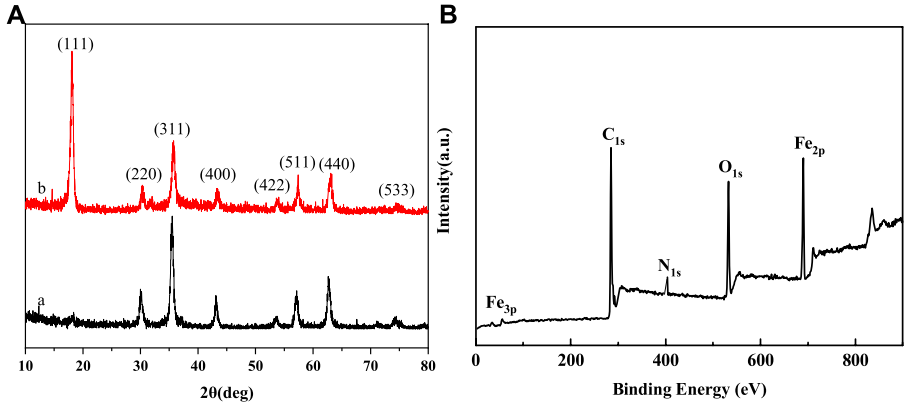

FIGURE 4 | (A) XRD spectra of (a) bare Fe_3O_4 (b) Fe_3O_4@PNIPAM-b-PAzoMA nanoparticles and **(B)** XPS spectra of Fe_3O_4@PNIPAM-b-PAzoMA nanoparticles.

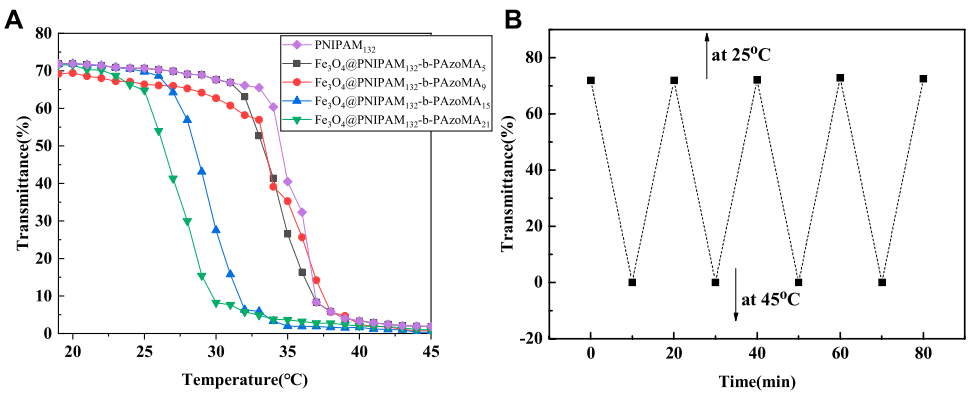

FIGURE 5 | (A) Cloud point curve for the aqueous solution of macro-CTA and Fe_3O_4@PNIPAM-b-PAzoMA nanoparticles. **(B)** Plots of optical transmittance as a function of temperature for Fe_3O_4@(PNIPAM-b-PAzoMA) aqueous solution with the concentration of 1 mg/ml (10 min for each temperature four heating/cooling cycles between 25 and 45°C).

products that had a narrow molecular weight distribution range of 1.06–1.20, as shown in **Figure 2B** and **Supplementary Table S2**. The GPC traces of the block copolymer demonstrated a clean shift toward a lower elution volume. The macro-CTA was a polymer containing 132 PNIPAM units because it had the highest LCST among many macromolecular chain initiators prepared by our study.

The architecture of the PNIPAM-b-PAzoMA and Fe_3O_4@PNIPAM-b-PAzoMA nanoparticles was authenticated by FT-IR spectra and ^{1}HNMR. From **Figure 3A**, compared with AzoMA (**Supplementary Figure S1**), a characteristic signal of PNIPAM representing nitrogen atoms was shifted to 6.53 ppm. The peaks at 7.85, 6.98, 3.99, and 3.89 ppm were the characteristic signals of AzoMA. It was seen clearly that the new characteristic peak of PNIPAM at 3,286 cm^{-1} was assigned to the stretching vibration (ν_{N-H}) of the acylamino group in **Figure 3B**. The band at 1,645 $fcm^{-1}$was ascribed to amide I [mainly the carbonyl stretching vibration ($\nu_{C=O}$)], and the band at 1,544cm^{-1} was ascribed to amide II [mainly the N–H bending vibration (δ_{N-H})], which has overridden the characteristic absorption peaks of AzoMA because of its high content of PNIPAM in the polymer. Two characteristic peaks appeared in the Fe_3O_4@PNIPAM-b-PAzoMA nanoparticles, which were located in 1,080 cm^{-1} and 583cm^{-1}, and possessed the ester acid bond and Fe-O band.

XPS and XRD spectra were used to further investigate the composition of the nanoparticles. **Figure 4A** showed the XRD pattern of the bare Fe_3O_4 and Fe_3O_4@PNIPAM-b-PAzoMA nanoparticles. The characteristic diffraction peaks for Fe_3O_4 (2θ = 18.07, 30.32, 35.68, 43.32, 53.78, 57.38, 62.89, and 74.56) marked by their indices on (111), (220), (311), (400), (422), (511), (440), and (533) crystal planes can be observed. All the peak positions were basically consistent with the standard data of the Fe_3O_4 structure (JCPDS card file No. 85–1,436) (Cullity, 1978). The peak position did no't change, but the peak intensity changed differently. The dispersion of nanoparticles in the solution was different because of the effect of the surface polymer. In **Figure 4B**, peaks at the binding energies (BEs) of 284.39, 403, and 533.23eV were corresponding to C_{1s}, N_{1s}, and O_{1s}, which were from the copolymer. The BE values of about 55.86eV and 688eV were ascribed to Fe_{3p} and Fe_{2p}. These results indicated that

TABLE 1 | Summarized data on Fe3O4@PNIPAM-b-PAzoMA.

Sample	Amount of AzoMA (mol%)	LCST (%) before irradiation (oC)	LCST after irradiation (oC)	Δ (°C)LCST (oC)
F (°C)e3O4@(PNIPAM132-b-PAzoMA5)	3.6	31.5	31.8	0.3
Fe3O4@(PNIPAM132-b-PAzoMA9)	6.4	30	30.9	0.9
Fe3O4@(PNIPAM132-b-PAzoMA15)	10.2	26.9	29.8	2.9
Fe3O4@(PNIPAM132-b-PAzoMA21)	13.7	25	29	4

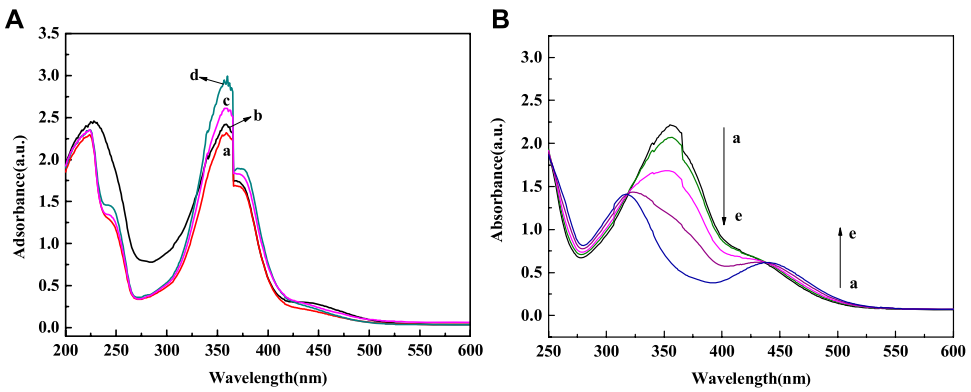

FIGURE 6 | (A) Spectral changes of Fe_3O_4@PNIPAM-b-PAzoMA in aqueous solution during UV irradiation (365 nm, 8 W) (a) Fe_3O_4@$PNIPAM_{132}$-b-$PAzoMA_5$, (b) Fe_3O_4@$PNIPAM_{132}$-b-$PAzoMA_9$, (c) Fe_3O_4@$PNIPAM_{132}$-b-$PAzoMA_{15}$, and (d)Fe_3O_4@$PNIPAM_{132}$-b-$PAzoMA_{21}$. **(B)** Spectral changes of Fe_3O_4@$PNIPAM_{132}$-b-$PAzoMA_{21}$ under irradiation time: (a) 0 min, (b) 5 min, (c) 10 min, (d) 15 min, and (e) 20 min.

the copolymer was successfully grafted onto the exterior surface of the Fe_3O_4 nanoparticles.

3.2 Thermo- and Light- Responsivity of Nanoparticles

It was found that the LCST of macro-CTA was 33.9°C in **Figure 5A**. It was higher than the homopolymer PNIPAM due to the hydrophilic carboxyl group of the macro-CTA. The LCSTs of all Fe_3O_4@PNIPAM-b-PAzoMA nanoparticles were lower than those of macro-CTA. This might be caused by the hydrophobic interaction of AzoMA in the nanoparticles. Also, the content of AzoMA in nanoparticles was inversely proportional to LCST, as shown in **Supplementary Figure S3**.

The effect of AzoMA's content on the LCST of the polymer was also reflected in the change of LCST of nanoparticles before and after UV irradiation, as shown in **Table 1**. The reason for this phenomenon was that the azo group of AzoMA was in a low dipole moment of the trans configuration without UV irradiation, and the polarity of AzoMA was weak, and this resulted in the strong hydrophobicity of AzoMA, and the LCST of the nanoparticles was lower than that of the macro-CTA. After UV irradiation, the azo group underwent a trans-cis transition. Compared with the trans configuration, the dipole moment of the azo group in the cis configuration was much higher, and the polarity of the AzoMA was also increased so that the hydrophilicity of nanoparticles was significantly enhanced. Another possible reason was that the azo of AzoMA in the trans configuration was a planar configuration. Compared with the cis structure, the superposition between molecules was more likely to occur so as to enhance the hydrophobic association ability, which was manifested by the increased phase transition temperature of the product after UV irradiation. After the aqueous solution of the sample irradiated by UV light was placed in the shade or exposed to visible light, its LCST returned to the temperature before UV irradiation. This was due to a cis-trans configuration transition of the azo group in **Figure 5B**.

Figure 6 showed the UV spectrum changes of Fe_3O_4@PNIPAM-b-PAzoMA aqueous solutions with different contents of AzoMA that were irradiated by UV light. In the **Figure 6A**, the absorbance was proportional to the content of AzoMA. The sample showed a strong absorption peak at 358 nm, while the absorption peak at 450 nm was relatively weak. This was because AzoMA mainly with its trans configuration under such conditions, and the trans configuration of azobenzene was relatively low. Therefore, this study focused on Fe_3O_4@PNIPAM-b-PAzoMA nanoparticles with high AzoMA contents. However, in **Figure 6B**, the characteristic absorption peak of AzoMA's cis configuration at 450 nm increased with the extension of UV irradiation time. This was because the azo groups in AzoMA gradually changed from trans configuration to cis configuration with the extension of UV irradiation time.

3.3 Thermostability and Magnetism of Nanoparticles

The thermogravimetric analysis (TG) is shown in **Figure 7**. We could clearly determine that below 600°C, after grafting

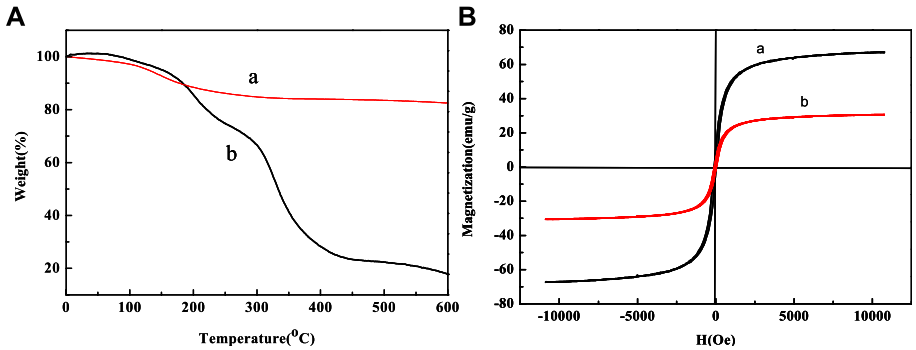

FIGURE 7 | (A) TG curves of (a) Fe_3O_4 and (b) Fe_3O_4@PNIPAM-b-PAzoMA and **(B)** hysteresis loops of (a)bare Fe_3O_4 nanoparticles and (b)Fe_3O_4@PNIPAM-b-PAzoMA nanoparticles at room temperature.

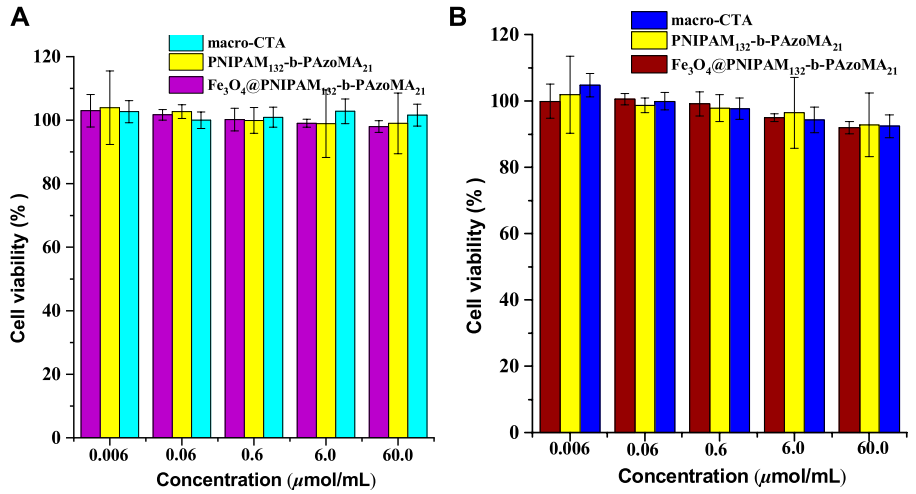

FIGURE 8 | Cell viability of **(A)** the L-929 cells and **(B)** the MCF-7 cells incubated with the samples (macro-CTA, PNIPAM-b-PAzoMA, and Fe_3O_4@PNIPAM-b-PAzoMA nanoparticles), over a range of sample concentrations from 0.006 to 60 μmol/ml by MTT assay for 48 h.

PNIPAM-b-PAzoMA onto the surface of the Fe_3O_4@PNIPAM-b-PAzoMA nanoparticles, the weight loss was about 56%, while only about 7% of weight loss for bare Fe_3O_4 nanoparticles. Compared with bare Fe_3O_4 nanoparticles, the weight loss of Fe_3O_4@PNIPAM-b-PAzoMA is generally concentrated in three stages which were 70°C~150°C, 150°C~300, and 300°C~500°C. In the first phase, the quality loss was about 5%, which was roughly consistent with the loss in 1), and this value was identified as the loss of Fe_3O_4. The mass loss in the second phase was mainly due to the thermal decomposition of PAzoMA. The weight loss in the third period was relatively large, especially due to the thermal decomposition of PNIPAM in the polymer, which was basically consistent with the data measured by GPC.

Figure 7B shows the hysteresis graph of Fe_3O_4 and Fe_3O_4@PNIPAM-b-PAzoMA nanoparticles. Due to the small particle size, the saturation magnetization (Ms) of Fe_3O_4 was about 68.02 emu/g. The Ms of Fe_3O_4@PNIPAM-b-PAzoMA nanoparticles decreased significantly, which was 30.01 emu/g. This was because polymer-coated Fe_3O_4 changed the magnetic anisotropy and increased the directional obstruction on the surface. Fe_3O_4@PNIPAM-b-PAzoMA nanoparticles showed no coercivity, so we could judge that the nanoparticles had a certain degree of super-paramagnetism.

3.4 Assessment of the Cell Viability

The cytotoxicity study on normal cells (L-929, with high activity) and tumor cells (MCF-7, with insensitive to apoptosis induced by various chemotherapeutic drugs) was carried out to investigate the preliminary biocompatibility of the resulting Fe_3O_4@PNIPAM-b-PAzoMA nanoparticles in **Figure 8**. MTT studies showed that macro-CTA, PNIPAM-b-PAzoMA, and Fe_3O_4@PNIPAM-b-PAzoMA nanoparticles had very low toxicity to L-929 cells and MCF-7 cells, and the cell survival rate remained above 80% even at sample concentrations up to 60 μmol/ml.

4 CONCLUSION

In this study, the thermo- and light-responsive polymer-coated magnetic nanoparticles were synthesized. The size of the Fe_3O_4@PNIPAM-b-PAzoMA nanoparticles was about 40–50 nm. Fe_3O_4@PNIPAM-b-PAzoMA nanoparticles had excellent temperature sensitivity, photosensitivity, thermostability, and super-paramagnetism and no significant cytotoxicity. Fe_3O_4@PNIPAM-b-PAzoMA may be used for good drug delivery in the tumor microenvironment and for potential antitumor therapy.

DATA AVAILABILITY STATEMENT

The original contributions presented in the study are included in the article/**Supplementary Material**; further inquiries can be directed to the corresponding authors.

AUTHOR CONTRIBUTIONS

All authors listed have made a substantial, direct, and intellectual contribution to the work and approved it for publication.

FUNDING

We are grateful to the Jilin science and technology department, science and technology development project No. 20200201098JC, the Jilin Province Education Department the Science and Technology development project (Nos. JJKH20170415KJ, JJKH20191059KJ, JJKJ20200461KJ, and JJKH20220469KJ), the National College Student Innovation Training Program (202013706063), the Jilin University Student Innovation Program (S202113706036), and Jilin province science and technology project of traditional Chinese medicine (2022088), for financial support.

ACKNOWLEDGMENTS

The authors would like to thank all reviewers of this article for their comments and suggestions.

SUPPLEMENTARY MATERIAL

The Supplementary Material for this article can be found online at: https://www.frontiersin.org/articles/10.3389/fbioe.2022.931830/full#supplementary-material

REFERENCES

Alimoradi, H., Matikonda, S. S., Gamble, A. B., Giles, G. I., and Greish, K. (2016). Hypoxia Responsive Drug Delivery Systems in Tumor Therapy. *Curr. Pharm. Des.* 22 (19), 2808–2820. doi:10.2174/1381612822666160217130049

Baggiolini, A., Callahan, S. J., Montal, E., Weiss, J. M., Trieu, T., Tagore, M. M., et al. (2021). Developmental Chromatin Programs Determine Oncogenic Competence in Melanoma. *Science* 373, 1–10. doi:10.1126/science.abc1048

Bathfield, M., Reboul, J., Cacciaguerra, T., Lacroix-Desmazes, P., and Gérardin, C. (2016). Thermosensitive and Drug-Loaded Ordered Mesoporous Silica: A Direct and Effective Synthesis Using PEO-B-PNIPAM Block Copolymers. *Chem. Mat.* 28 (10), 3374–3384. doi:10.1021/acs.chemmater.6b00595

Brazel, C. S. (2009). Magnetothermally-responsive Nanomaterials: Combining Magnetic Nanostructures and Thermally-Sensitive Polymers for Triggered Drug Release. *Pharm. Res.* 26 (3), 644–656. doi:10.1007/s11095-008-9773-2

Chen, J., Wang, X., Yuan, Y., Chen, H. T., Zhang, L. P., Xiao, H. H., et al. (2021). Exploiting the Acquired Vulnerability of Cisplatin-Resistant Tumors with a Hypoxia-Amplifying DNA Repair-Inhibiting (HYDRI) Nanomedicine. *Sci. Adv.* 7, 13–25. doi:10.1126/sciadv.abc5267

Couzin-Frankel, J. (2013). Breakthrough of the Year 2013. Cancer Immunotherapy. *Science* 342 (6165), 1432–1433. doi:10.1126/science.342.6165.1432

Cui, G. H., Dong, S. G., Sui, C. H., Duan, Q., and Feng, B. (2020). Fabrication of Composite Fe_3O_4 Nanoparticles Coupled by Thermo-Responsive and Fluorescent Eu Complex on Surface *Int. J. Polym. Mater. Polym. Biomaterials* 8, 1–7.

Cui, G., Zhao, K., You, K., Gao, Z., Kakuchi, T., Feng, B., et al. (2020). Synthesis and Characterization of Phenylboronic Acid-Containing Polymer for Glucose-Triggered Drug Delivery+. *Sci. Technol. Adv. Mater.* 21, 1–10. doi:10.1080/14686996.2019.1700394

Cullity, B. D. (1978). *Elements of X-Ray Diffraction*. Phillippines: Addison-Wesley Publishing Company Inc.

Du, J., Shi, C., Wu, W., Bian, X., Chen, P., Cui, Q., et al. (2017). Synthesis of Core-Shell Structured FAU/SBA-15 Composite Molecular Sieves and Their Performance in Catalytic Cracking of Polystyrene. *Sci. Technol. Adv. Mater.* 18 (1), 939–949. doi:10.1080/14686996.2017.1396561

Eberhardt, C. S., Kissick, H. T., Patel, M. R., Cardenas, M. A., Prokhnevska, N., Obeng, R. C., et al. (2021). Functional HPV-specific PD-1+ Stem-like CD8 T Cells in Head and Neck Cancer. *Nature* 597, 279–284. doi:10.1038/s41586-021-03862-z

Farokhzad, O., and Langer, R. (2006). Nanomedicine: Developing Smarter Therapeutic and Diagnostic Modalities☆. *Adv. Drug Deliv. Rev.* 58, 1456–1459. doi:10.1016/j.addr.2006.09.011

Ge, J., Neofytou, E., Cahill, T. J., Beygui, R. E., and Zare, R. N. (2012). Drug Release from Electric-Field-Responsive Nanoparticles. *ACS Nano* 6 (1), 227–233. doi:10.1021/nn203430m

Ge, R., Liu, C., Zhang, X., Wang, W., Li, B., Liu, J., et al. (2018). Photothermal-Activatable Fe3O4 Superparticle Nanodrug Carriers with PD-L1 Immune Checkpoint Blockade for Anti-metastatic Cancer Immunotherapy. *ACS Appl. Mat. Interfaces* 10 (24), 20342–20355. doi:10.1021/acsami.8b05876

Girase, M. L., Patil, P. G., and Ige, P. P. (2019). Polymer-drug Conjugates as Nanomedicine: a Review. *Int. J. Polym. Mater. Polym. Biomaterials* 69 (15), 990–1014. doi:10.1080/00914037.2019.1655745

Gotwals, P., Cameron, S., Cipolletta, D., Cremasco, V., Crystal, A., Hewes, B., et al. (2017). Prospects for Combining Targeted and Conventional Cancer Therapy with Immunotherapy. *Nat. Rev. Cancer* 17, 286–301. doi:10.1038/nrc.2017.17

Hawkins, M. J., Soon-Shiong, P., and Desai, N. (2008). Protein Nanoparticles as Drug Carriers in Clinical Medicine. *Adv. Drug Deliv. Rev.* 60, 876–885. doi:10.1016/j.addr.2007.08.044

He, G., Ma, Y., Zhou, H., Sun, S., Wang, X., Qian, H., et al. (2019). Mesoporous NiS2 Nanospheres as a Hydrophobic Anticancer Drug Delivery Vehicle for Synergistic Photothermal-Chemotherapy. *J. Mat. Chem. B* 7, 143–149. doi:10.1039/c8tb02473a

Huo, M., Yuan, J., Tao, L., and Wei, Y. (2014). Redox-responsive Polymers for Drug Delivery: from Molecular Design to Applications. *Polym. Chem.* 5 (5), 1519–1528. doi:10.1039/c3py01192e

IARC (2020). *Latest Global Burden of Cancer Data for 2020*. (Lyon, France: International Agency for Research on Cancer).

Jia, S., Fong, W.-K., Graham, B., and Boyd, B. J. (2018). Photoswitchable Molecules in Long-Wavelength Light-Responsive Drug Delivery: From Molecular Design

to Applications. *Chem. Mat.* 30, 2873–2887. doi:10.1021/acs.chemmater.8b00357

Karimi, M., Ghasemi, A., Zangabad, P. S., Rahighi, R., Moosavi Basri, S. M., Mirshekari, H., et al. (2016). Smart Micro/nanoparticles in Stimulus-Responsive Drug/gene Delivery Systems. *Chem. Soc. Rev.* 45, 1457–1501. doi:10.1039/c5cs00798d

Lai, J. T., Filla, D., and Shea, R. (2002). Functional Polymers from Novel Carboxyl-Terminated Trithiocarbonates as Highly Efficient RAFT Agents. *Macromolecules* 35, 6754–6756. doi:10.1021/ma020362m

Li, M., Luo, Z., and Zhao, Y. (2018). Self-Assembled Hybrid Nanostructures: Versatile Multifunctional Nanoplatforms for Cancer Diagnosis and Therapy. *Chem. Mat.* 30, 25–53. doi:10.1021/acs.chemmater.7b03924

Lin, L.-S., Cong, Z.-X., Cao, J.-B., Ke, K.-M., Peng, Q.-L., Gao, J., et al. (2014). Multifunctional Fe3O4@Polydopamine Core-Shell Nanocomposites for Intracellular mRNA Detection and Imaging-Guided Photothermal Therapy. *ACS Nano* 8, 3876–3883. doi:10.1021/nn500722y

Liu, F., Kozlovskaya, V., Medipelli, S., Xue, B., Ahmad, F., Saeed, M., et al. (2015). Temperature-Sensitive Polymersomes for Controlled Delivery of Anticancer Drugs. *Chem. Mat.* 27 (23), 7945–7956. doi:10.1021/acs.chemmater.5b03048

Liu, J., Bao, X., Kolesnik, I., Jia, B., Yu, Z., Xing, C., et al. (2022). Enhancing the *In Vivo* Stability of Polycation Gene Carriers by Using PEGylated Hyaluronic Acid as a Shielding System. *BIO Integr* 2 (2), 50–56. doi:10.15212/bioi-2021-0033

Liu, J., Huang, Y., Kumar, A., Tan, A., Jin, S., Mozhi, A., et al. (2014). pH-Sensitive Nano-Systems for Drug Delivery in Cancer Therapy. *Biotechnol. Adv.* 32 (4), 693–710. doi:10.1016/j.biotechadv.2013.11.009

Lu, S., Wang, Q., Zhang, G., Dong, X., Yang, C. T., Song, Y., et al. (2020). *American Association for Cancer Research (AACR) Annual Meeting 2020*. (New Orleans: LA: American Association for Cancer Research).

Ndebele, R. T., Yao, Q., Shi, Y.-N., Zhai, Y.-Y., Xu, H.-L., Lu, C.-T., et al. (2021). Progress in the Application of Nano- and Micro-based Drug Delivery Systems in Pulmonary Drug Delivery. *BIO Integr*. doi:10.15212/bioi-2021-0028

Nguyen, M., Felidj, N., and Mangeney, C. (2016). Looking for Synergies in Molecular Plasmonics through Hybrid Thermoresponsive Nanostructures. *Chem. Mat.* 28 (11), 3564–3577. doi:10.1021/acs.chemmater.6b00230

Olejniczak, J., Carling, C.-J., and Almutairi, A. (2015). Photocontrolled Release Using One-Photon Absorption of Visible or NIR Light. *J. Control. Release* 219, 18–30. doi:10.1016/j.jconrel.2015.09.030

Rwei, A. Y., Wang, W., and Kohane, D. S. (2015). Photoresponsive Nanoparticles for Drug Delivery. *Nano Today* 10 (4), 451–467. doi:10.1016/j.nantod.2015.06.004

Satarkar, N., and Hilt, J. (2008). Magnetic Hydrogel Nanocomposites for Remote Controlled Pulsatile Drug Release. *J. Control. Release* 130 (3), 246–251. doi:10.1016/j.jconrel.2008.06.008

Schroeder, A., Kost, J., and Barenholz, Y. (2009). Ultrasound, Liposomes, and Drug Delivery: Principles for Using Ultrasound to Control the Release of Drugs from Liposomes. *Chem. Phys. Lipids* 162 (1–2), 1–16. doi:10.1016/j.chemphyslip.2009.08.003

Shanmugam, V., Selvakumar, S., and Yeh, C.-S. (2014). Near-infrared Light-Responsive Nanomaterials in Cancer Therapeutics. *Chem. Soc. Rev.* 43 (17), 6254–6287. doi:10.1039/c4cs00011k

Shi, C., Wu, Z., Yang, F., and Tang, Y. (2021a). Janus Particles with pH Switchable Properties for High-Efficiency Adsorption of PPCPs in Water. *Solid State Sci.* 119, 106702–106709. doi:10.1016/j.solidstatesciences.2021.106702

Shi, C., Zhang, X., Zhang, X., Chen, P., and Xu, L. (2021b). Ultrasonic Desulfurization of Amphiphilic Magnetic-Janus Nanosheets in Oil-Water Mixture System. *Ultrason. Sonochemistry* 76, 105662–125668. doi:10.1016/j.ultsonch.2021.105662

Shibaev, V., Bobrovsky, A., and Boiko, N. (2003). Photoactive Liquid Crystalline Polymer Systems with Light-Controllable Structure and Optical Properties. *Prog. Polym. Sci.* 28 (5), 729–836. doi:10.1016/s0079-6700(02)00086-2

Sortino, S. (2012). Photoactivated Nanomaterials for Biomedical Release Applications. *J. Mat. Chem.* 22 (2), 301–318. doi:10.1039/c1jm13288a

Swain, A. K., Pradhan, L., and Bahadur, D. (2015). Polymer Stabilized Fe3O4-Graphene as an Amphiphilic Drug Carrier for Thermo-Chemotherapy of Cancer. *ACS Appl. Mat. Interfaces* 7 (15), 8013–8022. doi:10.1021/acsami.5b02536

Tong, R., Tang, L., and Cheng, J. (2012). Development and Application of Anticancer Nanomedicine. *Cheng J.* 1, 31–46. doi:10.1007/978-1-4614-2305-8_3

Wang, X., Yang, Y., Gao, P., Yang, F., Shen, H., Guo, H., et al. (2015). Synthesis, Self-Assembly, and Photoresponsive Behavior of Tadpole-Shaped Azobenzene Polymers. *ACS Macro Lett.* 4, 1321–1326. doi:10.1021/acsmacrolett.5b00698

Wu, F., Li, Q., Zhang, X., Liu, L., Wu, S., Sun, D., et al. (2012). Fabrication and Characterization of Thermo-Sensitive Magnetic Polymer Composite Nanoparticles. *J. Magnetism Magnetic Mater.* 324, 1326–1330. doi:10.1016/j.jmmm.2011.11.032

Yao, Y., Yu, Y., Wan, X., Yan, D., Chen, Y., Luo, J., et al. (2021). Azobenzene-Based Cross-Linked Small-Molecule Vesicles for Precise Oxidative Damage Treatments Featuring Controlled and Prompt Molecular Release. *Chem. Mat.* 33, 7357–7366. doi:10.1021/acs.chemmater.1c01860

Zhang, Y., Zhang, Y., Song, G., He, Y., Zhang, X., Liu, Y., et al. (2019). A DNA-Azobenzene Nanopump Fueled by Upconversion Luminescence for Controllable Intracellular Drug Release. *Angew. Chem. Int. Ed.* 58, 18207–18211. doi:10.1002/anie.201909870

Conflict of Interest: The authors declare that the research was conducted in the absence of any commercial or financial relationships that could be construed as a potential conflict of interest.

Publisher's Note: All claims expressed in this article are solely those of the authors and do not necessarily represent those of their affiliated organizations, or those of the publisher, the editors, and the reviewers. Any product that may be evaluated in this article, or claim that may be made by its manufacturer, is not guaranteed or endorsed by the publisher.

Copyright © 2022 Cui, Wang, Long, Zhang, Guo, Chen, Kakuchi, Duan and Zhao. This is an open-access article distributed under the terms of the Creative Commons Attribution License (CC BY). The use, distribution or reproduction in other forums is permitted, provided the original author(s) and the copyright owner(s) are credited and that the original publication in this journal is cited, in accordance with accepted academic practice. No use, distribution or reproduction is permitted which does not comply with these terms.

frontiers | Frontiers in Bioengineering and Biotechnology

ORIGINAL RESEARCH
published: 17 August 2022
doi: 10.3389/fbioe.2022.915067

Iodine-Rich Nanoadjuvants for CT Imaging–Guided Photodynamic Immunotherapy of Breast Cancer

Xiaoyan Xin[1†], Xiaoyue Ni[2†], Kang Shi[1], Jie Shao[3], Yanqiu Zhang[1], Xin Peng[1], Wen Yang[1], Chuanshuai Tian[1], Wen Zhou[2] and Bing Zhang[1*]*

[1]Department of Radiology, Nanjing Drum Tower Hospital, The Affiliated Hospital of Nanjing University Medical School, Nanjing, China, [2]Key Laboratory for Organic Electronics and Information Displays, Jiangsu Key Laboratory for Biosensors, Institute of Advanced Materials (IAM), Jiangsu National Synergetic Innovation Center for Advanced Materials (SICAM), Nanjing University of Posts and Telecommunications, Nanjing, China, [3]The Comprehensive Cancer Center of Drum Tower Hospital, Medical School of Nanjing University, Clinical Cancer Institute of Nanjing University, Nanjing, China

OPEN ACCESS

Edited by:
Jianxun Ding,
Changchun Institute of Applied Chemistry (CAS), China

Reviewed by:
Xianwen Wang,
Anhui Medical University, China
Honglin Jin,
Huazhong Agricultural University, China
Nikhil Pandey,
University of Maryland, United States
Xu Zhen,
Nanjing University, China

***Correspondence:**
Wen Zhou
iamwzhou@njupt.edu.cn
Bing Zhang
zhangbing_nanjing@nju.edu.cn

[†]These authors have share first authorship

Specialty section:
This article was submitted to Biomaterials, a section of the journal Frontiers in Bioengineering and Biotechnology

Received: 07 April 2022
Accepted: 18 May 2022
Published: 17 August 2022

Citation:
Xin X, Ni X, Shi K, Shao J, Zhang Y, Peng X, Yang W, Tian C, Zhou W and Zhang B (2022) Iodine-Rich Nanoadjuvants for CT Imaging–Guided Photodynamic Immunotherapy of Breast Cancer. Front. Bioeng. Biotechnol. 10:915067. doi: 10.3389/fbioe.2022.915067

Immunotherapy, which stimulates the body's own immune system to kill cancer cells, has shown great promise in the field of cancer therapy. However, the uncontrolled biodistribution of immunotherapeutic drugs may cause severe side effects. Herein, we report an iodine-rich nanoadjuvant (INA) for photo-immunotherapy. INA is prepared by encapsulating a toll-like receptor 7 agonist (R837) and a photosensitizer (phthalocyanine) into an iodine-rich amphiphilic copolymer PEG-PHEMA-I. By virtue of the enhanced permeation and retention (EPR) effect, INA can effectively accumulate into the tumor site. Under light irradiation, photodynamic therapy (PDT) triggered by INA will induce immunogenic cell death (ICD) in the tumor region to trigger the release of immune-associated cytokines. Such a process may further induce the maturation of dendritic cells which will be accelerated by R837, leading to the proliferation of effector T cells for immunotherapy. The photo-immunotherapy mediated by INA shows good anticancer efficacy both *in vitro* and *in vivo*. Meanwhile, INA is also a CT contrast agent owing to its high density of iodine, which can successfully illuminate tumors by CT imaging. Thus, our study develops a light-triggered nanoadjuvant for CT imaging–guided enhanced photo-immunotherapy.

Keywords: nanoadjuvant, immunotherapy, photodynamic therapy, breast cancer, CT imaging

INTRODUCTION

Immunotherapy is a kind of promising cancer therapeutic modality that stimulates the body's own immune system to attack cancer cells (Pardoll, 2012; Intlekofer and Thompson, 2013; Topalian et al., 2015). Until now, several immunotherapeutic modalities have been successfully applied, such as chimeric antigen receptor (CAR) T cell, immune checkpoint blockade, and cytokine therapy (Pardoll, 2012; Intlekofer and Thompson, 2013; Hargadon et al., 2018). However, because of the uncontrolled tissue accumulation of immunotherapeutic drugs, immunotherapy may suffer from the issue of immune-related adverse events (IRAEs), including hypokalemia, hypophysitis, myocarditis, and thyroid dysfunction (Kumar et al., 2017; Pollack et al., 2017; Darnell et al., 2020). To address such an issue, increasing the tumor accumulation of immunotherapeutic agents is a key point (Lu et al., 2018; Liu et al., 2019). Compared with small-molecular anticancer drugs, nanomedicines have been proven to exhibit better tumor accumulation (Shi et al., 2017; Tran et al., 2017; Youn and Bae, 2018;

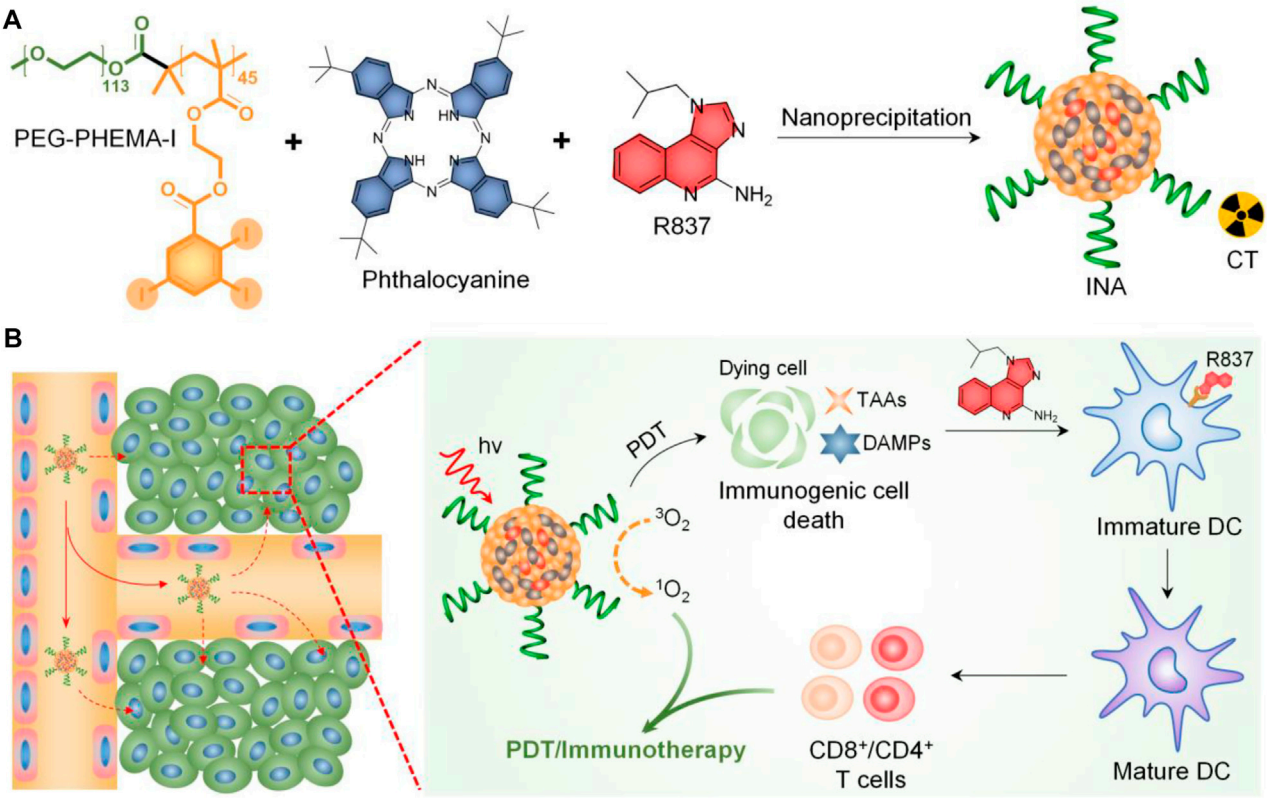

FIGURE 1 | (A) Schematic illustration of INA preparation. **(B)** Schematic illustration of the mechanism of INA for NIR light synergistic photodynamic immunotherapy.

Miao et al., 2019; Wang X. et al., 2021). By virtue of such advantage, numerous nanomaterials have been designed for cancer immunotherapy to achieve a better therapeutic efficacy with lower IRAEs (Meng et al., 2019; Ji et al., 2020; Mai et al., 2020; Allen et al., 2021). In addition, owing to the multifunctionality of nanomaterials, different kinds of immune stimulants and agonists, and therapeutic modalities, can be easily integrated into one system (Meng et al., 2019; Wang H. et al., 2019; Wang T. et al., 2019; Guo et al., 2021; Wang Z. et al., 2021). Therefore, developing novel nanomedicines is of great significance for cancer immunotherapy.

Despite the improved tumor accumulation of nanomedicine, most therapeutic modalities for immunotherapy activation still have the issue of low specificity. Among different modalities, phototherapy which uses light as an exogenous stimulus has the advantages of high spatiotemporal resolution and low side effects (Chen et al., 2016; Jia et al., 2020). Such a feature makes light an ideal choice for immunotherapy as it can ensure the therapeutic process and induction of immunogenic cell death (ICD) only to occur in the tumor site (Xu et al., 2017; Ding et al., 2018; Li et al., 2019). Until now, nanomaterial-based phototherapy-induced ICD has been applied for treating both primary and metastatic tumors *in vivo* (Wang Z. et al., 2019). In addition to ICD, such a nanosystem may also trigger the delivery of inhibitors, enzymes, adjuvants, and hydrogen sulfide to enhance the immunotherapeutic efficacy (Han et al., 2017; Shi et al., 2018; Wang H. et al., 2019; Sun et al., 2021; Zhang et al., 2022). All of these examples indicate the great promise of nanomaterials in light-induced immunotherapy. But how to integrate light-induced nano-immunotherapy with reliable clinical imaging methods *via* a facile strategy is still a challenge. The combination of a reliable clinical imaging method can not only help examine the location of the tumor but also benefit the observation of the curative effect evaluation of light-induced immunotherapy.

Herein, we report iodine-rich nanoadjuvants (INAs) for photodynamic immunotherapy. Such a nanoadjuvant is prepared by co-encapsulating a near-infrared (NIR)–absorbing phthalocyanine and a toll-like receptor-7 (TLR7) agonist (R837) into an iodine-rich amphiphilic copolymer, PEG-PHEMA-I (**Figure 1A**). After accumulation into the tumor site *via* enhanced permeation and retention (EPR) effect, INA may conduct photodynamic therapy (PDT) under NIR light irradiation. The ICD induced by PDT subsequently triggers the release of danger-associated molecular patterns (DAMPs) and tumor-associated antigens (TAAs) from dying tumor cells. The ICD combined with released R837 will trigger the maturation of dendritic cells (DCs), which further promote the proliferation of effector T cells. As a result, photodynamic immunotherapy is achieved by INA under NIR light irradiation (**Figure 1B**). In addition, the high concentration of iodine makes INA an ideal candidate for X-ray computed tomography (CT) contrast agents.

Thus, INA can be applied as a CT imaging–guided photodynamic immunotherapy for cancer.

EXPERIMENTAL

Materials

All the chemicals and solvents are purchased from Sigma-Aldrich and used as received unless otherwise mentioned. PEG-PHEMA-I was synthesized based on our previous study (Zhou et al., 2020).

Characterizations

Dynamic light scattering (DLS) was performed on a Brookhaven ZetaPALS. Transmission electron microscopy (TEM) images were captured on an HT7700 transmission electron microscope (acceleration voltage 100 kV). Absorption and fluorescence spectra were recorded on a Shimadzu UV-3600 ultraviolet–visible-near-infrared spectrophotometer and a Fluoromax-3 spectrophotometer (JobinYvon), respectively.

Preparation of Nanoparticles

INA was prepared *via* a nanoprecipitation method. Briefly, PEG-PHEMA-I, phthalocyanine, and R837 were dissolved into 1 ml of tetrahydrofuran (THF). The resulting solution was rapidly injected into 9 ml of water under vigorous sonication for 1 min. THF was then removed by gentle nitrogen gas flow, and the nanoparticle solution was filtered through a 0.22-μm filter to remove the aggregates. The obtained solution was stored at 4°C for further usage. The preparation of PEG-PHEMA-I nanoparticles was based on a similar procedure without the addition of R837.

Cellular Uptake

Fluorescein isothiocyanate (FITC) (5% w/w) was doped into INA to give INA-FITC a strong green fluorescence signal for confocal imaging. 4T1 cells were cultured in Dulbecco's modified Eagle's medium (DMEM) with 10% fetal bovine serum (FBS) and antibiotics (10 mg/ml of streptomycin and 10 U/mL of penicillin) at 37°C in an atmosphere of 5% carbon dioxide. The cells were then seeded into confocal dishes, and INA-FITC (4 μg/ml) was co-incubated with the cells for 4 h. After incubation, the cells were washed with fresh DMEM, and the cell nuclei were stained with DAPI. The cells were then imaged by an LSM880 confocal laser scanning microscope (Carl Zeiss, Germany) with an excitation wavelength of 405 nm for DAPI and 488 nm for INA-FITC.

Cytotoxicity Study

4T1 cells were seeded into 96-well plates for 24 h. INA with different concentrations was co-incubated with the cells for another 24 h. The cells were treated with or without 635-nm laser irradiation (1 W/cm^2) for 10 min. MTT assay was applied to determine the viability of cells.

In Vitro and *In Vivo* CT Imaging Measurement

Aqueous solutions of INA at different concentrations (3.125 μg/ml, 6.25 μg/ml, 12.5 μg/ml, 25 μg/ml, 50 μg/ml, 100 μg/ml, 200 μg/ml 400 μg/ml, and 400 μg/ml) were directly imaged using Hiscan XM Micro CT (Suzhou Hiscan Information Technology Co., Ltd.). The X-ray attenuation for regions of interest was quantified with Hiscan Analyzer software (Suzhou Hiscan Information Technology Co., Ltd.). 4T1 tumor–bearing mice (n = 3) were injected with INA (0.5 mg/ml, 10 μL) and PBS (10 μL) *via* tumor subcutaneous tissue. Then, the mice were scanned using a CT imaging system for 30 min post injection. The 3D reconstruction images and CT values (Hounsfield units, HU) were obtained through RadiAnt DICOM Viewer software.

In Vitro DC Stimulation Experiments

Bone-marrow-derived dendritic cells were generated from the bone marrow of 8-week-old BALB/c mice from Nanjing Peng Sheng Biological Technology Co. Ltd. according to an established method. For *in vitro* DC stimulation experiments, we cocultured free R837, PEG-PHEMA-I, or INA nanoparticles [(PEG-PHEMA-I) = 100 μg/ml (phthalocyanine) = 25 μg/ml (R837) = 15 μg/ml] with 10^6 bone-derived DCs from BALB/c mice for 48 h. After various treatments, DCs stained with anti–CD11c-BB700 (BD Biosciences), anti–CD86-PE-Cy7 (BD Biosciences), and anti–CD80-APC (BD Biosciences) antibodies were then analyzed by flow cytometry (CytoFLEX LX). Data analysis was carried out using FCS express software.

In Vito DC Stimulation Experiments

After 4T1 tumors grown on BALB/c mice reached 100 mm^3, 200 μL of PEG-PHEMA-I or INA (0.2 mg/ml PEG-PHEMA-I, 0.12 mg/ml R837) was injected intravenously. After injection for 48 h, the mice were exposed to a 680-nm laser with 0.5 W/cm^2 for 30 min with 1-min interval for every 2 min of light exposure. The mice were killed 2 days after PDT treatment, the draining lymph nodes were cut off, and we assessed the expression levels of CD80 and CD86 by flow cytometry.

Cytometric Bead Array Analysis of Cytokines

The cytokines from sera and DC medium supernatants were measured by the BD CBA mouse Th1/Th2 kit according to the manufacturer's protocol (BD Biosciences) with an appropriate diluent. The samples were run and FACS data were collected using an Accuri C6 Plus (BD Biosciences) flow cytometer and analyzed using FCAP version 3.0 array software (Soft Flow).

In Vivo PDT

The Ethics Committee of Nanjing Drum Tower Hospital approved all experiments in this study. All animal procedures were carried out in compliance with the guidelines set by the Animal Care Committee at Nanjing Drum Tower Hospital (Nanjing, China). The investigators were not blinded for animal studies. All efforts were made to minimize the number of animals used and their suffering. The mice were randomized on the basis of age and weight.

Female BALB/c mice (6–8 weeks) were purchased from Nanjing Peng Sheng Biological Technology Co. Ltd. and used under protocols approved by Drum Tower Hospital Animal Center. The mice were divided into groups randomly. For tumor inoculation, 4T1 cells (5×10^4) suspended in PBS were

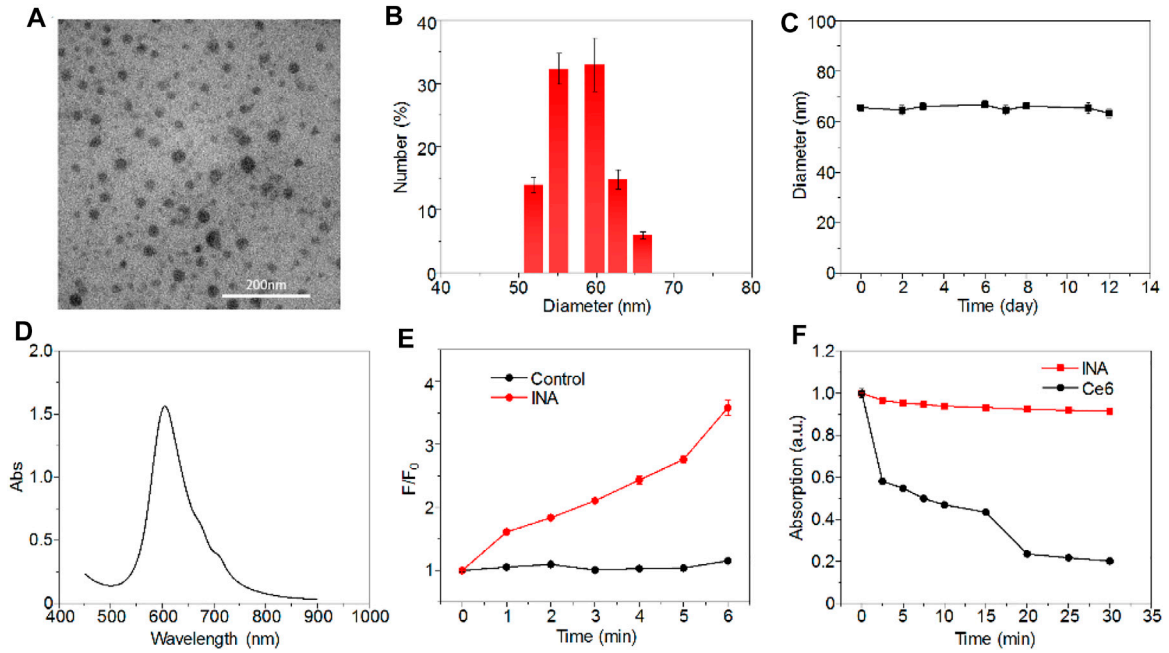

FIGURE 2 | Characterizations of INA. **(A)** Representative TEM image of INA. **(B)** Hydrodynamic size distribution of INA. **(C)** Average hydrodynamic size of INA is a function of storage time. **(D)** Absorption spectrum of INA. **(E)** Fluorescence intensity change (F/F_0) of SOSG with or without INA as a function of 635-nm laser irradiation time. **(F)** Normalized absorption changes of INA and phthalocyanine at 660 nm as a function of 635-nm laser irradiation time (0.1 W cm^{-2}). Error bars represent the standard deviations of three different measurements.

subcutaneously injected into the left flank of each female BALB/c mouse. The tumor volume was calculated according to the following formula: $width^2 \times length \times 0.5$. When those tumors reached ~100 mm^3, PEG-PHEMA-I or INA nanoparticles were injected into the vein at the INA dose of 0.8 mg per mouse. After 24 h, the mice were irradiated with a 680-nm laser with a power density of 0.5 W/cm^2 for 30 min with 1 min interval for every 2 min of light exposure.

In Vivo Immune Response Analysis

To analyze the immune cells in the tumors, those tumors mentioned above were harvested from mice and digested using 1500 U/mL collagenase (Sigma), 1000 U/mL hyaluronidase (Sigma), and Sigma DNase (Sigma) at 37°C for 30 min. The cells were filtered through nylon mesh filters and washed with PBS containing 1% FBS. The single-cell suspension was incubated with anti–CD3-AF700 (BD Biosciences) antibody. Afterward, those cells were washed with PBS containing 1% FBS and analyzed using flow cytometry analysis. Data analysis was carried out using FCS express software.

Statistical Analysis

The Graphpad Prism 5.0 software (Graphpad Software, La Jolla, CA, United States) was used for all statistical analyses. The mean ± SEM was determined for each treatment group in the individual experiments, and Student's t-test was used to determine the significance between the treatment and control groups. The results of multiple groups including tumor volume curves have been compared using the variance (ANOVA) test. p-values < 0.05 were significant, as indicated with asterisks (*p < 0.05, **p < 0.01, ***p < 0.001, and ****p < 0.0001).

RESULTS AND DISCUSSION

INA was prepared *via* a nanoprecipitation method, which used iodine-grafted amphiphilic copolymer PEG-PHEMA-I as the carrier to load hydrophobic phthalocyanine and R837. The color of the INA solution was blue, and the solution was transparent without the precipitate (**Supplementary Figure S1**). Transmission electron microscopy (TEM) imaging showed that INA had a spherical morphology with a diameter of approximately 30 nm (**Figure 2A**). The XRD spectrum of INA was recorded (**Supplementary Figure S2**). The hydrodynamic size of INA was calculated as 56 nm from dynamic light scattering (DLS), which was much higher than the size measured from the TEM image (**Figure 2B**). Such difference can be attributed to the shrinkage of nanoparticles during TEM sample preparation. The physiological stability of INA was tested by storing nanoparticle samples under 4°C, and DLS was used to determine the average hydrodynamic size of INA over time. The size remained almost the same even after storing for 12 days, indicating the good stability of INA (**Figure 2C**). The optical properties of INA were then studied. INA showed maximum absorption at around 600 nm, which was derived from the absorption of encapsulated phthalocyanine (**Figure 2D**). Almost no fluorescence was detected for INA maybe because of the self-quenching of phthalocyanine in the core of INA. A singlet oxygen

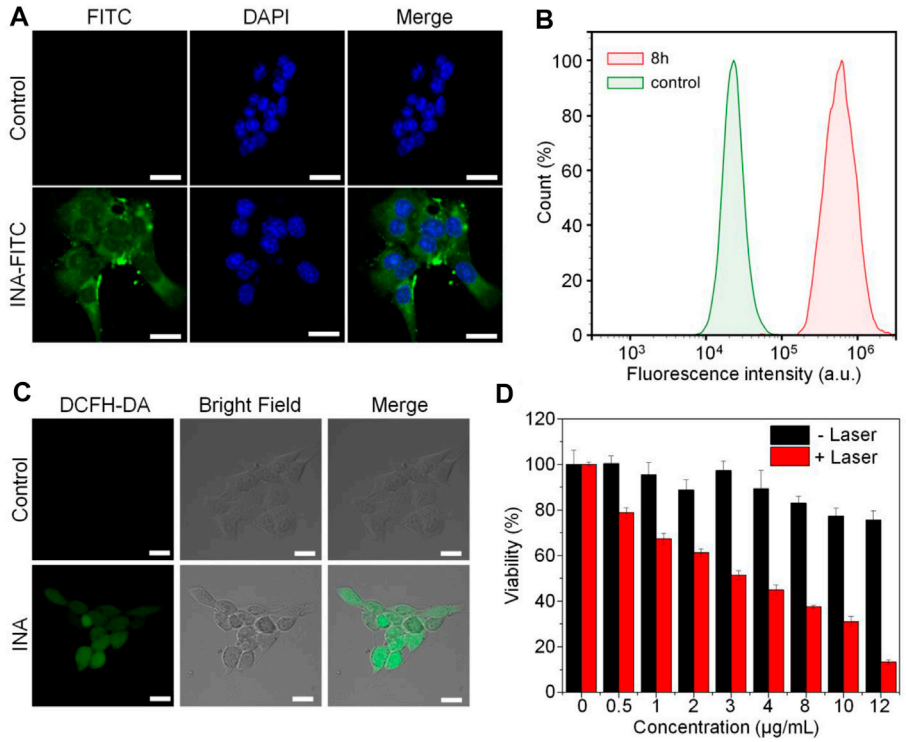

FIGURE 3 | Cell studies. **(A)** Confocal images of 4T1 cells with or without INA-FITC incubation for 8 h. The cell nuclei were stained with DAPI which indicated as blue color. **(B)** Quantification of fluorescence intensity in 4T1 cells incubated with INA-FITC for 8 h by flow cytometry. **(C)** Confocal images of 4T1 cells incubated with INA and DCFH-DA under 635-nm laser irradiation for 12 min **(D)** Cell viability of 4T1 cells after incubating with INA for 24 h at different concentrations with or without 635-nm laser irradiation (1 W cm^{-2}). The scale bars represent 20 μm. The error bars represent the standard deviation of three separate measurements.

($^1O_2$) fluorescence probe and a singlet oxygen sensor green (SOSG) were then used to study the $^1O_2$ generation of INA. Although INA showed no fluorescence emission, obvious fluorescence enhancement was observed for SOSG treated with INA under 635-nm laser irradiation, indicating the generation of $^1O_2$ from INA (**Figure 2E**). Such a phenomenon may be attributed to the high concentration of iodine within INA, which can enhance the ^{1}O2 quantum yield according to our previous study. Under laser irradiation for 30 min, the absorption of INA was nearly unchanged, while the absorption of phthalocyanine decreased 80% under the same condition (**Figure 2F**). Such a result demonstrated the superior photostability of INA. These data indicated that INA had good physiological and photo-stability and was a good candidate for PDT.

INA was then applied for cell studies to evaluate its *in vitro* biocompatibility and anticancer efficacy, 4T1 cell was chosen as the cell model. As INA showed no fluorescence signal, 5% w/w fluorescein isothiocyanate (FITC) was loaded into INA to give INA-FITC. INA-FITC showed a strong green fluorescence signal, which was suitable for confocal imaging. After incubating INA-FITC with 4T1 cells for 8 h, strong green fluorescence was detected in the cytoplasm of cells, which showed that INA-FITC can be effectively internalized into 4T1 cells (**Figure 3A**). A quantification study showed that INA-FITC-incubated cells had a much higher fluorescence intensity than the cells without INA-FITC, further confirming the successful internalization of INA-FITC (**Figure 3B**). The fluorescence intensity within cells after 8 h incubation was 27-fold higher than that before incubation. To confirm whether INA could generate $^1O_2$ within 4T1 cells under laser irradiation, a $^1O_2$ fluorescence probe, dichloro-dihydro-fluorescein diacetate (DCFH-DA), was used. After irradiating 4T1 cells which were incubated with both INA and DCFH-DA by the 635-nm laser for 12 min, a strong green fluorescence signal was detected within cells, while almost no fluorescence signal was detected for the cells without INA incubation (**Figure 3C**). Such a phenomenon indicated that INA can efficiently generate $^1O_2$ within 4T1 cells under laser irradiation. Then, *in vitro* biocompatibility and PDT efficacy of INA against 4T1 cells were evaluated by 3-(4,5-dimethylthiazol-2-yl)-2,5-diphenyltetrazolium bromide (MTT) assay. For the cells without laser irradiation, the cell viability was almost 80% even under the highest concentration of INA, indicating the good biocompatibility of INA. In contrast, under laser irradiation, the cell viability decreased gradually with the increase of INA concentration, and the cell viability was only 13.3% at the highest concentration, demonstrating the good *in vitro* PDT efficacy of INA.

Live/dead assay was then utilized to further confirm the PDT of INA against 4T1 cells. 4T1 cells were treated under different conditions, and calcium green (Calcium-AM) and propidium iodide (PI) were stained for live and dead cells, respectively. For

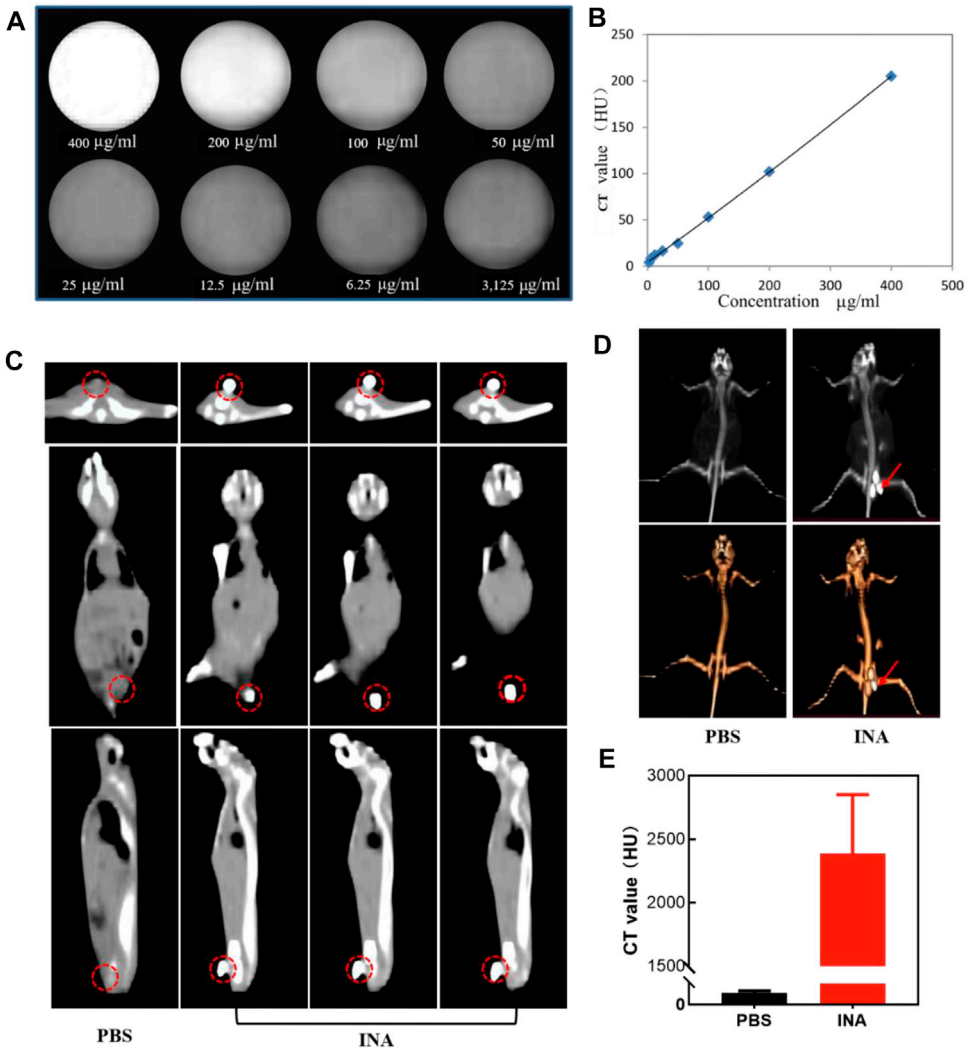

FIGURE 4 | (A,B) CT images and the corresponding plot of the CT value (HU) of INA at different concentrations. **(C)** Axial, coronal, and sagittal CT images of 4T1 tumor–bearing mice after intratumoral injection of PBS or INA. Red circles indicate the location of the tumors. **(D)** 3D reconstruction images from CT scan images of 4T1 tumor–bearing mice after intratumoral injection of PBS or INA. Red arrows indicate the location of the tumors. **(E)** Corresponding CT values of tumors after intratumoral injection of PBS or INA.

the control groups with or without laser irradiation and the INA group without laser irradiation, almost all the cells were alive. However, for the INA group with 635-nm laser irradiation, almost no living cells were observed, which further confirmed the *in vitro* PDT efficiency of INA (**Supplementary Figure S3A**). The flow cytometry analysis gave similar results, and only both treated with INA and 635-nm laser irradiation can significantly kill 4T1 cells (**Supplementary Figure S3B**). All these results demonstrated the superior PDT efficacy of INA, which showed its potential for *in vivo* anticancer evaluation.

CT is one of the most extensive imaging techniques for clinical diagnosis due to its deep penetration and high spatial resolution (Schlemmer et al., 2018; Ward et al., 2020; Hricak et al., 2021). The contrast agents used in clinical CT enhancement examination are generally water-soluble compounds containing iodine, which show strong X-ray attenuation capability (Chalela and Aguilar, 2016; Yeh et al., 2017; Zou et al., 2017). Thus, the high density of iodine in INA made it an excellent candidate for positive contrast agents of CT imaging. The CT contrast efficiency of INA was then evaluated, the image brightness was elevated, and the CT value reached about 200 HU at a high concentration (400 μg/ml) of INA (**Figures 4A,B**). A linear relationship of CT value versus concentration was confirmed (**Figure 4B**), validating the feasibility of the quantitative study. The ability of *in vivo* CT imaging of INA was further investigated by intratumoral injection of the nanoparticles into 4T1 tumor–bearing mice. The PBS injection group was used as a control. The three pictures on a continuous slice of axial, coronal, and sagittal CT images showed that the tumor which was injected with INA exhibited strong enhancement, while the PBS group showed no obvious contrast (**Figure 4C**). To observe the enhancement of the

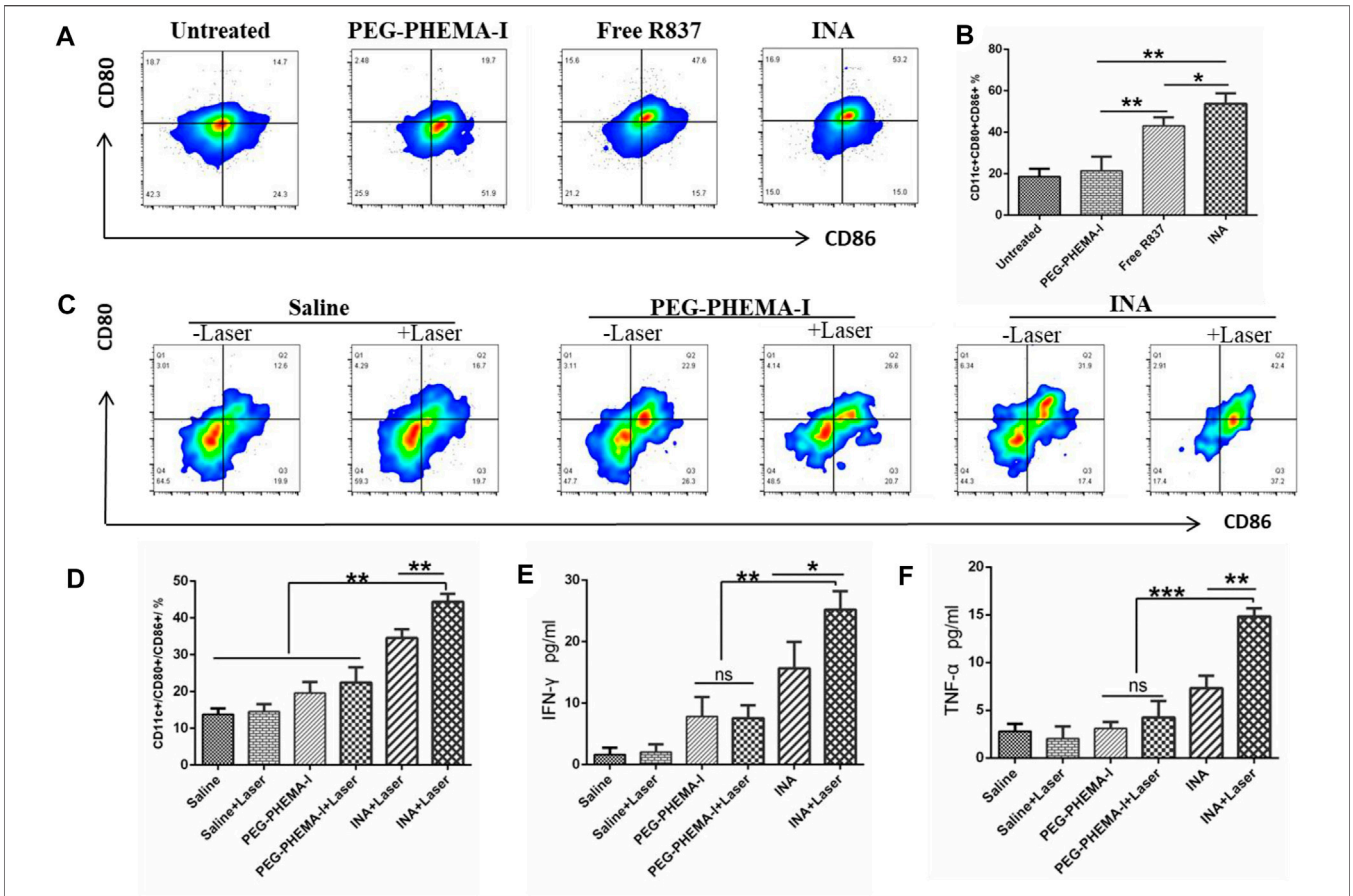

FIGURE 5 | (A) Flow cytometry of CD86 and CD80 expressions of DCs after incubation with PEG-PHEMA-I, free R837, or INA for 24 h **(B)** Quantification results of flow cytometry from figure **(A)**. **(C)** Flow cytometry of CD11c, CD80, and CD86 expression of DCs under different treatments. **(D)** Quantification results of flow cytometry from figure **(C) (E,F)** Cytokine levels of IFN-γ and TNF-α in sera from mice isolated on day 2 post INA-based PDT. Three mice were measured in each group. Error bars represent the standard deviation (SD) of at least three replicates.

tumor site more intuitively, we reconstruct the 3D VR (Virtual Reality) images from the 2D CT images. Severe enhancement of the tumor was detected on the subcutaneous flank of the mice (**Figure 4D**). The CT values were further analyzed to evaluate the CT imaging ability of INA. The results showed that the CT value of the tumors at 30 min post injection increased over 2000 HU, about forty-fold higher than that of the control group (**Figure 4E**). These results taken together indicate a strong CT contrast efficiency *in vitro* and *vivo* was achieved by INA.

The immune activation ability of the nanoparticles was then evaluated *in vitro*. Dendritic cells (DCs) are the most potent cells for activating and polarizing naive T cells. DCs are specialized immune cells that scan the surrounding tissue for foreign objects or abnormal cells, and they travel to the lymph nodes to activate T cells and immune response when they spot a danger signal. When they present peptide major histocompatibility complex (MHC) to the T cell receptors (TCR) of T cells, the costimulatory molecules (CD80 and CD86) are upregulated. The surface costimulatory molecules of DCs can reflect the degree of DC maturation. Therefore, we assessed the expression levels of CD80 and CD86 in bone marrow–derived DCs of BALB/C mice treated with PEG-PHEMAA-I, INA, or free R837 for 24 h. Flow cytometry analysis showed that the proportion of mature DC ($CD11c+CD80^{+}CD86^{+}$) treated by INA nanoparticles was significantly higher than that induced by the same dose of free R837, while PEG-PHEMAA-I nanoparticles without R837 had no obvious immune response to DC (**Figure 5A** and **Supplementary Figure S4**). As shown in **Figures 5B,C**, the INA group contained more $CD11c+CD80^{+}CD86^{+}$ DCs than the free R837 group (53.73 ± 2.899 vs. 43.13 ± 2.322, $n = 3$) and PEG-PHEMA-I group (53.73 ± 2.899 vs. 21.43 ± 3.964, $n = 3$). Taken together, these data represented that INA nanoparticles could act as a strong immune nanoadjuvant.

Recent studies have shown that PDT therapy can activate tumor-specific immune responses by generating tumor-associated antigens from tumor cell residues, which may then be processed by APCs such as DCs and presented to T cells (Chen et al., 2016; Han et al., 2017; Li et al., 2019). We thus wonder whether PDT induced by INA, which could also act as an immune adjuvant, would be able to trigger strong immune responses *in vivo*. After 4T1 tumors grown on BALB/c mice reached 100 mm^3, 200 μL of PEG-PHEMA-I or INA (0.2 mg/ml

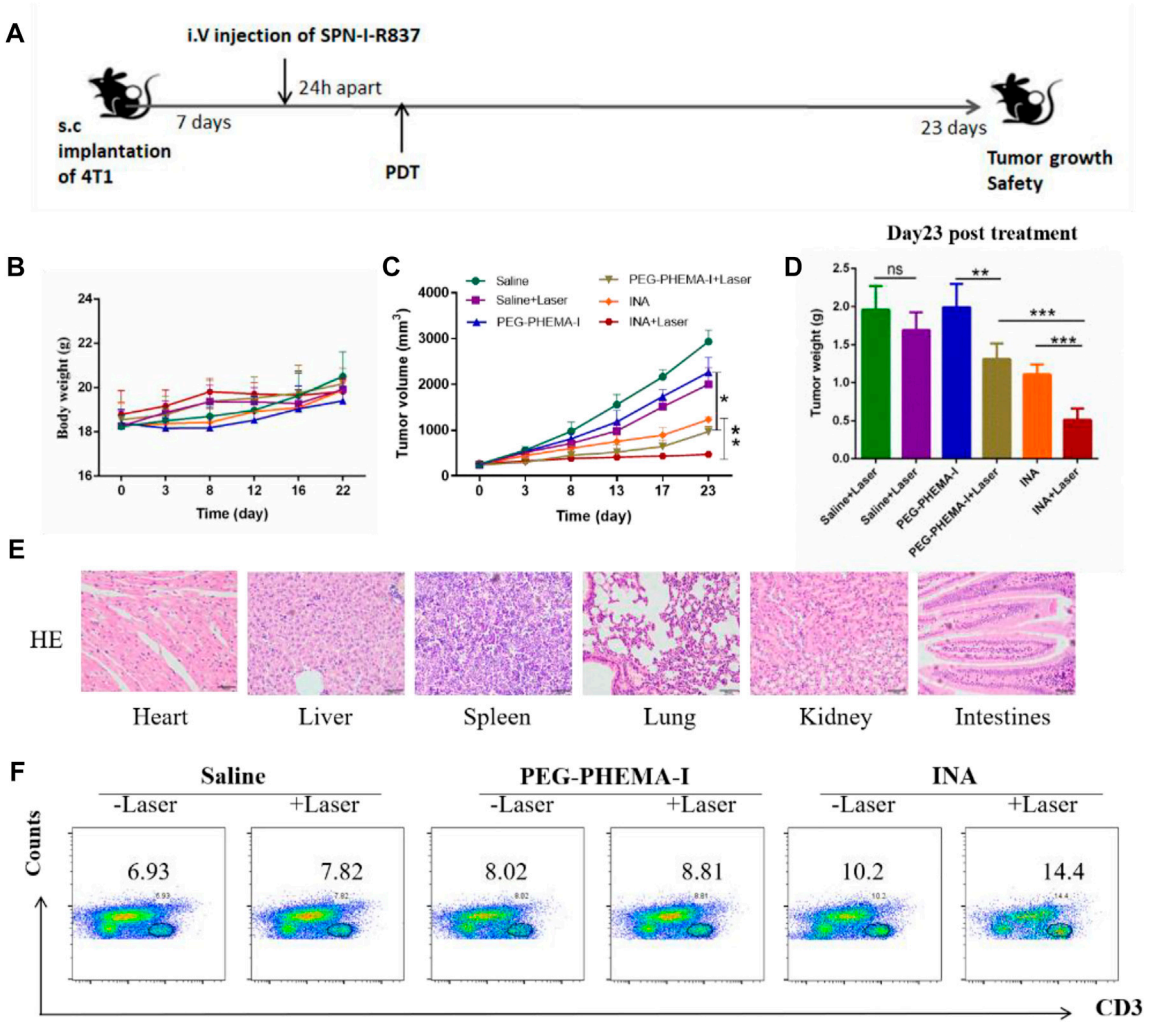

FIGURE 6 | *In vivo* antitumor effects. **(A)** Schematic illustration of our experiment design. Mice with 4T1 tumors were used in our experiment. **(B)** Mice body weight curves of different groups of mice (six mice per group). **(C)** Tumor growth curves of different groups of mice (six mice per group). **(D)** Tumor weight of the treated mice 23 d since the start of the therapy. **(E)** H&E staining of the major organs of INA + laser group of mice. **(F)** Proportions of tumor-infiltrating $CD3^+$ T cells.

PEG-PHEMA-I, 0.12 mg/ml R837) was injected intravenously. After injection for 48 h, the mice were exposed to a 680-nm laser with 0.5 W/cm^2 for 30 min with a 1-min interval for every 2 min of light exposure. The mice were killed 2 days after PDT treatment, the draining lymph nodes were cut off, and the mature level of DC was detected by flow cytometry. It was found that INA-based PDT therapy promoted a much higher level of DC maturation than that observed for PDT therapy with PEG-PHEMA-I in the absence of R837 (44.43 ± 1.247 vs. 22.43 ± 2.396, n = 3) and those with INA injection without laser irradiation (34.57 ± 1.34 vs. 19.60 ± 1.706, n = 3), as shown in **Figure 5D** and **Supplementary Figure S5**.

Meanwhile, the BD CBA mouse Th1/Th2 kit was used to analyze the changes of IFN-γ, TNF-α, and other cytokines in the serum of mice after different treatments. The expression of important cytokines IFN-γ and TNF-α was significantly upregulated after INA-induced PDT treatment (**Figures 5E,F**), and their levels were higher than those of PEG-PHEMA-I-induced PDT with laser irradiation (25.19 ± 1.752 vs. 7.570 ± 1.192 for IFN-γ, and 14.82 ± 0.4888 vs. 4.247 ± 1.006 for TNF-α), suggesting that INA-induced PDT had the highest capability for cellular immunity activation *in vivo*. These data indicated that R837 can effectively elevate the PDT-triggered immune response.

As INA has been demonstrated to trigger effective immune response under laser irradiation both *in vitro* and *in vivo*, INA was further applied for *in vivo* anticancer study. BALB/c mice bearing subcutaneous 4T1 tumors were intravenously injected (i.v.) with PEG-PHEMA-I or INA and then irradiated by a 680-nm laser at 0.5 W/cm^2 for 30 min with 1-min interval for every 2 min of light exposure. The design of our animal experiment is shown in **Figure 6A**. The growth of tumors in different groups was measured by a caliper every 4 days. The photo-immunotherapy triggered by INA had better therapeutic efficacy than PDT-induced by PEG-PHEMA-I nanoparticles,

indicating that the presence of R837 can enhance the therapeutic efficacy of photo-immunotherapy (**Figures 6C,D** and **Supplementary Figures S6, S8–S9**). The gradual increase of body weight of mice in all the groups demonstrated the safety of treatments (**Figure 6B**). In addition, no obvious damage was observed from H&E staining of major organs collected from INA-treated mice under laser irradiation, which further proved the biosafety of INA-induced photo-immunotherapy (**Figure 6E**, **Supplementary Figure S7**).

The population of $CD3^+$ T cells in the tumor region under different treatments was then determined to evaluate the level of immune activation. Flow cytometry results showed that INA-treated mice had a higher population of $CD3^+$ T cells in the tumor than PEG-PHEMA-I nanoparticles, demonstrating that R837 can increase the effector T cells in the tumor region. Without laser irradiation, a higher percentage of $CD3^+$ T cells was observed in the INA-treated mice (10.2 vs. 8.2). When using laser irradiation, the percentage of $CD3^+$ T cells was also higher in the INA-treated mice (14.4 vs. 8.1). The highest population was observed in the INA with the laser group. Such a result indicated that the best anticancer efficacy of INA with laser can be attributed to the highest level of effector T cells in the tumor region (**Figure 6F**).

CONCLUSION

In summary, we have designed a CT imaging–guided photo-immunotherapeutic nanosystem (INA) for cancer theranostics. INA was prepared by co-loading a TLR agonist, R837, and a photosensitizer phthalocyanine into an iodine-grafted amphiphilic copolymer (PEG-PHEMA-I). Under laser irradiation, INA could conduct PDT to trigger ICD, which released immune-related cytokines to induce the maturation of DCs. Meanwhile, R837 in the INA accelerates the maturation of DCs, further leading to the proliferation of effector T cells for immunotherapy. INA showed good $^1O_2$ quantum yield and photostability. The *in vitro* study indicated that INA could be effectively internalized into cancer cells and killed under NIR laser irradiation. Owing to the high density of iodine, INA had a relatively high CT attenuation coefficient and could indicate the location of the tumor *via* CT imaging. *In vivo* study demonstrated that INA induced the proliferation of cytotoxic T lymphocytes (CTLs) in the tumor region under laser irradiation and could inhibit the tumor growth *via* the photo-immunotherapy.

Our study thus provided a theranostic nanoplatform for imaging-guided photo-immunotherapy. In addition to CT imaging, optical imaging such as fluorescence or PA imaging could be incorporated into the nanoplatform by encapsulating optical materials other than phthalocyanine. In addition, other hydrophobic drugs may be loaded into the nanoplatform to achieve combination therapy for cancer.

DATA AVAILABILITY STATEMENT

The raw data supporting the conclusions of this article will be made available by the authors, without undue reservation.

ETHICS STATEMENT

The animal study was reviewed and approved by The Ethics Committee of Nanjing Drum Tower Hospital.

AUTHOR CONTRIBUTIONS

XX and XN contributed equally to this work and finished the most part in performing experiments analyzing data and editing the manuscript. KS and JS helped conduct animal experiments. YZ, XP, WY, and CT helped analyze data and formulate figures. WZ and BZ designed the study project.

FUNDING

This study was supported in part by the 66th Batch of China Postdoctoral Science Foundation Projects (No. 2019M661805), the National Natural Science Foundation of China (No. 81902914), a Research Grant of Key Project supported by the Medical Science and Technology Development Foundation, Nanjing Department of Health (No. YKK18062), Jiangsu Province, China, the Fundamental Research Funds for the Central Universities (No.021414380484), the Research Start-up Fund of NJUPT (NY220149), Natural Science Foundation of Jiangsu University (No. 21KJB150022), and Natural Science Foundation of NJUPT (No. NY221088).

SUPPLEMENTARY MATERIAL

The Supplementary Material for this article can be found online at: https://www.frontiersin.org/articles/10.3389/fbioe.2022.915067/full#supplementary-material

REFERENCES

Allen, S. D., Liu, X., Jiang, J., Liao, Y.-P., Chang, C. H., Nel, A. E., et al. (2021). Immune Checkpoint Inhibition in Syngeneic Mouse Cancer Models by a Silicasome Nanocarrier Delivering a GSK3 Inhibitor. *Biomaterials* 269, 120635. doi:10.1016/j.biomaterials.2020.120635

Chalela, J. G., and Aguilar, L. (2016). Images in Clinical Medicine. Iododerma from Contrast Material. *N. Engl. J. Med.* 374 (25), 2477. doi:10.1056/NEJMicm1512512

Chen, Q., Xu, L., Liang, C., Wang, C., Peng, R., and Liu, Z. (2016). Photothermal Therapy with Immune-Adjuvant Nanoparticles Together with Checkpoint Blockade for Effective Cancer Immunotherapy. *Nat. Commun.* 7, 13193. doi:10.1038/ncomms13193

Darnell, E. P., Mooradian, M. J., Baruch, E. N., Yilmaz, M., and Reynolds, K. L. (2020). Immune-Related Adverse Events (irAEs): Diagnosis, Management, and Clinical Pearls. *Curr. Oncol. Rep.* 22 (4), 39. doi:10.1007/s11912-020-0897-9

Ding, B., Shao, S., Yu, C., Teng, B., Wang, M., Cheng, Z., et al. (2018). Large-Pore Mesoporous-Silica-Coated Upconversion Nanoparticles as Multifunctional

Immunoadjuvants with Ultrahigh Photosensitizer and Antigen Loading Efficiency for Improved Cancer Photodynamic Immunotherapy. *Adv. Mat.* 30 (52), 1802479. doi:10.1002/adma.201802479

Guo, S., Li, K., Hu, B., Li, C., Zhang, M., Hussain, A., et al. (2021). Membrane-Destabilizing Ionizable Lipid Empowered Imaging-guided siRNA Delivery and Cancer Treatment. *Exploration* 1 (1), 35–49. doi:10.1002/exp.20210008

Han, Q., Wang, X., Jia, X., Cai, S., Liang, W., Qin, Y., et al. (2017). CpG Loaded MoS2 Nanosheets as Multifunctional Agents for Photothermal Enhanced Cancer Immunotherapy. *Nanoscale* 9 (18), 5927–5934. doi:10.1039/c7nr01460k

Hargadon, K. M., Johnson, C. E., and Williams, C. J. (2018). Immune Checkpoint Blockade Therapy for Cancer: An Overview of FDA-Approved Immune Checkpoint Inhibitors. *Int. Immunopharmacol.* 62, 29–39. doi:10.1016/j.intimp.2018.06.001

Hricak, H., Abdel-Wahab, M., Atun, R., Lette, M. M., Paez, D., Brink, J. A., et al. (2021). Medical Imaging and Nuclear Medicine: A Lancet Oncology Commission. *Lancet Oncol.* 22 (4), 136–172. doi:10.1016/s1470-2045(20)30751-8

Intlekofer, A. M., and Thompson, C. B. (2013). At the Bench: Preclinical Rationale for CTLA-4 and PD-1 Blockade as Cancer Immunotherapy. *J. Leukoc. Biol.* 94 (1), 25–39. doi:10.1189/jlb.1212621

Ji, Y., Liu, X., Li, J., Xie, X., Huang, M., Jiang, J., et al. (2020). Use of Ratiometrically Designed Nanocarrier Targeting CDK4/6 and Autophagy Pathways for Effective Pancreatic Cancer Treatment. *Nat. Commun.* 11 (1), 4249. doi:10.1038/s41467-020-17996-7

Jia, Y., Song, Y., Qu, Y., Peng, J., Shi, K., Du, D., et al. (2020). Mesoporous PtPd Nanoparticles for Ligand-Mediated and Imaging-Guided Chemo-Photothermal Therapy of Breast Cancer. *Nano Res.* 13, 1739–1748. doi:10.1007/s12274-020-2800-2

Kumar, V., Chaudhary, N., Garg, M., Floudas, C. S., Soni, P., and Chandra, A. B. (2017). Current Diagnosis and Management of Immune Related Adverse Events (irAEs) Induced by Immune Checkpoint Inhibitor Therapy. *Front. Pharmacol.* 8, 49. doi:10.3389/fphar.2017.00049

Li, W., Yang, J., Luo, L., Jiang, M., Qin, B., Yin, H., et al. (2019). Targeting Photodynamic and Photothermal Therapy to the Endoplasmic Reticulum Enhances Immunogenic Cancer Cell Death. *Nat. Commun.* 10 (1), 3349. doi:10.1038/s41467-019-11269-8

Liu, X., Zheng, J., Sun, W., Zhao, X., Li, Y., Gong, N., et al. (2019). Ferrimagnetic Vortex Nanoring-Mediated Mild Magnetic Hyperthermia Imparts Potent Immunological Effect for Treating Cancer Metastasis. *ACS Nano* 13 (8), 8811–8825. doi:10.1021/acsnano.9b01979

Lu, Y., Yang, Y., Gu, Z., Zhang, J., Song, H., Xiang, G., et al. (2018). Glutathione-Depletion Mesoporous Organosilica Nanoparticles as a Self-Adjuvant and Co-Delivery Platform for Enhanced Cancer Immunotherapy. *Biomaterials* 175, 82–92. doi:10.1016/j.biomaterials.2018.05.025

Mai, X., Zhang, Y., Fan, H., Song, W., Chang, Y., Chen, B., et al. (2020). Integration of Immunogenic Activation and Immunosuppressive Reversion Using Mitochondrial-Respiration-Inhibited Platelet-Mimicking Nanoparticles. *Biomaterials* 232, 119699. doi:10.1016/j.biomaterials.2019.119699

Meng, Z., Zhou, X., Xu, J., Han, X., Dong, Z., Wang, H., et al. (2019). Light-Triggered *In Situ* Gelation to Enable Robust Photodynamic-Immunotherapy by Repeated Stimulations. *Adv. Mat.* 31 (24), e1900927. doi:10.1002/adma.201900927

Miao, Z., Chen, S., Xu, C.-Y., Ma, Y., Qian, H., Xu, Y., et al. (2019). PEGylated Rhenium Nanoclusters: A Degradable Metal Photothermal Nanoagent for Cancer Therapy. *Chem. Sci.* 10 (21), 5435–5443. doi:10.1039/C9SC00729F

Pardoll, D. M. (2012). The Blockade of Immune Checkpoints in Cancer Immunotherapy. *Nat. Rev. Cancer* 12 (4), 252–264. doi:10.1038/nrc3239

Pollack, M. H., Betof, A., Dearden, H., Rapazzo, K., Valentine, I., Brohl, A. S., et al. (2017). Safety of Resuming Anti-PD-1 in Patients with Immune-Related Adverse Events (irAEs) during Combined Anti-CTLA-4 and Anti-PD1 in Metastatic Melanoma. *Ann. Oncol.* 29 (1), 250–255. doi:10.1093/annonc/mdx642

Schlemmer, H.-P., Bittencourt, L. K., D'Anastasi, M., Domingues, R., Khong, P.-L., Lockhat, Z., et al. (2018). Global Challenges for Cancer Imaging. *J. Glob. Oncol.* 4, 1–10. doi:10.1200/jgo.17.00036

Shi, B., Yan, Q., Tang, J., Xin, K., Zhang, J., Zhu, Y., et al. (2018). Hydrogen Sulfide-Activatable Second Near-Infrared Fluorescent Nanoassemblies for Targeted Photothermal Cancer Therapy. *Nano Lett.* 18 (10), 6411–6416. doi:10.1021/acs.nanolett.8b02767

Shi, J., Kantoff, P. W., Wooster, R., and Farokhzad, O. C. (2017). Cancer Nanomedicine: Progress, Challenges and Opportunities. *Nat. Rev. Cancer* 17 (1), 20–37. doi:10.1038/nrc.2016.108

Sun, Y., Feng, X., Wan, C., Lovell, J. F., Jin, H., and Ding, J. (2021). Role of Nanoparticle-Mediated Immunogenic Cell Death in Cancer Immunotherapy. *Asian J. Pharm. Sci.* 16 (2), 129–132. doi:10.1016/j.ajps.2020.05.004

Topalian, S. L., Drake, C. G., and Pardoll, D. M. (2015). Immune Checkpoint Blockade: A Common Denominator Approach to Cancer Therapy. *Cancer Cell* 27 (4), 450–461. doi:10.1016/j.ccell.2015.03.001

Tran, S., DeGiovanni, P. J., Piel, B., and Rai, P. (2017). Cancer Nanomedicine: A Review of Recent Success in Drug Delivery. *Clin. Transl. Med.* 6 (1), 44. doi:10.1186/s40169-017-0175-0

Wang, H., Han, X., Dong, Z., Xu, J., Wang, J., and Liu, Z. (2019a). Hyaluronidase with pH-Responsive Dextran Modification as an Adjuvant Nanomedicine for Enhanced Photodynamic-Immunotherapy of Cancer. *Adv. Funct. Mat.* 29 (29), 1902440. doi:10.1002/adfm.201902440

Wang, T., Zhang, H., Han, Y., Liu, H., Ren, F., Zeng, J., et al. (2019b). Light-Enhanced O2-Evolving Nanoparticles Boost Photodynamic Therapy to Elicit Antitumor Immunity. *ACS Appl. Mat. Interfaces* 11 (18), 16367–16379. doi:10.1021/acsami.9b03541

Wang, X., Zhong, X., Li, J., Liu, Z., and Cheng, L. (2021a). Inorganic Nanomaterials with Rapid Clearance for Biomedical Applications. *Chem. Soc. Rev.* 50 (15), 8669–8742. doi:10.1039/D0CS00461H

Wang, Z., Little, N., Chen, J., Lambesis, K. T., Le, K. T., Han, W., et al. (2021b). Immunogenic Camptothesome Nanovesicles Comprising Sphingomyelin-Derived Camptothecin Bilayers for Safe and Synergistic Cancer Immunochemotherapy. *Nat. Nanotechnol.* 16 (10), 1130–1140. doi:10.1038/s41565-021-00950-z

Wang, Z., Zhang, F., Shao, D., Chang, Z., Wang, L., Hu, H., et al. (2019c). Janus Nanobullets Combine Photodynamic Therapy and Magnetic Hyperthermia to Potentiate Synergetic Anti-Metastatic Immunotherapy. *Adv. Sci.* 6 (22), 1901690. doi:10.1002/advs.201901690

Ward, Z. J., Scott, A. M., Hricak, H., Abdel-Wahab, M., Paez, D., Lette, M. M., et al. (2020). Estimating the Impact of Treatment and Imaging Modalities on 5-Year Net Survival of 11 Cancers in 200 Countries: A Simulation-Based Analysis. *Lancet Oncol.* 21 (8), 1077–1088. doi:10.1016/S1470-2045(20)30317-X

Xu, J., Xu, L., Wang, C., Yang, R., Zhuang, Q., Han, X., et al. (2017). Near-Infrared-Triggered Photodynamic Therapy with Multitasking Upconversion Nanoparticles in Combination with Checkpoint Blockade for Immunotherapy of Colorectal Cancer. *ACS Nano* 11 (5), 4463–4474. doi:10.1021/acsnano.7b00715

Yeh, B. M., FitzGerald, P. F., Edic, P. M., Lambert, J. W., Colborn, R. E., Marino, M. E., et al. (2017). Opportunities for New CT Contrast Agents to Maximize the Diagnostic Potential of Emerging Spectral CT Technologies. *Adv. Drug Deliv. Rev.* 113, 201–222. doi:10.1016/j.addr.2016.09.001

Youn, Y. S., and Bae, Y. H. (2018). Perspectives on the Past, Present, and Future of Cancer Nanomedicine. *Adv. Drug Deliv. Rev.* 130, 3–11. doi:10.1016/j.addr.2018.05.008

Zhang, S., Wang, J., Kong, Z., Sun, X., He, Z., Sun, B., et al. (2022). Emerging Photodynamic Nanotherapeutics for Inducing Immunogenic Cell Death and Potentiating Cancer Immunotherapy. *Biomaterials* 282, 121433. doi:10.1016/j.biomaterials.2022.121433

Zhou, W., Chen, Y., Zhang, Y., Xin, X., Li, R., Xie, C., et al. (2020). Iodine-Rich Semiconducting Polymer Nanoparticles for CT/Fluorescence Dual-Modal Imaging-Guided Enhanced Photodynamic Therapy. *Small* 16 (5), e1905641. doi:10.1002/smll.201905641

Zou, Y., Wei, Y., Wang, G., Meng, F., Gao, M., Storm, G., et al. (2017). Nanopolymersomes with an Ultrahigh Iodine Content for High-Performance X-Ray Computed Tomography Imaging *In Vivo*. *Adv. Mat.* 29 (10), 1603997. doi:10.1002/adma.201603997

Conflict of Interest: The authors declare that the research was conducted in the absence of any commercial or financial relationships that could be construed as a potential conflict of interest.

Publisher's Note: All claims expressed in this article are solely those of the authors and do not necessarily represent those of their affiliated organizations, or those of the publisher, the editors, and the reviewers. Any product that may be evaluated in this article, or claim that may be made by its manufacturer, is not guaranteed or endorsed by the publisher.

Copyright © 2022 Xin, Ni, Shi, Shao, Zhang, Peng, Yang, Tian, Zhou and Zhang. This is an open-access article distributed under the terms of the Creative Commons Attribution License (CC BY). The use, distribution or reproduction in other forums is permitted, provided the original author(s) and the copyright owner(s) are credited and that the original publication in this journal is cited, in accordance with accepted academic practice. No use, distribution or reproduction is permitted which does not comply with these terms.

frontiers | Frontiers in Bioengineering and Biotechnology

TYPE Review
PUBLISHED 07 October 2022
DOI 10.3389/fbioe.2022.1024143

Check for updates

OPEN ACCESS

EDITED BY
Mingqiang Li,
Third Affiliated Hospital of Sun Yat-sen University, China

REVIEWED BY
Chendong Han,
Binghamton University, United States
Li Quan,
Huaiyin Institute of Technology, China
Liye Wang,
University of Houston, United States

*CORRESPONDENCE
Wenliang Li,
wenliangl@ciac.ac.cn

SPECIALTY SECTION
This article was submitted to Biomaterials, a section of the journal Frontiers in Bioengineering and Biotechnology

RECEIVED 21 August 2022
ACCEPTED 16 September 2022
PUBLISHED 07 October 2022

CITATION
Xiao X, Teng F, Shi C, Chen J, Wu S, Wang B, Meng X, Essiet Imeh A and Li W (2022), Polymeric nanoparticles—Promising carriers for cancer therapy.
Front. Bioeng. Biotechnol. 10:1024143.
doi: 10.3389/fbioe.2022.1024143

COPYRIGHT
© 2022 Xiao, Teng, Shi, Chen, Wu, Wang, Meng, Essiet Imeh and Li. This is an open-access article distributed under the terms of the Creative Commons Attribution License (CC BY). The use, distribution or reproduction in other forums is permitted, provided the original author(s) and the copyright owner(s) are credited and that the original publication in this journal is cited, in accordance with accepted academic practice. No use, distribution or reproduction is permitted which does not comply with these terms.

Polymeric nanoparticles—Promising carriers for cancer therapy

Xiao Xiao[1], Fei Teng[1], Changkuo Shi[1], Junyu Chen[1], Shuqing Wu[1], Bao Wang[2], Xiang Meng[1], Aniekan Essiet Imeh[3] and Wenliang Li[1,4]*

[1]School of Pharmacy, Jilin Medical University, Jilin, China, [2]School of Chemistry and Environmental Engineering, Changchun University of Science and Technology, Changchun, China, [3]School of Clinical Medicine, Jilin Medical University, Jilin, China, [4]Jilin Collaborative Innovation Center for Antibody Engineering, Jilin Medical University, Jilin, China

Polymeric nanoparticles (NPs) play an important role in controlled cancer drug delivery. Anticancer drugs can be conjugated or encapsulated by polymeric nanocarriers, which are known as polymeric nanomedicine. Polymeric nanomedicine has shown its potential in providing sustained release of drugs with reduced cytotoxicity and modified tumor retention, but until now, few delivery systems loading drugs have been able to meet clinical demands, so more efforts are needed. This research reviews the current state of the cancer drug-loading system by exhibiting a series of published articles that highlight the novelty and functions from a variety of different architectures including micelles, liposomes, dendrimers, polymersomes, hydrogels, and metal–organic frameworks. These may contribute to the development of useful polymeric NPs to achieve different therapeutic purposes.

KEYWORDS

polymeric nanoparticle, nanocarrier, cancer drug delivery, thermo-sensitive, pH-sensitive

1 Introduction

It has been noticed for long that clinical application of many potent remedial drugs in cancer and other diseases have been limited due to the following reasons: 1) poor aqueous solubility, and consequently, minimal systemic bioavailability (Anitha et al., 2011; Tosca et al., 2021). During the treatment, patients need to be injected with a large amount of saline, which easily causes water intoxication (Lauersen and Birnbaum, 1975). 2) Instability *in vivo*—the drugs are dispersible in the whole living body and tend to be metabolized and eliminated, which causes the change of drug concentration *in vivo* and reduces its efficacy (Marczynski et al., 2021; Fontana et al., 2021). 3) Toxic side effects—the drugs are always toxic to the normal cells at the same time, including nephrotoxicity, neurovirulence, and gastrointestinal reactions (Chen Y. et al., 2020; Deng et al., 2021). Patients need to take cytoprotective agents, which increases their pain. So large doses are not acceptable at all, and the efficacy of the drug is limited. 4) Drug

resistance—it is easy to cause multidrug resistance and reduce the effect of further treatment (Patil et al., 2010; Kim et al., 2013). Therefore, the development of new cancer drugs, the improvement of the absorption of the drugs, and the delivery of the drugs are urgent tasks.

Nanoparticles (NPs) are promising effective delivery tools as the candidates that overcome the difficulties in clinical applicability (Haley and Frenkel, 2008; Saw and Jon, 2020; Zheng et al., 2021). The colloidal particles with the size of 10–1,000 nm are termed as NPs. NPs can supply efficient therapeutic strategies by improving the bioavailability, stability, and target specificity to reduce side effects and overcome the limitations of conventional treatment methods (Gaumet et al., 2008; Yang et al., 2020; Ndebele et al., 2021). In addition, NPs have the potential to improve drug solubility, prolong cyclic half-life, and optimize drug pharmacokinetics (Verdurmen et al., 2021). NP-based drug delivery approaches have the potential of multifunction. They can disperse hydrophobic agents in aqueous media, thus improving the poor solubility, protecting the stability of drugs, and prolonging their circulation in the blood. They deliver the drugs to the target, therefore reducing the side effects and drug resistance. In general, NPs efficiently carry therapeutics to the target and are stable *in vivo* (Cotí et al., 2009; Sun et al., 2018; Li et al., 2020).

Nowadays, drug-loaded NPs are particularly viable for efficient cancer therapy due to their improved drug delivery and therapeutic effects in various types of cancer (Wang et al., 2010; Rejinold et al., 2011; Truong et al., 2015). Polymeric nanocarriers with conjugated or encapsulated anticancer drugs, also known as polymeric nanomedicines, show a variety of different architectures including polymer–drug conjugates, micelles, nanospheres, nanogels, vesicles, and dendrimers (Alexis et al., 2010; Liu et al., 2014) (Figure 1). They attract more attention for their ability to co-deliver multiple therapeutic agents and to target the tumor cells (Liu et al., 2020). Broad classes of therapeutics including cytotoxic agents, small interference RNA (siRNA), chemosensitizer, antiangiogenic agents, and so on can be carried by the nanoparticle platforms (Hu et al., 2010; Liao et al., 2014; Lammers and Ferrari, 2020). NPs enhance their retention effect and permeability on the basis of the exclusive pathophysiology of cancerous cells. NPs accumulate in cells without being recognized by P-glycoprotein, which results in the increased intracellular concentration of drugs. NPs can deliver chemotherapies to tumor cells at the right time when needed. They take the drugs to the right place, at the right concentration with greater efficacy and reduced cytotoxicity in peripheral healthy tissues (Gaitanis and Staal, 2010; Ambasta et al., 2011; Shao et al., 2015). Therein, a targeting strategy as a multitargeting system (MTS) has attracted extensive attention (Purushottamachar et al., 2013). In this strategy, the surface of NPs is decorated with two or more functional ligands for recognizing different receptors on the cells, which can enhance the multivalent interactions between the NPs and cell surface, and help to improve cell recognition and internalization. In addition, there are other strategies including adding pH-sensitive groups to improve drug efficacy (Asad et al., 2021). As NPs modify the cancer treatment techniques, various multifunctional NPs are now being investigated. Following are the overview of some typical polymeric NPs.

2 Typical polymeric nanoparticle carriers

2.1 Micelles

The polymeric micelle delivery of anticancer drugs improve the tumor targeting of drugs and reduce the drug resistance, which has aroused extensive research interest in recent years (Chen J. J. Y. et al., 2020; Mignani et al., 2021; Son et al., 2021). The polymeric micelle consists of a hydrophobic core and hydrophilic shell. Their sizes vary in tens to hundreds of nanometers. Its hydrophobic core is capable of packaging various hydrophobic drugs, such as cisplatin, doxorubicin, camptothecin, paclitaxel, and so on (Wu Y. et al., 2010; Soltantabar et al., 2020). Most of the hydrophilic shells are made of polyethylene glycol (PEG). PEG helps micelles to escape recognition and capture by the reticuloendothelial system. So the drugs inside could stay in the bloodstream long enough. Through the enhanced permeability and retention (EPR) effect, drugs will be accumulated in tumor tissue passively (Hori et al., 2010; Liu T. J. et al., 2011; Zhao et al., 2020). In addition to these, by introducing small organic molecules, peptides, protein, sugar moieties, nucleic acid ligands (e.g., aptamer), antibodies, and other tumor-targeting groups to the surface of the micelles, or through the combination with magnetic nanoparticles, micelles may even target tumor proactively (Chen et al., 2013; Yu et al., 2014; Yu Z. et al., 2015). Therefore, the use of micelles as drug delivery can significantly increase the bioavailability and the anti-cancer ability of drugs such as chemotherapeutic compounds, DNA, and siRNA and at the same time, reduce their toxicity and side effects (Jiang et al., 2021). The first to prove the potential of clinic application of the micelles with active targeting capacity is the clinical study of PSMA-targeted polymeric nanoparticles (Hrkach et al., 2012). So far, various methods for anticancer drugs have been explored to enhance cell internalization and subcellular distribution. The basic standpoint is to discover the self-changes of physiological properties of tumors and therefore take advantage of these changes to improve the related structure of micelles and increase the anticancer efficacy.

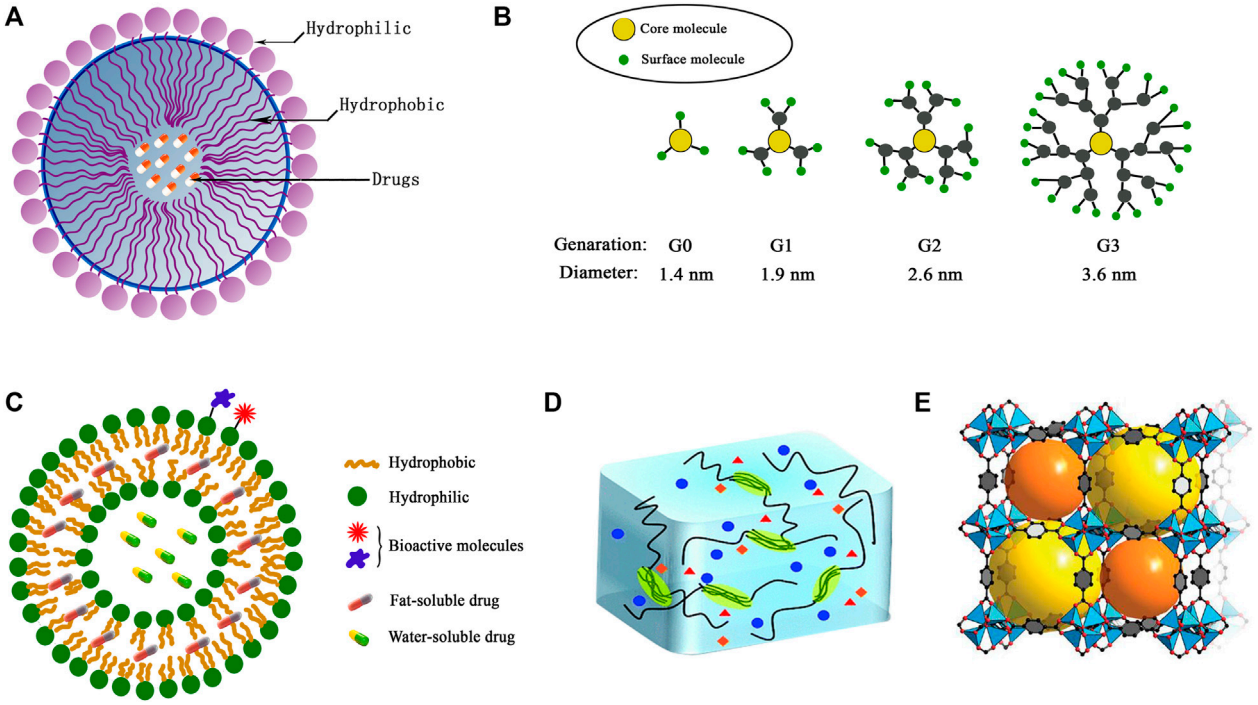

FIGURE 1
The structures of typical polymeric nanoparticles: **(A)** micelles, **(B)** dendrimers, **(C)** polymersomes, **(D)** hydrogel, **(E)** metal–organic framework (MOF).

2.1.1 pH-responsive micelles

In previous decades, it had been found that the delivery of polymeric micelles for anticancer drugs responding to tumor acidity may be an effective way. Plenty of pH-responsive copolymers responsive to weakly acidic tumor microenvironments (pH: 6.5–7.0) have been explored (Wu X. L. et al., 2010; Yang et al., 2010). Tumors show different acidic environments, including the extracellular pH (pH_E), and the environment is more acidic in the endosomal and lysosomal compartments of cancer cells (endosomes: pH 5.5–6.3 and lysosomes: pH 5.0–5.5) (Jiang et al., 2012). The average pH of normal tissue is around 7.4. Anoxia in the tumor cell prompts the anaerobic glycolysis to produce lactic acid. But the lack of a vascular system in tumor cells does not allow the lactic acid to be excreted completely, which leads to the acidic environment in tumor cells (Crayton and Tsourkas, 2011; Shen et al., 2012). The acidic environments in tumors can be treated as a signal to trigger the drug release of micelle carriers.

pH-responsive polymer micelles are mainly prepared by self-assembly of amphiphilic blocks or grafted copolymers (Basak and Ghosh, 2013; Kim et al., 2014). pH-responsive polymer segments must be contained, which can be made by protonated or deprotonated polymers. A deprotonated polymer is alkalescent with amine, pyridine, imidazolyl, or other basic groups. The protonated polymer may contain a carboxylic acid group which shows weak acidity. When pH value varies, the ionization state of the copolymer changes, causing the difference of the solubility of micelles in water. Poly (N,N-diethylaminoethyl methacrylate) (PDEA), poly (4- or 2-vinylpyridine) (PVP), poly (L-histidine) (PHis), and poly (β-amino ester) (PbAE) are the most common alkalescence copolymers (Figure 2) (Vamvakaki et al., 2005; Manganiello et al., 2012; Cai et al., 2015). These coploymers are not soluble in neutral or alkaline circumstances. When they are in acidic environments, the basic group is going to be protonated and positively charged, which results in their solubility. The ones with carboxylic acid group are on the contrary. They are soluble in basic environments, such as the groups of poly (2-alkyl acrylic acid), poly acrylic acid, and so on. The pH of the transition state from insolubility to solubility (pH_T) can be adjusted by the substituents (Gastaldi et al., 1996). The pH_T of pH-responsive polymer micelles suitable for the delivery of anticancer drugs should be 4.0–7.0 according to the acidic tumor environment (Xu et al., 2009). Another type of polymer used to prepare pH-responsive micelles is the acid-labile polymer. They can rapidly hydrolyze in a weakly acidic environment and complete the conversion from hydrophobicity to hydrophilia. To date, the chemical bonds rapidly hydrolyzing under acidic conditions are hydrazone, β-carboxamide, ester bonds, and so on (Agut et al., 2010; Lee et al., 2014; Shi et al., 2015). In general, pH-responsive micelles all have

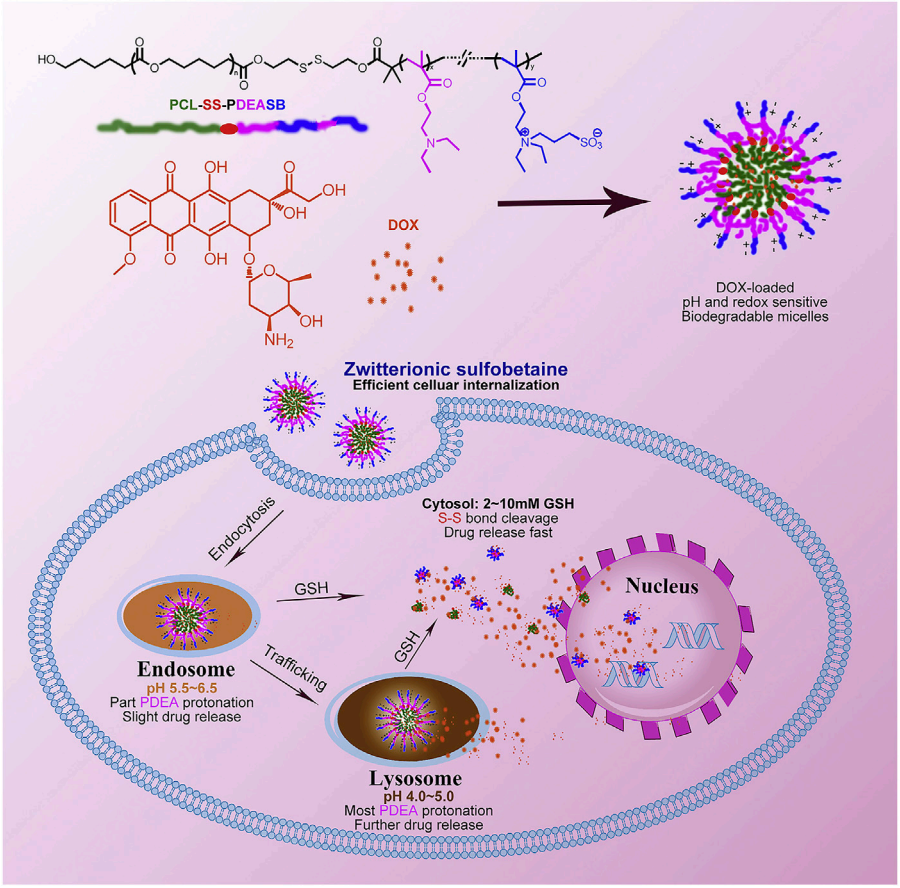

FIGURE 2
pH- and redox-sensitive micelles containing sulfobetaine for intracellular cell drug release. Adapted with permission from Cai et al. (2015).

the ability to dissociate in tumor microenvironment and release the drugs.

People now focus more on the multifunctional pH-responsive micelles. Recently, a kind of micellar-like polymeric amphiphile modulated by host–guest interactions in the presence of a lipophilic dye to induce assembly and phase transition under precise pH control was studied (Figure 3) (Kawano et al., 2021). Jun Hu has reported a paclitaxel-loaded cationic micelle from a block copolymer of poly (L-histidine) (3.7 kDa) and shortly branched polyethyleneimine (1.8 kDa) (Hu et al., 2013). The micelle is cationic, and its surface can be shielded by a negatively charged complex mPEG (2 kDa)-block-polysulfadimethoxine (4 kDa) (mPEG-b-PSDM) at pH 7.4. That made the micelle charge shielded. It was proven by the experiment that at pH 7.4, two human cancer cell lines, MCF-7 and SKOV-3, uptake the unshielded and deshielded micelle rapidly, while the uptake of the shielded micelle was minimal. The *in vivo* results from a mouse model also showed significant anticancer therapeutic efficacy. Pengcheng Yu also reported a mitochondria-targeted pH-responsive micelle: it is DOX-loaded and pH-responsive (Yu P. et al., 2015). The micelles were synthesized by a pH-responsive diblock copolymer, poly (ethylene glycol)-block-poly (2-(diisopropylamino)ethyl methacrylate) (PEGb-PDPA), and a vitamin E derivate (D-a-tocopheryl polyethylene glycol 1000 succinate, TPGS). DOX was released by the acidic pH-triggered micelle dissociation. At the same time, the TPGS segment assisted the drug by targeting mitochondrial organelles and reduced the mitochondrial transmembrane potential. *In vitro* experiments on DOX-resistant MCF-7/ADR cells demonstrated the micelles reduced the IC_{50} of DOX by a sixfold magnitude. *In vivo* animal studies also showed its powerful efficacy. Many other pH-responsive micelles like these are still being explored. All these results imply that the pH-responsive micelles have significant potential for drug delivery.

2.1.2 Reduction-responsive micelles

Reduction-responsive micelle is another effective delivery which has extensively been utilized for intracellular drug release as well. The point of reduction-responsive micelles is

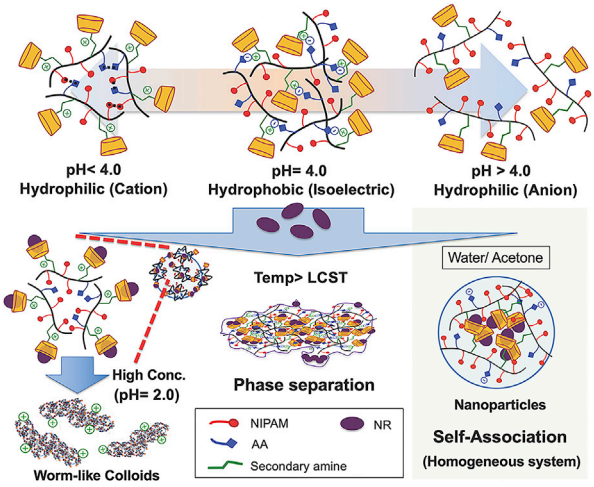

FIGURE 3
Colloidal assembly system comprising the poly (NIPAM-AA-β-CD) solution as a function of pH and temperature in both the homogeneous and inhomogeneous NR inclusion systems. Adapted with permission from Kawano et al. (2021).

mainly based on the over-expressed glutathione (GSH) in cancer cells. GSH in the cytoplasm of tumor has a concentration of up to 10 mmol/L. Compared to normal tissues, the cancer cells exhibit an notably reduced microenvironment due to the higher concentration of GSH (Yan et al., 2012). For this kind of micelles, an important reduction-responsive bond–disulfide bond has to be mentioned, which generally cross-links the core and shell or acts as the linkage between PEG shell and micellar core (Xia et al., 2018). High intracellular GSH levels result in the break of this bond, and PEG (or the shell) detaches from micelles, which triggers drug release. A typical example with this function is the biocompatible reduction-responsive micellar system reported by Ding et al. (2013). It is made of methoxyl poly (ethylene glycol) (mPEG) and poly (3-benzyloxycarbonyl-L-lysine) (PZLL) with disulfide-link. DOX can be loaded by the micelles with loading efficiency of about 30 wt%. In phosphate-buffered saline with 10.0 mmol/L GSH, DOX-loaded micelle was accelerated to release DOX and show higher cellular proliferation inhibition toward HeLa and HepG2 cell lines. In addition to that, the water-soluble reduction-sensitive reversibly core-cross-linked micelles were also studied (Rapp and Deforest, 2021). It is based on poly (ethylene glycol)-b-poly (N-2-hydroxypropyl methacrylamide)-lipoic acid (PEG-b-PHPMA-LA) conjugates and can be triggered to release DOX in the presence of 10 mmol/L catalytic dithiothreitol (DTT) which provides the reduction environment.

2.1.3 Photosensitive micelles

Photosensitive micelles mainly rely on the photosensitive segment. On exposure to light of appropriate wavelengths, the photosensitizers lead to the formation of reactive oxygen and therefore trigger the disruption of endosomal or lysosomal membranes (Ding et al., 2013; Xia et al., 2018; Rapp and Deforest, 2021). For instance, the polymeric micelles loading camptothecin (CPT) exhibited photosensitive endosomal escape, which reduced the cytotoxicity of camptothecin on photoirradiation (Nishiyama et al., 2009). Photosensitive platinum (IV) prodrugs (UVA-Pt2) are attached to polymers and self-assembled into micelles. The synthesized NP-UVA-Pt2 can be actively transported by tumor endocytosis, activated under UVA irradiation, and can release cisplatin to eliminate the tumor (Rong et al., 2014). Moreover, photosensitive platinum drugs can overcome the resistance of cisplatin (Hai et al., 2015).

The photosensitive supramolecular drug-loaded irradiated micelles had more potent cytotoxic effects against cancer cells exhibiting much higher cellular uptake efficiency (Figure 4) (Alemayehu et al., 2019). They rapidly entered the tumor cells to induce massive cell death. In addition to all the above, temperature-sensitive and enzyme-responsive micelles are also studied and show the potential to reach improved antitumor efficiency (Lee et al., 2007).

In general, the micelles can be used as carriers for the insoluble drugs which are with good therapeutic effect but have high toxicity. They are capable of loading insoluble anticancer drugs such as paclitaxel, hydroxycamptothecin, and doxorubicin with good results as we mentioned. They improve the solubility, the concentration, and the retention time of the drug at the tumor site, so as to improve the efficacy and reduce the side effects of the drugs. The micelles are also the carriers of gene drugs and protein drugs. The biodegradable micelle carriers have many advantages in gene delivery therapy, such as stability, non-toxicity, non-antigenicity, and gene protection. They act as non-viral vectors for plasmid DNA, small interfering RNA (siRNA), oligonucleotide, and so on. The development of safe delivery systems of the micelles will be the breakthrough of gene therapy. Furthermore, micelles also have applications in the traditional Chinese medicine. The micelles used in the study of active components, simple recipe, and compound recipe help to improve the dosage form and the therapeutic effect of the traditional Chinese medicine, which features in the modernization of traditional Chinese medicine. The group of Yan has obtained cationic nanomicelles as carriers of Chinese herbal medicine active components of ursolic acid. They enhance the drug efficacy in colorectal cancer treatment (Shu et al., 2020). At present, there are many researches on the multifunctional micelles. It is believed that with the developments of interdisciplinary research and new materials, nanomicelles will show more applications in pharmacy.

2.2 Dendrimers

A dendrimer is a synthetic nanomaterial. It was found and successfully synthesized by American chemist Tomalia D. A. in

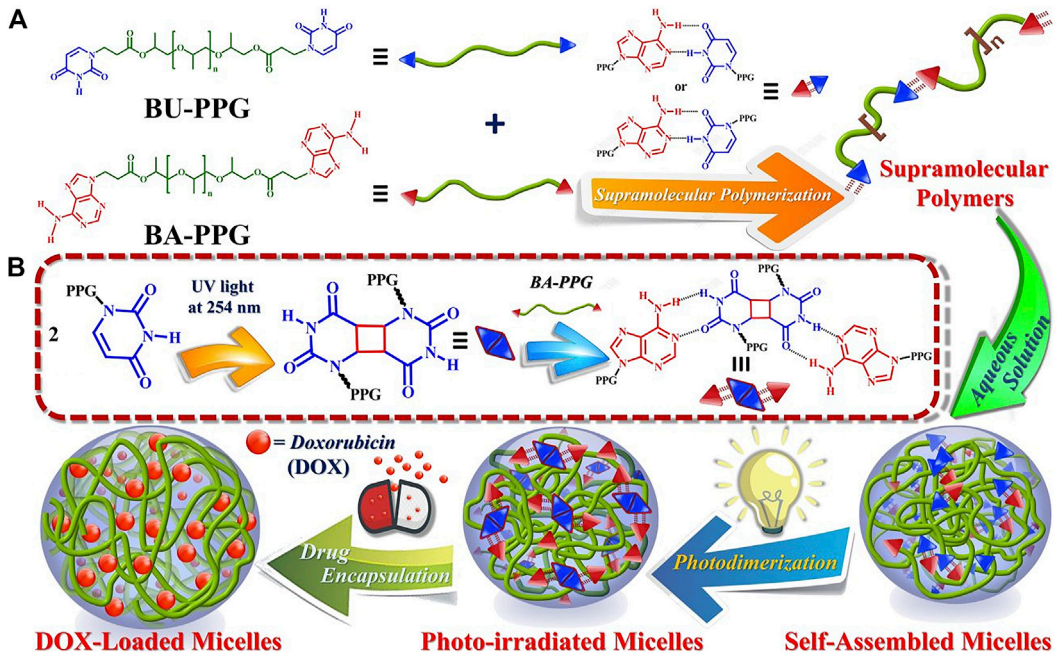

FIGURE 4
Schematic illustration of micelle formation and drug loading/release by photosensitive BA-PPG/BU-PPG in aqueous buffer solutions. Adapted with permission from Alemayehu et al. (2019).

the early 1980s (Padias et al., 1987). In the past 20 years, dendrimers, with their unique structures and performance, have received attention in many fields such as material science and biomedicine (Liu X. et al., 2011; Li et al., 2016). The basic research and practical application of dendrimers have been studied continuously. With the development of the study on drug delivery, the delivery of dendrimers was explored. The dendrimers have been hot for a long time as the gene and drug delivery. Dendrimers have specific three-dimensional structures. It is the macromolecule which is synthesized nanometer by nanometer. Dendrimers can be distinguished from other polymers by its highly branched, tree-like structure. All branching monomers originate from one core, which can be divided into two types according to their growth directions: divergent growth and convergent growth. Different from ordinary polymers, dendrimers show low viscosity, high solubility, mixability, and high reactivity. At the same time, their volume and shape can be controlled in the synthesis process. The surface can be made into a dense area composed of different molecular groups, which play the role of hooks. In particular, each terminal functional group can be combined with the attachment point of polyvalent molecules on the surface of viruses and cells, so as to facilitate the adhesion of various useful molecules. A dendrimer parcels the drug in two ways. The drug molecules can be physically captured in the interior of the dendritic structure or covalently bonded to the surface or other groups of dendrimers forming polymer–drug conjugates. As drug or gene carriers, dendrimers selectively accumulate in the tumor tissue site actively by some targeted groups or passively through the EPR effect, which makes the delivery system targeted. It can be designed and synthesized for specific application. With these features, dendrimers are becoming a new type of promising cancer drug carrier. Dendrimers are safe and efficient non-biological carriers for the cancer drugs. In spite of these, there are still many problems to be solved, especially the specific toxicology and biocompatibility of dendrimers, which need to be further studied. It is believed that with the development of nanotechnology and the improvement of design and synthetic methods, dendrimers will eventually go into clinical application generally.

2.2.1 Divergent growth dendrimer

The divergent growth method refers to the dendrimer growing and spreading from a initiator like ethanediamine or propylamine through gradual polymerization. Each polymerization reaction may form a new layer (or called generation) on the surface, marked as G_0, G_1, G_2···G_{10}. So the size and number of generations are decided by the synthesis procedure. For the steric hindrance effect formed by the compression of high-density branches, the self-growth will be limited. After the cyclic reaction, the generations can be up to 10 at most. The choice of initiator is very important, which

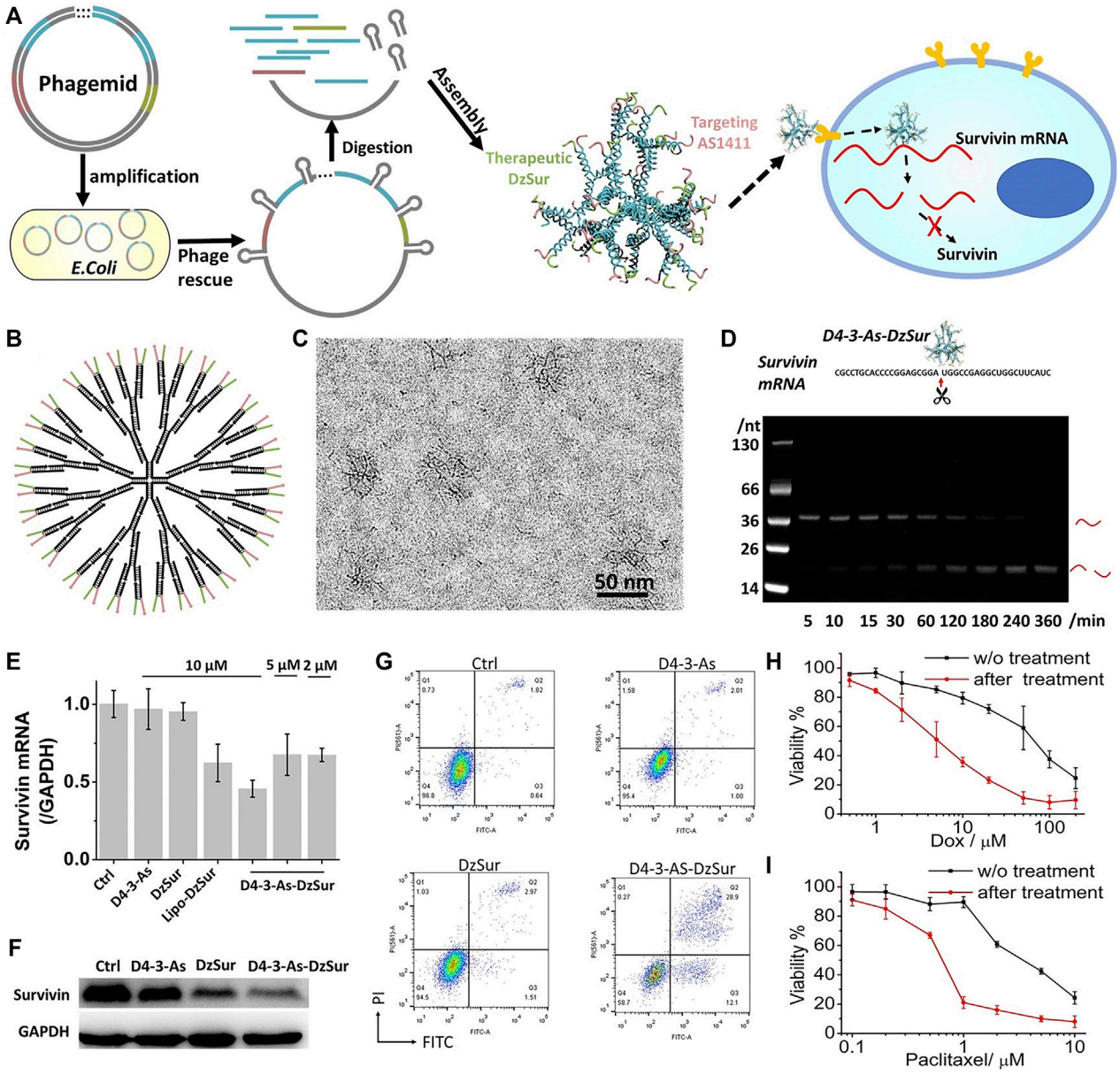

FIGURE 5
Targeted survivin regulation by the DNA-dendrimer-based nanomedicine D4–3-As-DzSur. **(A)** Biotechnological production. **(B)** 2D structure. **(C)** Cryo-TEM image. **(D)** Survivin mRNA cleavage property. **(E)** qPCR tests. **(F)** Western blot analysis of survivin suppression in A549 cells. **(G)** Apoptosis analysis of A549 cell. **(H,I)** Chemosensitization effect on DOX **(H)** and paclitaxel **(I)**. (Lu et al., 2021).

determines the charge density of the whole polymer and the surface charge. The end functional groups are added at the end generation. The chemical properties of the molecules depend on the type of end-functional groups and their physical properties, such as solubility and viscosity, are also affected by the end groups. For example, the dendrimer-entrapped gold nanoparticles synthesized by Xiangyang Shi belong to this type. They are modified by folic acid (FA) and fluorescein isothiocyanate (FI) molecules which are water-soluble, stable, and biocompatible (Shi et al., 2007). FA and FI help the anti-cancer drug to exhibit bioactivity better. As the author reported, the FA- and FI-modified dendrimer-entrapped gold nanoparticles show high inhibition to kB cells (a human epithelial carcinoma cell line). PAMAM-G7 reported by Mitra Gholami was synthesized by the divergent growth method (Gholami et al., 2017), and a 6th generation dendrimer was synthesized in a single day by Per Antoni through the divergent growth method (Antoni et al., 2010). DNA-dendrimer-based

nanomedicine constructed by the flexible 3-arm building blocks with a highly efficient one-pot DNA assembly was designed (Figure 5) (Lu et al., 2021). This is the first DNA nanomedicine (D4–3-As-DzSur in literature 109) genetically encoded, biotechnologically produced, and directly self-assembled. The good targeted gene regulation has been proved by *in vitro* and *in vivo* tests.

2.2.2 Convergent growth dendrimers

The convergent growth method is the second way to synthesize dendrimers. It refers to the dendrimer growing in reverse order as compared to the divergent growth method. It is triggered by the dendrons coupled with branch units. The dendrons target and link in one direction to the core molecule, and produce the tree-like polymer. The advantage of convergent growth method is that different terminal groups can be selected for different application requirements. The highly asymmetrical dendritic macromolecules containing well-defined functionalities at their periphery were synthesized by Craig J. Hawker using the convergent growth approach (Hawker and Fréchet, 1990). It was shown that the convergent growth method offered unparalleled control over the placement and number of functional groups at the periphery of dendritic macromolecules.

In summary, dendrimers achieved efficient gene transfer in a variety of cell tissues, which will lead to the targeted and multifunctional anticancer therapy. The dendrimers have many advantages such as no gene size limitation, being suitable for mass production with good reproducibility and low cost, and being easy to modify. They offer a new direction for the study of non-viral carriers. Different types of dendrimers have their own advantages and play a role in gene therapy, particularly the ones with the modifications of amino acids and peptides realize high transfection efficiency and targeting in specific cells. However, their biotoxicity and biocompatibility limit their development, so chemical modifications are needed. The modifications increase the uptake rate of cells, improve the efficiency of gene transfection *in vivo*, and expand the application of dendrimers. The modification of supramolecular parent material improves the membrane penetration of dendrimer, but the supramolecular parent material itself needs to be modified before binding to the dendrimer. Almost all the supramolecular parent materials, except natural cyclodextrin, were synthesized with complex steps, which limits their application. The modification from inorganic group confers dendrimers new properties and makes multifunctional gene vectors. However, inorganic substances cause the antigen and antibody reactions *in vivo*, which makes them unsuitable for safe gene therapy. Some functional responsive dendrimers improve the efficacy of drugs, while the clinical applications of them is still lacking. Therefore, the combination of organic and inorganic materials with dendrimers through physical or chemical methods is going to be explored to complete the safe multifunctional therapy of the dendrimers.

2.3 Polymersomes

Polymersomes are a kind of supramolecular aggregates formed by the self-assembly of amphiphilic molecules. They own spherical single-chamber or multi-chamber structures formed by closed bilayers, which are similar to the structure of cell membranes (Christian et al., 2009; Kim et al., 2009). As drug carriers, polymersomes modify the distribution of drugs in body, prevent drug degradation and inactivation, extend the action time of drugs, and reduce side effects. After being parceled by polymersomes, the drugs may prolong their circulation time in blood and target tumor selectively. The polymersomes are self-assembled by the synthetic or natural modified amphiphilic polymers (Pangburn et al., 2012). Compared with surfactants, liposomes, and other small vesicles, polymersomes show the advantages of easy molecular design, high intensity, good stability, strong permeability, and so on. In recent years, due to the rapid development of macromolecular self-assembly technology, as a new type of drug carrier, polymersomes have developed well and become the important current research on novel self-assembly drug delivery. Because the structure of polymersomes is similar to that of liposomes, they have a hydrophilic inner cavity and a hydrophobic membrane bilayer (Chandrawati and Caruso, 2012). So, similar to a liposome, it delivers hydrophilic drugs and hydrophobic drugs at the same time, being a unique drug carrier for these two kinds of active constituents. In addition, the hydrophilic shell on the surface of polymersomes shows better stability, enhanced permeability, and retention. Bioactive molecules, such as antibodies, polypeptides, and ligands, can be attached to the surface of polymersomes stably. These molecules also make the polymersome an active target or show other biological effects. Polymersomes can also be used as carriers for artificial oxygen (Wen et al., 2014). Different amphiphilic polymer molecules (different species, molecular weight, block proportion, polymer structure, etc.) affect the physical and chemical characteristics (particle size, film thickness, permeability, drug loading, etc.) and the *in vivo* behavior of the polymersome, which makes the polymersome system more controllable. Therefore, polymersome, as a new type multifunctional drug delivery, because of its high drug loading, high encapsulation efficiency, stability, and controllability, can be used to improve the targeting delivery and bioavailability of anti-cancer drugs. Like their low molecular weight analogues liposomes, they can be stimuli-sensitive (Li and Kellera, 2009; Siegel, 2014). Stimuli include pH, temperature hydrolysis, oxidation, reduction, light, and so on. Here, we discuss the thermo- and pH-sensitive polymersomes.

2.3.1 Thermo-sensitive polymersomes

For the polymers sensitive to temperature stimulation, their hydrophobicity increases as the temperature changes, and the polymersomes are formed so. The hydrophobic segment most commonly used for thermo-sensitive polymer is poly (N-isopropylacrylamide) (PNIPAAm) (Lorenzo et al., 2005; Cao et al., 2007). PNIPAAm has lower critical solution temperature (LCST) of 30–50°C. It is completely soluble in aqueous solution when the temperature is lower than LCST, while it becomes insoluble when the temperature is higher than LCST. The polymers with PNIPAAm block self-assembly to form micelles or polymersomes when they are more hydrophobic. Drugs can be loaded in these polymersomes at temperatures below LCST. When the temperature is above LCST, these polymersomes are collapsed to release the drugs. The drug release responding to the temperature change makes thermo-sensitive polymersomes, and they become excellent carriers for controlled drug release applications. So far, the blocks have been used for thermo-sensitive polymersomes including poly (N-(3-aminopropy1)-methacrylamide hydrochloride)-b-PNIPAAm, poly (2-einnamoylethyl methacrylate)-b-PNIPAAm, PEG-PNIPAAm, and so on (Pamies et al., 2009; Zhang et al., 2011; Quan et al., 2013). Thermo-sensitive poly (N-isopropylacrylamide-co-acrylamide- coallylamine) (NIPA-AAm-AH) polymersomes reported by Maham Rahimi with lower LCST can be incorporated with various molecules at the surface (Rahimi et al., 2008). The polymersomes were synthesized by the approach of free-radical polymerization. They can release the DOX most at 41°C. Biao Yang prepared the pore-covering polymer brushes by PNIPAAm onto the PET (Yang and Yang, 2003). With the change of the temperature, the pore size varied with the swelling and shrinkage of poly-PNIPAAm brushes and the membranes' fluxes were adjusted.

2.3.2 pH-sensitive polymersomes

pH-sensitive polymers have titratable functional groups and can be protonated or deprotonated by adjusting environmental pH value. Thus, the solubility of the polymer will be changed to prepare pH-sensitive polymersomes. The pH-response can be obtained either by polyacid blocks which lose H^+ and become ionized by a higher pH variation, or by polybase blocks that can be protonated and insoluble at lower pH. The best advantage of pH-triggered release is the fast response of the system. The release occurs almost instantaneously. For example, in the case of poly (2-(methacryloyloxy)ethyl phosphorylcholine)-b-poly (2-(diisoprop ylamino) ethylm ethacrylate (PMPC-PDPA) polymersomes reported by Du Jian-zhong, when the pH value of the solution altered from 2 to greater than 6, the hydrophobicity of PDPA was enhanced due to the deprotonation of the tertiary amine group in the PDPA segment, and the di-block copolymer PMPC-PDPA formed polymersomes (Du et al., 2005). In a similar way, for the di-block copolymer poly (butadiene)-b-poly (L-glutamic acid) (PBD-PGA), the particle size of 100–150 nm can be prepared through deprotonation of PGA by adjusting pH value. Polymersomes composed of poly (ethylene glycol)-polyester reported by Fariyal Ahmed were shown to break down into membranelytic micelles within hours at low pH (Ahmed et al., 2006). The antitumor drug with their delivery kill growing tumor rapidly and effectively. Thermo- and pH-sensitive polymers synthesized by N-isopropylacrylamide and methacrylate monomers derived from cholic acid with ethylene glycol and oligo spacers through free-radical polymerization were also reported by Benrebouh et al. (2001).

The polymersomes have so many advantages as we mentioned and they can deliver the water-soluble and hydrophobic drug molecules at the same time. They are widely used to encapsulate vulnerable proteins and genetic drugs. The time in blood circulation of the polymersomes can be extended with PEG modification. Drug release can be regulated by changing the type of polymer and the proportion of hydrophilic and hydrophobic segments. Stimulus-responsive polymersomes avoid unnecessary drug leakage, improve bioavailability, and reduce side effects. Targeted polymersomes enable targeted drug delivery. Compared with liposomes and other traditional NP delivery systems, polymersomes are easier to be prepared using cheaper raw materials and with better stability, which has become a new predominant NP delivery system. However, the clinical application of polymersomes still faces some challenges. First of all, the sterilization of polymersomes is the main obstacle to be used as nano-carriers. Because the sterilization temperature is higher than the transition temperature of gel liquid in the polymersome preparation, heat energy will break their structures, leading to drug leakage from the polymersomes, so heat sterilization (such as dry heat sterilization and high pressure steam sterilization) is not suitable for the polymersomes. Membrane hyperfiltration is not suitable for polymersomes with particle diameters larger than the membrane aperture (0.22 μm) either. The preparation of polymersomes under aseptic conditions may be a solution. Many pharmaceutical preparations, such as eye ointment, eye drops, and injections, are sterilized by gamma ray, which produces less heat. Therefore, gamma-ray sterilization has the potential to be applied to the sterilization of polymersomes. In addition, the potential toxicity is another limitation for the clinical application of polymersomes. The biodegradability of polymersomes, their responses to stimuli, and targeting ability need further study. Meanwhile, the mechanisms of circulation, distribution, and metabolism of polymersomes in the body are not very clear. Solving these problems will be an important task for researchers.

2.4 Hydrogels

Under certain conditions, colloidal particles connect with each other in the dispersion medium to form a spatial network. Meanwhile, the dispersion medium is filled in the interspace of

the structure. The dispersion system formed thereby is called hydrogel. The hydrogel contains large amount of liquid without mobility. Their affinity to imbibe water is attributed to the hydrophilic groups such as -OH, -CONH-, -$CONH_2$-, and -SO_3H in the structures (Hamidi et al., 2008). So hydrogels are described as three-dimensional configurations capable of absorbing large amounts of water or biological fluids. Hydrogels composed of 3D hydrophilic polymer chains have unique configurations and adjustable physicochemical properties (Peng et al., 2020). Even though the hydrogels absorb water well, they cannot be dissolved in an aqueous solution. When in aqueous surrounding environment, hydrogels will swell as a consequence of the critical crosslinks in the structure. These crosslinks can be physically (entanglements or crystallites) or chemically (tie-points and junctions) formed by the present of covalent bonds, hydrogen bonds, van der Waals interactions, or physical entanglements (Bernhard and Tibbitt, 2021; Zhang et al., 2021). The hydrogels can be generally divided into two groups: elastic hydrogel and brittle hydrogel. Elastic hydrogel is permeable. With the loss of the dispersion medium, the volume of elastic hydrogel will obviously decrease, and when the dispersion medium is reabsorbed, the volume increases, such as gelatin. The shape and volume of brittle hydrogel, such as silica gel, do not change when the dispersion medium is released and absorbed. Because of the small particle size, high water content, long retention time in blood, and degradability, hydrogel can be used as a carrier for cancer drugs. However, nanogels are mostly prepared in traditional ways. The release process is difficult to control, and some cross-linking agents are toxic to the body. In order to improve the safety and efficiency of hydrogel carriers in clinical drug delivery, new materials and cross-linking agents are synthesized to obtain multifunctional nanogels with high drug load, strong controllability, and good safety, so as to benefit from its advantages in drug delivery. Controlled-release or stimuli-induced-release hydrogel systems have become the focus of attention.

2.4.1 Temperature-sensitive hydrogels

Due to the special constituents, the hydrogels repeat swelling-deswelling conversion. Temperature-sensitive hydrogels, also known as thermo-responsive hydrogels, are the ones accomplishing the conversion by responding to the environmental temperature changes. Most of the temperature-sensitive hydrogels have hydrophobic groups, such as methyl, ethyl, and propyl groups. As we mentioned, among the polymersomes, PNIPAAm is probably the most widely used. The hydrogels made up of LCST polymers display shrinkage when the temperature rises above the LCST. At lower temperatures, the hydrogen bonds in the hydrophilic block of polymer and water dominate to increase the dissolution in water. While with the temperature increases, hydrophobic interactions in hydrophobic segments dominate, and hydrogen bonding becomes weaker. That results in the hydrogel net shrinking because of interpolymer chain association through hydrophobic interactions. The more the hydrophobic constituents are contained, the lower the LCST becomes. LCST could be controlled by the ratio of hydrophilic and hydrophobic segments. The hydrogels with PNIPAAm show faster shrinkage and sensitivity to additional stimuli. For example, the temperature-sensitive hydrogels based on the interpenetrating network of PNIPAAm was immobilized on porous silica gel and hydroxyapatite (Shin et al., 2001; Shin et al., 2002). The ones with chitosan and hyaluronic acid were studied with their physicochemical characteristics. *In vitro* drug release and *in vivo* pharmacodynamics were examined in detail (Ayon et al., 2015). The ones with loaded carboplatin for controlled drug delivery have also been explored (Andre et al., 2007). These series of studies on the temperature-sensitive hydrogels in the pharmaceutical field showed promising results. Recent studies on temperature-sensitive hydrogels have shown that hydrogen bonding and hydrophilicity of polymers are important factors affecting the quality of delivery. At the same time, the large concentration and the addition of non-water-soluble agents will bring up safety problems. So modifying its structure or being mixed with other auxiliary materials or environmentally sensitive materials are the effective ways to improve the response to temperature, so as to prolong the drug retention time and improve the efficiency.

2.4.2 pH-sensitive hydrogels

pH-sensitive hydrogels have been most frequently used to develop controlled release systems. pH-sensitive hydrogels generally contain ionic groups—acidic or basic groups that either give out or accept protons in response to environmental pH changes. The change of the pH value will affect the electric charge of ionic groups of the hydrogels, which leads to the increase of charge repulsion, thus causing the hydrogel to change from collapsing state to stretching state. That is the process of swelling and deswelling. The microenvironment pH of tumor cells is more acidic than the normal ones, so the tumor cell can be the trigger of drug release of the pH-sensitive hydrogels. The hydrogels dissolve more or swell more at low pH due to ionization. Different comonomers give different hydrophobicity to the hydrogels, causing different pH-sensitive behaviors. Examples of these are hydrogels based on poly (lactic acid), methoxyl poly (ethylene glycol), and itaconic acid prepared by Ke Wang; pH-responsive co-polymeric hydrogels studied by Umaira Rehman; and polyacrylamide grafted pectin pH-sensitive hydrogel reported by Prashant B. Sutar (Omidia et al., 2019; Sarfraz et al., 2019; Rehman et al., 2021).

2.4.3 Other stimuli-sensitive hydrogels

Electro-sensitive hydrogels shrink or swell in the presence of an applied extra electric field. In some cases, the hydrogels show

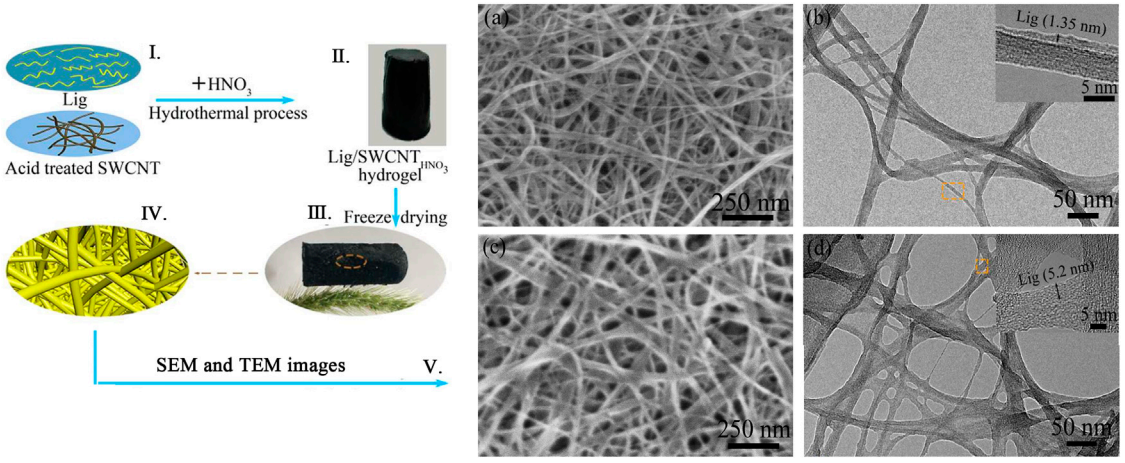

FIGURE 6
(I–IV) Aerogel assembled by Lig (lignosulfonate) and acid treated SWNCT (single-walled carbon nanotubes). (V) SEM and TEM images of Lig/SWCNT and Lig/SWCNT$_{HNO3}$. Adapted with permission from Peng et al. (2018).

swelling on one side and deswelling on the other side, resulting in the hydrogels bending. The hydrogel shape changes (swelling, shrinking, and bending) with the trigger of the electric field. That is the basis of the electro-sensitive hydrogels, such as carbon nanotube-coated hydrogel hybrids made by Servant et al. (2013). The visible light-sensitive hydrogel is readily available, low-priced, safe, clean, and easily manipulated. They are prepared by introducing a light-sensitive chromophore to the hydrogels, such as the polypeptide hydrogel synthesized by Charati et al. (2010). In addition to these, pressure-sensitive, specific ion-sensitive, and antigen-responsive hydrogels were all studied (Ikeda et al., 2010; Liu et al., 2013; Peng et al., 2018). The dibenzo-18-crown-6 copolymer was introduced into the PNIPAM system, which showed ionic sensitivity due to selective complexation with the crown ether unit, making the hydrogel show good ionic response to potassium (Figure 6) (Peng et al., 2018).

Hydrogels have been widely used in drug delivery due to their excellent biocompatibility and high water content. They can release drugs selectively and continuously respond to different environments. Related products especially the transdermal hydrogels are already on the market. The dosage forms are diverse and show different advantages such as high drug loading efficiency, good permeability, and high bioavailability. Hydrogels control drug release more accurately, significantly improve the solubility of some drugs, and they are easy to remove. At present, hydrogel is still a hot topic in academic research. As can be seen from the launch of the hydrogel products, hydrogel has broad application and market prospect. However, some problems still restrict the application of hydrogel in drug delivery. For example: 1) most of the hydrogels have relatively low tensile strength and elasticity, which makes them easy to break; 2) water swelling occurs and the swelling rate is high; and 3) hydrogels do not degrade easily and lack biological functions. Therefore, there are two directions for the future research of hydrogels. One is the structural transformation of existing hydrogel materials. The other is exploring new hydrogels with better performance, and designing a stimulation-responsive hydrogel drug delivery system.

2.5 Metal–organic frameworks

Metal–organic frameworks (MOFs) refer to the infinite network of crystalline materials formed by the self-assembly of transition metal ions or a metal cluster with the organic ligand. They are mainly used in the field of chemistry research such as magnetism, optics, and biological imaging (Chen G. et al., 2020; Chang et al., 2021). In recent years, medical researchers have reduced the size of such materials to the nanometer scale (NMOFs) and tried to use them in the fields of biological medicine storage, slow release, biological imaging, and the transmission of gaseous signal molecules (Liang et al., 2016; Wang et al., 2020). NMOFs can be synthesized by reprecipitation, reverse microemulsion, solvothermal method, or template synthesis method. NMOF has a large specific surface area, which makes it possible to be used as a drug carrier. NMOF shows good polymorphism and tunability due to the diverse types of the metals and the various coordinating abilities of the ligands. The coordination numbers of different metal ions are different, and the same metal ion may have different coordination numbers in different coordination environments. There are numerous organic ligands, especially those containing multiple carboxyl groups. Therein, the

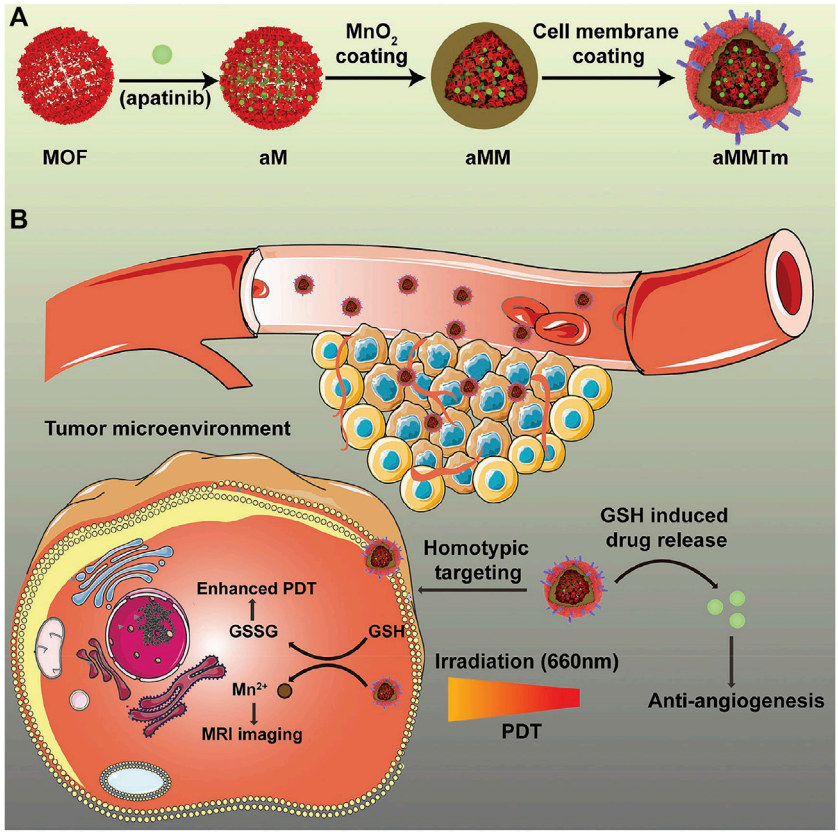

FIGURE 7
Schematic illustration of an integrated nanosystem apatinib-loaded MOFs (aMMTm) preparation and proposed combination therapy of photodynamic therapy and antiangiogenesis. Adapted with permission from Min et al. (2019). **(A)** The construction of porphyrinic metal-organic framework nanoparticle aMMTm through drug loading, MnO_2 coating and tumor cell membrane decoration. **(B)** Proposed action mechanism of aMMTm in a mouse tumor model. The tumor cell membrane camouflage may help the nanoparticles to escape early clearance and to target tumor tissue through homotypic affinity.

carboxyl group has a variety of coordination modes, and there may be two or more carboxyl groups in the ligand, so the coordination mode is very complicated. These all increase the adjustability of NMOFs. The structure of NMOFs is also affected by the synthesis condition. So, numerous various kinds of NMOFs are obtained by now, such as square shape, brick wall shape, diamond shape, quartz shape, ladder shape, lattice structure, and so on (Tavra et al., 2015; Chen J. et al., 2020; Lazaro et al., 2020). Storage and the release of drugs in the porous material are determined by a series of factors, including the pore size, pore morphology, pore-to-pore connectivity, and guest affinity. For traditional porous materials such as silicon, the capacity is not high enough, so loaded drugs are difficult to release. Porous NMOFs with large volume of aperture and regular structure can achieve high drug loadings and controlled drug release. The reported NMOFs as carriers have shown high drug loading. They load nonsteroidal anti-inflammatory drugs, antiviral drugs, and the antitumor drugs. The active exchange of NMOFs was completed almost exclusively through clathrin-mediated endocytosis, while the uptake was concerned with both clathrin and caveolae-mediated endocytosis. The NMOF is situated mostly in lysosomes against lysosomal degradation for further degradation in the cytosol, and drugs are released and distributed to different cellular organelles (Figure 7) (Min et al., 2019). The advantage of the NMOF is that it can be administered through a variety of ways and improve the pharmacokinetics of loaded drugs. Experiments showed it improves the antitumor activity of the controlled release system applied to the drugs based on Pt. Moreover, Maspoch etc. chose doxorubicin, camptothecin, and several other anticancer drugs to be loaded by MOFs through the self-assembly process (Imaz et al., 2010). Because these drugs have fluorescent properties, the release process was monitored. The NMOF as a drug delivery carrier greatly reduces side effects for the body and improves the drug efficacy in the focal area of body. Through chemical modification, NMOF forms a new drug release system and has become a hot research topic.

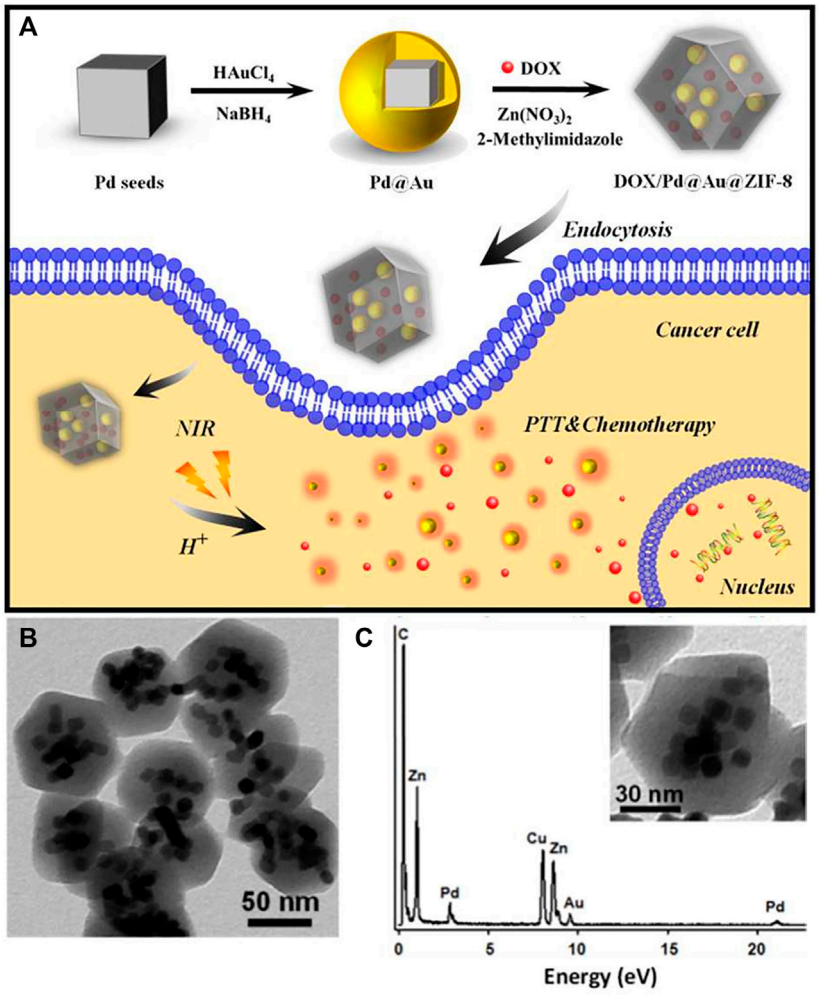

FIGURE 8
(A) DOX/Pd@Au@ZIF-8 and its application in pH and near-infrared-triggered chemotherapy photothermal synergistic treatment of cancer cells; **(B)** DOX/Pd@Au@ZIF-8 TEM images; **(C)** DOX/Pd@Au@ZIF-8 TEM-associated EDX spectra. Adapted with permission from Yang et al. (2017).

2.5.1 Ordinary metal–organic frameworks

Here, the ordinary MOFs refer to the ones that are not environmentally sensitive. Through the modification to make them carry a variety of functional groups, MOFs for cancer drug delivery show different characteristics. Such as the NMOFs modified by folic acid, through the mutual connections of organic groups, the surface is filled with folic acid, which make the NMOF a folate receptor with targeting property (Sun et al., 2012). 5-FU uracil was loaded in, and the release could be sustained. This NMOF with larger drug loading capacity reduced the side effects and overcame the disadvantages. It has application prospects in antitumor treatment. The group of Lin synthesized Fe(III)-carboxylate nanoscale metal–organic frameworks with high specific surface area by the rapid microwave method (Rieter et al., 2008; Pashow et al., 2009). The ferric center is Fe^{3+} ion. 1,3,5,7-tetramethyl-4,4-difluoro-8-bromomethyl-4-bora-3a,4a-diaza-s-indaeene (Br-BODIPY) and ethoxysueeinato-cisplatin (ES-CP) were used to increase the histocompatibility. Coated with a shell of SiO_2 with Na_2SiO_3 as the silicon source, the MOF was bonded with fluorescence and anticancer drug through a modified covalent bond. The drug loaded in the ferric MOF showed biotoxicity similar with cisplatin to human colon cancer cell line HT-29 at the same concentration. The nanoscale MOFs for the co-delivery of cisplatin and pooled siRNAs was also studied by Lin (Kathryn et al., 2009; He et al., 2014). The MOFs enhanced therapeutic efficacy in drug-resistant ovarian cancer cells.

2.5.2 Stimuli-sensitive metal–organic frameworks

Compared with other drug deliveries, the study of MOFs started late and is under development. Even though

TABLE 1 The materials, cargo and *in vivo*/vitro test status of some typical nanoparticles.

Type	Function	Materials	Cargo (not limited to this)	*In vivo* test	*In vitro* test	References
Micelles	pH-responsive	AP peptide/PEG-poly$_{(D,L\text{-lactic acid})}$/(ethylene glycol) (MPEG)-poly (β-amino ester	Doxorubicin	Done	Done	Wu X. L. et al. (2010)
		Hyperbranched aliphatic polyester, Boltorn H40/poly (ε-Caprolactone/poly (malic acid) (PMA-co-PCL)/poly (ethylene glycol)/folate	Doxorubicin	-	Done	Yang et al. (2010)
		Polymethacrylates (PMA)-grafted poly (amidoamine) (PAMAM)/folate-PEGylation	Paclitaxel	Done	Done	Shen et al. (2012)
		Poly (ε-caprolactone)-SS-poly (N,N-diethylaminoethyl methacrylate)-r-poly (N-(3-sulfopropyl)-N-methacrylate-N,N-diethylammonium-betaine) (PCL-SS-PDEASB)	Doxorubicin	-	Done	Cai et al. (2015)
	Reduction-responsive	Hyaluronic acid-tocopherol succinate (HA-ss-TOS) polymers/hyaluronic acid-tocopherol succinate (HA-TOS)	Paclitaxe	Done	Done	Xia et al. (2018)
		Poly (L-histidine)-block-short branched polyethyleneimine (PHis-b-sbPEI)/mPEG-block-polysulfadimethoxine (mPEG-b-PSDM),	Doxorubicin	-	Done	Ding et al. (2013)
	Photosensitive	Methoxyl-poly (ethylene glycol)-block-poly (lactide-co-2-methyl-2-carboxyl-propylene carbonate-ethanol amine)	Platinum (IV) prodrug (UVA-Pt2)	-	Done	Rong et al. (2014)
		Methoxy-poly (ethylene glycol)-block-poly (e-caprolactone)-block-poly-L-lysine, mPEG$_{114}$-b-PCL$_{20}$-PLL$_{10}$	Cisplatin	Done	-	Hai et al. (2015)
		MMPs-specific PEGylated peptide	Doxorubicin	Done	Done	Lee et al. (2007)
Dendrimers	Ordinary	FA- and FI-modified {(Au^0)$_{51.2}$-G5·NH$_2$} DENPs	-	Done	-	Shi et al. (2007)
		D4@3-As-DzSur with AS1411 as targeting ligands and anti-survivin DNAzyme as therapeutic agents	Doxorubicin	Done	Done	Gholami et al. (2017)
Polymersomes	Thermo-sensitive	Poly (N-isopropylacrylamide)-chitosan (PNIPAAm-CS)	Ocular drug	Done	Done	Cao et al. (2007)
		Poly (N-isopropylacrylamide-co-acrylamide-co-allylamine) (NIPA-AAm-AH) nan	Doxorubicin	Done	-	Rahimi et al. (2008)
	PH-sensitive	Poly (ethylene glycol)-polyester	Doxorubicin/Paclitaxe	Done	Done	Ahmed et al. (2006)
Hydrogel	Temperature-sensitive	Poly (N-isopropylacrylamide) gels/tailored nanoporous silica	Indomethacin	-	-	Shin et al. (2001)
		Hydroxyapatite-poly (N-isopropylacrylamide) (HAP–PNIPAAm)	Indomethacin	-	-	Shin et al. (2002)
	pH-sensitive	HP-β-CD/agarose-g-poly (MAA)	Capecitabine	Done	-	Rehman et al. (2021)
	Electroresponsive	Poly (methylacrylic acid) (PMAA)/pristine multiwalled carbon nanotubes (pMWNT)	Radio-labelled sucrose	Done	-	Servant et al. (2013)
MOFs	Ordinary	$ZrCl_4$/terephthalic acid	5-fluorouracil (5-FU)/dichloroacetate (DCA)/ibuprofen (IBU)/alendronate (AL)	Done	-	Lazaro et al. (2020)
		Amino-triphenyldicarboxylic acid (amino-TPDC)/$ZrCl_4$/amino-TPDC	Cisplatin/siRNAs	-	Done	He et al. (2014)
	Stimuli-sensitive	2-Methylimidazole/chloroauric acid/sodium palladium tetra-chloride (Na_2PdCl_4)/poly (vinyl pyrrolidone) (PVP, 30,000 W)/L-ascorbic acid (AA)	Doxorubicin	Done	-	Yang et al. (2017)

environment-sensitive MOFs are at the early stage, various stimuli-sensitive MOFs have been synthesized. A class of thermo- and solvatochromic metal–organic frameworks based on 4-(pyridin-4-yl)benzoic acid reported by Gift Mehlana was synthesized by solvothermal methods (Mehlana et al., 2012). pH-sensitive MOF with co-encapsulation of Pd@Au nanoparticles and doxorubicin for pH- and NIR-triggered synergistic chemo-photothermal treatment of cancer cells showed an excellent synergistic treatment effect on SMMC-7721 cells even at low concentrations (Figure 8) (Yang et al., 2017). Other pH-sensitive MOF like hollow mesoporous silica (HMS)@MOF capsules for DOX showed much higher cytotoxicity than the free drugs (Yang et al., 2017). Additionally, a core@shell nanocomposite material with biocompatible bovine serum albumin (BSA) as the core and pH-sensitive MOF as the shell loading DOX was prepared (Liang et al., 2018). It released DOX at low pH (5.0–6.0) with higher efficacy against the breast cancer cell line MCF-7. These all accelerate the development of MOFs for anticancer drug deliveries.

As a new type of organic-inorganic hybrid crystalline porous material, MOF has the advantages of large specific surface area, high porosity, and diverse structures. However, there are also some problems to be solved in the application of MOFs: 1) The present preparation technology for most MOFs is not suitable for industrial production. It requires high precision of the instrument, which is still mostly confined to laboratory preparation. To overcome it, we need to make more efforts in the production process and instrument specifications. 2) There is some toxicity of the MOFs. The preparation of MOFs mostly relies on organic solvents as the medium, resulting in the residue of organic solvents in the pores, causing toxicity. However, the selectivity and synthesis efficiency of organic ligands will be affected if water is used as the synthetic medium due to the poor solubility. At the same time, the surface tension of water is large, and in the activation process before drug loading, the stress on the pores will be generated with the removal of water, leading to the pore collapse and the reduction of drug loading. This can be improved by the optimization of the solvent and activation process. A good synthetic medium should be non-toxic, volatile, and with low surface tension. The freeze-drying method and supercritical CO_2 fluid can protect the pore structure of MOFs by the sublimation process and less stress of supercritical CO_2 fluid on pore, so as to improve drug loading efficiency. More methods will be studied. 3) At the beginning of the development, many MOFs are used for adsorption, catalysis and so on. The organic ligands are chosen according to the chemical properties, which is inevitably irritating to the human body. From the medicinal point of view, researchers should pay attention to the optimization of their organic ligands. The use of ligands with specific functions or anticancer pharmacological effects can further improve the anti-tumor effect, and shows the advantage of combining drugs with adjuvants. 4) Different MOFs may have different stability and safety. There are many configurations and types of MOFs. However, few studies evaluated the metabolic process, safety, or biocompatibility of different types of MOFs *in vivo* and *in vitro*, so specific studies are necessary in this field to provide sufficient evidence of the safety and support the clinical application of MOFs. Interdisciplinary cooperation of chemistry, materials, and biomedicine is deepening. The research is expected to further develop MOF materials in biomedicine. The materials, cargo and *in vivo*/*vitro* test status of some typical nanoparticles mentioned above are summarized in Table 1.

3 Conclusion and outlook

Polymeric NPs, as a group full of vigor, have excellent prospects and commercial value. The whole development of polymeric NPs is based on theory, experiment, and practical application. At present, there are more than 60 nano-drugs being approved for marketing in the world, and more than 200 are under clinical research, among which anti-tumor drugs are the main ones, including antiviral drugs, anti-inflammatory drugs, polypeptide protein drugs, RNA drugs, and drugs for diagnostic imaging. Compared with other dosage form, NPs have the advantages of improving drug stability—avoiding the drugs being rapidly destroyed or degraded, prolonging circulation time of drugs, enhancing penetrating and retention effects, specific binding with tumor cells and achieving targeted delivery, blocking angiogenesis of tumor tissues, and so on. Nanomedicine shows great potential in improving drug distribution and improving bioavailability. It is developing steadily and lively. However, challenges in the preparation of NP materials, improvement of their biological compatibility, the unknown mechanism of drug carrying, and the toxicity of polymeric NP materials *in vivo* are the problems remaining to be solved. Additionally, the pharmacokinetic of most NPs *in vivo* and the intracorporal processes of drugs are still not clear, which lead to the different results between clinical efficacy and preclinical studies. This is also one of the important reasons that the clinical development of nanomedicine has been restricted. Based on the promising application prospect of NPs, we remain committed to solving these problems. First, diversified synthesis methods need to be used. Different nanocarriers need to be synthesized and selected for different drug molecules. At present, the synthesis of nanocarrier drugs is mostly in liquid phase, including hydrothermal synthesis, template synthesis, interface synthesis, and so on. More syntheses with new techniques need to be explored. Second, most of the polymeric NPs cannot be used in clinics because of their toxicity. Although a large number of biocompatible polymeric NP materials have been used, the study of their toxicity is still limited by the imperfect analysis methods for the mechanism of drug carriers. Third, the mechanism of action of NPs *in vivo* is under improvement. The pharmacokinetic study of NPs should also flourish with the development of drug delivery

systems. To obtain the transport rate between plasma drug concentration and tissue drug concentration by establishing a reasonable pharmacokinetic model has an important meaning for the design and optimization of NPs. To sum up, it can be predicted that polymeric NP carriers will be developed and widely applied with the further improvement of synthetic methods, analytical methods, and the basic experimental work of pharmacology. In addition, with the development of sensing, interconnection, and big data technologies, mobile medical system and miniaturization of drug delivery are also important tasks in the future.

Author contributions

XX wrote the main draft under WL's supervision. FT, CS, and AE helped in paper writing. BW, XM, and SW helped in compilation of literature. All authors read and approved the final manuscript.

Funding

Financial support by the Grant of Jilin Province Science and Technology Committee (No. 20180101194JC), the Jilin Province Development and Reform Commission (No. 2021C039-3). Jilin Education Bureau (Youth Project No. JJKH20200451KJ), Health Commission of Jilin Province (Young Science and Technology Backbone Project No. 2019Q030), Youth Growth—Science and technology project of Science and Technology Department of Jilin Province (No. 20220508069RC), Foundations of Undergraduate Innovation, and Venture Competition Project (No. 202013706046, S202113706073, and S202113706090X) are acknowledged.

Conflict of interest

The authors declare that the research was conducted in the absence of any commercial or financial relationships that could be construed as a potential conflict of interest.

Publisher's note

All claims expressed in this article are solely those of the authors and do not necessarily represent those of their affiliated organizations, or those of the publisher, the editors, and the reviewers. Any product that may be evaluated in this article, or claim that may be made by its manufacturer, is not guaranteed or endorsed by the publisher.

References

Agut, W., Brûlet, A., Schatz, C., Taton, D., and Lecommandoux, S. (2010). pH and temperature responsive polymeric micelles and polymersomes by self-assembly of poly[2-(dimethylamino)ethylmethacrylate]-b-poly(glutamic acid) double hydrophilic block copolymers. *Langmuir* 26, 10546–10554. doi:10.1021/la1005693

Ahmed, F., Pakunlu, R. I., Srinivas, G., Brannan, A., Bates, F., Klein, M. L., et al. (2006). Shrinkage of a rapidly growing tumor by drug-loaded polymersomes: pH-triggered release through copolymer degradation. *Mol. Pharm.* 3, 340–350. doi:10.1021/mp050103u

Alemayehu, Y. A., Gebeyehu, B. T., and Cheng, C. C. (2019). Photosensitive supramolecular micelles with complementary hydrogen bonding motifs to improve the efficacy of cancer chemotherapy. *Biomacromolecules* 20, 4535–4545. doi:10.1021/acs.biomac.9b01322

Alexis, F., Pridgen, E. M., Langer, R., and Farokhzad, O. C. (2010). Nanoparticle technologies for cancer therapy. *Handb. Exp. Pharmacol.* 197, 55–86. doi:10.1007/978-3-642-00477-3_2

Ambasta, R. K., Sharma, A., and Kumar, P. (2011). Nanoparticle mediated targeting of VEGFR and cancer stem cells for cancer therapy. *Vasc. Cell* 3, 26. doi:10.1186/2045-824x-3-26

Andre, M. B., Gobin, A. M., Whitmire, R. E., and West, J. L. (2007). Temperature-sensitive hydrogels with SiO_2-Au nanoshells for controlled drug delivery. *J. Control. Release* 123, 219–227. doi:10.1016/j.jconrel.2007.08.013

Anitha, A., Maya, S., Deepa, N., Chennazhi, K. P., Nair, S. V., Tamura, H., et al. (2011). Efficient water soluble O-carboxymethyl chitosan nanocarrier for the delivery of curcumin to cancer cells. *Carbohydr. Polym.* 83, 452–461. doi:10.1016/j.carbpol.2010.08.008

Antoni, P., Robb, M. J., Campos, L., Montanez, M., Hult, A., Malmström, E., et al. (2010). Pushing the limits for thiol-ene and CuAAC reactions: Synthesis of a 6th generation dendrimer in a single day. *Macromolecules* 43, 6625–6631. doi:10.1021/ma101242u

Asad, M. I., Khan, D., Rehman, A. U., Elaissari, A., and Ahmed, N. (2021). Development and *in vitro*/*in vivo* evaluation of pH-sensitive polymeric nanoparticles loaded hydrogel for the management of psoriasis. *Nanomaterials* 11, 3433. doi:10.3390/nano11123433

Ayon, M. A. G., Barajas, J. A. S., Corrales, L. A. P., and Claverie, A. L. (2015). PNVCL-PEGMA nanohydrogels with tailored transition temperature for controlled delivery of 5-fluorouracil. *J. Polym. Sci. Part A Polym. Chem.* 53, 2662–2672. doi:10.1002/pola.27766

Basak, D., and Ghosh, S. (2013). PH-regulated controlled swelling and sustained release from the core functionalized amphiphilic block copolymer micelle. *ACS Macro Lett.* 2, 799–804. doi:10.1021/mz400357g

Benrebouh, A., Avoce, D., and Zhu, X. X. (2001). Thermo- and pH-sensitive polymers containing cholic acid derivatives. *Polymer* 42, 4031–4038. doi:10.1016/s0032-3861(00)00837-5

Bernhard, S., and Tibbitt, M. W. (2021). Supramolecular engineering of hydrogels for drug delivery. *Adv. Drug Deliv. Rev.* 171, 240–256. doi:10.1016/j.addr.2021.02.002

Cabral, H., Nakanishi, M., Kumagai, M., Jang, W. D., Nishiyama, N., and Kataoka, K. (2009). A photo-activated targeting chemotherapy using glutathione sensitive camptothecin-loaded polymeric micelles. *Pharm. Res.* 26, 82–92. doi:10.1007/s11095-008-9712-2

Cai, M., Leng, M., Lu, A., He, L., Xie, X., Huang, L., et al. (2015). Synthesis of amphiphilic copolymers containing zwitterionic sulfobetaine as pH and redox responsive drug carriers. *Colloids Surfaces B Biointerfaces* 126, 1–9. doi:10.1016/j.colsurfb.2014.12.005

Cao, Y., Zhang, C., Shen, W., Cheng, Z., Yu, L. L., and Ping, Q. (2007). Poly(N-isopropylacrylamide)-chitosan as thermosensitive *in situ* gel-forming system for ocular drug delivery. *J. Control. Release* 120, 186–194. doi:10.1016/j.jconrel.2007.05.009

Chandrawati, R., and Caruso, F. (2012). Biomimetic liposome- and polymersome-based multicompartmentalized assemblies. *Langmuir* 28, 13798–13807. doi:10.1021/la301958v

Chang, M., Wei, Y., Liu, D., Wang, J. X., and Chen, J. F. (2021). A general strategy for instantaneous and continuous synthesis of ultrasmall metal-organic framework nanoparticles. *Angew. Chem. Int. Ed. Engl.* 60, 26594–26600. doi:10.1002/ange.202112250

Charati, M. B., Lee, I., Hribar, K. C., and Burdick, J. A. (2010). Light-sensitive polypeptide hydrogel and nanorod composites. *Small* 6, 1608–1611. doi:10.1002/smll.201000162

Chen, D., Song, P., Jiang, F., Meng, X., Sui, W., Shu, C., et al. (2013). pH-responsive mechanism of a deoxycholic acid and folate comodified chitosan micelle under cancerous environment. *J. Phys. Chem. B* 117, 1261–1268. doi:10.1021/jp310677p

Chen, G., Kou, X., Huang, S., Tong, L., Shen, Y., Zhu, W., et al. (2020). Modulating the biofunctionality of metal-organic-framework-encapsulated enzymes through controllable embedding patterns. *Angew. Chem. Int. Ed. Engl.* 59, 2889–2896. doi:10.1002/ange.201913231

Chen, J., Chao, M. Y., Liu, Y., Xu, B. W., Zhang, W. H., and Young, D. J. (2020). An N, N'-diethylformamide solvent-induced conversion cascade within a metal-organic framework single crystal. *Chem. Commun.* 56, 5877–5880. doi:10.1039/d0cc02420a

Chen, J. J. Y., Vliesb, A. J., and Hasegawa, U. (2020). Hydrogen sulfide-releasing micelles for promoting angiogenesis. *Polym. Chem.* 11, 4454–4463. doi:10.1039/d0py00495b

Chen, Y., Du, M., Yu, J., Rao, L., Chen, X., and Chen, Z. (2020). Nanobiohybrids: A synergistic integration of bacteria and nanomaterials in cancer therapy. *BIO Integr.* 1, 25–36. doi:10.15212/bioi-2020-0008

Christian, D. A., Cai, S., Bowen, D. M., Kim, Y., Pajerowski, J. D., and Discher, D. E. (2009). Polymersome carriers: From self-assembly to siRNA and protein therapeutics. *Eur. J. Pharm. Biopharm.* 71, 463–474. doi:10.1016/j.ejpb.2008.09.025

Cotí, K. K., Belowich, M. E., Liong, M., Ambrogio, M. W., Lau, Y. A., Khatib, H. A., et al. (2009). Mechanised nanoparticles for drug delivery. *Nanoscale* 1, 16–39. doi:10.1039/b9nr00162j

Crayton, S. H., and Tsourkas, A. (2011). pH titratable superparamagnetic iron oxide for improved nanoparticle accumulation in acidic tumor microenvironments. *ACS Nano* 5, 9592–9601. doi:10.1021/nn202863x

Deng, Y., Huang, R., Huang, S., and Xiong, M. (2021). Nanoparticles enable efficient delivery of antimicrobial peptides for the treatment of deep infections. *BIO Integr.* 2, 50–56. doi:10.15212/bioi-2021-0003

Ding, J., Chen, J., Li, D., Xiao, C., Zhang, J., He, C., et al. (2013). Biocompatible reduction-responsive polypeptide micelles as nanocarriers for enhanced chemotherapy efficacy *in vitro*. *J. Mat. Chem. B* 1, 69–81. doi:10.1039/c2tb00063f

Du, J., Tang, Y., Lewis, A. L., and Armes, S. P. (2005). pH-sensitive vesicles based on a biocompatible zwitterionic diblock copolymer. *J. Am. Chem. Soc.* 127, 17982–17983. doi:10.1021/ja056514l

Fontana, F., Carollo, E., Melling, G. E., and Carter, D. R. F. (2021). Extracellular vesicles: Emerging modulators of cancer drug resistance. *Cancers (Basel)* 13, 749. doi:10.3390/cancers13040749

Furukawa, H., Cordova, K. E., O'Keeffe, M., and Yaghi, O. M. (2013). The chemistry and applications of metal-organic frameworks. *Science* 341, 1230444. doi:10.1126/science.1230444

Gaitanis, A., and Staal, S. (2010). Liposomal doxorubicin and nab-paclitaxel: Nanoparticle cancer chemotherapy in current clinical use. *Methods Mol. Biol.* 624, 385–392. doi:10.1007/978-1-60761-609-2_26

Gastaldi, E., Lagaude, A., and Fuente, B. T. D. L. (1996). Micellar transition state in casein between pH 5.5 and 5.0. *J. Food Sci.* 61, 59–64. doi:10.1111/j.1365-2621.1996.tb14725.x

Gaumet, M., Vargas, A., Gurny, R., and Delie, F. (2008). Nanoparticles for drug delivery: The need for precision in reporting particle size parameters. *Eur. J. Pharm. Biopharm.* 69, 1–9. doi:10.1016/j.ejpb.2007.08.001

Gholami, M., Mohammadi, R., Arzanlou, M., Dourbash, F. A., Majidi, E. K. G., Mohseni, S. M., et al. (2017). *In vitro* antibacterial activity of poly (amidoamine)-G7 dendrimer. *BMC Infect. Dis.* 17, 395–406. doi:10.1186/s12879-017-2513-7

Hai, Q. S., Wen, L. L., Ruo, G. Q., Le, S. Y., Xia, B. J., Zheng, M., et al. (2015). Delivering a photosensitive transplatin prodrug to overcome cisplatin drug resistance. *Chem. Commun.* 51, 11493–11495. doi:10.1039/c5cc03692e

Haley, B., and Frenkel, E. (2008). Nanoparticles for drug delivery in cancer treatment. *Urologic Oncol. Seminars Orig. Investigations* 26, 57–64. doi:10.1016/j.urolonc.2007.03.015

Hamidi, M., Azadi, A., and Rafiei, P. (2008). Hydrogel nanoparticles in drug delivery. *Adv. Drug Deliv. Rev.* 60, 1638–1649. doi:10.1016/j.addr.2008.08.002

Hawker, C. J., and Fréchet, J. M. J. (1990). Control of surface functionality in the synthesis of dendritic macromolecules using the convergent-growth approach. *Macromolecules* 23, 4726–4729. doi:10.1021/ma00223a036

He, C., Lu, K., Liu, D., and Lin, W. (2014). Nanoscale metal-organic frameworks for the Co-delivery of cisplatin and pooled siRNAs to enhance therapeutic efficacy in drug-resistant ovarian cancer cells. *J. Am. Chem. Soc.* 136, 5181–5184. doi:10.1021/ja4098862

Hori, K., Nishihara, M., and Yokoyama, M. (2010). Vital microscopic analysis of polymeric micelle extravasation from tumor vessels: Macromolecular delivery according to tumor vascular growth stage. *J. Pharm. Sci.* 99, 549–562. doi:10.1002/jps.21848

Hrkach, J., Hoff, D. V., Ali, M. M., Andrianova, E., Auer, J., Campbell, T., et al. (2012). Preclinical development and clinical translation of a PSMA-targeted docetaxel nanoparticle with a differentiated pharmacological profile. *Sci. Transl. Med.* 4, 128ra39. doi:10.1126/scitranslmed.3003651

Hu, C. M., Aryal, S., and Zhang, L. (2010). Nanoparticle-assisted combination therapies for effective cancer treatment. *Ther. Deliv.* 1, 323–334. doi:10.4155/tde.10.13

Hu, J., Miura, S., Na, K., and Bae, Y. H. (2013). pH-responsive and charge shielded cationic micelle of poly(L-histidine)-block-short branched PEI for acidic cancer treatment. *J. Control. Release* 172, 69–76. doi:10.1016/j.jconrel.2013.08.007

Ikeda, M., Ochi, R., Wada, A., and Hamachi, I. (2010). Supramolecular hydrogel capsule showing prostate specific antigen-responsive function for sensing and targeting prostate cancer cells. *Chem. Sci.* 1, 491–498. doi:10.1039/c0sc00278j

Imaz, I., Martínez, M. R., Fernández, L. G., García, F., Molina, D. R., Hernando, J., et al. (2010). Coordination polymer particles as potential drug delivery systems. *Chem. Commun.* 46, 4737–4739. doi:10.1039/c003084h

Jiang, T., Qiao, Y., Ruan, W., Zhang, D., Yang, Q., Wang, G., et al. (2021). Cation-free siRNA micelles as effective drug delivery platform and potent RNAi nanomedicines for glioblastoma therapy. *Adv. Mat.* 33, 2104779. doi:10.1002/adma.202104779

Jiang, T., Zhang, Z., Zhang, Y., Lv, H., Zhou, J., Li, C., et al. (2012). Dual-functional liposomes based on pH-responsive cell-penetrating peptide and hyaluronic acid for tumor-targeted anticancer drug delivery. *Biomaterials* 33, 9246–9258. doi:10.1016/j.biomaterials.2012.09.027

Kathryn, M. L., Pashow, T., Rocca, J. D., Xie, Z., Tran, S., and Lin, W. (2009). Post-synthetic modifications of iron-carboxylate nanoscale metal-organic frameworks for imaging and drug delivery. *J. Am. Chem. Soc.* 131, 14261–14263. doi:10.1021/ja906198y

Kawano, S., Lie, J., Ohgi, R., Shizuma, M., and Muraoka, M. (2021). Modulating polymeric amphiphiles using thermo- and pH-responsive copolymers with cyclodextrin pendant groups through molecular recognition of the lipophilic dye. *Macromolecules* 11, 5229–5240. doi:10.1021/acs.macromol.1c00265

Kim, K. R., Kim, D. R., Lee, T., Yhee, J. Y., Kim, B. S., Kwon, I. C., et al. (2013). Drug delivery by a self-assembled DNA tetrahedron for overcoming drug resistance in breast cancer cells. *Chem. Commun.* 49, 2010–2012. doi:10.1039/c3cc38693g

Kim, K. S., Park, W., Hu, J., Bae, Y. H., and Na, K. (2014). A cancer-recognizable MRI contrast agents using pH-responsive polymeric micelle. *Biomaterials* 35, 337–343. doi:10.1016/j.biomaterials.2013.10.004

Kim, Y., Tewari, M., Pajerowski, J. D., Cai, S., Sen, S., Williams, J. H., et al. (2009). Polymersome delivery of siRNA and antisense oligonucleotides. *J. Control. Release* 134, 132–140. doi:10.1016/j.jconrel.2008.10.020

Lammers, T., and Ferrari, M. (2020). The success of nanomedicine. *Nano Today* 31, 100853. doi:10.1016/j.nantod.2020.100853

Lauersen, N. H., and Birnbaum, S. J. (1975). Water intoxication associated with oxytocin administration during saline-induced abortion. *Am. J. Obstet. Gynecol.* 121, 2–6. doi:10.1016/0002-9378(75)90965-5

Lazaro, I. A., Wells, C. J. R., and Forgan, R. S. (2020). Multivariate modulation of the Zr MOF UiO for defect-controlled multimodal anticancer drug delivery. *Angew. Chem. Int. Ed.* 59, 5249–5255. doi:10.1002/anie.201915848

Lee, G. Y., Park, K., Kim, S. Y., and Byun, Y. (2007). MMPs-specific PEGylated peptide-DOX conjugate micelles that can contain free doxorubicin. *Eur. J. Pharm. Biopharm.* 67, 646–654. doi:10.1016/j.ejpb.2007.03.023

Lee, S. Y., Lee, H., In, I., and Park, S. Y. (2014). pH/redox/photo responsive polymeric micelle via boronate ester and disulfide bonds with spiropyran-based photochromic polymer for cell imaging and anticancer drug delivery. *Eur. Polym. J.* 57, 1–10. doi:10.1016/j.eurpolymj.2014.04.020

Li, H. J., Du, J. Z., Du, X. J., Xu, C. F., Sun, C. Y., Wang, H. X., et al. (2016). Stimuli-responsive clustered nanoparticles for improved tumor penetration and therapeutic efficacy. *Proc. Natl. Acad. Sci. U. S. A.* 113, 4164–4169. doi:10.1073/pnas.1522080113

Li, M. H., and Kellera, P. (2009). Stimuli-responsive polymer vesicles. *Soft Matter* 5, 927–937. doi:10.1039/b815725a

Li, Z., Xiao, C., Yong, T., Li, Z., Gan, L., and Yang, X. (2020). Influence of nanomedicine mechanical properties on tumor targeting delivery. *Chem. Soc. Rev.* 49, 2273–2290. doi:10.1039/c9cs00575g

Liang, K., Richardson, J. J., Cui, J., Caruso, F., Doonan, C. J., and Falcaro, P. (2016). Metal-organic framework coatings as cytoprotective exoskeletons for living cells. *Adv. Mat.* 28, 7910–7914. doi:10.1002/adma.201602335

Liang, Z., Yang, Z., Yuan, H., Wang, C., Qi, J., Liu, K., et al. (2018). A protein@ metal-organic framework nanocomposite for pH-triggered anticancer drug delivery. *Dalton Trans.* 47, 10223–10228. doi:10.1039/c8dt01789a

Liao, L., Liu, J., Dreaden, E. C., Morton, S. W., Shopsowitz, K. E., Hammond, P. T., et al. (2014). A convergent synthetic platform for single-nanoparticle combination cancer therapy: Ratiometric loading and controlled release of cisplatin, doxorubicin, and camptothecin. *J. Am. Chem. Soc.* 136, 5896–5899. doi:10.1021/ja502011g

Liu, J., Meng, Z. X., and Zhen, Y. (2020). Immunoscore guided cold tumors to acquire "temperature" through integrating physicochemical and biological methods. *BIO Integr.* 1, 6–14. doi:10.15212/bioi-2020-0002

Liu, T. J., Liu, S., Hu, X. L., Sheng, S. H., Huang, Y. B., and Jing, X. B. (2011). EPR effect of amphiphilic copolymer micelles observed by fluorescent imaging. *Chem. Res. Chin. U.* 27, 628–634.

Liu, X., Wu, J., Yammine, M., Zhou, J., Posocco, P., Viel, S., et al. (2011). Structurally flexible triethanolamine core PAMAM dendrimers are effective nanovectors for DNA transfection *in vitro* and *in vivo* to the mouse thymus. *Bioconjug. Chem.* 22, 2461–2473. doi:10.1021/bc200275g

Liu, X. W., Zhu, S., Wu, S. R., Wang, P., and Han, G. Z. (2013). Response behavior of ion-sensitive hydrogel based on crown ether. *Colloids Surfaces A Physicochem. Eng. Aspects* 417, 140–145. doi:10.1016/j.colsurfa.2012.09.044

Liu, Y., Feng, L., Liu, T., Zhang, L., Yao, Y., Yu, D., et al. (2014). Multifunctional pH-sensitive polymeric nanoparticles for theranostics evaluated experimentally in cancer. *Nanoscale* 6, 3231–3242. doi:10.1039/c3nr05647c

Lorenzo, C. A., Concheiro, A., Dubovik, A. S., Grinberg, N. V., Burova, T. V., and Grinberg, V. Y. (2005). Temperature-sensitive chitosan-poly(N-isopropylacrylamide) interpenetrated networks with enhanced loading capacity and controlled release properties. *J. Control. Release* 102, 629–641. doi:10.1016/j.jconrel.2004.10.021

Lu, H. L., Syu, W. J., Nishiyama, N., Kataoka, K., and Lai, P. S. (2009). Dendrimer phthalocyanine-encapsulated polymeric micelle-mediated photochemical internalization extends the efficacy of photodynamic therapy and overcomes drug-resistance *in vivo*. *J. Control. Release* 155, 458–464. doi:10.1016/j.jconrel.2011.06.005

Lu, J., Hu, P., Cao, L., Wei, Z., Xiao, F., Chen, Z., et al. (2021). Genetically encoded and biologically produced all-DNA nanomedicine based on one-pot assembly of DNA dendrimers for targeted gene regulation. *Angew. Chem. Int. Ed.* 60, 5377–5385. doi:10.1002/anie.202012916

Manganiello, M. J., Cheng, C., Convertine, A. J., Bryers, J. D., and Stayton, P. S. (2012). Diblock copolymers with tunable pH transitions for gene delivery. *Biomaterials* 33, 2301–2309. doi:10.1016/j.biomaterials.2011.11.019

Marczynski, M., Kimna, C., and Chitosan, O. L. (2021). Purified mucins in drug delivery research. *Adv. Drug Deliv. Rev.* 178, 113845–113865. doi:10.1016/j.addr.2021.113845

Mehlana, G., Bourne, S. A., and Ramon, G. (2012). A new class of thermo- and solvatochromic metal-organic frameworks based on 4-(pyridin-4-yl)benzoic acid. *Dalton Trans.* 41, 4224–4231. doi:10.1039/c2dt12016j

Mignani, S., Shi, X., Zablocka, M., and Majoral, J. P. (2021). Dendritic macromolecular architectures: Dendrimer-based polyion complex micelles. *Biomacromolecules* 22, 262–274. doi:10.1021/acs.biomac.0c01645

Min, H., Wang, J., Qi, Y., Zhang, Y., Han, X., Xu, Y., et al. (2019). Biomimetic metal–organic framework nanoparticles for cooperative combination of antiangiogenesis and photodynamic therapy for enhanced efficacy. *Adv. Mat.* 31, 1808200. doi:10.1002/adma.201808200

Ndebele, R. T., Yao, Q., Shi, Y. N., Zhai, Y. Y., Xu, H. L., Lu, C. T., et al. (2021). Progress in the application of nano- and micro-based drug delivery systems in pulmonary drug delivery. *BIO Integr.* 3, 71–83. doi:10.15212/bioi-2021-0028

Nishiyama, N., Morimoto, Y., Jang, W. D., and Kataoka, K. (2009). Design and development of dendrimer photosensitizer-incorporated polymeric micelles for enhanced photodynamic therapy. *Adv. Drug Deliv. Rev.* 61, 327–338. doi:10.1016/j.addr.2009.01.004

Omidia, S., Pirhayatib, M., and Kakanejadifard, A. (2019). Co-delivery of doxorubicin and curcumin by a pH-sensitive, injectable, and *in situ* hydrogel composed of chitosan, graphene, and cellulose nanowhisker. *Carbohydr. Polym.* 231, 115745. doi:10.1016/j.carbpol.2019.115745

Padias, A. B., Hall, H. K., Tomalia, D. A., and McConnell, J. R. (1987). Starburst polyether dendrimers. *J. Org. Chem.* 52, 5305–5312. doi:10.1021/jo00233a002

Pamies, R., Zhu, K., Kjøniksen, A. L., and Nyström, B. (2009). Thermal response of low molecular weight poly-(N-isopropylacrylamide) polymers in aqueous solution. *Polym. Bull.* 62, 487–502. doi:10.1007/s00289-008-0029-4

Pangburn, T. O., Georgiou, K., Bates, F. S., and Kokkoli, E. (2012). Targeted polymersome delivery of siRNA induces cell death of breast cancer cells dependent upon Orai3 protein expression. *Langmuir* 28, 12816–12830. doi:10.1021/la300874z

Pashow, K. M. T., Rocca, J. D., Xie, Z., Tran, S., and Lin, W. (2009). Post-synthetic modifications of iron-carboxylate nanoscale metal-organic frameworks for imaging and drug delivery. *J. Am. Chem. Soc.* 131, 14261–14263. doi:10.1021/ja906198y

Patil, Y. B., Swaminathan, S. K., Sadhukha, T., Ma, L., and Panyam, J. (2010). The use of nanoparticle-mediated targeted gene silencing and drug delivery to overcome tumor drug resistance. *Biomaterials* 31, 358–365. doi:10.1016/j.biomaterials.2009.09.048

Peng, P. X., Jian, D. Y., Qing, Y., Ying, Z. Z., and He, L. X. (2020). Bioactive factors-imprinted scaffold vehicles for promoting bone healing: The potential strategies and the confronted challenges for clinical production. *BIO Integr.* 1, 37–54. doi:10.15212/bioi-2020-0010

Peng, Z., Zou, Y., Xu, S., Zhong, W., and Yang, W. (2018). High-performance biomass-based flexible solid-state supercapacitor constructed of pressure-sensitive lignin-based and cellulose hydrogels. *ACS Appl. Mat. Interfaces* 10, 22190–22200. doi:10.1021/acsami.8b05171

Purushottamachar, P., Godbole, A. M., Gediya, L. K., Martin, M. S., Vasaitis, T. S., Afful, A. K. K., et al. (2013). Systematic structure modifications of multitarget prostate cancer drug candidate galeterone to produce novel androgen receptor down-regulating agents as an approach to treatment of advanced prostate cancer. *J. Med. Chem.* 56, 4880–4898. doi:10.1021/jm400048v

Quan, Z., Zhu, K., Knudsen, K. D., Nyström, B., and Lund, R. (2013). Tailoring the amphiphilicity and self-assembly of thermosensitive polymers: End-capped PEG-PNIPAAM block copolymers. *Soft Matter* 9, 10768–10778. doi:10.1039/c3sm51945g

Rahimi, M., Kilaru, S., Sleiman, G. E. H., Saleh, A., Rudkevich, D., and Nguyen, K. (2008). Synthesis and characterization of thermo-sensitive nanoparticles for drug delivery applications. *J. Biomed. Nanotechnol.* 4, 482–490. doi:10.1166/jbn.2008.014

Rapp, T. L., and Deforest, C. A. (2021). Targeting drug delivery with light: A highly focused approach. *Adv. Drug Deliv. Rev.* 171, 94–107. doi:10.1016/j.addr.2021.01.009

Rehman, U., Sarfraz, R. M., Mahmood, A., Hussain, Z., Batool, N., Zafar, N., et al. (2021). Smart pH-responsive co-polymeric hydrogels for controlled delivery of capecitabine: Fabrication, Optimization and *in vivo* toxicology screening. *Curr. Drug Deliv.* 18, 1256–1271. doi:10.2174/1567201818666210212085912

Rejinold, N. S., Muthunarayanan, M., Divyarani, V. V., Sreerekha, P. R., Chennazhi, K. P., Nair, S. V., et al. (2011). Curcumin-loaded biocompatible thermoresponsive polymeric nanoparticles for cancer drug delivery. *J. Colloid Interface Sci.* 360, 39–51. doi:10.1016/j.jcis.2011.04.006

Rieter, W. J., Pott, K. M., Taylor, K. M., and Lin, W. (2008). Nanoscale coordination polymers for platinum-based anticancer drug delivery. *J. Am. Chem. Soc.* 130, 11584–11585. doi:10.1021/ja803383k

Rong, D., Hai, H. X., Guan, N. G., Bin, J., Xing, Y., Wen, L. L., et al. (2014). Nanoparticle delivery of photosensitive Pt(IV) drugs for circumventing cisplatin cellular pathway and on-demand drug release. *Colloids Surfaces B Biointerfaces* 123, 734–741. doi:10.1016/j.colsurfb.2014.10.015

Sarfraz, R. M., Akram, M. R., Ali, M. R., Mahmood, A., Khan, M. U., Ahmad, H., et al. (2019). Development and *in-vitro* evaluation of pH responsive polymeric nano hydrogel carrier system for gastro-protective delivery of naproxen sodium. *Adv. Polym. Technol.* 4, 1–13. doi:10.1155/2019/6090965

Saw, P. E., and Jon, S. (2020). Understanding of the entry mechanism of nanoparticles into tumors determines the future direction of nanomedicine development. *BIO Integrat* 1, 193–195. doi:10.15212/bioi-2020-0033

Servant, A., Methven, L., Williams, R. P., and Kostarelos, K. (2013). Electroresponsive polymer-carbon nanotube hydrogel hybrids for pulsatile drug delivery *in vivo*. *Adv. Healthc. Mat.* 2, 806–811. doi:10.1002/adhm.201200193

Shao, K., Singha, S., Casares, X. C., Tsai, S., Yang, Y., and Santamaria, P. (2015). Nanoparticle-based immunotherapy for cancer. *ACS Nano* 9, 16–30. doi:10.1021/nn5062029

Shen, M., Huang, Y., Han, L., Qin, J., Fang, X., Wang, J., et al. (2012). Multifunctional drug delivery system for targeting tumor and its acidic microenvironment. *J. Control. Release* 161, 884–892. doi:10.1016/j.jconrel.2012.05.013

Shi, X., Wang, S., Meshinchi, S., Antwerp, M. E. V., Bi, X., Lee, I., et al. (2007). Dendrimer-entrapped gold nanoparticles as a platform for cancer-cell targeting and imaging. *Small* 3, 1245–1252. doi:10.1002/smll.200700054

Shi, Y., Nostrum, C. V., and Hennink, W. (2015). Interfacially hydrazone cross-linked thermosensitive polymeric micelles for acid-triggered release of paclitaxel. *ACS Biomater. Sci. Eng.* 1, 393–404. doi:10.1021/acsbiomaterials.5b00006

Shin, Y., Chang, J. H., Liu, J., Williford, R., Shin, Y., and Exarhos, G. J. (2001). Hybrid nanogels for sustainable positive thermosensitive drug release. *J. Control. Release* 73, 1–6. doi:10.1016/s0168-3659(01)00247-4

Shin, Y., Liu, J., Chang, J. H., and Exarhos, G. J. (2002). Sustained drug release on temperature-responsive poly(N-isopropylacrylamide)-integrated hydroxyapatite. *Chem. Commun.* 16, 1718–1719. doi:10.1039/b204703a

Shu, W. C., Chun, H. L., Shu, N. L., Chee, H. T., Phei, E. S., and Xu, X. (2020). Enhancing chemotherapy by RNA interference. *BIO Integr.* 2, 64–81. doi:10.15212/bioi-2020-0003

Siegel, R. A. (2014). Stimuli sensitive polymers and self regulated drug delivery systems: A very partial review. *J. Control. Release* 190, 337–351. doi:10.1016/j.jconrel.2014.06.035

Soltantabar, P., Calubaquib, E. L., Mostafavi, E., Biewer, M. C., and Stefan, M. C. (2020). Enhancement of loading efficiency by coloading of doxorubicin and quercetin in thermoresponsive polymeric micelles. *Biomacromolecules* 21, 1427–1436. doi:10.1021/acs.biomac.9b01742

Son, I., Lee, Y., Baek, J., Park, M., Kim, B. S., Min, S. K., et al. (2021). pH-responsive amphiphilic polyether micelles with superior stability for smart drug delivery. *Biomacromolecules* 22, 2043–2056. doi:10.1021/acs.biomac.1c00163

Sun, C., Qin, C., Wang, X., Yang, G. S., Shao, K. Z., Lan, Y. Q., et al. (2012). ZeoliticImidazolate framework-8 as efficient pH-sensitive drug delivery vehicle. *Dalton Trans.* 41, 6906–6909. doi:10.1039/c2dt30357d

Sun, X., Wang, G., Hao, Z., Hu, S., Liu, X., Tang, J., et al. (2018). The blood clearance kinetics and pathway of polymeric micelles in cancer drug delivery. *ACS Nano* 12, 6179–6192. doi:10.1021/acsnano.8b02830

Tavra, C. O., Baxter, E. F., Tian, T., Bennett, T. D., Slater, N. K., Cheetham, A. K., et al. (2015). Amorphous metal-organic frameworks for drug delivery. *Chem. Commun.* 51, 13878–13881. doi:10.1039/c5cc05237h

Tosca, E. M., Bartolucci, R., and Magni, P. (2021). Application of artificial neural networks to predict the intrinsic solubility of drug-like molecules. *Pharmaceutics* 13, 1101–1121. doi:10.3390/pharmaceutics13071101

Truong, N. P., Whittaker, M. R., Mak, C. W., and Davis, T. P. (2015). The importance of nanoparticle shape in cancer drug delivery. *Expert Opin. Drug Deliv.* 12, 129–142. doi:10.1517/17425247.2014.950564

Vamvakaki, M., Papoutsakis, L., Katsamanis, V., Afchoudia, T., Fragouli, P. G., Iatrou, H., et al. (2005). Micellization in pH-sensitive amphiphilic block copolymers in aqueous media and the formation of metal nanoparticles. *Faraday Discuss.* 128, 129–147. doi:10.1039/b403414g

Verdurmen, W. P. R., Oude Egberink, R., Sait, A., Andree, L., Sala, B. M., Hassani Besheli, N., et al. (2021). Mimicking the biology of engineered protein and mRNA nanoparticle delivery using a versatile microfluidic platform. *Pharmaceutics* 13, 1944. doi:10.3390/pharmaceutics13111944

Wang, P., Zhao, X., Wang, Z., Meng, M., Li, X., and Ning, Q. (2010). Generation 4 polyamidoamine dendrimers is a novel candidate of nano-carrier for gene delivery agents in breast cancer treatment. *Cancer Lett.* 298, 34–49. doi:10.1016/j.canlet.2010.06.001

Wang, X. G., Xu, L., Li, M. J., and Zhang, X. Z. (2020). Construction of flexible-on-rigid hybrid-phase metal-organic frameworks for controllable multi-drug delivery. *Angew. Chem. Int. Ed. Engl.* 59, 18234–18242. doi:10.1002/ange.202008858

Wen, L. L., Wen, J. Z., Xiu, Y. Y., Zhi, G. X., and Xia, B. J. (2014). Biodegradable polymersomes from four-arm PEG-b-PDLLA for encapsulating hemoglobin. *J. Appl. Polym. Sci.* 131, 1–5. doi:10.1002/app.40433

Wu, X. L., Kim, J. H., Koo, H., Bae, S. M., Shin, H., Kim, M. S., et al. (2010). Tumor-targeting peptide conjugated pH-responsive micelles as a potential drug carrier for cancer therapy. *Bioconjug. Chem.* 21, 208–213. doi:10.1021/bc9005283

Wu, Y., Sefah, K., Liu, H., Wang, R., and Tan, W. (2010). DNA aptamer-micelle as an efficient detection/delivery vehicle toward cancer cells. *Proc. Natl. Acad. Sci. U. S. A.* 107, 5–10. doi:10.1073/pnas.0909611107

Xia, J., Du, Y., Huang, L., Chaurasiya, B., Tu, J., Webster, T. J., et al. (2018). Redox-responsive micelles from disulfide bond-bridged hyaluronic acid-tocopherol succinate for the treatment of melanoma. *Nanomedicine Nanotechnol. Biol. Med.* 14, 713–723. doi:10.1016/j.nano.2017.12.017

Xu, J. X., Tang, J. B., Zhao, L. H., and Shen, Y. Q. (2009). Advances in the study of tumor pH-responsive polymeric micelles for cancer drug targeting delivery. *Acta Pharmacol. Sin.* 44, 1328–1335.

Yan, L., Wu, W., Zhao, W., Qi, R., Cui, D., Xie, Z., et al. (2012). Reduction-sensitive core-cross-linked mPEG-poly(ester-carbonate) micelles for glutathione-triggered intracellular drug release. *Polym. Chem.* 3, 2403–2412. doi:10.1039/c2py20240a

Yang, B., and Yang, W. (2003). Thermo-sensitive switching membranes regulated by pore-covering polymer brushes. *J. Memb. Sci.* 218, 247–255. doi:10.1016/s0376-7388(03)00182-0

Yang, F., Medik, Y., Li, L., Tian, X., Wang, A. Z., Brouwer, K. L. R., et al. (2020). Nanoparticle drug delivery can reduce the hepatotoxicity of therapeutic cargo. *Small* 16, e1906360. doi:10.1002/smll.201906360

Yang, X., Grailer, J. J., Pilla, S., Steeber, D. A., and Gong, S. (2010). Tumor-targeting, pH-responsive, and stable unimolecular micelles as drug nanocarriers for targeted cancer therapy. *Bioconjug. Chem.* 21, 496–504. doi:10.1021/bc900422j

Yang, X., Li, L., He, D., Hai, L., Tang, J., Li, H., et al. (2017). A metal-organic framework based nanocomposite with co-encapsulation of Pd@Au nanoparticles and doxorubicin for pH- and NIR-triggered synergistic chemo-photothermal treatment of cancer cells. *J. Mat. Chem. B* 5, 4648–4659. doi:10.1039/c7tb00715a

Yu, H., Xu, Z., Chen, X., Xu, L., Yin, Q., Zhang, Z., et al. (2014). Reversal of lung cancer multidrug resistance by pH-responsive micelleplexes mediating co-delivery of siRNA and paclitaxel. *Macromol. Biosci.* 14, 100–109. doi:10.1002/mabi.201300282

Yu, P., Yu, H., Guo, C., Cui, Z., Chen, X., Yin, Q., et al. (2015). Reversal of doxorubicin resistance in breast cancer by mitochondria-targeted pH-responsive micelles. *Acta Biomater.* 14, 115–124. doi:10.1016/j.actbio.2014.12.001

Yu, Z., Guan, N. G., Ben, M., Rong, D., Hai, H. X., Yang, X., et al. (2015). A hybrid platinum drug dichloroacetate-platinum(II) overcomes cisplatin drug resistance through dual organelle targeting. *Anticancer. Drugs* 26, 698–705. doi:10.1097/cad.0000000000000234

Zhang, Z., Ai, S., Yang, Z., and Li, X. (2021). Peptide-based supramolecular hydrogels for local drug delivery. *Adv. Drug Deliv. Rev.* 174, 482–503. doi:10.1016/j.addr.2021.05.010

Zhang, Z. X., Liu, K. L., and Li, J. (2011). Self-assembly and micellization of a dual thermoresponsive supramolecular pseudo-block copolymer. *Macromolecules* 44, 1182–1193. doi:10.1021/ma102196q

Zhao, D., Wang, E., and Lodge, T. P. (2020). Hybridization of a bimodal distribution of copolymer micelles. *Macromolecules* 53, 7705–7716. doi:10.1021/acs.macromol.0c01419

Zheng, C., Li, M., and Ding, J. (2021). Challenges and opportunities of nanomedicines in clinical translation. *BIO Integr.* 2, 57–60. doi:10.15212/bioi-2021-0016

Glossary

NPs nanoparticles

PEG polyethylene glycol

EPR enhanced permeability and retention effect

pH_E extracellular pH

PDEA poly(N,N-diethylaminoethyl methacrylate)

PVP poly(4- or 2-vinylpyridine)

PHis poly(L-histidine)

PbAE poly(β-amino ester)

pH_T pH of the transition state from insolubility to solubility

DOX doxorubicin

PEGb-PDPA poly(ethylene glycol)-block-poly(2-(diisopropylamino)ethyl methacrylate)

TPGS d-a-tocopheryl polyethylene glycol 1000 succinate

GSH glutathione

mPEG methoxyl poly(ethylene glycol)

PZLL poly(3-benzyloxycarbonyl-L-lysine)

PEG-b-PHPMA-LA poly(ethylene glycol)-b-poly(N-2-hydroxypropyl methacrylamide)-lipoic acid

DTT dithiothreitol

CPT camptothecin

UVA ultraviolet A

BU-PPG uracil-end-capped oligomeric poly(propylene glycol)

BA-PPG adenine-end-capped oligomeric poly(propylene glycol)

RES reticuloendothelial system

LCL long circulation liposomes

GM-1 gangliosides

PEGS polyethylene glycol derivatives

PEI 1800-TA polyethylenimine 1800-triamcinolone acetonide

CHEDLA [(2-lactoylamido) ethylamino]formic acid cholesterol ester

STL successive targeting liposomes

PE phosphatidyl ethanolamine

DOPE dioleoyl phosphatidyl ethanolamine

FA folic acid

FI fluorescein isothiocyanate

KB cells a human epithelial carcinoma cell line

PAMAM-G7 dendritic polyamides-generation 7

PNIPAAm poly(N-isopropylacrylamide)

LCST lower critical solution temperature

PMPC-PDPA poly (2-(methacryloyloxy)ethyl phosphorylcholine)-b-poly (2-(diisoprop ylamino) ethylm ethacrylate

PBD-PGA di-block copolymer poly(butadiene)-b-poly(L-glutamic acid)

Lig lignosulfonate

SWNCT single-walled carbon nanotubes

MOFs metal–organic frameworks

NMOFs nanometer scale metal–organic frameworks

aMMTm apatinib-loaded MOFs coated with MnO_2 and decorated with membranes

5-FU uracil 5-fluorouracil

Br-BODIPY 1,3,5,7-tetramethyl-4,4-difluoro-8-bromomethyl-4-bora-3a,4a-diaza-s-indaeene

ES-CP ethoxysueeinato-cisplatin

HMS hollow mesoporous silica

AFM atomic force microscopy

TEM transmission electron microscopy.

frontiers | Frontiers in Bioengineering and Biotechnology

TYPE Review
PUBLISHED 21 October 2022
DOI 10.3389/fbioe.2022.1047598

Check for updates

OPEN ACCESS

EDITED BY
Michel Assad,
Charles River Laboratories, Canada

REVIEWED BY
Fengchao Cui,
Northeast Normal University, China
Xinan Shi,
Guangxi University, China
Tsung-Rong Kuo,
Taipei Medical University, Taiwan

*CORRESPONDENCE
Leijiao Li,
lileijiao@cust.edu.cn
Wenliang Li,
wenlilangl@ciac.ac.cn

SPECIALTY SECTION
This article was submitted to Biomaterials, a section of the journal Frontiers in Bioengineering and Biotechnology

RECEIVED 18 September 2022
ACCEPTED 07 October 2022
PUBLISHED 21 October 2022

CITATION
Wang B, Xu Y, Shao D, Li L, Ma Y, Li Y, Zhu J, Shi X and Li W (2022), Inorganic nanomaterials for intelligent photothermal antibacterial applications. *Front. Bioeng. Biotechnol.* 10:1047598. doi: 10.3389/fbioe.2022.1047598

COPYRIGHT
© 2022 Wang, Xu, Shao, Li, Ma, Li, Zhu, Shi and Li. This is an open-access article distributed under the terms of the Creative Commons Attribution License (CC BY). The use, distribution or reproduction in other forums is permitted, provided the original author(s) and the copyright owner(s) are credited and that the original publication in this journal is cited, in accordance with accepted academic practice. No use, distribution or reproduction is permitted which does not comply with these terms.

Inorganic nanomaterials for intelligent photothermal antibacterial applications

Bao Wang[1], Yan Xu[1], Donghan Shao[1,2], Leijiao Li[1,2]*, Yuqin Ma[1,2], Yunhui Li[1,2], Jianwei Zhu[2], Xincui Shi[1,2] and Wenliang Li[3]*

[1]School of Chemistry and Environmental Engineering, Changchun University of Science and Technology, Changchun, China, [2]Zhongshan Institute of Changchun University of Science and Technology, Zhongshan, China, [3]Engineering Research Center of Antibody, Jilin Medical University, Jilin, China

Antibiotics are currently the main therapeutic agent for bacterial infections, but they have led to bacterial resistance, which has become a worldwide problem that needs to be addressed. The emergence of inorganic nanomaterials provides a new opportunity for the prevention and treatment of bacterial infection. With the continuous development of nanoscience, more and more inorganic nanomaterials have been used to treat bacterial infections. However, single inorganic nanoparticles (NPs) are often faced with problems such as large dosage, strong toxic and side effects, poor therapeutic effect and so on, so the combination of inorganic nano-materials and photothermal therapy (PTT) has become a promising treatment. PTT effectively avoids the problem of bacterial drug resistance, and can also reduce the dosage of inorganic nanomaterials to a certain extent, greatly improving the antibacterial effect. In this paper, we summarize several common synthesis methods of inorganic nanomaterials, and discuss the advantages and disadvantages of several typical inorganic nanomaterials which can be used in photothermal treatment of bacterial infection, such as precious metal-based nanomaterials, metal-based nanomaterials and carbon-based nanomaterials. In addition, we also analyze the future development trend of the remaining problems. We hope that these discussions will be helpful to the future research of near-infrared (NIR) photothermal conversion inorganic nanomaterials.

KEYWORDS

inorganic nanomaterials, photothermal therapy, near infrared-induced, antibacterial, biomedicine

1 Introduction

The risk of bacterial infection is common in living environment and public facilities. Especially after surgery, the risk of infection with pathogenic bacteria is extremely high and difficult to treat (Sethulekshmi et al., 2022). Minor delay wound healing, and heavy produce life-threatening complications. Bacterial infections have become one of the enemies of human health. In order to effectively fight against bacterial infections, a series

of antibiotics are manufactured and widely used, such as: penicillin, roxithromycin, vancomycin, cephalosporin, etc. (Hochvaldová et al., 2022). But antibiotic abuse has led to bacterial resistance, forming multiple multidrug-resistant (MDR) bacteria, such as methicillin-resistant *Staphylococcus aureus* (MRSA), vancomycin-resistant *Staphylococcus aureus* (VRSA) and vancomycin-resistant Enterococcus (Abbas et al., 2022). It is reported that 10 million people may die every year from 2022 to 2050 due to bacterial antibiotic resistance (O'Neill 2016). Antimicrobial-resistant (AMR) and multidrug-resistant (MDR) infections will have a higher mortality rate than all types of cancer combined, according to projections from the Centers for Disease Control and Prevention (CDC) (Pormohammad et al., 2021). Therefore, it is of great significance to develop unconventional antibiotic drugs to treat bacterial infections (Chaudhary 2016).

In recent years, nanotechnology has become increasingly linked to biomedicine, and some nanomaterials with antibacterial activity are considered an ideal way to treat and prevent bacterial infections. Nanomaterials generally refer to materials in the range of 1–100 nm in at least one dimension in three-dimensional space. Inorganic nanomaterials are widely used in the treatment of tumors, cancers and bacterial infections due to their low toxicity, small size, good biocompatibility, easy modification and large surface energy (Chaudhary et al., 2016). At present, a variety of inorganic nanomaterials have been synthesized, including: metal-based nanomaterials, transition metal-based nanomaterials and carbon-based nanomaterials. The size and morphology of nanomaterials are the main indicators affecting their performance, and among the nanomaterials that have been synthesized, the morphology mainly includes: nanorods (Zhang et al., 2021), nanospheres (Li et al., 2022), nanowires (Han et al., 2022), nanoflower (Mutalik et al., 2021), nanotubes (Zhao et al., 2023), nanosheets (Mutalik et al., 2022), etc. The unique antibacterial mechanisms of nanomaterials are the following: 1) Destruction of bacterial DNA and proteins through the release of metal ions or the production of reactive oxygen species (ROS); 2) Destruction of bacterial cell membranes through the aggregation of nanoparticles (Qi et al., 2020); 3) NPs accumulate on the surface of the cell membrane to block the transmembrane transmission of electrons; 4) Heat shock/stress caused by temperature increase (Hamblin 2016; Wang C. et al., 2020). However, many times a single nanomaterial has problems such as insignificant therapeutic effect, large dose of material used, and strong toxicity in the treatment of bacterial infection. To this end, the search for safer and more effective treatments for bacterial infections has become a major focus for scientists.

As a controllable and non-invasive treatment method, PTT has been widely used in biomedical fields as a new treatment model in recent years. The PTT converts light energy into thermal energy through physical means, and a photothermal agent is required during the conversion process. It has become a popular trend to carry out nanomaterials as photothermal agents in combination with photothermal therapy and applied in antibacterial therapy. The advantages of photothermal therapy are mainly in the good penetration of tissues, and this non-contact treatment can effectively avoid bacteria developing drug resistance. Ultraviolet light (<380 nm), visible light (380–760 nm), and NIR light (>760 nm) are commonly used light sources for several photothermal therapies. The wavelength of visible light is between 380 and 760 nm, accounting for about 52% of the solar spectrum, and the wavelength of ultraviolet light is less than 380 nm, which is in the invisible region along with NIR light, accounting for 4% and 44% of the solar spectrum, respectively. By adjusting the band structure engineering of the photothermal agent, the surface plasmon resonance effect or the addition of light enhancers to reduce the very small proportion of ultraviolet light in the solar spectrum, resulting in its photothermal conversion efficiency cannot be satisfactory. Therefore, achieve full use of the light source is a very meaningful thing (Wang L. et al., 2021).

Inorganic nano-photothermal conversion materials for the treatment of bacterial infections are fully discussed here (Figure 1). Starting from the synthesis method, the preparation and modification methods of inorganic nanomaterials of different morphologies and sizes, the antibacterial mechanism under different light sources, and various factors affecting the photothermal conversion efficiency of nanomaterials are described. Finally, the application of photothermal conversion nanomaterials in antimicrobials is described, and its future development direction and challenges are prospected. Here, we summarize several synthesis methods of inorganic nanomaterials and their advantages and disadvantages (Table 1), as well as the advantages and antibacterial mechanism (Table 2) of several inorganic nanomaterials used in photothermal treatment of bacterial infection.

2 Synthesis of inorganic nanomaterials

The synthesis of nanomaterials is usually mainly divided into "top-down" and "bottom-up" methods (Saravanan et al., 2021). Top-down generally refers to the decomposition of large pieces of material into smaller parts by physical or chemical methods such as ultrasonic crushing or laser etching (Nekoueian et al., 2019; Cui et al., 2022). Bottom-up generally refers to the formation of new materials by assembling different materials together by chemical or biological means such as one-pot method or biosynthesis (Jamkhande et al., 2019). In view of the fact that the internal stresses introduced by top-down synthesis methods in many cases will destroy the morphology of nanomaterials and affect the surface effect of NPs, most nanomaterials choose bottom-up methods for synthesis (Xia et al., 2019).

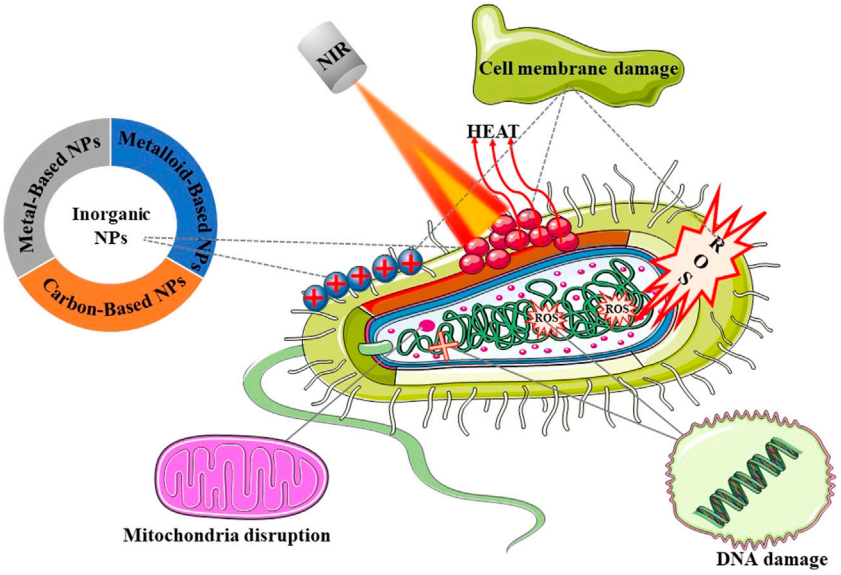

FIGURE 1
Schematic illustration of the main topics covered in this review.

TABLE 1 Synthesis methods and advantages and disadvantages of Inorganic nanoparticles.

Synthesis method	Synthesis principle	Advantages	Disadvantages	References
Radiation induced	Irradiate a solution containing precursors with accelerated electrons or gamma rays	Not affected by temperature, and the purity of the product is high	Radiation does great harm to human health and has the risk of causing cancer	Güven (2021)
Biosynthesis	Extract required elements from plants or organisms	The raw materials are cheap and easy to obtain, and the biosafety is high	The extraction process is complicated and the output is low	Rambabu et al. (2021)
Seed mediated method	The extremely small nanocrystals were added to the supersaturated solution for secondary nucleation	Avoid the homogeneous nucleation process which is difficult to control	The purity of the reaction reagent is high, and the concentration of the precursor is not easy to be controlled	Shi et al. (2021)
Assisted synthesis of capping agent	The capping agent is selectively adsorbed on the surface of nanocrystals by changing the surface free energy	Nanoparticles with multiple morphologies can be obtained by using end-capping agents	The dispersion and solubility of nanoparticles will be affected	Huang et al. (2020)

Commonly used bottom-up synthesis methods are mainly as follows:

2.1 Radiation induced

Radiation induced technology has become a very popular method for the synthesis of nanomaterials because it is simple, fast, green and is not affected by the experimental temperature. It has been widely used in the fields of medicine and environment (Xiong et al., 2021). In the process of synthesis, the solution containing the corresponding precursor can be irradiated with accelerating electrons or gamma rays to synthesize NPs with smaller size (Čubová and Čuba. 2019), and high-purity products can be obtained without strictly controlling the experimental conditions. Ionizing radiation with high-energy gamma photons and accelerated electrons can uniformly generate free radicals in the transmitted medium (Güven 2021).This property makes ionizing radiation technology widely used in the preparation of nanomaterials.

By irradiating the carbon nanotubes with γ ray, the carbon nanotubes can be uniformly dispersed and kept stable without using a dispersant (Saif et al., 2018) (Figure 2A). Radiation induced technology is also commonly used in the synthesis of quantum dots (Gidwani et al., 2021). Li et al. (2011) Synthesized SnSe quantum dots by using ionizing radiation technology and adding surfactant CTAB at room temperature, which effectively avoided the problems of high synthesis

TABLE 2 Summary of inorganic nanomaterials for NIR photothermal antibacterial.

Nanoparticles	Advantage	Treatment strategy	References
Au NPs	It has strong light absorption, surface plasmon resonance and photothermal effect	When used in photothermal therapy, the lattice is heated, the temperature of the material rises, and bacteria are killed	Ma et al. (2019)
Ag NPs	It has adjustable surface plasmon resonance effect, has certain antibacterial properties and is easy to synthesize	Ag itself can interact with phosphate and other substances inside and outside the cell, and inhibit the growth of bacteria. When combined with NIR, it can destroy the cell membrane and lead to bacterial death due to local heating	Tamboli and Lee (2013)
B NPs	It has the functions of anti-inflammation and metabolic regulation, can maintain the stability of cell membrane and has targeting	The existence of element B promotes the separation of holes and electrons, improves the optical properties, and can produce more ROS to kill bacteria under light conditions	Ran et al. (2022)
Te NPs	It can specifically bind to glutathione in cells and has a certain antibacterial effect	Te (0) accumulates in cells, produces ROS under NIR laser irradiation and activates intracellular oxidative stress, resulting in the death of bacteria	Huang et al. (2022)
CQDs	It has small size, good water dispersibility, biocompatibility and optical properties, and is easy to be removed from the body	CQDs can produce ROS under laser irradiation, and the temperature increases at the same time	Ghirardello et al. (2021)
Graphene	It has good thermal conductivity and optical transmittance and has full spectrum absorption	Graphene itself has a targeted effect on bacteria, graphene produces high temperature under NIR laser irradiation, and the two synergistically enhance the antibacterial effect	Wang H. et al. (2020)

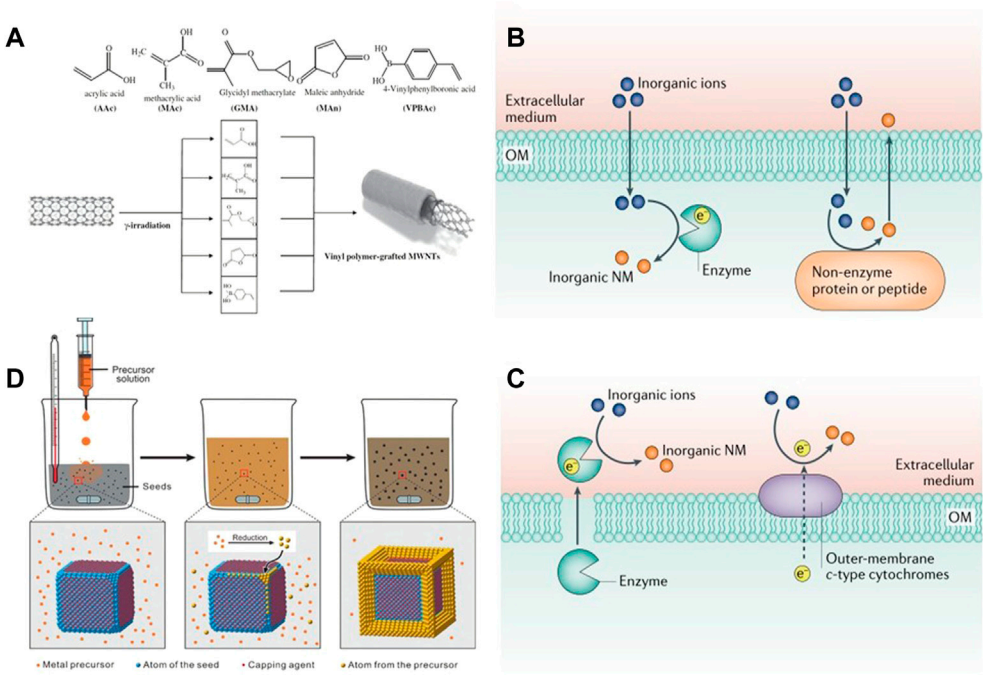

FIGURE 2
(A) Linking the surface of MWCNT's with different vinyl monomers by laser irradiation. Reproduced from (Yang et al., 2010) with permission from Radiation Physics and Chemistry. The biosynthesis of inorganic nanomaterials can be generated by **(B)** secreted enzymes and membrane proteins extracellularly, or **(C)** intracellularly, by combining proteins/peptides with inorganic ions or oxidoreductases. Reproduced from (Choi and Lee. 2020) with permission from Nature Reviews Chemistry. **(D)** General procedure for obtaining desired nanocrystals from metal precursors using a seed-mediated method. Inorganic-nanomaterial synthesis in microbial cells and bacteriophages. Reproduced from (Xia et al., 2016) with permission from Angewandte Chemie.

temperature and the use of toxic precursors. In addition to the above nanoparticles, nano gel can also be synthesized by radiation-induced method. Recently, Sabatino et al. (2020) reviewed the progress made by γ ray, electron beam and ultraviolet radiation are used to mediate the formation of nano gel, and the application of the synthesized gel is

briefly summarized (Matusiak et al., 2020; Sabatino et al., 2020). Radiation induced technology provides a simpler way for the synthesis of inorganic nanoparticles and is expected to be widely used in the future synthesis process.

2.2 Biosynthesis

Green synthesis is one of the effective methods to reduce the biological toxicity of nanoparticles, which can effectively improve the biocompatibility of nanoparticles (Zonaro et al., 2015). In the process of green synthesis, biosynthesis mainly extracts the required elements from organisms or plant organisms. It is favored for its advantages of economy, safety and easy availability (Rambabu et al., 2021). There is no need to add additional reductant or capping agent during the synthesis process, nor high pressure and high temperature (Salem and Fouda 2021). Plants are more favorable for the synthesis of nanoparticles due to their various biological molecules such as polyphenols, proteins, flavonoids and bioactive amines (Lee et al., 2020). The method of synthesizing nanoparticles with plant extracts is a one-step synthesis method (Wang D. et al., 2019). Plant synthesis has the advantages of cheap and easy access to raw materials, low biological toxicity, high economic efficiency and safety. The synthesis of nanoparticles from plant extracts was first proposed by Gardea-Torresdey et al. (2003) using alfalfa sprouts to synthesize Ag-NPs. After that, some people successively proposed the biosynthesis of silver and gold NPs by golden rutin flower; Ag NPs with very small size (2–4 nm) were synthesized with Camellia sinensis (Rolim et al., 2019); Fe NPs with a size in the range of 30–100 nm were synthesized with tea leaves extract (Lin et al., 2020).

Microbial synthesis is the second largest biological source of nanoparticles. The mechanism for the synthesis of nanoparticles is that numerous metal or non-metal ions (such as Cu^{2+}, Mg^{2+}, Ag^{+}, Cd^{2+}) will interact electrostatically with the negatively charged cell membrane and adsorb to the surface of the cell membrane, transferring through the microbial membrane to the cell, which in turn activates the cell's over-defence mechanism and is exported as a monomer by the cell using the efflux pump. The output monomer is the synthesized nanoparticles (Choi and Lee. 2020). The biosynthetic pathway of NPs can be divided into intracellular synthesis and extracellular synthesis (Figures 2B,C). The reducibility of enzymes is a very important factor for biomolecules to reduce metals and nonmetals. In extracellular synthesis, inorganic ions are mainly reduced to NPs by enzymes secreted by cells. For example, with Shewanella oneidensis MR-1, Pd NPs with a size of 10–100 nm can be synthesized in and out of the cell by enzymes secreted by the cell or enzymes on the extracellular membrane under the action of bioelectrochemistry (Wang W. et al., 2019). During intracellular synthesis, it mainly depends on reductase, polypeptide or non-enzymatic protein. Through the gene expression of protein MT, glutathione can be oligomerized into polypeptide PC to participate in the reduction of Cu^{2+}, Ag^{+} and other inorganic ions (Jung et al., 2018), so that nanoparticles can be synthesized and grown in cells. For example, Ag nanospheres with a size of 20–70 nm can be synthesized by using the covering protein of *Pseudomonas* sp. and a wide range of secondary secretions (John et al., 2020). In addition, Fungi and yeast, also one of the bacterial genera, are also broadly used for the synthesis of NPs. The fungus itself has a large amount of mycelium, which enables it to synthesize nanoparticles with high efficiency (Kitching et al., 2022).

Biomolecules contain functional groups. In most cases, they can be used not only for the synthesis of nanoparticles, but also for the stabilization and functionalization of NPs (Choi and Lee 2020). This also provides a new idea for the application of nanoparticles in the field of antibacterial.

2.3 Seed mediated method

In the traditional sense, most nanocrystals are directly generated by using the one pot method in the presence of salt precursor and reducing agent, and by external conditions such as microwave, ultrasonic wave and current. Sometimes, the above methods cannot obtain ideal size and morphology, so Chen et al. (2013) proposed the seed mediated method to accurately control the synthesis of nanocrystals. The seed-mediated method divides growth and nucleation into two steps. Seed crystals of very small size (about a few nanometres) are added to a solution below supersaturated concentration to continue growth. It avoids the difficult to control homogeneous nucleation process by directing the newly formed atoms to nucleate twice on the surface of the pre-synthesised seeds (Xia et al., 2016) (Figure 2D).

The following problems should be paid attention to in the seed mediated method: 1) High purity reaction reagents should be used; 2) Control the concentration of precursor to ensure that no other reaction occurs except heterogeneous nucleation; 3) Be careful that the seed crystal is oxidized before use (Thanh et al., 2014). In order to ensure the accurate synthesis of crystal seeds, inert gas or capping agent is often introduced in the process of synthesis to protect the crystal seeds. The most typical seed mediated method is to use surfactants to prepare Au nanorods (GNRs). For example, cetyltrimethylammonium bromide (CTAB) is often used as a "soft template" to guide the directional growth of nanocrystals. This template is a simple and effective method to prepare rare and precious metal materials. Firstly, chloroauric acid was reduced by sodium borohydride in CTAB aqueous solution to prepare smaller Au seed solution. Secondly, the growth solution was prepared by reducing Au (III) complex ion to Au (I) complex ion with ascorbic acid (AA) in CTAB aqueous solution. Finally, a certain quantity of seed solution was added to the growth

solution. The biggest advantage of seed mediated method is that any existing nanocrystalline seed can be added to the growth solution composed of capping agent or reducing agent to obtain high yield and new morphology nanocrystals (Shi et al., 2021).

2.4 Assisted synthesis of capping agent

The growth of nanocrystals usually requires stable control of capping agents (Loza et al., 2020). The addition of capping agent will have an important impact on the internal structure, surface structure and shape of nanocrystals, so it is widely used in nanomaterials and synthesis (Yang et al., 2019). At present, a great many capping agents have been reported to be used, such as biomolecules, anionic/cationic species, small molecules and macromolecular polymers (Abadi et al., 2022). The capping agent is mainly used to selectively adsorb on a plane of nanocrystals by changing the free energy of the surface to prevent further deposition and growth of atoms on the plane. There are many examples where the use of capping agent has changed the morphology of nanomaterials. For example, when fructose is used as capping agent to synthesize tellurium nanocrystals, tellurium nanorods are synthesized without fructose, and triangular tellurium nanostar is synthesized after fructose is added (Huang et al., 2020). In addition, when eight different chain lengths of CTAB (C_nTAB, n = 2–16, Even) are used to synthesise GNRs, GNRs of different sizes from nanometres to micrometres can be obtained (Ye et al., 2013; Inaba et al., 2019).

A single capping agent cannot fully satisfy the basic needs of NPs in the synthesis process. In addition to morphology and size, dispersion and solubility are also important indicators to evaluate NPs. The future development direction will be toward the simultaneous use of two different types of capping agents, which can not only effectively improve the yield, but also obtain more nanocrystals with uniform size and good dispersion (Jana 2005; Zheng et al., 2021).

3 Antibacterial application and antibacterial mechanism of photothermal conversion inorganic nanomaterials

In clinical applications, there are high requirements for the biocompatibility of photothermal therapy nanomaterials. Although many nanomaterials reported so far have excellent photothermal conversion properties, their long-term safety is doubtful and it is difficult to be directly applied to clinical treatment. For example, metal NPs have poor biological metabolic capacity, and carbon-based materials have been shown to trigger many toxic reactions, such as oxidative stress and lung inflammation. Therefore, improving the biocompatibility of photothermal materials to provide better biodegradability and low toxicity is also a key factor.

In the treatment of bacterial infection, PTT has been widely used because it can effectively prevent bacteria from producing drug resistance. In view of the poor penetration of visible light to tissues, NIR light is often used as the light source of PTT. The commonly used NIR photothermal conversion nanomaterials mainly include noble metal-based nanomaterials, transition metal-based nanomaterials and carbon-based nanomaterials.

3.1 Noble metal-based nanomaterials

3.1.1 Au

Noble metal-based nanomaterials have attracted extensive attention in photothermal therapy and imaging due to their surface plasmon enhanced fluorescence, plasma resonance effect and plasma photothermal effect. Among many noble metal nanomaterials, the preparation methods of nano Au have been very mature. Au nanoparticles have the benefits of easy surface modification and great biocompatibility. When irradiated with NIR light of a certain frequency, the Au NPs not only have high absorption capacity for light, but also can increase the absorption of light by the Au NPs through its adjustable regional plasmon resonance (LSPR). In view of the wonderful light absorption properties of Au NPs, they are often used as photothermal agents for the treatment of bacterial infections.

At present, the low photothermal conversion efficiency of Au is an urgent problem to be solved. In order to remove the application limitation brought by the photothermal conversion efficiency, scientists have explored the Au NPs with different morphologies and modified by different methods. GNRs are one of the most common morphologies in the synthesized gold nanomaterials, with strong absorption in the range of 600–900 nm (Vankayala and Hwang. 2018). When used for PTT, plasma resonance begins to attenuate with the heating of the lattice, resulting in an increase in the ambient temperature. In the process of photothermal conversion, the more electrons, the higher the thermal energy conversion. Based on this principle, Ma et al. (2019) constructed a core-shell nanostructure GNR@LDH of GNRs and layered double hydroxide (LDH). Under 2 Wcm^{-2} 808 nm laser irradiation, the temperature of individual GNRs could be increased by 31.8°C. GNR@LDH containing the same concentration of GNRs is 50°C warmer and can achieve a photothermal conversion efficiency of 60%.When using PEG GNR@LDH after functionalization, 300 μg ml^{-1} GNR@LDH-PEG (including 30 μg ml^{-1} GNRs) for 5 min, the bactericidal rates of *Escherichia coli* (*E. coli*) and *Staphylococcus aureus* (*S. aureus*) were 99.25% and 88.44%, respectively (Figures 3A,B). Compared with single component GNRs, noble metal semiconductor heterostructures exhibit new functions and better performance

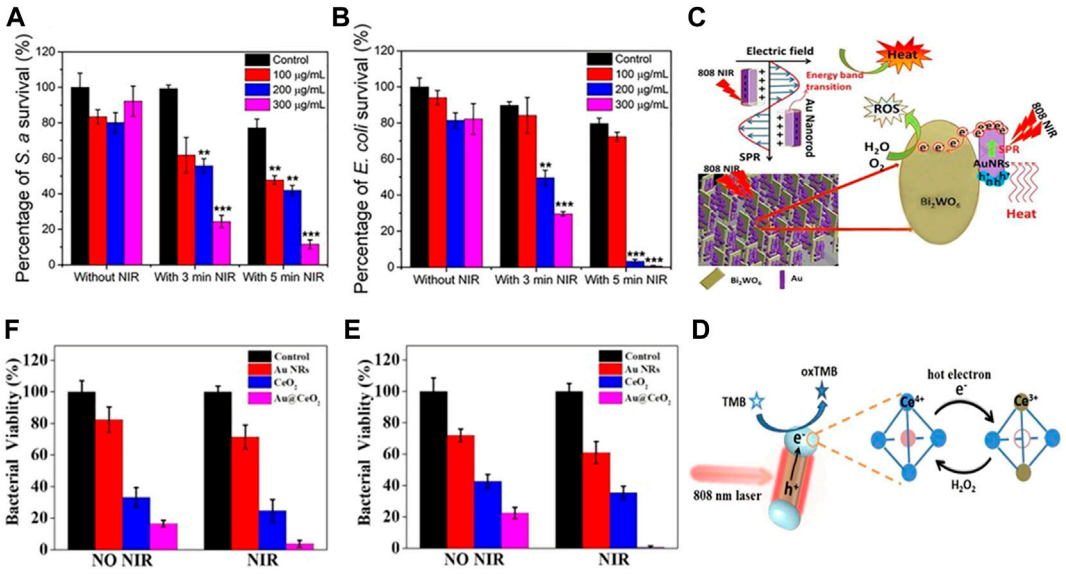

FIGURE 3
(A) Survival rate of *S. aureus* in corresponding group (n = 3); **(B)** Survival rate of E. *coli* in corresponding group (n = 3). Reproduced from (Ma et al., 2019) with permission from ACS Appl. Mater. Interfaces. **(C)** Photocatalytic mechanism of the Au@Bi2WO6 composite. Reproduced from (Li et al., 2019) with permission from Journal of Hazardous Materials. **(D)** Schematic diagram of carrier dynamics and carrier reaction of Au@CeO_2 for peroxidase-like reaction under plasmon excitation. Enhanced antibacterial activity of Au@CeO_2 nanozyme. Bacteriostatic activity of **(E)** *S. aureus* and **(F)** *E. coli* with different samples without and with NIR irradiation, respectively. Reproduced from (Liu et al., 2021) with permission from Applied Catalysis B: Environmental.

due to the synergistic effect between different components of heterostructures. The charge separation and light absorption at the heterostructure interface can be promoted by the surface plasmon resonance (SPR) of noble metals, which can effectively improve the photothermal conversion efficiency of GNRs (Leng et al., 2018). Li et al. (2019) combined GNRs and Bi_2WO_6 nanosheets, reduced the recombination of electrons and holes through the SPR effect induced by 808 nm NIR, improved the photocatalytic performance of Au@Bi_2WO_6 coatings, and was more likely to produce a large amount of ROS. When irradiated with NIR laser for 15 min, it was able to kill 99.96% and 99.62% of *E. coli* and *S. aureus*, and the sterilization rate was much higher than that when GNRs were used alone (Figure 3C). Sibidou et al. confirmed through experiments that the Au nanomaterials with biconical shape with (111) crystal plane have better photothermal effect than GNRs with (200) crystal plane (Yougbare et al., 2021a), and can kill all *E. coli* when irradiated at 808 nm for 7 min. In addition to the large Au nanostructures, the ultra-small gold nanoclusters also have ideal antibacterial effects. The use of biomolecules plays an important role in the synthesis of gold nanoclusters. Common biomolecules such as glucose, DNA, polypeptide, protein, etc. are reductive and have rich functional groups. They can not only act as reductants in the synthesis of gold nanoclusters, but also as ligands to realize the functionalization of Au nanoclusters (Pranantyo et al., 2019). Among many biomolecules, antimicrobial peptides (AMPs), as a kind of non-antibiotic biomolecules, can not only kill bacteria, but also be used as reducing agents to prepare gold nanoclusters with fluorescence emission. When the photothermal conversion efficiency reached 34.2%, the AMPs modified Au nanoclusters achieved the progressive killing of *E. coli* and HT-29 (Zhu et al., 2020) (Figure 3D). The unique SPR effect of noble metals enables it to be used in combination with a variety of materials to improve the therapeutic effect. GNRs can show a huge electric field enhancement at both ends of the rod under resonance excitation (Chen et al., 2013). Among them, the combination with nano enzymes has been proven to be effective in the treatment of bacterial infections. Liu et al. (2021) Deposited CeO_2 nano enzyme at the end of GNRs to form a spatially separated dumbbell shaped nanostructure, which can simultaneously have plasma induced hot carriers and thermal effects (Figure 3E). Under 808 nm irradiation, Au@CeO_2 The significant enhancement of peroxidase like activity of the Au composite enables the Au composite to have a broad-spectrum antibacterial effect (Liu et al., 2021) (Figure 3F).

The above antibacterial mechanism of Au NPs can be simply summarized as follows: Metal NPs are oxidized by NIR laser and released in the form of particles, generating ROS, destroying bacterial cell membranes, causing internal ribosomal instability, mitochondria and protein damage, and finally causing bacterial death (Faisal et al., 2013; Fu et al., 2014).

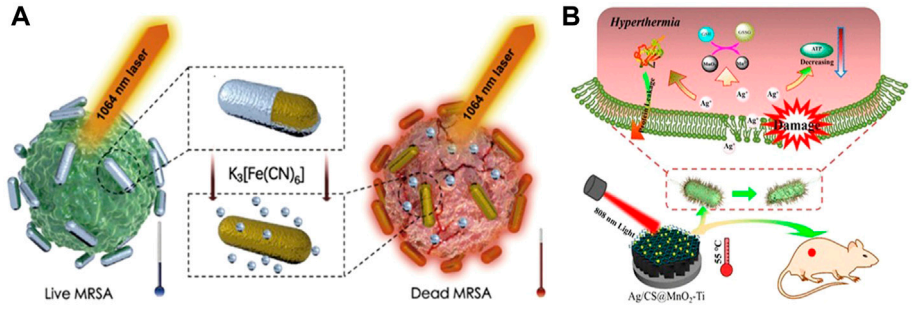

FIGURE 4
(A) Schematic diagram of NIR II combined with released Ag^+ in the treatment of MRSA. Reproduced from (Mei et al., 2020) with permission from Biomaterials. **(B)** Synergistic antibacterial mechanism of Ag/CS@MnO_2-Ti and 808 nm NIR. Reproduced from (Wang X. et al., 2019) with permission from ACS Appl. Mater. Interfaces.

3.1.2 Ag

Ag NPs have similar chemical properties to Au NPs. For example, large specific surface area, enhanced optical performance and the same LSPR effect. However, due to the size, shape, dosage and other reasons, Ag has non negligible biological toxicity.

Behravan et al. proved that the use of biosynthesis to obtain Ag NPs that can be used for the treatment of bacterial infection can effectively reduce the biological toxicity of Ag NPs, and the aqueous extract of Berberis leaves and roots was successfully used to synthesize Ag NPs with a size of 30–70 nm (Behravan et al., 2019). The antimicrobial performance was tested by disk diffusion method, which proved that it has a great inhibitory effect on *E. coli* and *S. aureus*. As a common biomolecule, polysaccharides also have low biological toxicity and are often used in the synthesis of hydrogels. Liu et al. (2020) embedded the Ag NPs synthesized with gallic acid (GA) into the network structure synthesized by polysaccharide carrageenan, and obtained a GA-Ag NP hydrogel with coagulation, air permeability, anti-dehydration and good bactericidal effect under 808 nm laser irradiation. It can also promote wound healing while treating bacterial infection. In the follow-up study, Mei et al. (2020) combined Ag and Au and also synthesized micro-Au/Ag NRs that can promote wound healing and can be used for the treatment of MRSA infection. On this basis, the micro-NPs can also be used for photoacoustic imaging (PA). *In vitro* and *in vivo* experiments showed that the synergistic effect of free Ag^+ and 1,640 nm NIR could effectively eliminate MRSA and the biological toxicity was extremely low (Figure 4A). Meanwhile, activatable NIR PA can monitor the treatment process and provide timely feedback.

It has been proved in medicine that Ag nanoparticles have excellent antibacterial properties, and its antibacterial mechanism can be summarized as follows: when Ag NPs are used alone for antibacterial, Ag NPs have a high tendency to sulfur and phosphorus in cells, and can interact with phosphate and sulfur-containing proteins inside and outside cells. When the nanoparticles reach a certain concentration, they can achieve complete inhibition of bacterial growth (Tamboli and Lee, 2013). When Ag NPs are combined with PTT and hydrogel, under the irradiation of NIR light and heat, the hydrogel coated on the wound surface is locally heated, causing protein denaturation and membrane damage in bacterial cells (Liu et al., 2020), and promoting the release of Ag NPs. Ag NPs with larger surface area and smaller size are more likely to enter the cell and interact with thiol groups, causing bacterial death (Wang X. et al., 2019) (Figure 4B). Different antibacterial mechanisms show the great potential of Ag nano photothermal conversion materials in the biomedical field, and the combined treatment system of Ag NPs will effectively improve the therapeutic effect.

3.2 Metal like nanomaterials

3.2.1 Boron

Boron (B) is one of the necessary trace elements for organisms. It can not only fight inflammation and regulate metabolism, but also maintain the stability of cell membrane (Xie et al., 2020; Duo et al., 2021; Jakubczak et al., 2021). In the past decade, many boron containing drugs have been approved for clinical use. However, due to potential toxicity, some boron compounds are still in the research stage. In recent years, researchers have paid much attention to the property that boron compounds can transform between neutral triangular plane sp^2 and tetrahedral hybrid state sp^3.

Boron derived compounds play a significant antibacterial role. In many previous studies, boric acid was considered as a promising drug that can resist antibiotic resistance (Song et al., 2021) (Figure 5A). Since 2015, tuberculosis (TB) caused by Mtb has caused about 250,000 deaths every year, and the treatment success rate of multi drug resistant tuberculosis (MDR-TB) is only 56%. It is reported that boric acid can treat

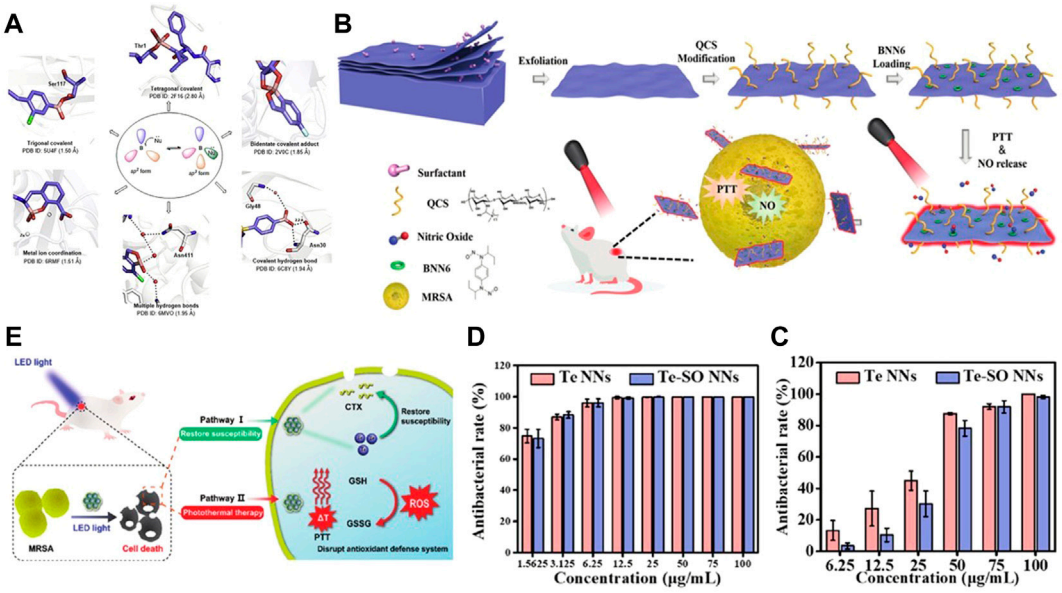

FIGURE 5
(A) Boron compounds and their interaction modes with biological targets. Reproduced from (Song et al., 2021) with permission from Acta Pharmaceutica Sinica B. **(B)** Preparation of B-QCS-BNN6 and its application in photothermal-NO synergistic antibacterial. Reproduced from (Lv et al., 2022) with permission from Biomaterials Science. Antibacterial activity of Te and Te-SO nanoneedles (NNs) toward **(C)** *S. aureus*. **(D)** and *E. coli*. antibacterial rate in the presence of Te and Te-SO NNs at different concentrations. Reproduced from (Huang et al., 2022) with permission from Materials Today Bio. **(E)** Bactericidal action of Te–CTX nanocomposites. The intracellular CTX and PTT synergism against MRSA for accelerating wound healing in mice. Reproduced from (Wu et al., 2022) with permission from Journal of Materials Chemistry B.

tuberculosis by selectively killing MTB, and can also be used as an inhibitor of *Staphylococcus aureus caseinolytic* protease P (SaClpP) (Song et al., 2021). Under the driving of visible light, the boron doped TiO_2 thin film can exhibit the inhibitory effect on *S. aureus*, *Acinetobacter* baumannii and *Streptococcus* pyogenes through the combined action of photocatalysis and B (Wong et al., 2020; Wang et al., 2022). The doping of B increases the specific surface area of nanoparticles, promotes the separation of electrons and holes, further improves the photocatalytic activity, and can produce a large number of ROS under light conditions, thus greatly improving the antibacterial activity (Ran et al., 2022).

Recently, someone proposed a photothermal antibacterial mode for B nanosheets. The multifunctional nano platform with B nanosheets as the carrier can capture negatively charged bacteria, and the NO generated after 808 nm illumination can better diffuse to the bacterial surface, thus achieving the ideal therapeutic effect of typical Gram-negative bacteria and Gram-positive bacteria (Lv et al., 2022) (Figure 5B). In conclusion, boron based photothermal nanomaterials still have a lot of space to explore in the field of antibacterial.

3.2.2 Tellurium

Tellurium (Te) is a semiconductor metal, which belongs to the chalcogenide group together with Se and O. after the biological application of Se was developed, scientists were surprised to find that Te in the same group also has excellent biomedical application prospects. In fact, the antibacterial activity of Te was discovered earlier than the use of antibiotics (FLEMING and F. R. C. S., 1940), which also shows that tellurium is a promising antibacterial agent.

Lin et al. (2012) synthesized four different morphologies of Te NPs using TeO_2 as raw material and N_2H_4 as reducing agent, and preliminarily explored their antibacterial activities, laying a foundation for the subsequent antibacterial application of tellurium nanoparticles. Tellurium is rarely natural, and most tellurium exists in the form of oxidized state, for example, −2 (telluride: Te^{2-}), 0 (elemental element: Te^0), + 4 (tellurite: TeO_3^{2-}), and + 6 (tellurite: TeO_4^{2-}) (Vahidi et al., 2021). The antibacterial effect of inorganic Te nanoparticles alone is not ideal (Lin et al., 2012). In order to expand its efficacy without affecting the performance of nanoparticles, many researchers choose to dope tellurium with other metals or some non-metallic materials or functionalize the synthesized tellurium nanoparticles to enhance the therapeutic effect. Brown D. et al. coated polyvinylpyrrolidone (PVP) on the surface of Te nanorods and analyzed the parameters representing the bacterial growth lag time λ, it was confirmed that the coating of PVP could delay the maturation of bacteria and then inhibit the growth of bacteria (Brown et al., 2018). However, the toxicity of tellurium nanoparticles remains a concern.

In order to reduce the toxicity of Te, scientists have made many attempts. On the one hand, plant extracts were selected as precursors for the synthesis of tellurium NPs (Zambonino et al., 2021). On the other hand, the reducing agent or capping agent needed in the synthesis process is changed. For example, Rosales-Conrado et al. synthesized spherical Te nanomaterials of different sizes using extracts from different kinds of tea leaves (Rosales-Conrado et al., 2021); Medina Cruz et al. Synthesized cubic Te NPs with lemon juice and lime juice respectively, and confirmed that when the concentration of nanoparticles was greater than 15 μg ml^{-1}, they had a significant inhibitory effect on MDR *E. coli* and MRSA (Medina Cruz et al., 2019); Huang et al. green synthesized triangular star Te NPs (Huang et al., 2020) with common fructose as reductant; Vahidi et al. synthesized Te NPs (Vahidi et al., 2021) with strong antioxidant and bactericidal properties using fungi.

The research data show that the size of nanoparticles has a significant impact on their antibacterial activity. In fact, the smaller size nanoparticles will show higher antibacterial activity than the larger size nanoparticles (Pormohammad et al., 2021). The lethality of tellurium NPs to bacteria is mainly due to the specific binding of tellurium oxyanion and GSH in bacterial cells, which makes TeO_3^{2-} be reduced to Te (0) and accumulated in cells. At the same time, ROS is generated in cells due to Fenton reaction, which activates the oxidative stress reaction in cells and finally kills bacteria (Huang et al., 2022) (Figures 5C,D). Secondly, Te NPs can also damage the integrity of bacterial biofilms, resulting in impaired function of cell membranes or cell walls. However, according to the previous research results, the antibacterial properties of many tellurium NPs synthesized at present are not ideal. Based on the great photothermal properties of tellurium NPs, the combination of tellurium NPs and PTT has gradually become a new popular trend. Wu et al. (2022) used cefotaxime (CTX)-loaded tellurium nanoparticles (Te-CTX NPs) as a photothermal agent, which, when irradiated by laser, produced a combined antibacterial effect of two synergistic pathways of PTT and CTX. On the one hand, Te restores the sensitivity of CTX to MRSA; on the other hand, the high temperature effect induced by PTT can destroy the antioxidant defense system of bacteria (Figure 5E). Under the synergistic effect of the two, 50 μg ml^{-1} Te-CTX NPs could effectively kill more than 90% of MRSA. The successful synergistic treatment of tellurium NPs and PTT provides more directions and possibilities for subsequent experiments. There are still more unknown about the combined use of the two.

3.3 Carbon-based nanomaterials

3.3.1 Carbon quantum dots

Carbon quantum dots (CQDs) generally refer to carbon-based nanomaterials with a size less than 10 nm. The small size gives CQDs excellent photostability, water dispersibility, photocatalytic activity, biocompatibility, and bacteriostatic properties (Mintz et al., 2019). The excellent optical properties of CQDs have been widely used in the biomedical field in recent years (Nekoueian et al., 2019). In addition to being widely used in biological imaging, photodynamic therapy and photothermal therapy of tumors (Liu et al., 2022), it is also widely used in antibacterial.

As a promising photothermal inorganic nanomaterial, it has been reported that CQDs have intrinsic antibacterial properties in the blue light region of 400–470 nm. Under the excitation of 470 nm blue light, carbon dots can generate ROS by light to destroy MRSA and *E. coli* (Wang B. et al., 2021). The greatest advantage of CQDs is that they can be easily removed from the body and have low biological toxicity (Chung et al., 2020). The absorption coefficient of CQDs is low in the NIR region, but the temperature can be increased to the required range by adjusting the power density of the irradiated laser or doping other elements or modifying (Geng et al., 2020). Some researchers have synthesized composite fluorescent carbon dots ($CsWO_3$-FCD) with the function of detecting and clearing bacteria. The carbon dots were coated with tungsten oxide ($CsWO_3$). On the one hand, it can target bacteria; on the other hand, it can also use the strong NIR absorption of catechol and $CsWO_3$ on the FCD surface to achieve photothermal antibacterial. At a small dose, it can effectively kill most *E. coli* and *S. aureus* within 5 min (Robby et al., 2021).

Qie et al. (2022) functionalized CQD with chiral biomolecules to prepare a bacterial affinity photothermal carbon point (BAPYCDs) for MurD ligase, and combined 808 nm 1.5 W cm^{-2} NIR laser with BAPYCDs. In 10 min, the BAPYCDs temperature of 200 μg ml^{-1} can be raised to 70.3°C. The temperature shows that BAPYCDs has excellent photothermal conversion efficiency. The addition of chiral molecule D-glutamic acid (D-Glu) enables BAPYCDs to be targeted and can be accurately localized to bacterial infection sites (Xin et al., 2017). When BAPYCDs were used alone for *in vitro* bacteriostatic experiments, 89.27% of *S. aureus* and 80.33% of *E. coli* were killed. When the above carbon dots were combined with NIR laser, almost all *S. aureus* and *E. coli* were killed (Figures 6A,B).

The antibacterial effect of the above CQDs is closely related to the charge and N content on the surface of CQDs (Verma et al., 2020). Most of the CQDs synthesized with amines or quaternary ammonium salts have certain antibacterial properties, but only the cationic groups of CQDs have limited antibacterial effect. Positively charged CQDs and negatively charged bacteria enter the cell interior through electrostatic interaction (Figure 6C) and cause cell wall damage and cytoplasmic leakage (Figure 6D) (Ghirardello et al., 2021), Irradiation with NIR raised the local temperature of bacteria and produced ROS, which further accelerated bacterial apoptosis (Figure 6E).

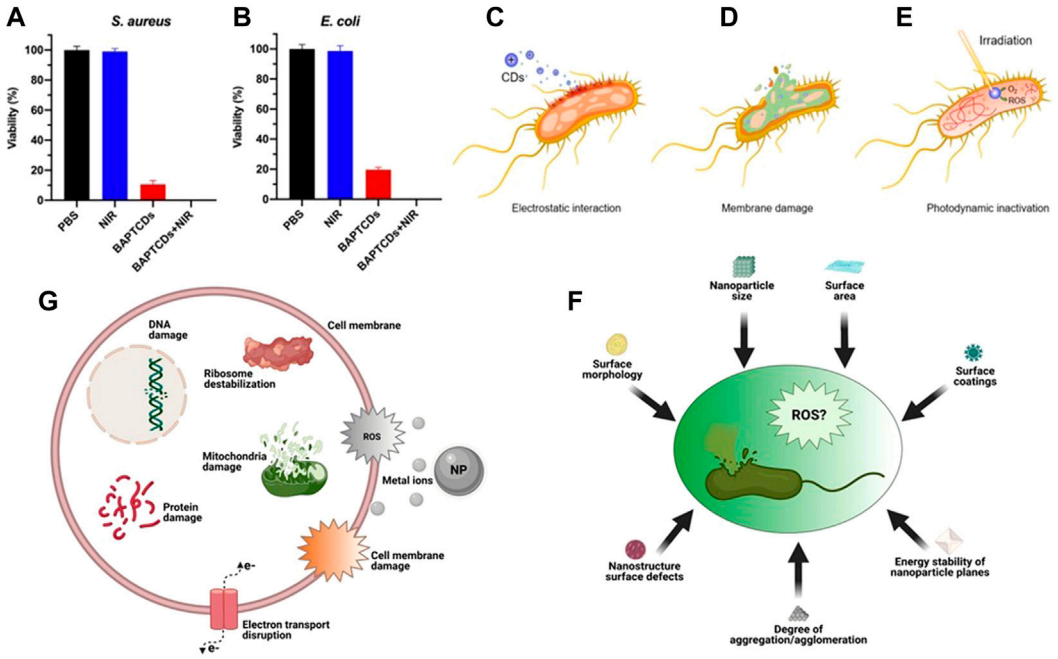

FIGURE 6
Bacterial viability of *E. coli* **(A)** and *S. aureus* **(B)** were obtained by the colony-forming count method. Reproduced from (Qie et al., 2022) with permission from Frontiers in Bioengineering and Biotechnology. General bactericidal mechanisms of action of CDs. **(C)** Electrostatic interactions between CDs and bacterial cell walls. **(D)** Internalization of CDs leads to irreversible damage caused by cytoplasmic leakage **(E)** CDs generate ROS under laser irradiation causing DNA damage. **(F)** Some factors of ROS production induced by carbon points and inhibition of bacteria. **(G)** Some mechanisms of toxicity of NPs. Reproduced from (Yougbare et al., 2021b) with permission from International Journal of Nanomedicine.

3.3.2 Graphene and its derivatives

Since the discovery of graphene in 2004, graphene has become a hot scientific research field due to its good thermal conductivity and optical transmittance, high intrinsic mobility, large specific surface area and excellent conductivity (Yang et al., 2016). With the continuous expansion of the research field of photothermal nanomaterials, graphene and its derivatives have also become one of the research objects. The full-spectrum absorption properties of graphene and its derivatives make it very representative in the field of photothermal materials, which are widely used in antibacterial applications. The excellent heat transport characteristics also give graphene more important practical significance. When covid-19 broke out in 2019, in order to better resist the virus, Zhong et al. (2020) prepared a graphene coated mask with both photothermal and hydrophobic properties. Under the Sun, the coating can quickly heat up and kill bacteria. Wang H. et al. (2020) prepared a graphene quaternary ammonium salt platform functionalized by boric acid. The platform can not only use the targeting effect generated by electrostatic adsorption to mediate the antibacterial effect, but also synergistically enhance the antibacterial effect through the high temperature generated by 808 nm NIR laser irradiation. The experiments show that the nano platform can effectively treat biofilm infection and multi drug resistant gram-negative bacterial infection. In addition to the above-described PTT using laser light of the first near infrared window (NIR-I), PTT in the second near infrared window (NIR-II) has also been reported in recent studies. Geng et al. (2022) Selected 1,064 nm (NIR-II) NIR laser with stronger penetration ability than NIR-I as the treatment light source and graphene quantum dots (N-GQDs) doped with graphitized nitrogen as the treatment platform. Under the irradiation of 1,064 nm laser, N-GQDs showed nearly 100% inhibition and biofilm efficiency against multidrug-resistant bacteria. It also showed a function of promoting wound healing in a mouse model after being infected with MRSA.

Most of the graphene-based materials reported at present have relatively sharp edges and high photothermal conversion efficiency. Therefore, in addition to using photothermal effect to kill bacteria, mechanical/physical destruction can also be used to kill bacteria (Xin et al., 2019). The antibacterial mechanism is mainly to destroy the cell membrane and cell wall of bacteria.

To sum up, the antibacterial mechanism of the common photothermal conversion nanomaterials at present mainly includes three viewpoints: first, the generation of ROS (Figure 6F), and the damage mechanism of ROS to bacteria can be summarized into two ways: 1) Destroying the permeability

of plasma membrane, causing some substances to flow out, or affecting the metabolic activities of bacteria (Ma et al., 2021); 2) DNA strand breaks and depolymerizes to produce stable oxidation products (Gao et al., 2017; Wentao et al., 2019); Second, release metal ions to destroy bacterial DNA and proteins (Figure 6G); Third, NPs gather on the surface of bacterial cell membrane and destroy the cell membrane and cell wall (Qi et al., 2020), blocking transmembrane electron transfer. The damage of cell membrane or cell wall will lead to the dysfunction of bacteria or the leakage of cytoplasmic components, and eventually cause the death of bacteria (Xin et al., 2019).

4 Summary and prospect

The toxicity and potential side effects of inorganic nanomaterials limit their application in the treatment of bacterial infection to a certain extent (Pormohammad et al., 2021). At present, modifying the synthesized inorganic nanoparticles or doping with other metal or non-metallic elements is an effective measure to deal with the toxicity of materials. However, in the specific implementation process, it often needs to face the problems of complex reaction process and harsh reaction conditions. The introduction of PTT successfully avoids the above-mentioned problems, and can achieve a more ideal bacteriostatic effect when using less nanomaterial dosage.

In recent years, the development of inorganic nanomaterials has also created more convenience for the use of PTT. More and more metal and non-metal inorganic nanomaterials with different sizes, morphologies and synthesis methods have shown excellent bacteriostatic effects in the process of combined use with PTT. However, some complications such as skin rash, allergic reaction, itching, etc. of these bactericides synthesized at present may still exist (Punjataewakupt et al., 2019). We still need to conduct a large number of clinical experiments to prove the safety of inorganic photothermal nanomaterials in terms of antibacterial.

We hope to turn the existing challenges into opportunities and develop inorganic photothermal nanomaterials that can be used for both antibacterial and wound healing in the near future.

Author contributions

BW and YX designed and wrote the manuscript under LL and WL's supervision. DS, YM, and XS searched articles relating to the subject. YL and JZ helped in final editing. All authors contributed to the article and approved the submitted version.

Acknowledgments

We acknowledge the support of this work by National Natural Science Foundation of China (No. 21871246), Natural Science Foundation project of Jilin province (No. 20200201082JC), the Jilin Province Development and Reform Commission (No. 2021C039-3), and Jilin Province Science and Technology Development Program (20190302001GX).

Conflict of interest

The authors declare that the research was conducted in the absence of any commercial or financial relationships that could be construed as a potential conflict of interest.

Publisher's note

All claims expressed in this article are solely those of the authors and do not necessarily represent those of their affiliated organizations, or those of the publisher, the editors and the reviewers. Any product that may be evaluated in this article, or claim that may be made by its manufacturer, is not guaranteed or endorsed by the publisher.

Supplementary material

The Supplementary Material for this article can be found online at: https://www.frontiersin.org/articles/10.3389/fbioe.2022.1047598/full#supplementary-material

References

Abadi, B., Hosseinalipour, S., Nikzad, S., Pourshaikhali, S., Fathalipour-Rayeni, H., Shafiei, G., et al. (2022). Capping agents for selenium nanoparticles in biomedical applications. *J. Clust. Sci*. doi:10.1007/s10876-022-02341-3

Abbas, M., Ovais, M., Atiq, A., Ansari, T. M., Xing, R., Spruijt, E., et al. (2022). Tailoring supramolecular short peptide nanomaterials for antibacterial applications. *Coord. Chem. Rev.* 460, 214481. doi:10.1016/j.ccr.2022.214481

Behravan, M., Hossein Panahi, A., Naghizadeh, A., Ziaee, M., Mahdavi, R., and Mirzapour, A. (2019). Facile green synthesis of silver nanoparticles using Berberis vulgaris leaf and root aqueous extract and its antibacterial activity. *Int. J. Biol. Macromol.* 124, 148–154. doi:10.1016/j.ijbiomac.2018.11.101

Brown, C. D., Cruz, D. M., Roy, A. K., and Webster, T. J. (2018). Synthesis and characterization of PVP-coated tellurium nanorods and their antibacterial and anticancer properties. *J. Nanopart. Res.* 20, 254. doi:10.1007/s11051-018-4354-8

Chaudhary, A. S. (2016). A review of global initiatives to fight antibiotic resistance and recent antibiotics discovery. *Acta Pharm. Sin. B* 6, 552–556. doi:10.1016/j.apsb.2016.06.004

Chaudhary, S., Umar, A., and Mehta, S. K. (2016). Selenium nanomaterials: An overview of recent developments in synthesis, properties and potential applications. *Prog. Mater. Sci.* 83, 270–329. doi:10.1016/j.pmatsci.2016.07.001

Chen, H., Shao, L., Li, Q., and Wang, J. (2013). Gold nanorods and their plasmonic properties. *Chem. Soc. Rev.* 42, 2679–2724. doi:10.1039/c2cs35367a

Choi, Y., and Lee, S. Y. (2020). Biosynthesis of inorganic nanomaterials using microbial cells and bacteriophages. *Nat. Rev. Chem.* 4, 638–656. doi:10.1038/s41570-020-00221-w

Chung, Y. J., Kim, J., and Park, C. B. (2020). Photonic carbon dots as an emerging nanoagent for biomedical and healthcare applications. *ACS Nano* 14, 6470–6497. doi:10.1021/acsnano.0c02114

Čubová, K., and Čuba, V. (2019). Synthesis of inorganic nanoparticles by ionizing radiation – A review. *Radiat. Phys. Chem.* 158, 153–164. doi:10.1016/j.radphyschem.2019.02.022

Cui, F., Li, T., Wang, D., Yi, S., Li, J., and Li, X. (2022). Recent advances in carbon-based nanomaterials for combating bacterial biofilm-associated infections. *J. Hazard. Mat.* 431, 128597. doi:10.1016/j.jhazmat.2022.128597

Duo, Y., Xie, Z., Wang, L., Mahmood Abbasi, N., Yang, T., Li, Z., et al. (2021). Borophene-based biomedical applications: Status and future challenges. *Coord. Chem. Rev.* 427, 213549. doi:10.1016/j.ccr.2020.213549

Faisal, M., Saquib, Q., Alatar, A. A., Al-Khedhairy, A. A., Hegazy, A. K., and Musarrat, J. (2013). Phytotoxic hazards of NiO-nanoparticles in tomato: A study on mechanism of cell death. *J. Hazard. Mat.* 250, 318–332. doi:10.1016/j.jhazmat.2013.01.063

Fleming, A.F. R. C. S. (1940). On the specific antibacterial properties of penicillin and potassium tellurite. *J. Pathology* 576, 33.

Fu, P. P., Xia, Q., Hwang, H. M., Ray, P. C., and Yu, H. (2014). Mechanisms of nanotoxicity: Generation of reactive oxygen species. *J. Food Drug Anal.* 22, 64–75. doi:10.1016/j.jfda.2014.01.005

Gao, F., Sun, M., Ma, W., Wu, X., Liu, L., Kuang, H., et al. (2017). A singlet oxygen generating agent by chirality-dependent plasmonic shell-satellite nanoassembly. *Adv. Mat.* 29, 1606864. doi:10.1002/adma.201606864

Gardea-Torresdey, J. L., Gomez, E., Peralta-Videa, J. R., Parsons, J. G., Troiani, H., and Jose-Yacaman, M. (2003). Alfalfa sprouts: A natural source for the synthesis of silver nanoparticles. *Langmuir* 4, 1357–1361. doi:10.1021/la020835i

Geng, B., Li, Y., Hu, J., Chen, Y., Huang, J., Shen, L., et al. (2022). Graphitic-N-doped graphene quantum dots for photothermal eradication of multidrug-resistant bacteria in the second near-infrared window. *J. Mat. Chem. B* 10, 3357–3365. doi:10.1039/d2tb00192f

Geng, B., Shen, W., Fang, F., Qin, H., Li, P., Wang, X., et al. (2020). Enriched graphitic N dopants of carbon dots as F cores mediate photothermal conversion in the NIR-II window with high efficiency. *Carbon* 162, 220–233. doi:10.1016/j.carbon.2020.02.053

Ghirardello, M., Ramos-Soriano, J., and Galan, M. C. (2021). Carbon dots as an emergent class of antimicrobial agents. *Nanomater. (Basel)* 11, 1877. doi:10.3390/nano11081877

Gidwani, B., Sahu, V., Shukla, S. S., Pandey, R., Joshi, V., Jain, V. K., et al. (2021). Quantum dots: Prospectives, toxicity, advances and applications. *J. Drug Deliv. Sci. Technol.* 61, 102308. doi:10.1016/j.jddst.2020.102308

GüVEN, O. (2021). Radiation-assisted synthesis of polymer-based nanomaterials. *Appl. Sci.* 11, 7913–7930. doi:10.3390/app11177913

Hamblin, M. R. (2016). Antimicrobial photodynamic inactivation: A bright new technique to kill resistant microbes. *Curr. Opin. Microbiol.* 33, 67–73. doi:10.1016/j.mib.2016.06.008

Han, L., Zhan, W., Liang, X., Zhang, W., Huang, R., Chen, R., et al. (2022). *In-situ* generation Cu2O/CuO core-shell heterostructure based on copper oxide nanowires with enhanced visible-light photocatalytic antibacterial activity. *Ceram. Int.* 48, 22059–22071. doi:10.1016/j.ceramint.2022.04.192

Hochvaldová, L., Večeřová, R., KoláŘ, M., Prucek, R., KvíTEK, L., LapčíK, L., et al. (2022). Antibacterial nanomaterials: Upcoming hope to overcome antibiotic resistance crisis. *Nanotechnol. Rev.* 11, 1115–1142. doi:10.1515/ntrev-2022-0059

Huang, L., Liu, M., Feng, Z., Xu, X., Chen, L., Ma, Z., et al. (2022). Biocompatible tellurium nanoneedles with long-term stable antibacterial activity for accelerated wound healing. *Mat. Today Bio* 15, 100271. doi:10.1016/j.mtbio.2022.100271

Huang, W., He, L., Ouyang, J., Chen, Q., Liu, C., Tao, W., et al. (2020). Triangle-shaped tellurium nanostars potentiate radiotherapy by boosting checkpoint blockade immunotherapy. *Matter* 3, 1725–1753. doi:10.1016/j.matt.2020.08.027

Inaba, T., Takenaka, Y., Kawabata, Y., and Kato, T. (2019). Effect of the crystallization process of surfactant bilayer lamellar structures on the elongation of high-aspect-ratio gold nanorods. *J. Phys. Chem. B* 123, 4776–4783. doi:10.1021/acs.jpcb.8b10897

Jakubczak, M., Szuplewska, A., Rozmysłowska-Wojciechowska, A., Rosenkranz, A., and Jastrzębska, A. M. (2021). Novel 2D MBenes—synthesis, structure, and biotechnological potential. *Adv. Funct. Mat.* 31, 2103048. doi:10.1002/adfm.202103048

Jamkhande, P. G., Ghule, N. W., Bamer, A. H., and Kalaskar, M. G. (2019). Metal nanoparticles synthesis: An overview on methods of preparation, advantages and disadvantages, and applications. *J. Drug Deliv. Sci. Technol.* 53, 101174–101225. doi:10.1016/j.jddst.2019.101174

Jana, N. R. (2005). Gram-scale synthesis of soluble, near-monodisperse gold nanorods and other anisotropic nanoparticles. *Small* 1, 875–882. doi:10.1002/smll.200500014

John, M. S., Nagoth, J. A., Ramasamy, K. P., Mancini, A., Giuli, G., Natalello, A., et al. (2020). Synthesis of bioactive silver nanoparticles by a Pseudomonas strain associated with the antarctic psychrophilic protozoon euplotes focardii. *Mar. Drugs* 18, 38. doi:10.3390/md18010038

Jung, J. H., Lee, S. Y., and Seo, T. S. (2018). *In vivo* synthesis of nanocomposites using the recombinant *Escherichia coli*. *Small* 14, e1803133. doi:10.1002/smll.201803133

Kitching, M., Inguva, S., Ramani, M., Gao, Y., Marsili, E., and Cahill, P. (2022). Biosynthesis of gold nanoparticles by vascular cells *in vitro*. *Front. Microbiol.* 13, 813511. doi:10.3389/fmicb.2022.813511

Lee, K. X., Shameli, K., Yew, Y. P., Teow, S. Y., Jahangirian, H., Rafiee-Moghaddam, R., et al. (2020). <p>Recent developments in the facile bio-synthesis of gold nanoparticles (AuNPs) and their biomedical applications<. *Int. J. Nanomedicine* 15, 275–300. doi:10.2147/IJN.S233789

Leng, C., Zhang, X., Xu, F., Yuan, Y., Pei, H., Sun, Z., et al. (2018). Engineering gold nanorod-copper sulfide heterostructures with enhanced photothermal conversion efficiency and photostability. *Small* 14, e1703077. doi:10.1002/smll.201703077

Li, B., Tan, L., Liu, X., Li, Z., Cui, Z., Liang, Y., et al. (2019). Superimposed surface plasma resonance effect enhanced the near-infrared photocatalytic activity of Au@Bi2WO6 coating for rapid bacterial killing. *J. Hazard. Mat.* 380, 120818. doi:10.1016/j.jhazmat.2019.120818

Li, P., Feng, Y., Cheng, D., and Wei, J. (2022). Self-template synthesis of mesoporous vanadium oxide nanospheres with intrinsic peroxidase-like activity and high antibacterial performance. *J. Colloid Interface Sci.* 625, 435–445. doi:10.1016/j.jcis.2022.06.049

Li, Z., Peng, L., Fang, Y., Chen, Z., Pan, D., and Wu, M. (2011). Synthesis of colloidal SnSe quantum dots by electron beam irradiation. *Radiat. Phys. Chem.* 80, 1333–1336. doi:10.1016/j.radphyschem.2011.04.017

Lin, Z. H., Lee, C. H., Chang, H. Y., and Chang, H. T. (2012). Antibacterial activities of tellurium nanomaterials. *Chem. Asian J.* 7, 930–934. doi:10.1002/asia.201101006

Lin, Z., Weng, X., Owens, G., and Chen, Z. (2020). Simultaneous removal of Pb(II) and rifampicin from wastewater by iron nanoparticles synthesized by a tea extract. *J. Clean. Prod.* 242, 118476. doi:10.1016/j.jclepro.2019.118476

Liu, C., Zhang, M., Geng, H., Zhang, P., Zheng, Z., Zhou, Y., et al. (2021). NIR enhanced peroxidase-like activity of Au@CeO2 hybrid nanozyme by plasmon-induced hot electrons and photothermal effect for bacteria killing. *Appl. Catal. B Environ.* 295, 120317. doi:10.1016/j.apcatb.2021.120317

Liu, H., Mo, L., Chen, H., Chen, C., Wu, J., Tang, Z., et al. (2022). Carbon dots with intrinsic bioactivities for photothermal optical coherence tomography, tumor-specific therapy and postoperative wound management. *Adv. Healthc. Mat.* 11, e2101448. doi:10.1002/adhm.202101448

Liu, Y., Li, F., Guo, Z., Xiao, Y., Zhang, Y., Sun, X., et al. (2020). Silver nanoparticle-embedded hydrogel as a photothermal platform for combating bacterial infections. *Chem. Eng. J.* 382, 122990–123030. doi:10.1016/j.cej.2019.122990

Loza, K., Heggen, M., and Epple, M. (2020). Synthesis, structure, properties, and applications of bimetallic nanoparticles of noble metals. *Adv. Funct. Mat.* 30, 1909260–1909274. doi:10.1002/adfm.201909260

Lv, J., Qi, Y., Tian, Y., Wang, G., Shi, L., Ning, G., et al. (2022). Functionalized boron nanosheets with near-infrared-triggered photothermal and nitric oxide release activities for efficient antibacterial treatment and wound healing promotion. *Biomater. Sci.* 10, 3747–3756. doi:10.1039/d2bm00519k

Ma, H., Yang, S., Li, M., Tang, X., Xia, Z., and Dai, R. (2021). Preparation and photocatalytic antibacterial mechanism of porous metastable β-Bi2O3 nanosheets. *Ceram. Int.* 47, 34092–34105. doi:10.1016/j.ceramint.2021.08.319

Ma, K., Li, Y., Wang, Z., Chen, Y., Zhang, X., Chen, C., et al. (2019). Core-shell gold Nanorod@Layered double hydroxide nanomaterial with highly efficient photothermal conversion and its application in antibacterial and tumor therapy. *ACS Appl. Mat. Interfaces* 11, 29630–29640. doi:10.1021/acsami.9b10373

Matusiak, M., Kadlubowski, S., and Rosiak, J. M. (2020). Nanogels synthesized by radiation-induced intramolecular crosslinking of water-soluble polymers. *Radiat. Phys. Chem.* 169, 108099. doi:10.1016/j.radphyschem.2018.12.019

Medina Cruz, D., Tien-Street, W., Zhang, B., Huang, X., Vernet Crua, A., Nieto-Arguello, A., et al. (2019). Citric juice-mediated synthesis of tellurium nanoparticles with antimicrobial and anticancer properties. *Green Chem.* 21, 1982–1998. doi:10.1039/c9gc00131j

Mei, Z., Gao, D., Hu, D., Zhou, H., Ma, T., Huang, L., et al. (2020). Activatable NIR-II photoacoustic imaging and photochemical synergistic therapy of MRSA infections using miniature Au/Ag nanorods. *Biomaterials* 251, 120092. doi:10.1016/j.biomaterials.2020.120092

Mintz, K. J., Zhou, Y., and Leblanc, R. M. (2019). Recent development of carbon quantum dots regarding their optical properties, photoluminescence mechanism, and core structure. *Nanoscale* 11, 4634–4652. doi:10.1039/c8nr10059d

Mutalik, C., Krisnawati, D. I., Patil, S. B., Khafid, M., Atmojo, D. S., Santoso, P., et al. (2021). Phase-Dependent MoS2 nanoflowers for light-driven antibacterial application. *ACS Sustain. Chem. Eng.* 9, 7904–7912. doi:10.1021/acssuschemeng.1c01868

Mutalik, C., Okoro, G., Krisnawati, D. I., Jazidie, A., Rahmawati, E. Q., Rahayu, D., et al. (2022). Copper sulfide with morphology-dependent photodynamic and photothermal antibacterial activities. *J. Colloid Interface Sci.* 607, 1825–1835. doi:10.1016/j.jcis.2021.10.019

Nekoueian, K., Amiri, M., Sillanpaa, M., Marken, F., Boukherroub, R., and Szunerits, S. (2019). Carbon-based quantum particles: An electroanalytical and biomedical perspective. *Chem. Soc. Rev.* 48, 4281–4316. doi:10.1039/c8cs00445e

O'Neill, J. (2016). Jim O'Neill. *Nat. Rev. Drug Discov.* 15, 526. doi:10.1038/nrd.2016.160

Pormohammad, A., Monych, N. K., Ghosh, S., Turner, D. L., and Turner, R. J. (2021). Nanomaterials in wound healing and infection control. *Antibiot. (Basel)* 10, 473. doi:10.3390/antibiotics10050473

Pranantyo, D., Liu, P., Zhong, W., Kang, E. T., and Chan-Park, M. B. (2019). Antimicrobial peptide-reduced gold nanoclusters with charge-reversal moieties for bacterial targeting and imaging. *Biomacromolecules* 20, 2922–2933. doi:10.1021/acs.biomac.9b00392

Punjataewakupt, A., Napavichayanun, S., and Aramwit, P. (2019). The downside of antimicrobial agents for wound healing. *Eur. J. Clin. Microbiol. Infect. Dis.* 38, 39–54. doi:10.1007/s10096-018-3393-5

Qi, K., Xing, X., Zada, A., Li, M., Wang, Q., Liu, S.-Y., et al. (2020). Transition metal doped ZnO nanoparticles with enhanced photocatalytic and antibacterial performances: Experimental and DFT studies. *Ceram. Int.* 46, 1494–1502. doi:10.1016/j.ceramint.2019.09.116

Qie, X., Zan, M., Gui, P., Chen, H., Wang, J., Lin, K., et al. (2022). Design, synthesis, and application of carbon dots with synergistic antibacterial activity. *Front. Bioeng. Biotechnol.* 10, 894100. doi:10.3389/fbioe.2022.894100

Rambabu, K., Bharath, G., Banat, F., and Show, P. L. (2021). Green synthesis of zinc oxide nanoparticles using Phoenix dactylifera waste as bioreductant for effective dye degradation and antibacterial performance in wastewater treatment. *J. Hazard. Mat.* 402, 123560. doi:10.1016/j.jhazmat.2020.123560

Ran, B., Ran, L., Hou, J., and Peng, X. (2022). Incorporating boron into niobic acid nanosheets enables generation of multiple reactive oxygen species for superior antibacterial action. *Small* 18, e2107333. doi:10.1002/smll.202107333

Robby, A. I., Kim, S. G., Lee, U. H., In, I., Lee, G., and Park, S. Y. (2021). Wireless electrochemical and luminescent detection of bacteria based on surface-coated CsWO3-immobilized fluorescent carbon dots with photothermal ablation of bacteria. *Chem. Eng. J.* 403, 126351–126396. doi:10.1016/j.cej.2020.126351

Rolim, W. R., Pelegrino, M. T., De AraújO Lima, B., Ferraz, L. S., Costa, F. N., Bernardes, J. S., et al. (2019). Green tea extract mediated biogenic synthesis of silver nanoparticles: Characterization, cytotoxicity evaluation and antibacterial activity. *Appl. Surf. Sci.* 463, 66–74. doi:10.1016/j.apsusc.2018.08.203

Rosales-Conrado, N., GóMEZ-GóMEZ, B., MatíAS-Soler, J., PéREZ-Corona, M. T., and Madrid-AlbarráN, Y. (2021). Comparative study of tea varieties for green synthesis of tellurium-based nanoparticles. *Microchem. J.* 169, 106511. doi:10.1016/j.microc.2021.106511

Sabatino, M. A., Ditta, L. A., Conigliaro, A., and Dispenza, C. (2020). A multifuctional nanoplatform for drug targeted delivery based on radiation-engineered nanogels. *Radiat. Phys. Chem.* 169, 108059–108075. doi:10.1016/j.radphyschem.2018.11.013

Saif, M. J., Naveed, M., Asif, H. M., and Akhtar, R. (2018). Irradiation applications for polymer nano-composites: A state-of-the-art review. *J. Industrial Eng. Chem.* 60, 218–236. doi:10.1016/j.jiec.2017.11.009

Salem, S. S., and Fouda, A. (2021). Green synthesis of metallic nanoparticles and their prospective biotechnological applications: An overview. *Biol. Trace Elem. Res.* 199, 344–370. doi:10.1007/s12011-020-02138-3

Saravanan, A., Kumar, P. S., Karishma, S., Vo, D. N., Jeevanantham, S., Yaashikaa, P. R., et al. (2021). A review on biosynthesis of metal nanoparticles and its environmental applications. *Chemosphere* 264, 128580. doi:10.1016/j.chemosphere.2020.128580

Sethulekshmi, A. S., Saritha, A., Joseph, K., Aprem, A. S., and Sisupal, S. B. (2022). MoS2 based nanomaterials: Advanced antibacterial agents for future. *J. Control. Release* 348, 158–185. doi:10.1016/j.jconrel.2022.05.047

Shi, Y., Lyu, Z., Zhao, M., Chen, R., Nguyen, Q. N., and Xia, Y. (2021). Noble-metal nanocrystals with controlled shapes for catalytic and electrocatalytic applications. *Chem. Rev.* 121, 649–735. doi:10.1021/acs.chemrev.0c00454

Song, S., Gao, P., Sun, L., Kang, D., Kongsted, J., Poongavanam, V., et al. (2021). Recent developments in the medicinal chemistry of single boron atom-containing compounds. *Acta Pharm. Sin. B* 11, 3035–3059. doi:10.1016/j.apsb.2021.01.010

Tamboli, D. P., and Lee, D. S. (2013). Mechanistic antimicrobial approach of extracellularly synthesized silver nanoparticles against gram positive and gram negative bacteria. *J. Hazard. Mat.* 260, 878–884. doi:10.1016/j.jhazmat.2013.06.003

Thanh, N. T., Maclean, N., and Mahiddine, S. (2014). Mechanisms of nucleation and growth of nanoparticles in solution. *Chem. Rev.* 114, 7610–7630. doi:10.1021/cr400544s

Vahidi, H., Kobarfard, F., Alizadeh, A., Saravanan, M., and Barabadi, H. (2021). Green nanotechnology-based tellurium nanoparticles: Exploration of their antioxidant, antibacterial, antifungal and cytotoxic potentials against cancerous and normal cells compared to potassium tellurite. *Inorg. Chem. Commun.* 124, 108385. doi:10.1016/j.inoche.2020.108385

Vankayala, R., and Hwang, K. C. (2018). Near-infrared-light-activatable nanomaterial-mediated phototheranostic nanomedicines: An emerging paradigm for cancer treatment. *Adv. Mat.* 30, e1706320. doi:10.1002/adma.201706320

Verma, A., Arshad, F., Ahmad, K., Goswami, U., Samanta, S. K., Sahoo, A. K., et al. (2020). Role of surface charge in enhancing antibacterial activity of fluorescent carbon dots. *Nanotechnology* 31, 095101. doi:10.1088/1361-6528/ab55b8

Wang, B., Song, H., Qu, X., Chang, J., Yang, B., and Lu, S. (2021). Carbon dots as a new class of nanomedicines: Opportunities and challenges. *Coord. Chem. Rev.* 442, 214010–214028. doi:10.1016/j.ccr.2021.214010

Wang, C., Li, J., Liu, X., Cui, Z., Chen, D. F., Li, Z., et al. (2020). The rapid photoresponsive bacteria-killing of Cu-doped MoS2. *Biomater. Sci.* 8, 4216–4224. doi:10.1039/d0bm00872a

Wang, D., Xia, X., Wu, S., Zheng, S., and Wang, G. (2019). The essentialness of glutathione reductase GorA for biosynthesis of Se(0)-nanoparticles and GSH for CdSe quantum dot formation in Pseudomonas stutzeri TS44. *J. Hazard. Mat.* 366, 301–310. doi:10.1016/j.jhazmat.2018.11.092

Wang, H., Zhao, B., Dong, W., Zhong, Y., Zhang, X., Gong, Y., et al. (2020). A dual-targeted platform based on graphene for synergistic chemo-photothermal therapy against multidrug-resistant Gram-negative bacteria and their biofilms. *Chem. Eng. J.* 393, 124595–124614. doi:10.1016/j.cej.2020.124595

Wang, L., Xu, X., Cheng, Q., Dou, S. X., and Du, Y. (2021). Near-infrared-driven photocatalysts: Design, construction, and applications. *Small* 17, 1904107. doi:10.1002/smll.201904107

Wang, W., Zhang, B., and He, Z. (2019). Bioelectrochemical deposition of palladium nanoparticles as catalysts by Shewanella oneidensis MR-1 towards enhanced hydrogen production in microbial electrolysis cells. *Electrochimica Acta* 318, 794–800. doi:10.1016/j.electacta.2019.06.038

Wang, X., Su, K., Tan, L., Liu, X., Cui, Z., Jing, D., et al. (2019). Rapid and highly effective non-invasive disinfection by hybrid Ag/CS@MnO2 nanosheets using near-infrared light. *ACS Appl. Mat. Interfaces* 11, 15014–15027. doi:10.1021/acsami.8b22136

Wang, Y., Wang, X., Li, L., Wu, Y., and Yu, Q. (2022). An experimental and theoretical study on the photocatalytic antibacterial activity of boron-doped TiO2 nanoparticles. *Ceram. Int.* 48, 604–614. doi:10.1016/j.ceramint.2021.09.139

Wentao, W., Tao, Z., Bulei, S., Tongchang, Z., Qicheng, Z., Fan, W., et al. (2019). Functionalization of polyvinyl alcohol composite film wrapped in a-ZnO@CuO@Au nanoparticles for antibacterial application and wound healing. *Appl. Mater. Today* 17, 36–44. doi:10.1016/j.apmt.2019.07.001

Wong, M.-S., Sun, M.-T., Sun, D.-S., and Chang, H.-H. (2020). Visible-light-responsive antibacterial property of boron-doped titania films. *Catalysts* 10, 1349. doi:10.3390/catal10111349

Wu, S., Liu, X., Li, Z., Lu, Z., Jiang, N., Yang, H., et al. (2022). Te-Cefotaxime nanocomposites with restored antibiotic susceptibility and the LED light activated photothermal effect for rapid MRSA eradication. *J. Mat. Chem. B* 10, 1571–1581. doi:10.1039/d1tb02538d

Xia, C., Zhu, S., Feng, T., Yang, M., and Yang, B. (2019). Evolution and synthesis of carbon dots: From carbon dots to carbonized polymer dots. *Adv. Sci. (Weinh).* 6, 1901316. doi:10.1002/advs.201901316

Xia, Y., Gilroy, K. D., Peng, H.-C., and Xia, X. (2016). Seed-mediated growth of colloidal metal nanocrystals. *Angew. Chem. Int. Ed.* 55, 60–95. doi:10.1002/anie.201604731

Xie, Z., Meng, X., Li, X., Liang, W., Huang, W., Chen, K., et al. (2020). Two-dimensional borophene: Properties, fabrication, and promising applications. *Research* 2020, 1–23. doi:10.34133/2020/2624617

Xin, Q., Liu, Q., Geng, L., Fang, Q., and Gong, J. R. (2017). Chiral nanoparticle as a new efficient antimicrobial nanoagent. *Adv. Healthc. Mat.* 6, 1601011. doi:10.1002/adhm.201601011

Xin, Q., Shah, H., Nawaz, A., Xie, W., Akram, M. Z., Batool, A., et al. (2019). Antibacterial carbon-based nanomaterials. *Adv. Mat.* 31, e1804838. doi:10.1002/adma.201804838

Xiong, G., Jia, J., Zhao, L., Liu, X., Zhang, X., Liu, H., et al. (2021). Non-thermal radiation heating synthesis of nanomaterials. *Sci. Bull.* 66, 386–406. doi:10.1016/j.scib.2020.08.037

Yang, D.-S., Jung, D.-J., and Choi, S.-H. (2010). One-step functionalization of multi-walled carbon nanotubes by radiation-induced graft polymerization and their application as enzyme-free biosensors. *Radiat. Phys. Chem.* 79, 434–440. doi:10.1016/j.radphyschem.2009.11.006

Yang, J., Qi, G.-Q., Liu, Y., Bao, R.-Y., Liu, Z.-Y., Yang, W., et al. (2016). Hybrid graphene aerogels/phase change material composites: Thermal conductivity, shape-stabilization and light-to-thermal energy storage. *Carbon* 100, 693–702. doi:10.1016/j.carbon.2016.01.063

Yang, T.-H., Shi, Y., Janssen, A., and Xia, Y. (2019). Surface capping agents and their roles in shape-controlled synthesis of colloidal metal nanocrystals. *Angew. Chem. Int. Ed.* 1, 15378–15401. doi:10.1002/anie.201911135

Ye, X., Gao, Y., Chen, J., Reifsnyder, D. C., Zheng, C., and Murray, C. B. (2013). Seeded growth of monodisperse gold nanorods using bromide-free surfactant mixtures. *Nano Lett.* 13, 2163–2171. doi:10.1021/nl400653s

Yougbare, S., Chou, H. L., Yang, C. H., Krisnawati, D. I., Jazidie, A., Nuh, M., et al. (2021a). Facet-dependent gold nanocrystals for effective photothermal killing of bacteria. *J. Hazard. Mat.* 407, 124617. doi:10.1016/j.jhazmat.2020.124617

Yougbare, S., Mutalik, C., Okoro, G., Lin, I. H., Krisnawati, D. I., Jazidie, A., et al. (2021b). Emerging trends in nanomaterials for antibacterial applications. *Int. J. Nanomedicine* 16, 5831–5867. doi:10.2147/IJN.S328767

Zambonino, M. C., Quizhpe, E. M., Jaramillo, F. E., Rahman, A., Santiago Vispo, N., Jeffryes, C., et al. (2021). Green synthesis of selenium and tellurium nanoparticles: Current trends, biological properties and biomedical applications. *Int. J. Mol. Sci.* 22, 989. doi:10.3390/ijms22030989

Zhang, X., Zhang, G., Chai, M., Yao, X., Chen, W., and Chu, P. K. (2021). Synergistic antibacterial activity of physical-chemical multi-mechanism by TiO2 nanorod arrays for safe biofilm eradication on implant. *Bioact. Mat.* 6, 12–25. doi:10.1016/j.bioactmat.2020.07.017

Zhao, P., Feng, Y., Zhou, Y., Tan, C., and Liu, M. (2023). Gold@Halloysite nanotubes-chitin composite hydrogel with antibacterial and hemostatic activity for wound healing. *Bioact. Mat.* 20, 355–367. doi:10.1016/j.bioactmat.2022.05.035

Zheng, J., Cheng, X., Zhang, H., Bai, X., Ai, R., Shao, L., et al. (2021). Gold nanorods: The most versatile plasmonic nanoparticles. *Chem. Rev.* 121, 13342–13453. doi:10.1021/acs.chemrev.1c00422

Zhong, H., Zhu, Z., Lin, J., Cheung, C. F., Lu, V. L., Yan, F., et al. (2020). Reusable and recyclable graphene masks with outstanding superhydrophobic and photothermal performances. *ACS Nano* 14, 6213–6221. doi:10.1021/acsnano.0c02250

Zhu, S., Wang, X., Li, S., Liu, L., and Li, L. (2020). Near-infrared-light-assisted *in situ* reduction of antimicrobial peptide-protected gold nanoclusters for stepwise killing of bacteria and cancer cells. *ACS Appl. Mat. Interfaces* 12, 11063–11071. doi:10.1021/acsami.0c00310

Zonaro, E., Lampis, S., Turner, R. J., Qazi, S. J., and Vallini, G. (2015). Biogenic selenium and tellurium nanoparticles synthesized by environmental microbial isolates efficaciously inhibit bacterial planktonic cultures and biofilms. *Front. Microbiol.* 6, 584. doi:10.3389/fmicb.2015.00584

frontiers | Frontiers in Bioengineering and Biotechnology

TYPE Review
PUBLISHED 31 October 2022
DOI 10.3389/fbioe.2022.1053197

Check for updates

OPEN ACCESS

EDITED BY
Wenliang Li,
Jilin Medical University, China

REVIEWED BY
Hongwei Cheng,
Xiamen University, China
Anjaneyulu Dirisala,
Innovation Centre of NanoMedicine (iCONM), Japan
Bin Wang,
Southwest University, China

*CORRESPONDENCE
Huping Jiao,
jiaohp@jlu.edu.cn
Bai Li,
li_bai@jlu.edu.cn

†These authors have contributed equally to this work

SPECIALTY SECTION
This article was submitted to Biomaterials, a section of the journal Frontiers in Bioengineering and Biotechnology

RECEIVED 25 September 2022
ACCEPTED 18 October 2022
PUBLISHED 31 October 2022

CITATION
Li Y, Fang H, Zhang T, Wang Y, Qi T, Li B and Jiao H (2022), Lipid-mRNA nanoparticles landscape for cancer therapy.
Front. Bioeng. Biotechnol. 10:1053197.
doi: 10.3389/fbioe.2022.1053197

COPYRIGHT
© 2022 Li, Fang, Zhang, Wang, Qi, Li and Jiao. This is an open-access article distributed under the terms of the Creative Commons Attribution License (CC BY). The use, distribution or reproduction in other forums is permitted, provided the original author(s) and the copyright owner(s) are credited and that the original publication in this journal is cited, in accordance with accepted academic practice. No use, distribution or reproduction is permitted which does not comply with these terms.

Lipid-mRNA nanoparticles landscape for cancer therapy

Yin Li[1†], Hengtong Fang[1†], Tao Zhang[1], Yu Wang[1], Tingting Qi[1], Bai Li[2*] and Huping Jiao[1*]

[1]College of Animal Science, Jilin University, Changchun, Jilin, China, [2]Department of Colorectal and Anal Surgery, General Surgery Center, First Hospital of Jilin University, Changchun, Jilin, China

Intracellular delivery of message RNA (mRNA) technique has ushered in a hopeful era with the successive authorization of two mRNA vaccines for the Coronavirus disease-19 (COVID-19) pandemic. A wide range of clinical studies are proceeding and will be initiated in the foreseeable future to treat and prevent cancers. However, efficient and non-toxic delivery of therapeutic mRNAs maintains the key limited step for their widespread applications in human beings. mRNA delivery systems are in urgent demand to resolve this difficulty. Recently lipid nanoparticles (LNPs) vehicles have prospered as powerful mRNA delivery tools, enabling their potential applications in malignant tumors *via* cancer immunotherapy and CRISPR/Cas9-based gene editing technique. This review discusses formulation components of mRNA-LNPs, summarizes the latest findings of mRNA cancer therapy, highlights challenges, and offers directions for more effective nanotherapeutics for cancer patients.

KEYWORDS

mRNA delivery, lipid nanoparticles (LNPs), ionizable lipids, cancer nano-vaccine, cancer immunotherapy, gene editing

Introduction

Messenger RNA (mRNA) is an unstable intermediate in the central dogma conveying genetic information from genes to proteins. As the therapeutic agent, compared with DNA, mRNA is safe and has no potential risk of integrating into the genome. Additionally, the mRNA is not needed to transfer into nucleus, which is relatively easy for transferring and translation. In 1990, it was proved that *in vitro* transcribed (IVT) naked mRNA is translated in mice by direct intramuscular injection (Wolff et al., 1990). However, mRNA is unstable in harsh physiological conditions and is rapidly degraded by endoribonucleases and exoribonucleases of the extracellular and intracellular milieu before translating an encoded therapeutic protein (Dirisala et al., 2019). To overcome these shortcomings, the first thing is to improve the stability of mRNA. The mature mRNA molecules consist of five key elements, 5′ cap structure, 5′ untranslated regions (UTRs), coding regions, 3′ untranslated regions (UTRs) and 3′ poly(A) tail. The sequence of modification and optimization strategies have been built up for the above structural elements to augment translation efficiency and stability and to become immune-silent

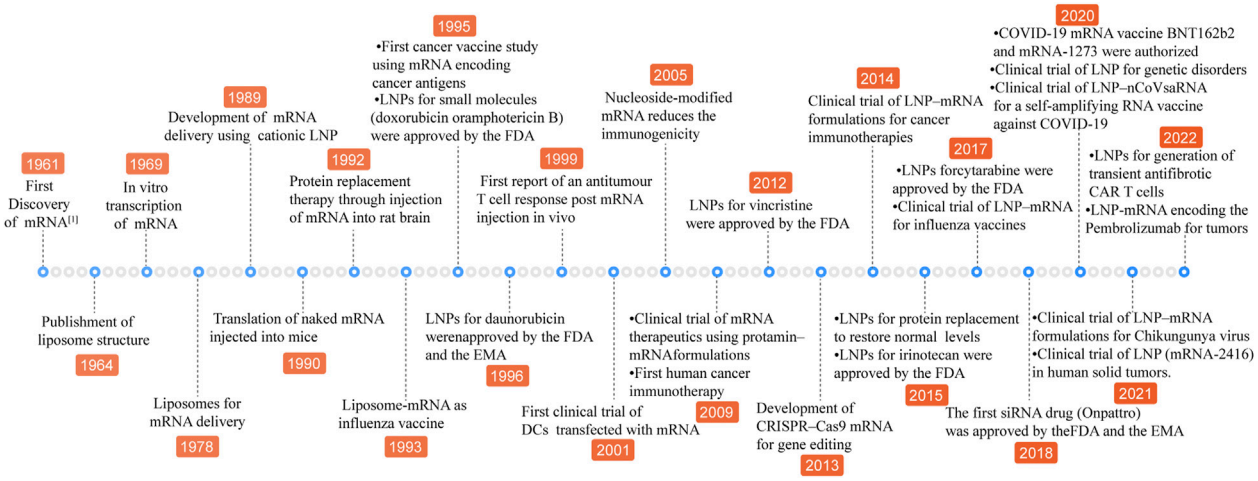

FIGURE 1
Hallmarks of mRNA-lipid nanoparticles. LNP, lipid nanoparticle; COVID-19, coronavirus disease 2019; CRISPR/Cas9, Clustered Regularly Interspaced Short Palindromic Repeats/CRISPR-associated protein 9.

including modification mRNA with cap structure analog, non-nature base substitution and polyA tail synthesis (Kaczmarek et al., 2021). On the other hand, the delivery system remains another limiting factor for the employment of mRNA therapy. Subsequently, non-viral nanoparticles, such as polymer- and lipid-based materials were applied to cancer therapy (Cheng et al., 2018a; Cheng et al., 2018b). However, lipid-based nanoparticles show the advantages of providing protection for mRNA from nuclease degradation, accelerating acidic endosome escape after introduction into the cell and high payloads over polymer (Liu et al., 2021) and advances have been achieved in LNP-mRNA therapy (Figure 1). Lipids, which are the basic fabric of cell membranes, could self-assemble into nanoparticles in polar solvents and are essential for performing their biological functions. LNPs have excellent physical and chemical properties including their shape, size, surface characteristics and interaction with anionic molecules, thus they are widely applied in the medicine and health field as a delivery carrier for active pharmaceutical ingredients (Ndebele et al., 2022). Since LNPs have been used to deliver mRNA, a series of cancer nanomedicine was rapidly developed and entered into clinical trials, which made mRNA molecules possible to become a potent therapeutic system for cancer treatment (Kazemian et al., 2022).

In this Review, we focus on the mRNA modification and the key component of lipid nanoparticles in the process of formulation improvement and optimization. Subsequently, we highlight the progress in cancer therapy fields and describe key steps in tumor treatment. Finally, we discuss the future perspectives toward developing mRNA-LNPs as next-generation therapy vehicles.

mRNA modification

Cap structure analog design

It is believed that mRNA lifespan is controlled by the 5′ cap structure and length of poly (A) tail. The mRNA is capped with the first base covalently linked with N^7-methylated guanosine group *via* a 5′-5′ triphosphate bond (Håkansson Wigley, 1998). *In vivo*, the RNA guanine-7-methyltransferase could cap the mRNA with GTP and Ado-met as the substrate. However, IVT RNA cap is inefficient. Both RNA polymerase and RNA ligase could ligate the cap structure ($m^7G(5')ppp(5')G$) to the IVT mRNA 5′ terminals. Since the cap structure has two 3′ OH, almost half cap structure is reversed cap, that is $Gpppm^7GpN$ cap, which cannot be recognized by translation machinery (Carberry et al., 1990). Hence, the “anti-reverse” cap analogs (ARCAs) were designed to eliminate the possibility of reverse ligation of cap structure, which could get 2.7-fold protein translation efficiency than normal m^7GpppG cap substrate (Figure 2).

mRNA body modification

The mRNA body modification can also enhance translation efficiency and stability. The first found mRNA modification is m^6A which is enriched in 5 termini of mRNA body. Inosine (I) is the intermediate of adenosine and guanosine, which is the nature modification found in the untranslated region. It is believed that inosine is a modulator for mRNA stability and translation efficiency. Pseudouridine also abounds in the mRNA coding region, which could increase levels of ribosome loading onto transcripts (Figure 2).

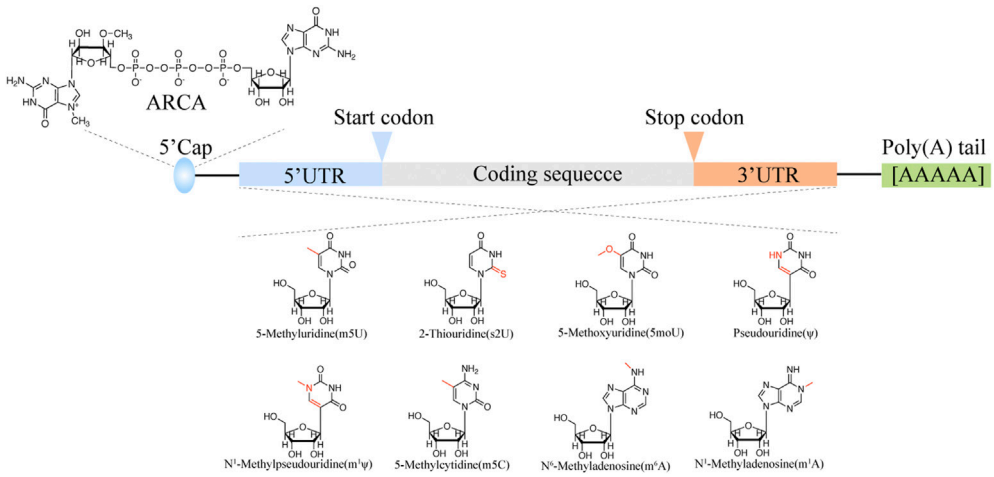

FIGURE 2
The optimization of IVT mRNA stability.

Representative lipid component materials

Over the past several decades, the groundwork for genetic drug delivery platforms was laid. With the approval of two COVID-19 mRNA vaccines (Comirnaty® (Pfizer-BioNTech), and Spikevax®(Moderna)), the preferred nano-delivery system is commonly lipid nanoparticles (LNPs) (Guerin Thompson, 2021). LNP can be prepared with different techniques, such as conventional lipid Thin-Film Hydration subsequent Size-Reduction Techniques, Ethanol-Injection Method, and next-generation In-line T-junction mixing and microfluidic mixing which are all based on a rapid mixing self-assembly process, namely a spontaneous organization of individual lipid molecule into a nanostructured sphere driven by non-covalent interactions (Figure 3) (Shepherd et al., 2021). Microfluidic mixing is a promising new method for preparing large-scale lipid-based cargos. It is well-made and can be expanded from the research laboratory to good manufacturing practice (GMP) production preferred nowadays for use in clinical trials and commercial pharmaceuticals. Another advantage of the microfluidics method is the ability to control various parameters. LNP formulations typically consist of 1) an ionizable or cationic lipid, possessing a positive charged tertiary or quaternary amines head to interact with the mRNA macromolecular; 2) a helper lipid (e.g., DSPC) acting like the phospholipid in the hydrophobic membrane; 3) cholesterol providing stabilization of the LNP bilayer; and 4) an outer PEGylated-surface to give the nanoparticle a hydrophilic surface, lengthen the blood circulation time and reduce nonspecific protein absorption (Kowalski et al., 2019).

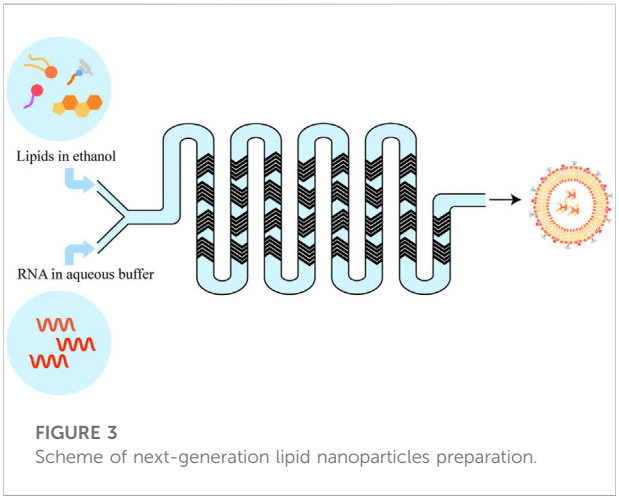

FIGURE 3
Scheme of next-generation lipid nanoparticles preparation.

Cationic and ionizable lipids

Cationic lipids or ionizable lipids consist of three parts: A hydrophilic amine head region, a nonpolar alkyl tail group, and a core linker connecting the two domains (Figures 4, 5), acting as a capable nanomaterial to increase the entrapment efficiency. Cationic lipids bear nonionic ammonium head groups and remain in their pH-independent positive charge, such as DOTMA, DOTAP, DOSPA, and EDOPC. The mRNA-lipoplexes (RNA-LPX) formulated on DOTMA combined with DOPE, can target to deliver the mRNA into dendritic cells (DCs) and macrophages by changing the surface charge ratio from positive to negative through intravenous administration, and induce an antigen-specific adaptive

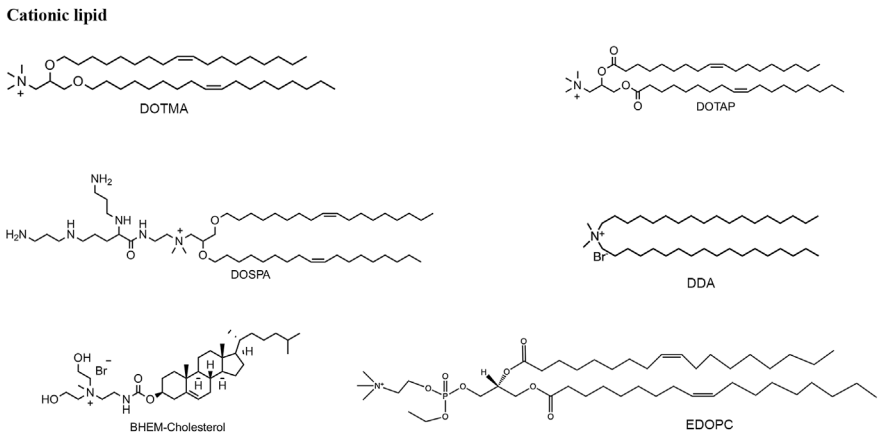

FIGURE 4
Structure of six typical cationic lipids.

immune response and type-I-IFN-associated innate immune response for cancer immunogenic therapy (Kranz et al., 2016). The same lipid formulation for the treatment of autoimmune encephalomyelitis is utilized as a non-inflammatory mRNA vaccine (Krienke et al., 2021 January 8). The hybrid Poly (lactic-co-glycolic acid) (PLGA)-DOTAP core carrying histone deacetylase inhibitors (HDACIs) mRNA to inhibit metastatic lung cancer was also developed (Peng et al., 2021). Metal–lipid hybrid nanoparticle (MLN) containing EDOPC to mediate genome editing transforming growth factor-β (TGF-β) can restructure the tumor microenvironment and prevent tumor recurrence in combination with near-infrared light to heat (Kim et al., 2021). BHEM-Cholesterol was developed by replacing the methyl group with two hydroxyl regions on the basis of DC-Cholesterol in the head group aimed to augment membrane/lipid interaction, combined with poly(ethylene glycol)-block-poly(lactic-co-glycolic acid) (PEG-b-PLG) and PLGA to synthesize a lipid–polymer hybrid particle for mRNA entrapment (Zeng et al., 2020b).

Cationic lipid-based nanoparticles have shown wide application prospects in mRNA therapy, not only for their capability to promote mRNA molecules to stay in LNPs core but also because they can elicit an innate immune response, thus acting as immune adjuvants to improve immunogenicity (Bevers et al., 2022). For example, DDAB is a cationic lipid as an immune adjuvant that stimulates an immune response, activates macrophages, and binds to antigens. The DOTAP-polymeric hybrid nanoparticles exhibited the most powerful results in inducing humoral and cellular immunity among other candidates *in vivo* (Anderluzzi et al., 2020).

However, we are still facing toxicity issues induced by the permanent positive charge of cationic lipid when broadening the applications of lipid-based non-viral vectors to mRNA therapy, hence, the pH-dependent tertiary amine ionizable lipids that could change to positive charges by protonation effect under lower acidic pH and become electrically neutral at physiological pH were developed to overcome this issue by changing structural domains of cationic compounds. Among fifty-six amino lipids, the most effective LNPs were confirmed with a high acid dissociation constant (pKa) between 6.2 and 6.4 which is close to the protonation point of ionizable lipids (CullisHope, 2017). In an acidified endosome, ionizable amino lipids receive hydrogen ions due to higher pKa than PH. The cationic lipids enhance interaction with negatively charged endosome bilayer and promote the endosome membrane unstableness and endosomal escape, which is a major obstacle in LNP technology, following internalization by the target cell and the release of RNA molecules into the cytosol (Farbiak et al., 2021; Dirisala et al., 2022). Hence, ionizable cationic lipids exhibit the advantage of minor toxicity and prolonged existing times in the body in comparison with cationic delivery vehicles after extracellular vaccination.

Ionizable lipids, such as DOGS, multivalent lipid 5 (MVL5), DC-Cholesterol and GL67, initially get development for DNA transfection, later, some have also been investigated for mRNA therapy. Heyes et al. synthesized DODMA by modifying DOTMA and further displaced the oleyl lipid tails with the linoleyl chains to form DLinDMA, and then compared the effect of different saturation degrees on gene silencing ability (Heyes et al., 2005). Taking linoleyl alcohol as raw material, DLin-KC2-DMA was synthesized through five steps reactions with pKa values between 6.2 and 6.7, and has vastly higher activity than DLinDMA (Semple et al., 2010). In order to screen for ionizable lipids, the Factor VII model offers a high-throughput approach for hepatic gene silencing with effective siRNA dose, and further modifications on the linker domain led to the development of DLin-MC3-DMA (MC3). It has been proven to work effectively in low doses and is a key component of Onpattro, the first siRNA drug approved by the United States

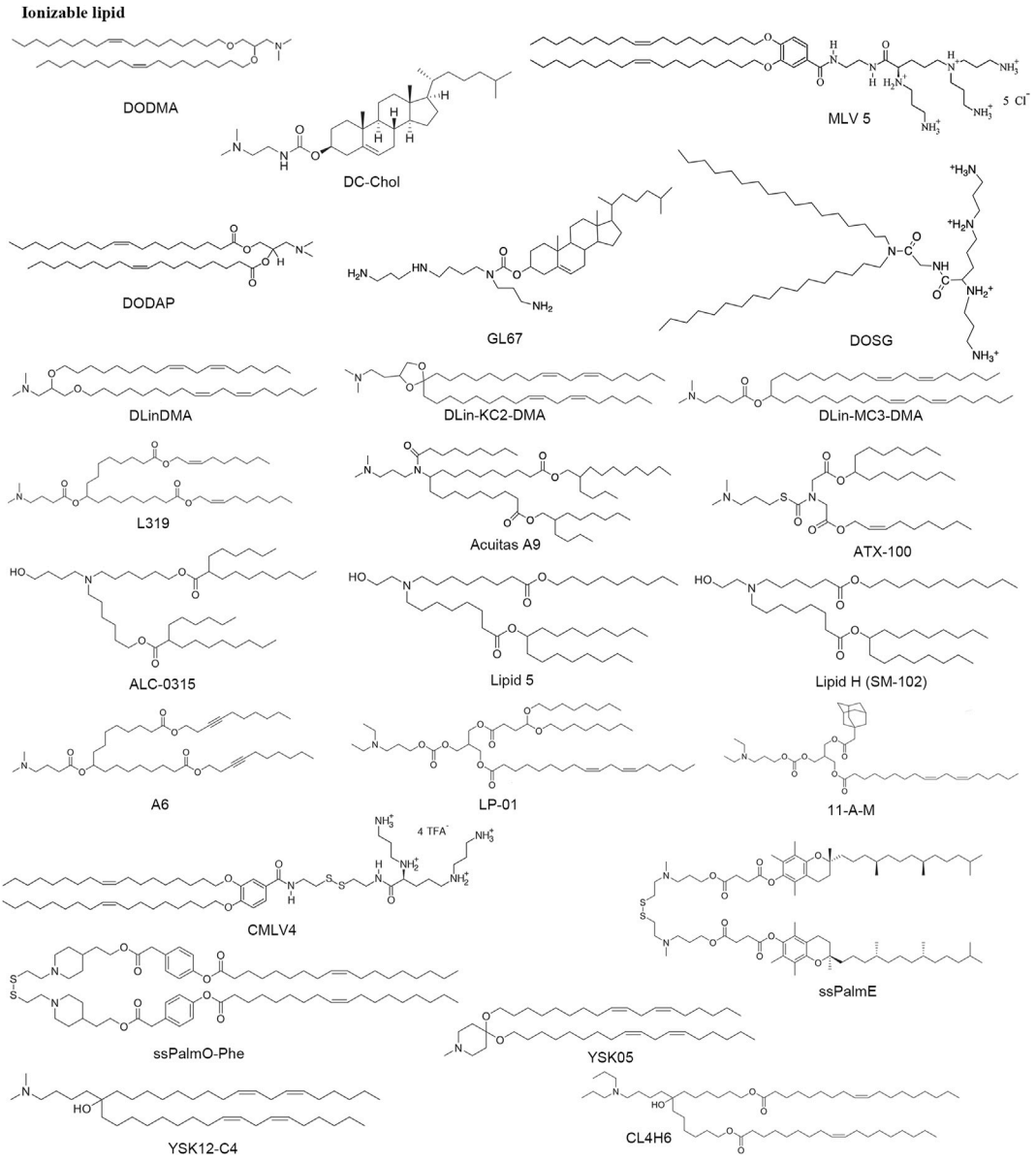

FIGURE 5
Structure of some typical ionizable lipids.,

Food and Drug Administration (FDA) (Akinc et al., 2019). To improve the biocompatibility of LNPs, the researchers focused on lipid biodegradable functionality by introducing ester groups into the hydrocarbon tail, which can be easily degraded to reduce potential toxicity, immunogenicity, and other side effects. By changing the ester bond position, L319 was proven to be the lead biodegradable tertiary amine lipid (Maier et al., 2013). In the same way, the biodegradable lipids ATX-100, Lipid 5, Lipid H (SM-102), ALC-0315, Acuitas A9 and LP-01 have better delivery ability *in vivo* pharmacokinetics (Buschmann et al., 2021). These results demonstrated that the branching alkyl tails may improve RNA molecules' release within the endosome. Additionally, Lipid H nanoparticles revealed a relationship between LNPs size and immunogenicity in mice from various formulations (Hassett et al., 2021). Further, A6 incorporating alkyne groups into the non-polar tails could facilitate their interaction with the endosome membrane, thus enhancing endosomal escape from aqueous inner core (Miao et al., 2020). In Lokugamage et al. (2019) synthesized a library of 16 diverse ionizable lipids using diethylamino head region or 1-pyrrodinyl head group conjugated to carbonate linkers and the 11-A-M LNPs perform the best effects than others. The CMVLn (n = 2–5), a new degradable

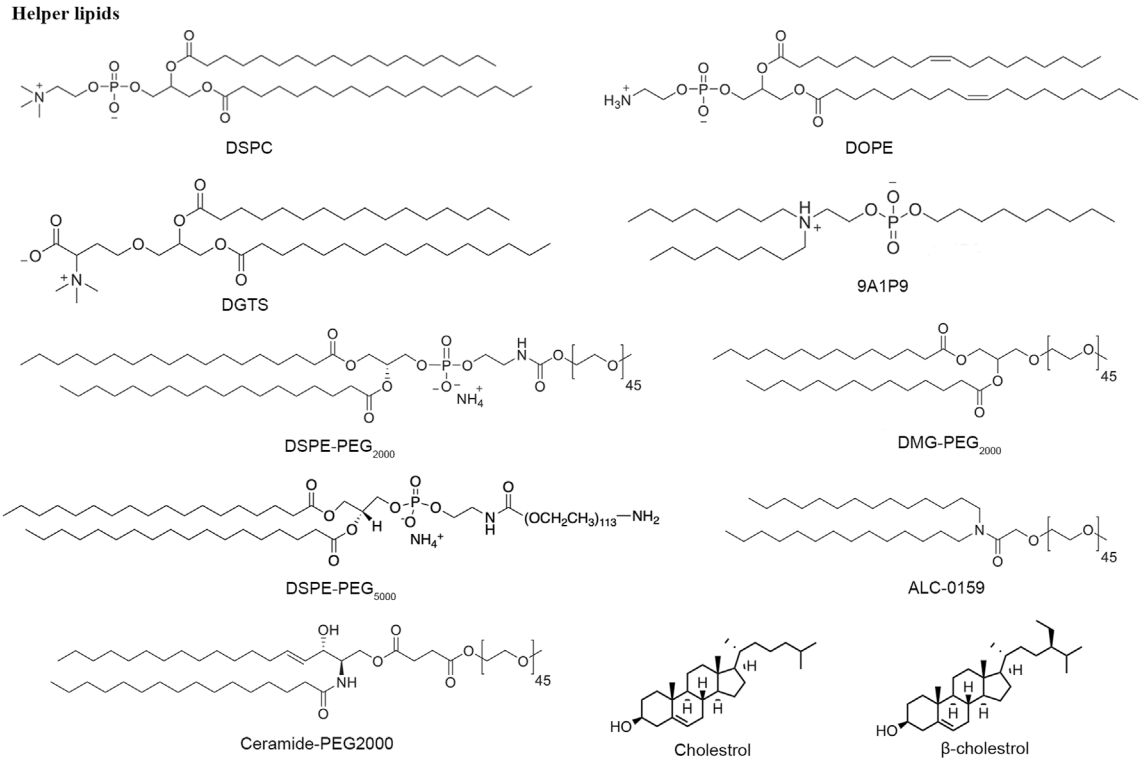

FIGURE 6
Structure of some helper lipids.

multivalent cationic lipids containing a disulfide-bond group between the head group and the hydrophobic tails, and this disulfide bond could be cleaved by reducing agents leading to attenuate toxicity (Shirazi et al., 2011). The ssPalmE, a lipid-like nanomaterial with a disulfide bond and incorporated alpha-tocopherol succinate as the lipid tails, could efficiently suppress tumor growth (Akita et al., 2015). ssPalmO-Phenyl-P4C2, optimized from ssPalmE, using oleic acid as the scaffold of biodegradable lipidoid material showed superior delivery efficiency. Additionally, the introduction of the aromatic ring surprisingly contributes to endosomal membrane destabilization (Tanaka et al., 2020).

The pH-sensitive amino lipid YSK05 displays high fusogenic with the cell membrane (Miyabe et al., 2014). Further optimization of the hydrophilic head region of YSK05 contributed to YSK12, which significantly facilitated gene silencing in mouse DCs (Warashina et al., 2016). The efficient gene silencing ability (50% effective dose: 0.0025 mg/kg) and biodegradability were observed in the third generation YSK series of ionizable lipids CL4H6 (Sato et al., 2019).

In 2014, ionizable truncated acyl backbone amino lipids with asymmetric tails were reported. They were well-tolerated and showed high scavenging capacity *in vivo* addressing a key pharmaceutical challenge through rational formulation optimization (Gindy et al., 2014). Derived from this work, Suzuki et al. (2017) synthesized a string of ionizable lipids with two asymmetric hydrocarbon tails (e.g., L021), and further optimization of ester bond into the lipid tail generated L101, a biodegradable lipid displayed potent gene-silencing activity in mouse hepatocytes and resulted in rapid pharmacokinetics of the lipid.

Combinatorial conjugation and screening approaches have been applied for the synthesis of ionizable lipidoid libraries to improve delivery efficiency. With Design of Experiment methods, several types of reactions have been applied for the synthesis of lipidoids, such as the ring-opening reaction of epoxides, reductive animation reaction and Michael Addition (Zhang et al., 2021; Hu et al., 2022). In 2008, Anderson's laboratory synthesized a large library of more than 1,200 structurally varied lipid-like materials, and the 98N12-5 acting as the top one performed potent specific gene knockdown in three animal models (Akinc et al., 2008). In addition, they developed two-generation libraries, $304O_{13}$ and $503O_{13}$ turned out to be the lead lipids respectively, with high levels of transportation efficiency (Whitehead et al., 2014). O_{i10}, a ten-carbon branched tail, was conjugated to alkyl-amine to synthesize $306O_{i10}$ which can potently ionize at low pH and facilitate more efficient mRNA delivery (Hajj et al., 2019). An ionizable lipid library was synthesized by the addition reaction of amine head and acrylate

tail containing the disulfide bond, among which, 306-O12B indicated the capability of liver targeting through co-delivery of Cas9 mRNA and gRNA for Angptl3 gene editing *in vivo* (Qiu et al., 2021). BAMEA-O16B, a biodegradable lipid integrated with disulfide bonds, can simultaneously deliver Cas9 mRNA and sgRNA into cells for gene editing (Liu et al., 2019). A library of over 1,500 bio-reducible lipidoids was constructed *via* addition between diverse amine groups and acrylate esters reacted with alkyl thiols. 5A2-SC8, the lead-performing lipid of the library, provided a potent therapeutic material for gene therapy system (Zhou et al., 2016). Based on 5A2-SC8, replacing amino scaffold 5A2 with 4A3 results in 4A3-SC8, which was formulated in dendrimer-based lipid nanoparticles and achieved gene editing through CRISPR/Cas9 protein (Farbiak et al., 2021 July). Anderson's group synthesized a lipidoid library *via* another ring-opening approach of epoxides altering carbon lengths with amine substances, such as C12-200 and cKK-E12. A1-D1-5 also called iLY 1809, a thermostable analog of cKK-E12, achieved an effective dose of 0.18 mg/kg of ED_{50} for siRNA (Hu et al., 2022) and enable robust gene editing *via* the delivery of plasmid which expresses both Cas9 protein and sgRNA targeted for Polo-like kinase 1 (PLK1) (Li et al., 2022). Additionally, 7C1 (Lokugamage et al., 2021) and G0-C14 (Islam et al., 2021) were synthesized *via* ring-opening of alkyl epoxide with PEI600 and generation 0 of poly (amidoamine) (PAMAM) respectively.

Amines, isocyanides, and alkyl ketones were used to synthesize a library of 1,080 ionizable lipids. The high-performing lipids, A18-Iso5-2DC18 can induce a strong immune response and show remarkable tumor growth suppression and the survival was prolonged in tumor models through the systematic administration of LNPs (Miao et al., 2019). Lipid-like derivatives (TT2-TT8) were developed *via* Reductive Amination. TT3-LNP can potently provide protection for human factor IX mRNA (Li et al., 2015), and in 2020, it was used to encapsulate the SARS-CoV-2 spike subunits mRNA (Zeng et al., 2020a). FTT5, a biodegradable analog of TT3, further facilitates the release of mRNA encoding human factor VIII into cytoplasm (Zhang et al., 2020). Most recently, Cornebise et al. (2022) reported that squaramides as a part of aromatic four-membered rings, participated in pi-pi interactions, hence, the top-performing lipid 29 can cause high expression of mRNA.

Helper lipids—phospholipid, cholesterol and PEGylating lipids

Extensive research has shown that LNP generally consists of additional lipid nanomaterials besides cationic or ionizable lipids to stabilize the RNA delivery system, such as phospholipids, cholesterol, and polyethylene glycol lipids (Figure 6). Phosphatidylcholines (PCs), characterized by cylindrical geometry structure, is the most abundant phospholipid of cell membrane bilayers, approximately accounting for about 50%. DSPC has two symmetric saturated tails with high melting temperatures and is typically used to formulate highly stable LNPs (Witzigmann et al., 2020). Recently, due to the pandemic of COVID-19, DSPC has been applied for mRNA-1273 and BNT162b2 vaccines (Puranik et al., 2022). DOPE, a phosphoethanolamine with two unsaturated tails groups, replacing DSPC in LNPs formulations achieves potent mRNA delivery efficiency *in vivo* because DOPE is inclined to adopt a hexagonal H(II) conformation transformation, which makes endosome bilayer more unstable and accelerates endosome escape of lipid nanoparticles after uptake (Hou et al., 2021). The 9A1P9 from a library of ionizable phospholipids through combinatorial reaction schemes got 40 and 965 times more efficient than DOPE and DSPC in mRNA delivery, respectively (Liu et al., 2021).

As a key member of the lipid nanoparticle formulation, cholesterol can serve as a helper lipid that can make nanoparticles more stable by filling in gaps between phospholipids and facilitating the fusion of the nanoparticles with the biological membrane (Zhang et al., 2021). The studies reported that the amount of cholesterol in LNP components is larger than what can be stably retained in LNPs. Moreover, it was demonstrated that about 30–40 mol% helper lipid is necessary for the encapsulation of siRNA into LNPs, providing another insight into the part of helper lipids.

The enhanced permeability and retention (EPR) effect influences the preferential accumulation of LNP into solid tumors (Sindhwani et al., 2020; Zheng and LiDing., 2021). However, this effect would depend on relatively longer circulation time and relatively small particle size. Liu et al. (2022) synthesized a new shielding material by conjugating low molecular weight polyethylene glycol (PEG) to a hyaluronic acid (HA) core forming a protective layer through electrostatic interactions. Hence, PEGylating lipids are incorporated into LNP formulations to extend the circulation time within the blood by reducing immune clearance regulated by the kidneys. (Forfull names of lipid compounds, see Supplementary Material).

Potent cancer treatment

International Agency for Research on Cancer (IRAC) reported that there are 19,292,789 new cancer cases and 9,958,133 cancer deaths all over the world with 40 types in 2020 and the top three are breast, lung, and colorectal cancer. Therefore, it is critical to develop the anti-tumor vaccine. More recently, Moderna and Pfizer/BioNTech LNP-mRNA vaccines approved by the FDA to prevent the pandemic of COVID-19, are receiving global attention. The main application associated with the use of LNP for cancer therapy has been broadly studied during the past years, and still, nanoparticles display potent interest because of their relatively small size and large surface-

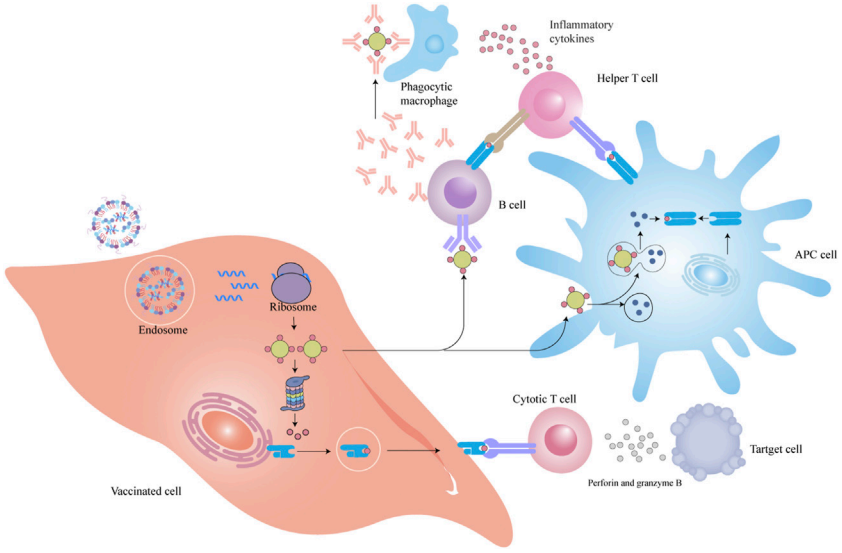

FIGURE 7
LNP-mRNA vaccines immune response process.

to-volume ratio, and they lead to absolutely novel revolution compared to the large vehicles of bulk material. Besides, LNP-mRNA vaccines have several advantages over conventional vaccines: 1) safety, they eliminate concerns associated with intracellular toxicity and infection risk (CullisHope, 2017). In contrast with DNA nucleoside vaccines and viral vehicle-based vaccines, the risk of genomic integration and toxicity is not posed in mRNA vaccines because they act in their activity in the cytoplasm. The transient property of mRNA molecules is beneficial to avoiding an overexpression of the target protein. Additionally, the researchers have developed a procession of favorable degradable biomaterials. 2) flexibility, mRNA vaccines can easily achieve different targets by changing the coding region and furthermore enable the co-delivery of multiple mRNA molecules to the same cell allowing the generation of multi-antigen complexes thus we can simultaneously prevent different pathogens by injecting a single vaccine. 3) Speediness and repeatability, GMP-leveled manufacture of mRNA vaccines enable reproducible and homogeneous production of lipid-mRNA nanoparticles within weeks (Gebre et al., 2021).

Immunotherapy

The majority of mRNA-LNP vaccines can be internalized by the uptake of vaccinated cells through systemic administration and can express into antigen proteins that are presented to T and B cells by MHC molecules to kill diseased cells and facilitate the death of tumor cells (Figure 7).

Cancer vaccines involve the elicitation of tumor-specific T lymphocyte response aiming at removing or rejecting tumor cells without harming normal cells by providing cancer antigens under the action of immune stimulators. The attempt to use mRNA to treat tumors can date back to 1995, which showed to elicit antigen-specific immune responses in mice (Hou et al., 2021). Prior to the broad application of the LNP-mRNA anti-cancer vaccine, one of the key manufacturing limitations is that it is difficult to select a target antigen. Following the discovery of Tumor-associated antigens (TAAs), we can design cancer vaccines to target TAAs that are preferentially translated into malignant cells. The proof-of-concept research of LNPs from 2016 by Kranz et al. reported that the RNA-LPX vaccine can target to DCs *in vivo via* intravenous injection of TAAs-lipoplexes based on DOTMA or DOTAP cationic lipid combined with DOPE (Kranz et al., 2016). The encapsulation of TAAs-mRNA into the lipoplex efficiently kept the TAAs molecules from extracellular ribonucleases and boosted their expression in various lymphoid organs. And the authors demonstrated that not only can the mRNA-lipoplex vaccine elicit a type I IFN-associated innate immune response, but also lead to a potent adaptive response, efficiently down-regulating the growth of tumors. DC-based immunotherapies make up the main part of mRNA cancer vaccines in clinical trials and delivery of mRNA molecules into DCs for adoptive immune was the first-in-human clinical trial based on an mRNA therapeutic cancer vaccine (Kowalski et al., 2019). And currently, lipid nanoparticle–mRNA formulations for cancer are extensively developed as a consequence of the promising

antitumor efficacy shown in CureVac, BioNTech, and Moderna as pioneers in the battle.

To further improve vaccine effects, we can optimize the processes of APC uptake and T cell activation by co-delivery of antigen mRNA cargos with adjuvants and co-stimulatory molecules to obtain a more comprehensive oncology therapeutic effect, for instance, mannose functionalized LNPs vaccines are preferentially taken up by DCs (Van der Jeught et al., 2018). Stimulator of interferon genes (STING) is key receptor proteins in the natural immune response that can co-adjust innate immunity and acquired immunity. After vaccination, STING will evoke type I interferon. The occurrence of cytokines and T lymph cell recruiting factors arouse tumor-specific cytotoxic T cells (CTLs) response, which can accelerate the expression of antigen *in vivo*, as well as evoke the STING signaling pathway, and remarkably promote the tumor-associated antigen immune activation (Li et al., 2022). At the same moment, it is worth noting that T cell initiation may better determine whether an immune response will be elicited rather than antigen expression as the final criteria for assessing the efficiency of an mRNA vaccine. Another mRNA-2752 involves OX40L/IL-23/IL-36 multiple mRNA macromolecules to treat lymphoma (NCT03739931). Within the mRNA-2752 cocktail vaccine, OX40L functions as the activated co-stimulating signal to potentiate T cell effector function and expansion. IL-36 acts as pro-inflammatory cytokines to further augment anticancer effects and elicit a favorable tumor microenvironments (TME) change. IL-23, as a member of the IL-12 family, functions both in innate immunity and adaptive immunity (Hewitt et al., 2019).

With the recent advancement in cancer immunotherapies, the application of immune checkpoint inhibitors, particularly the discovery of neo-antigens and the development of personalized vaccines, a series of improvements have been achieved to reveal the feasibility of mRNA vaccines to conquer cancer. Several immune checkpoint blockades, monoclonal antibodies (mAbs) targeting immune regulatory molecules have been found out in the last few years, such as anti-programmed cell death 1 (PD-1), programmed cell death-ligand 1 (PD-L1) and cytotoxic T-lymphocyte-associated protein 4 inhibitors. FixVac melanoma mRNA vaccine formulated with four non-mutated antigens combined with a checkpoint inhibitor, anti-PD-1 antibody mediates persistent immune responses in patients (Sahin et al., 2020). Wu et al. formulated IVT-mRNA encoding the Pembrolizumab, a commercial anti-PD-1 mAb in LNP *via* optimizing the addition of signal peptide and the molar ratio of heavy/light chain of antibody leading to an excellent tumor growth inhibition (Wu et al., 2022). Tumor-associated macrophages (TAMs) are extremely abundant and play an important part in provoking immunosuppression in liver malignancies. To eliminate this immunosuppression, an antibody that specifically neutralizes CCL2 and CCL5 (BisCCL2/5i), two key chemokines taking the responsibility for TAM infiltration, is developed. And BisCCL2/5i combined with PD-1 ligand inhibitor encapsulating in lipid nanoparticles leads to death inhibition in mouse models of primary or metastasizing liver cancer (Wang et al., 2021).

Cancer neo-antigens originated from non-synonymous somatic mutations in tumor cells represent a promising orientation for cancer immunotherapies and neo-antigen-based cancer vaccines currently exhibit prominent therapeutic capacity in both preclinical and clinical trials (Miao et al., 2021). The mRNA-4157 is a personalized therapeutic vaccine for melanoma from Moderna. An attractive therapeutic candidate approach that combined a novel CpG-B class oligodeoxynucleotide (CpG 2018B) enhanced cytokine generation with neo-antigen mRNA and promoted the antitumor effect *via* intratumoral injection (Li et al., 2021). Other recent work has paid attention to chimeric antigen receptor (CAR)-T-cell cancer immunotherapy. Specifically, synthetic mRNA molecules encoding CAR are internalized into T lymph cells, and then CAR protein scaffolds are expressed in T cells to identify and kill antigen-specific tumor cells (Gao et al., 2021). Ionizable lipids have delivered CAR mRNA to primary human T cells and achieved potent cancer-killing activity (Billingsley et al., 2020). To overwhelm the limitation of inefficient CAR-T cell stimulation *in vivo*, tight junction protein claudin 6 mRNA composed in RNA-LPX was delivered into lymphoid compartments and promoted the expansion of CAR-T cells in solid tumors (Reinhard et al., 2020). Margaret M. et al. synthesized sequential libraries of ionizable lipid harnessing Orthogonal Design of Experiments for mRNA engineering of CAR-T cells and achieved a 3-fold increase for mRNA expression and low cytotoxicity in comparison to a standard formulation (Billingsley et al., 2022).

Gene targeting therapy

mRNA therapeutics utilizing LNPs as a targeting delivery vehicle have provided a toolbox in disease states where gene mutations lead to abnormal and non-functional protein expression. In addition to direct delivery of the mutant mRNA to restore function, gene editing such as CRISPR/Cas9 technique served as the next promising application of mRNA therapeutics has been investigated to inactivate or correct mutated cancer-related genes (QiuLi, 2021). However, delivery of the CRISPR/Cas system to malignant tumors for efficient treatment keeps challenging and faces critical obstacles. Wang's laboratory published the report of hyperbranched poly (β-amino ester) based polyplex nanoparticles involving delivery of CRISPR/Cas9 and sgE7 targeted plasmid and achieved the treatment of HPV infection-associated cervical malignancy (Xiong et al., 2022). Zhang et al. utilized dLNPs for the co-delivery of focal adhesion kinase (FAK) siRNA, Cas9 mRNA and sgRNA-PD-L1 (siFAK + CRISPR-LNPs) to enhance >10-fold gene-editing efficacy in tumor tissues. FAK-knockdown

promoted cellular uptake and tumor EPR and CRISPR-LNPs significantly inhibited PD-L1 expression *via* CRISPR/Cas gene editing systems, which achieved a strong tumor growth inhibition and metastasis in four different mouse models of cancer (Zhang et al., 2022). Peer's laboratory synthesized a novel ionizable amino lipid involving co-delivery of Cas9 mRNA and sgRNAs-PLK1 (sgPLK1-cLNPs) to inhibit tumor growth and prolong survival by 80% (Rosenblum et al., 2020). Recently, TME, which play a critical role in activating immune cells, has gained attention for immunotherapy. TGF-β, a major immunosuppressive cytokine, widely interacts with various immune cells and can induce immune evasion of the TME. Kim et al. successfully used MLN encapsulating sgRNA targeting TGF-β and CRISPR/Cas9 system to restructure the TME and protect against tumor recurrence (Kim et al., 2021). The ability of gene editing to disrupt gene expression in tumors opens a new era for cancer treatment. And more research is desired to explore the next-generation nano-vectors to deliver the CRISPR/Cas9 mRNA genome editing tool to treat cancers for clinical application.

Summary and future prospective

LNP-based mRNA therapies have retained great appeal and a promising rank of drugs for diversified therapeutic applications were developed over the past few years by replacing ideal mRNA cargoes. Importantly, BNT162b2 (Pfizer/BioNTech) raises robust prevention for the COVID-19 pandemic and a new era of mRNA therapeutics has been opened up. Although significant advances have been achieved in recent years, it is worth noting that several obstacles still hamper the broad applications of LNP-mRNA therapies. It is a long road to optimize nonviral vector formulations for nucleic acid delivery, which the development of Patisiran perhaps best exemplified. Meanwhile, LNP-mRNA development has submitted fundamental insights into optimal formulations for delivery efficiency from endosome escape, GMP, safety profiles, stability, and cost-effectiveness to establish next-generation mRNA-LNPs.

At the same moment, the determinants of performance for LNP-mRNA delivery technology are multifactorial and interactive and they bear a versatile toolbox with many possibilities to promote future gene therapies. Future mRNA therapeutic platforms remain to be explored in the following directions: 1) selective organ targeting (SORT) technology needed to be detailed in the LNP corona composition 2) personalized framework 3) reprogramming the tumor microenvironment, to promote $CD4^+$ and $CD8^+$ cells infiltrates in the tumors 4) biodegradablity and biocompatibility, covalently coupling degradable chemical groups to reduce cytotoxicity 5) pharmacokinetics and pharmacodynamics, appropriate duration of pharmacological effects, and 6) adjuvanticity, the relationship between innate immune and inflammation. As these design criteria and modular parameters are rigorously investigated and established with large multidimensional spaces, it is anticipated that a therapeutic revolution that breaks through the current limits will come in the near future.

Author contributions

YL and HF writing the manuscripts. YW and TQ prepare the pictures, BL and HJ amended the whole paper.

Conflict of interest

The authors declare that the research was conducted in the absence of any commercial or financial relationships that could be construed as a potential conflict of interest.

Publisher's note

All claims expressed in this article are solely those of the authors and do not necessarily represent those of their affiliated organizations, or those of the publisher, the editors and the reviewers. Any product that may be evaluated in this article, or claim that may be made by its manufacturer, is not guaranteed or endorsed by the publisher.

Supplementary material

The Supplementary Material for this article can be found online at: https://www.frontiersin.org/articles/10.3389/fbioe.2022.1053197/full#supplementary-material

References

Akinc, A., Maier, M. A., Manoharan, M., Fitzgerald, K., Jayaraman, M., Barros, S., et al. (2019). The Onpattro story and the clinical translation of nanomedicines containing nucleic acid-based drugs. *Nat. Nanotechnol.* 14, 1084–1087. doi:10.1038/s41565-019-0591-y

Akinc, A., Zumbuehl, A., Goldberg, M., Leshchiner, E. S., Busini, V., Hossain, N., et al. (2008). A combinatorial library of lipid-like materials for delivery of RNAi therapeutics. *Nat. Biotechnol.* 26, 561–569. doi:10.1038/nbt1402

Akita, H., Ishiba, R., Togashi, R., Tange, K., Nakai, Y., Hatakeyama, H., et al. (2015). A neutral lipid envelope-type nanoparticle composed of a pH-activated and vitamin E-scaffold lipid-like material as a platform for a gene carrier targeting renal cell carcinoma. *J. Control. Release* 200, 97–105. doi:10.1016/j.jconrel.2014.12.029

Anderluzzi, G., Lou, G., Gallorini, S., Brazzoli, M., Johnson, R., O'hagan, D. T., et al. (2020). Investigating the impact of delivery system design on the efficacy of

self-amplifying RNA vaccines. *Vaccines (Basel)* 8, 212. doi:10.3390/vaccines8020212

Bevers, S., Kooijmans, S. a. A., Van De Velde, E., Evers, M. J. W., Seghers, S., Gitz-Francois, J., et al. (2022). mRNA-LNP vaccines tuned for systemic immunization induce strong antitumor immunity by engaging splenic immune cells. *Mol. Ther.* 30, 3078–3094. doi:10.1016/j.ymthe.2022.07.007

Billingsley, M. M., Hamilton, A. G., Mai, D., Patel, S. K., Swingle, K. L., Sheppard, N. C., et al. (2022). Orthogonal design of Experiments for optimization of lipid nanoparticles for mRNA engineering of CAR T cells. *Nano Lett.* 22, 533–542. doi:10.1021/acs.nanolett.1c02503

Billingsley, M. M., Singh, N., Ravikumar, P., Zhang, R., and JuneMitchell, C. H. M. J. (2020). Ionizable lipid nanoparticle-mediated mRNA delivery for human CAR T cell engineering. *Nano Lett.* 20, 1578–1589. doi:10.1021/acs.nanolett.9b04246

Buschmann, M. D., Carrasco, M. J., Alishetty, S., Paige, M., and AlamehWeissman, M. G. D. (2021). Nanomaterial delivery systems for mRNA vaccines. *Vaccines (Basel)* 9, 65. doi:10.3390/vaccines9010065

Carberry, S. E., Darzynkiewicz, E., Stepinski, J., Tahara, S. M., and RhoadsGoss, R. E. D. J. (1990). A spectroscopic study of the binding of N-7-substituted cap analogs to human protein synthesis initiation factor 4E. *Biochemistry* 29, 3337–3341. doi:10.1021/bi00465a027

Cheng, H., Fan, X., Wang, X., Ye, E., Loh, X. J., Li, Z., et al. (2018a). Hierarchically self-assembled supramolecular host-guest delivery system for drug resistant cancer therapy. *Biomacromolecules* 19, 1926–1938. doi:10.1021/acs.biomac.7b01693

Cheng, H., Wu, Z., Wu, C., Wang, X., Liow, S. S., Li, Z., et al. (2018b). Overcoming STC2 mediated drug resistance through drug and gene co-delivery by PHB-PDMAEMA cationic polyester in liver cancer cells. *Mater. Sci. Eng. C* 83, 210–217. doi:10.1016/j.msec.2017.08.075

Cornebise, M., Narayanan, E., Xia, Y., Acosta, E., Ci, L., Koch, H., et al. (2022). Discovery of a novel amino lipid that improves lipid nanoparticle performance through specific interactions with mRNA. *Adv. Funct. Mat.* 32, 2106727. doi:10.1002/adfm.202106727

CullisHope, P. R. M. J. (2017). Lipid nanoparticle systems for enabling gene therapies. *Mol. Ther.* 25, 1467–1475. doi:10.1016/j.ymthe.2017.03.013

Dirisala, A., Uchida, S., Li, J., Van Guyse, J. F. R., Hayashi, K., Vummaleti, S. V. C., et al. (2022). Effective mRNA protection by poly(l-ornithine) synergizes with endosomal escape functionality of a charge-conversion polymer toward maximizing mRNA introduction efficiency. *Macromol. Rapid Commun.* 43, e2100754. doi:10.1002/marc.202100754

Dirisala, A., Uchida, S., Tockary, T. A., Yoshinaga, N., Li, J., Osawa, S., et al. (2019). Precise tuning of disulphide crosslinking in mRNA polyplex micelles for optimising extracellular and intracellular nuclease tolerability. *J. Drug Target.* 27, 670–680. doi:10.1080/1061186X.2018.1550646

Farbiak, L. C. Q., Wei, T., Álvarez-Benedicto, E., Johnson, L., Lee, S., Siegwart, D., et al. (2021). All-in-one dendrimer-based lipid nanoparticles enable precise HDR-mediated gene editing *in vivo*. *Adv. Mat.* 33 (30), e2006619. doi:10.1002/adma.202006619

Farbiak, L., Cheng, Q., Wei, T., Álvarez-Benedicto, E., Johnson, L. T., Lee, S., et al. (2021). All-in-one dendrimer-based lipid nanoparticles enable precise HDR-mediated gene editing *in vivo*. *Adv. Mat.* 33, e2006619. doi:10.1002/adma.202006619

Gao, M., Zhang, Q., and FengLiu, X. H. J. (2021). Synthetic modified messenger RNA for therapeutic applications. *Acta Biomater.* 131, 1–15. doi:10.1016/j.actbio.2021.06.020

Gebre, M. S., Brito, L. A., Tostanoski, L. H., Edwards, D. K., and CarfiBarouch, A. D. H. (2021). Novel approaches for vaccine development. *Cell* 184, 1589–1603. doi:10.1016/j.cell.2021.02.030

Gindy, M. E., Feuston, B., Glass, A., Arrington, L., Haas, R. M., Schariter, J., et al. (2014). Stabilization of Ostwald ripening in low molecular weight amino lipid nanoparticles for systemic delivery of siRNA therapeutics. *Mol. Pharm.* 11, 4143–4153. doi:10.1021/mp500367k

GuerinThompson, S. D. (2021). Restriction boosts piezoelectricity. *Nat. Mat.* 20, 574–575. doi:10.1038/s41563-020-00890-4

Hajj, K. A., Ball, R. L., Deluty, S. B., Singh, S. R., Strelkova, D., Knapp, C. M., et al. (2019). Branched-tail lipid nanoparticles potently deliver mRNA *in vivo* due to enhanced ionization at endosomal pH. *Small* 15, e1805097. doi:10.1002/smll.201805097

HåkanssonWigley, K. D. B. (1998). Structure of a complex between a cap analogue and mRNA guanylyl transferase demonstrates the structural chemistry of RNA capping. *Proc. Natl. Acad. Sci. U. S. A.* 95, 1505–1510. doi:10.1073/pnas.95.4.1505

Hassett, K. J., Higgins, J., Woods, A., Levy, B., Xia, Y., Hsiao, C. J., et al. (2021). Impact of lipid nanoparticle size on mRNA vaccine immunogenicity. *J. Control. Release* 335, 237–246. doi:10.1016/j.jconrel.2021.05.021

Hewitt, S. B. A., Bailey, D., Ichikawa, K., Zielinski, J., Karp, R., Apte, A., et al. (2019). Durable anticancer immunity from intratumoral administration of IL-23, IL-36γ, and OX40L mRNAs. *Sci. Transl. Med.* 11 (477), eaat9143. doi:10.1126/scitranslmed.aat9143

Heyes, J., Palmer, L., and BremnerMaclachlan, K. I. (2005). Cationic lipid saturation influences intracellular delivery of encapsulated nucleic acids. *J. Control. Release* 107, 276–287. doi:10.1016/j.jconrel.2005.06.014

Hou, X., Zaks, T., and LangerDong, R. Y. (2021). Lipid nanoparticles for mRNA delivery. *Nat. Rev. Mat.* 6, 1078–1094. doi:10.1038/s41578-021-00358-0

Hu, B., Li, B., Li, K., Liu, Y., Li, C., Zheng, L., et al. (2022). Thermostable ionizable lipid-like nanoparticle (iLAND) for RNAi treatment of hyperlipidemia. *Sci. Adv.* 8, eabm1418. doi:10.1126/sciadv.abm1418

Islam, M. A., Rice, J., Reesor, E., Zope, H., Tao, W., Lim, M., et al. (2021). Adjuvant-pulsed mRNA vaccine nanoparticle for immunoprophylactic and therapeutic tumor suppression in mice. *Biomaterials* 266, 120431. doi:10.1016/j.biomaterials.2020.120431

Kaczmarek, J. C., Patel, A. K., Rhym, L. H., Palmiero, U. C., Bhat, B., Heartlein, M. W., et al. (2021). Systemic delivery of mRNA and DNA to the lung using polymer-lipid nanoparticles. *Biomaterials* 275, 120966. doi:10.1016/j.biomaterials.2021.120966

Kazemian, P., Yu, S. Y., Thomson, S. B., Birkenshaw, A., and LeavittRoss, B. R. C. J. D. (2022). Lipid-nanoparticle-based delivery of CRISPR/Cas9 genome-editing components. *Mol. Pharm.* 19, 1669–1686. doi:10.1021/acs.molpharmaceut.1c00916

Kim, D., Wu, Y., and ShimOh, G. Y. K. (2021). Genome-editing-Mediated restructuring of tumor immune microenvironment for prevention of metastasis. *ACS Nano* 15, 17635–17656. doi:10.1021/acsnano.1c05420

Kowalski, P. S., Rudra, A., and MiaoAnderson, L. D. G. (2019). Delivering the messenger: Advances in technologies for therapeutic mRNA delivery. *Mol. Ther.* 27, 710–728. doi:10.1016/j.ymthe.2019.02.012

Kranz, L. M., Diken, M., Haas, H., Kreiter, S., Loquai, C., Reuter, K. C., et al. (2016). Systemic RNA delivery to dendritic cells exploits antiviral defence for cancer immunotherapy. *Nature* 534, 396–401. doi:10.1038/nature18300

Krienke, C. K. L., Diken, E., Streuber, M., Kirchhoff, S., Bukur, T., Kranz, L., et al. (2021). A noninflammatory mRNA vaccine for treatment of experimental autoimmune encephalomyelitis. *Science* 371 (6525), 145–153. doi:10.1126/science.aay3638

Li, B., Luo, X., Deng, B., Wang, J., Mccomb, D. W., Shi, Y., et al. (2015). An orthogonal array optimization of lipid-like nanoparticles for mRNA delivery *in vivo*. *Nano Lett.* 15, 8099–8107. doi:10.1021/acs.nanolett.5b03528

Li, C., Yang, T., Weng, Y., Zhang, M., Zhao, D., Guo, S., et al. (2022a). Ionizable lipid-assisted efficient hepatic delivery of gene editing elements for oncotherapy. *Bioact. Mat.* 9, 590–601. doi:10.1016/j.bioactmat.2021.05.051

Li, M., Li, Y., Li, S., Jia, L., Wang, H., Li, M., et al. (2022b). The nano delivery systems and applications of mRNA. *Eur. J. Med. Chem.* 227, 113910. doi:10.1016/j.ejmech.2021.113910

Li, Q., Ren, J., Liu, W., and JiangHu, G. Q. R. K. (2021). CpG oligodeoxynucleotide developed to activate primate immune responses promotes antitumoral effects in combination with a neoantigen-based mRNA cancer vaccine. *Drug Des. devel. Ther.* 15, 3953–3963. doi:10.2147/dddt.S325790

Liu, J., Bao, X., Kolesnik, I., Jia, B., Yu, Z., Xing, C., et al. (2022). Enhancing the *in vivo* stability of polycation gene carriers by using PEGylated hyaluronic acid as a shielding system. *BIO Integr.* 3, 103–111. doi:10.15212/bioi-2021-0033

Liu, J., Chang, J., Jiang, Y., Meng, X., Sun, T., Mao, L., et al. (2019). Fast and efficient CRISPR/Cas9 genome editing *in vivo* enabled by bioreducible lipid and messenger RNA nanoparticles. *Adv. Mat.* 31, e1902575. doi:10.1002/adma.201902575

Liu, S., Cheng, Q., Wei, T., Yu, X., Johnson, L. T., Farbiak, L., et al. (2021). Membrane-destabilizing ionizable phospholipids for organ-selective mRNA delivery and CRISPR-Cas gene editing. *Nat. Mat.* 20, 701–710. doi:10.1038/s41563-020-00886-0

Lokugamage, M. P., Sago, C. D., Gan, Z., and KrupczakDahlman, B. R. J. E. (2019). Constrained nanoparticles deliver siRNA and sgRNA to T cells *in vivo* without targeting ligands. *Adv. Mat.* 31, e1902251. doi:10.1002/adma.201902251

Lokugamage, M. P., Vanover, D., Beyersdorf, J., Hatit, M. Z. C., Rotolo, L., Echeverri, E. S., et al. (2021). Optimization of lipid nanoparticles for the delivery of nebulized therapeutic mRNA to the lungs. *Nat. Biomed. Eng.* 5, 1059–1068. doi:10.1038/s41551-021-00786-x

Maier, M. A., Jayaraman, M., Matsuda, S., Liu, J., Barros, S., Querbes, W., et al. (2013). Biodegradable lipids enabling rapidly eliminated lipid nanoparticles for systemic delivery of RNAi therapeutics. *Mol. Ther.* 21, 1570–1578. doi:10.1038/mt.2013.124

Miao, L., Li, L., Huang, Y., Delcassian, D., Chahal, J., Han, J., et al. (2019). Delivery of mRNA vaccines with heterocyclic lipids increases anti-tumor efficacy by STING-mediated immune cell activation. *Nat. Biotechnol.* 37, 1174–1185. doi:10.1038/s41587-019-0247-3

Miao, L., Lin, J., Huang, Y., Li, L., Delcassian, D., Ge, Y., et al. (2020). Synergistic lipid compositions for albumin receptor mediated delivery of mRNA to the liver. *Nat. Commun.* 11, 2424. doi:10.1038/s41467-020-16248-y

Miao, L., Zhang, Y., and Huang, L. (2021). mRNA vaccine for cancer immunotherapy. *Mol. Cancer* 20, 41. doi:10.1186/s12943-021-01335-5

Miyabe, H., Hyodo, M., Nakamura, T., Sato, Y., and HayakawaHarashima, Y. H. (2014). A new adjuvant delivery system 'cyclic di-GMP/YSK05 liposome' for cancer immunotherapy. *J. Control. Release* 184, 20–27. doi:10.1016/j.jconrel.2014.04.004

Ndebele, R. T., Yao, Q., Shi, Y.-N., Zhai, Y.-Y., Xu, H.-L., Lu, C.-T., et al. (2022). Progress in the application of nano- and micro-based drug delivery systems in pulmonary drug delivery. *BIO Integr.* 3, 71–83. doi:10.15212/bioi-2021-0028

Peng, Q., Li, H., Deng, Q., Liang, L., Wang, F., Lin, Y., et al. (2021). Hybrid artificial cell-mediated epigenetic inhibition in metastatic lung cancer. *J. Colloid Interface Sci.* 603, 319–332. doi:10.1016/j.jcis.2021.06.066

Puranik, A., Lenehan, P. J., Silvert, E., Niesen, M. J. M., Corchado-Garcia, J., O'horo, J. C., et al. (2022). Comparative effectiveness of mRNA-1273 and BNT162b2 against symptomatic SARS-CoV-2 infection. *Med. (N Y)* 3, 28–41.e8. doi:10.1016/j.medj.2021.12.002

Qiu, M., Glass, Z., Chen, J., Haas, M., Jin, X., Zhao, X., et al. (2021). Lipid nanoparticle-mediated codelivery of Cas9 mRNA and single-guide RNA achieves liver-specific *in vivo* genome editing of Angptl3. *Proc. Natl. Acad. Sci. U. S. A.* 118, e2020401118. doi:10.1073/pnas.2020401118

QiuLi, M. P. (2021). CRISPR/Cas-based diagnostics and gene therapy. *BIO Integr.* 2, 121–129. doi:10.15212/bioi-2020-0048

Reinhard, K., Rengstl, B., Oehm, P., Michel, K., Billmeier, A., Hayduk, N., et al. (2020). An RNA vaccine drives expansion and efficacy of claudin-CAR-T cells against solid tumors. *Science* 367, 446–453. doi:10.1126/science.aay5967

Rosenblum, D., Gutkin, A., Kedmi, R., Ramishetti, S., Veiga, N., Jacobi, A. M., et al. (2020). CRISPR-Cas9 genome editing using targeted lipid nanoparticles for cancer therapy. *Sci. Adv.* 6, eabc9450. doi:10.1126/sciadv.abc9450

Sahin, U., Oehm, P., Derhovanessian, E., Jabulowsky, R. A., Vormehr, M., Gold, M., et al. (2020). An RNA vaccine drives immunity in checkpoint-inhibitor-treated melanoma. *Nature* 585, 107–112. doi:10.1038/s41586-020-2537-9

Sato, Y., Hashiba, K., Sasaki, K., Maeki, M., and TokeshiHarashima, M. H. (2019). Understanding structure-activity relationships of pH-sensitive cationic lipids facilitates the rational identification of promising lipid nanoparticles for delivering siRNAs *in vivo*. *J. Control. Release* 295, 140–152. doi:10.1016/j.jconrel.2019.01.001

Semple, S. C., Akinc, A., Chen, J., Sandhu, A. P., Mui, B. L., Cho, C. K., et al. (2010). Rational design of cationic lipids for siRNA delivery. *Nat. Biotechnol.* 28, 172–176. doi:10.1038/nbt.1602

Shepherd, S. J., Warzecha, C. C., Yadavali, S., El-Mayta, R., Alameh, M. G., Wang, L., et al. (2021). Scalable mRNA and siRNA lipid nanoparticle production using a parallelized microfluidic device. *Nano Lett.* 21, 5671–5680. doi:10.1021/acs.nanolett.1c01353

Shirazi, R. S., Ewert, K. K., Leal, C., Majzoub, R. N., and BouxseinSafinya, N. F. C. R. (2011). Synthesis and characterization of degradable multivalent cationic lipids with disulfide-bond spacers for gene delivery. *Biochimica Biophysica Acta - Biomembr.* 1808, 2156–2166. doi:10.1016/j.bbamem.2011.04.020

Sindhwani, S., Syed, A. M., Ngai, J., Kingston, B. R., Maiorino, L., Rothschild, J., et al. (2020). The entry of nanoparticles into solid tumours. *Nat. Mat.* 19, 566–575. doi:10.1038/s41563-019-0566-2

Suzuki, Y., Hyodo, K., Suzuki, T., Tanaka, Y., and KikuchiIshihara, H. H. (2017). Biodegradable lipid nanoparticles induce a prolonged RNA interference-mediated protein knockdown and show rapid hepatic clearance in mice and nonhuman primates. *Int. J. Pharm. X.* 519, 34–43. doi:10.1016/j.ijpharm.2017.01.016

Tanaka, H., Takahashi, T., Konishi, M., Takata, N., Gomi, M., Shirane, D., et al. (2020). Self-degradable lipid-like materials based on "hydrolysis accelerated by the intra-particle enrichment of reactant (HyPER)" for messenger RNA delivery. *Adv. Funct. Mat.* 30, 1910575. doi:10.1002/adfm.201910575

Van Der Jeught, K., De Koker, S., Bialkowski, L., Heirman, C., Tjok Joe, P., Perche, F., et al. (2018). Dendritic cell targeting mRNA lipopolyplexes combine strong antitumor T-cell immunity with improved inflammatory safety. *ACS Nano* 12, 9815–9829. doi:10.1021/acsnano.8b00966

Wang, Y., Tiruthani, K., Li, S., Hu, M., Zhong, G., Tang, Y., et al. (2021). mRNA delivery of a bispecific single-domain antibody to polarize tumor-associated macrophages and synergize immunotherapy against liver malignancies. *Adv. Mat.* 33, e2007603. doi:10.1002/adma.202007603

Warashina, S., Nakamura, T., Sato, Y., Fujiwara, Y., Hyodo, M., Hatakeyama, H., et al. (2016). A lipid nanoparticle for the efficient delivery of siRNA to dendritic cells. *J. Control. Release* 225, 183–191. doi:10.1016/j.jconrel.2016.01.042

Whitehead, K. A., Dorkin, J. R., Vegas, A. J., Chang, P. H., Veiseh, O., Matthews, J., et al. (2014). Degradable lipid nanoparticles with predictable *in vivo* siRNA delivery activity. *Nat. Commun.* 5, 4277. doi:10.1038/ncomms5277

Witzigmann, D., Kulkarni, J. A., Leung, J., Chen, S., and CullisVan Der Meel, P. R. R. (2020). Lipid nanoparticle technology for therapeutic gene regulation in the liver. *Adv. Drug Deliv. Rev.* 159, 344–363. doi:10.1016/j.addr.2020.06.026

Wolff, J. A., Malone, R. W., Williams, P., Chong, W., Acsadi, G., Jani, A., et al. (1990). Direct gene transfer into mouse muscle *in vivo*. *Science* 247, 1465–1468. doi:10.1126/science.1690918

Wu, L. P., Wang, W. W., Tian, J. L., Qi, C. R., Cai, Z. X., Yan, W. H., et al. (2022). Intravenous delivery of RNA encoding anti-PD-1 human monoclonal antibody for treating intestinal cancer. *J. Cancer* 13, 579–588. doi:10.7150/jca.63991

Xiong, J., Li, G., Mei, X., Ding, J., Shen, H., Zhu, D., et al. (2022). Co-delivery of p53 restored and E7 targeted nucleic acids by poly (Beta-Amino ester) complex nanoparticles for the treatment of HPV related cervical lesions. *Front. Pharmacol.* 13, 826771. doi:10.3389/fphar.2022.826771

Zeng, C., Hou, X., Yan, J., Zhang, C., Li, W., Zhao, W., et al. (2020a). Leveraging mRNA sequences and nanoparticles to deliver SARS-CoV-2 antigens *in vivo*. *Adv. Mat.* 32, e2004452. doi:10.1002/adma.202004452

Zeng, C., Zhang, C., and WalkerDong, P. G. Y. (2020b). Formulation and delivery technologies for mRNA vaccines. *Curr. Top. Microbiol. Immunol.* 2020, 1 doi:10.1007/82_2020_217

Zhang, D., Wang, G., Yu, X., Wei, T., Farbiak, L., Johnson, L. T., et al. (2022). Enhancing CRISPR/Cas gene editing through modulating cellular mechanical properties for cancer therapy. *Nat. Nanotechnol.* 17, 777–787. doi:10.1038/s41565-022-01122-3

Zhang, X., Zhao, W., Nguyen, G. N., Zhang, C., Zeng, C., Yan, J., et al. (2020). Functionalized lipid-like nanoparticles for *in vivo* mRNA delivery and base editing. *Sci. Adv.* 6, eabc2315. doi:10.1126/sciadv.abc2315

Zhang, Y., Sun, C., Wang, C., and JankovicDong, K. E. Y. (2021). Lipids and lipid derivatives for RNA delivery. *Chem. Rev.* 121, 12181–12277. doi:10.1021/acs.chemrev.1c00244

Zheng, C., and LiDing, M. J. (2021). Challenges and opportunities of nanomedicines in clinical translation. *BIO Integr.* 2, 57–60. doi:10.15212/bioi-2021-0016

Zhou, K., Nguyen, L. H., Miller, J. B., Yan, Y., Kos, P., Xiong, H., et al. (2016). Modular degradable dendrimers enable small RNAs to extend survival in an aggressive liver cancer model. *Proc. Natl. Acad. Sci. U. S. A.* 113, 520–525. doi:10.1073/pnas.1520756113

Frontiers in
Bioengineering and Biotechnology

Accelerates the development of therapies, devices, and technologies to improve our lives

A multidisciplinary journal that accelerates the development of biological therapies, devices, processes and technologies to improve our lives by bridging the gap between discoveries and their application.

Discover the latest Research Topics

See more →

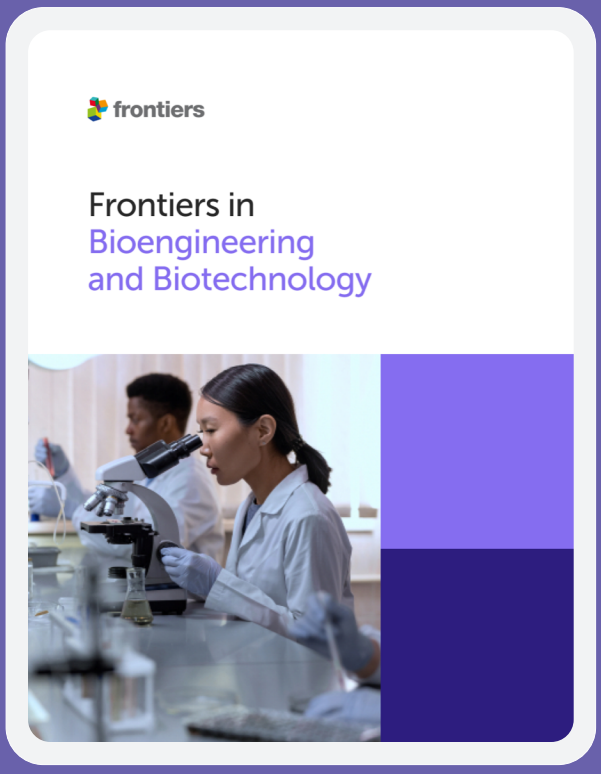

Frontiers

Avenue du Tribunal-Fédéral 34
1005 Lausanne, Switzerland
frontiersin.org

Contact us

+41 (0)21 510 17 00
frontiersin.org/about/contact